POLITECNICO DI MILANO

Facoltà di Ingegneria Industriale e dell'Informazione

Dipartimento di Energia

Dipartimento di Chimica, Materiali e Ingegneria Chimica "Giulio Natta"

FIRST-PRINCIPLES ASSESSMENT OF CO_2 ACTIVATION OVER METAL CATALYSTS

Relatore: Prof. Matteo Maestri

Correlatore: Dr. Simone Piccinin, (CNR/IOM Democritos, c/o SISSA, Trieste, Italy)

Tesi di Laurea in Ingegneria Chimica di:

Luca DIETZ Matr. 782589

Anno Accademico 2012-2013

Abstract

CO_2 activation on Platinum, Rhodium and Nickel has been studied in detail by the mean of a periodic planewave DFT analysis.

The evaluation of the reaction paths involving CO_2 is of increasing interest in emerging technologies that entail CO_2 conversion, such as “Power to Gas”, CO_2 methanation and Reverse Water Gas Shift for short contact time reforming processes.

The challenging issue related to the reduction of CO_2 emissions in power plants and the pressing need for independence from fossil fuels mobilized the research and development areas towards the production of electricity from renewable sources. A successful method to store energy in a chemical way may be grounded on water electrolysis for hydrogen production. However, this compound is neither easily transportable nor manageable with ease. It is in this context that one inserts the "Power to Gas" project. The hydrogen is converted into a chemical with wide range of use (synthetic natural gas), by means of the catalytic reaction of CO_2 methanation.

In this Thesis four pathways have been considered on different surface environments as representative steps for:

Direct decomposition: $CO_2 \rightarrow CO + O$

Boudouard reaction: $CO_2 + C \rightarrow 2CO$

Boudouard in coking condition: $CO_2 + nC \rightarrow 2CO + (n-1)C$

Direct hydrogenation: $CO_2 + H \rightarrow COOH$

In this regard, an approach based on the use of quantum mechanics has been selected as an ideal tool to make a theoretical modeling of the atomic scale. In particular, the adoption of "first-principles" methods, as Density Functional Theory, allows us to understand in detail the relevant processes such as those involved in energy conversion and storage. The Schrödinger equation is solved according to Kohn-Sham approximation; in relation to the calculation of the total energy of the examined system, it is possible to extract the essential information for the evaluation of the fundamental properties of an heterogeneous process, such as heats of adsorption and adsorbate's geometric features. By means of the CI-NEB algorithm, the Transition State has been located, activation energies have been calculated, and these variables have been correlated with other characteristic properties of the metallic catalysts.

This analysis showed a poor affinity of CO_2 towards metal substrates, while the other chemical species involved in the elementary steps, such as C, O, H, COOH and CO strongly adsorb on all the three considered metals. It was noticed that on Platinum, the mechanism of activation preferably occurs, in terms of energy, through the process of hydrogenation of carbon dioxide. In case of Rhodium and Nickel based catalysts, the favored reactive path is the one that concerns CO_2 direct decomposition. Given the presence of carbonaceous compounds, also the possible coke formation has been considered. It was found that the activation energies for the Boudouard reaction with high carbon coating collapse and appear scarcely affected by the type of metal.

.

Sommario

L'attivazione della CO_2 su Platino, Rodio e Nichel è stata studiata nel dettaglio grazie all'impiego di un'analisi DFT a onde piane.

La valutazione dei cammini di reazione che coinvolgono la CO_2 è di crescente interesse per le tecnologie emergenti volte a convertire la CO_2, come il "Power to Gas", la metanazione della CO_2 e la Reverse Water Gas Shift nei processi di reforming a basso tempo di contatto.

L'avvincente tema legato alla riduzione delle emissioni di CO_2 sugli impianti di generazione di potenza e la premente necessità d'indipendenza dai combustibili fossili ha mobilitato il settore di ricerca e sviluppo verso la produzione di energia elettrica da fonti rinnovabili. Un modo efficiente per accumulare energia entro un composto chimico può essere fondato sulla produzione di idrogeno, via elettrolisi dell'acqua. Tuttavia, questo composto non è né facilmente trasportabile né maneggiabile con sicurezza. È in questo contesto che si inserisce il progetto "Power to Gas". L'idrogeno è convertito in un composto ad ampio campo di utilizzo (gas naturale sintetico), mediante la reazione catalitica di metanazione della CO_2.

In questa tesi sono stati considerati quattro diversi cammini, e gli step rappresentativi che avvengono sulla superficie catalitica sono:

La decomposizione diretta: $CO_2 \rightarrow CO + O$

La reazione di Boudouard: $CO_2 + C \rightarrow 2CO$

La reazione di Boudouard in condizioni di coking: $CO_2 + nC \rightarrow 2CO + (n-1)C$

L'idrogenazione diretta: $CO_2 + H \rightarrow COOH$

A questo proposito, un approccio fondato sull'utilizzo della meccanica quantistica è stato selezionato come ideale per realizzare una modellazione teorica sulla scala atomica. In particolare l'impiego di metodi "first-principles", come la Density Functional Theory, permette di comprendere nel dettaglio processi rilevanti, quali quelli coinvolti nella conversione e accumulo dell'energia. L'equazione di Schrödinger viene risolta nell'approssimazione di Kohn-Sham; sulla base del calcolo dell'energia totale del sistema studiato, è possibile estrarre informazioni indispensabili per la valutazione delle proprietà fondamentali di un processo eterogeneo, come calori di adsorbimento e proprietà geometriche dell'adsorbato. Mediante l'algoritmo CI-NEB si è ricercato il Transition State, calcolato le energie di attivazione, e correlato queste ultime grandezze ad altre proprietà caratteristiche dei catalizzatori metallici.

Questa analisi ha evidenziato una scarsa affinità della CO_2 nei confronti del substrato metallico, mentre le altre specie chimiche coinvolte negli atti elementari, quali C, O, H, CO e COOH si adsorbono con forza su tutti e tre i metalli considerati. È stato osservato che su Platino, il meccanismo di attivazione avviene preferibilmente, da un punto di vista energetico, attraverso un processo idrogenazione del biossido di carbonio. Nel caso di catalizzatori a base di Rodio e Nichel il cammino reattivo favorito è quello che prevede la decomposizione diretta della CO_2. Data la presenza di composti carboniosi, anche la possibile formazione di coke è stata considerata. Si è riscontrato che ad alto ricoprimento di carbonio le energie di attivazione, per la reazione di Boudouard crollano e appaiono scarsamente influenzate dalla tipologia di metallo.

Table of Contents

CHAPTER 1

1 Introduction

1.1 Motivation

Solar power, wind and other renewable powers, once converted into electrical energy, are united by a fluctuating production, with seasonal periods, so in some times of the year the excess of energy cannot be exploited, while in other seasons a deficit of electrical energy occurs. Sustainable energy technologies are intrinsically intermittent and the need for a greater flexibility in electricity accommodation increases.

For this reason a new technology has been proposed to overcome the failure to readily store the excess of electricity. A matching between electricity supply and demand can be achieved and "green" electric energy can be produced on demand through the "Power to Gas" system.

This way the surplus in energy is stored in a lasting manner within a stable chemical compound that is methane, or the so-called synthetic natural gas.

The electricity from sustainable sources can be accumulated into hydrogen by means of the process of water electrolysis, with an average efficiency of 75% for recent alkaline cells used in industrial processes. To ensure an increase in the efficiency of this first transformation, the amount of energy that is lost as heat can be partially recovered by feeding it into the district heating network. On the other hand, oxygen , which is the byproduct of the H_2O splitting reaction, posses a significant economic value and a wide range of application in various branches such as medical technology, so it can be conveniently sold in the internal market.

However, limitations in the use of gaseous hydrogen are caused by several difficulties connected with transport issues that prevent hydrogen to be considered as an optimal power source.

Therefore, "Power to Gas" is involved in a further conversion, in fact this process exploits hydrogen to give rise to the methanation reaction, combining the previous molecule with CO_2 which can be extracted from air or from alternative sources such as cement or biogas plants. So synthetic methane

produced by “Power to Gas” can be easily gathered by entering it into the distribution network of natural gas.

The driving force of this innovative process is related to the numerous advantages of “Power to Gas”:

- The selection of methane as fuel allows to take advantage of the infrastructures commonly used to transport and store the natural gas, which are already available in all those countries that have a gas network.
- The choice that has led to change hydrogen into methane is related to the fact that hydrogen can be injected into the network only within certain percentages, which are modest, while synthetic natural gas is totally compatible with methane and allows stocks which guarantee more temporary storage.
- The transport of gas via pipelines is far more economical when compared with the distribution system of electrical energy, with a ratio of 20:1 in favor of natural gas per unit of transferred energy. In addition, the advantage becomes net if one considers the cost the public gas and electricity, referred to kilowatt per hour (0.06 €/kWh vs. 0.2 €/kWh).
- A greenhouse gas as CO_2, usually produced as flue gas of power plants and internal combustion engines of automotive vehicles, and then discharged in atmosphere, is recycled and turned into a propeller or fed as raw gas for further synthesis of chemicals.

However, methanation is strongly exothermic and reduces the overall efficiency of the “Power to Gas“ process, in fact efficiency decreases from 75 % (to convert electric current into hydrogen) to 65 % (to store electrical energy in CH_4). The only way to rationally increase these values and bring the process to higher performance than traditional natural gas combined-cycle or cogeneration plants needs a heat recovery system to be designed, in fact a large amount of high temperature heat is released by the methanation reactor.

At present, international organizations and industries are involved in this project. In Denmark Topsoe is working on a “Power to Gas” project , CEA, GEG and Saipem in France aim at creating a demonstration plant, instead in Germany Total, Siemens and other organizations have invested in the realization of a biogas plant, wind turbines and electrolysis unit for hydrogen generation. E.ON has launched in 2013 a project for the construction of a “Power to Gas” pilot plant. Institutions as FIW and IWES are investigating the conversion of the surplus of electric energy from wind turbines in synthetic natural gas.

In 2013, the developments of “Power to Gas” technology have brought the automaker AUDI to invest in this project; the installation of wind turbines in the North Sea, in order to produce "green" electric current has been planned. The surplus in electric energy will be used in a hydrolysis unit to break water into molecular oxygen and hydrogen; the latter will interact with carbon dioxide to give methane, renamed by AUDI “e-gas”. This way the CO_2 cycle can be closed as the content of CO_2 released into the atmosphere, due to the combustion of “e-gas”, is the same quantity of CO_2 that has to be removed from air or from the exhaust gas of a biogas plant. Global CO_2 emissions of an “e-gas” powered vehicle are estimated with a “well-to-wheel analysis” to be less than 30g of CO_2/km. Lower emissions (about 4g of CO_2/km) are only possible if electric vehicles, whose batteries are charged using power produced by wind turbines, or renewable sources, are considered. However, the real problem of the electric motors remains the limited autonomy and considerable expenditure of energy for the manufacture of batteries.

In 2011, DNV KEMA has started a project with the purpose to build a methanation unit on a laboratory scale that consumes hydrogen, co-fed with carbon dioxide and monoxide, in order to have synthetic natural gas. The process of heterogeneous catalysis was realized on a Nickel-based catalyst, at high temperature (400-500°C) and atmospheric pressure. Further analysis were planned out to quantify the influence of the operating parameters on conversion and selectivity, as well as to evaluate the performance of the catalyst for the methanation reaction.

It is therefore crucial to understand and study CO_2 activation on those metals that are typically employed at industrial level and that are possible methanation catalysts.

A rational investigation of the properties of the adopted catalyst has to be performed through physical-chemical analysis. The chemistry of the process must be accurately understood in fact it is important to assay in details the energetic of the elementary steps which are responsible of the CO_2 activation on metals at the atomic scale. Thus surface reactivity and the substrate-adsorbate interaction became the object of a preliminary assessment.

1.2 General overview

In this work the properties of reactive systems involving carbon dioxide on transition metals have been studied. The model we have used to simulate these systems is base on the Density Functional Theory. Through this tool the interaction between metals as Platinum, Rhodium and Nickel and chemisorbed species such as CO_2, CO, COOH, C, O, H has been investigated. Such kind of approach is commonly referred to as "first-principles" because it is based on mathematical and physical models that describe the atomic scale without adaptive parameters derived from laboratory experimentations. Therefore DFT allows the development of microkinetic models abandoning the need to introduce hypotheses on the reaction mechanism, commonly based on experimental data fittings. By introducing the basics of surface science and chemical-physics in the study of a catalytic process, the well known trial-and-error approach for the development of new substrates, with optimum electronic structure, can be replaced by a rational modeling of catalytic surface reactions at the atomic scale.

Such a type of investigation represents the first step towards the wide and complete multiscale approach:

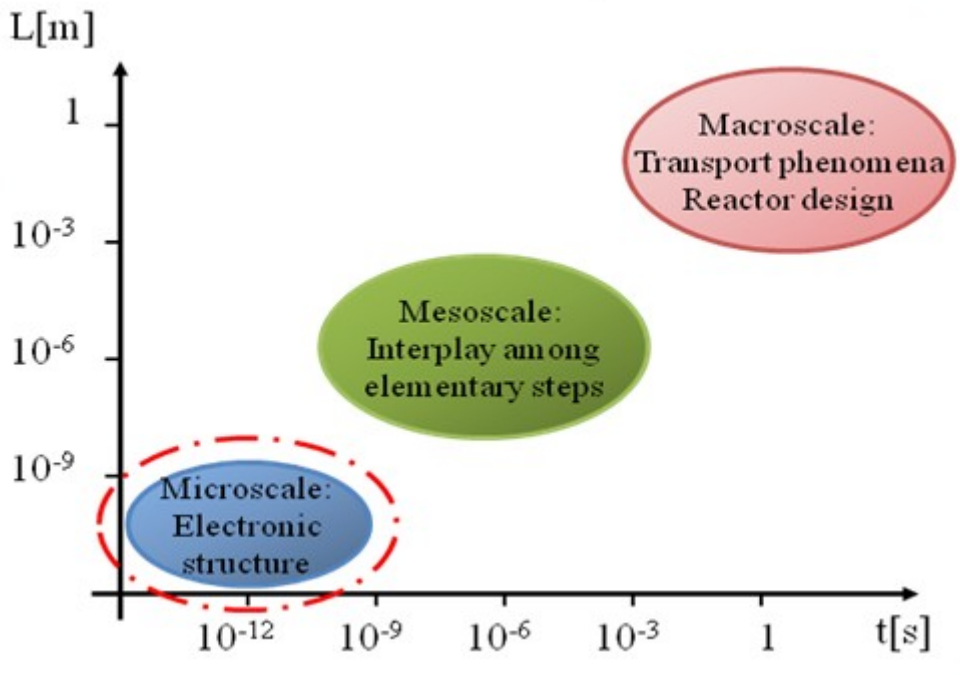

Figure 1.1: time and space range of a multiscale approach

Where microscale has the fundamental role to deal with kinetic parameters of elementary steps, which describe the breaking and the constitution of chemical bonds. Microscale is commonly the field of study of all eligible reaction paths that can occur at the catalytic surface, but only few of them are really relevant on the overall reaction rate of the process and can be used to properly model the system at the reactor scale. A bridge among the three levels, micro, meso, macro scale, must be realized since the lower levels exert influence on the upper ones and vice versa.

Heats of adsorption have been computed to identify the most stable adsorption sites, although the real target lies in the calculation of activation energies and the modeling of possible correlations that link the properties of the system as binding energies, activation energies, structure and metal sensitivity.

Explanations have been provided through the electronic structure analysis and the projection of the density of states onto the valence orbitals (PDOS), the Transition State has been rated according to its electronic and geometrical features.

This work is divided into 5 chapters:

Chapter 2

The second chapter is an introduction to quantum-mechanics that is a basic theory developed to allow the characterization of the matter at the atomic scale through the formulation of the Schrödinger equation. Since this equation is a function of the positions of all the atoms and electrons of the system, an enormous computational effort is involved in its resolution. Such intensive numerical resources can be supplied only with the aid of massive parallel supercomputers. A significant issue which adds to the complexity of the numerical calculation is due to a lack of an exact formulation of the expression of Schrödinger equation. The more intricate term is represented by the electron-electron interaction, whose contributions of exchange and correlation are not known explicitly but they are necessarily approximated.

The resolution of Schrödinger equation becomes computationally easier if the Density Functional Theory is implemented; in fact it guarantees an exact change of variable to reduce the dimensionality of the problem, that is the effective number of independent variables. The theorems of Hohenberg and Kohn assure that no approximation is introduced up to now.

However, the problem is still extremely complex so it is replaced by a simpler one, but some approximations have to be accepted:

- The many body system is turned into a one-electron system according to Kohn and Sham scheme,
- Only the valence electrons are individually treated, the ensemble of core electrons are described by a smooth potential called pseudopotential,
- The exchange and correlation contribution is built according to the Generalized Gradient approximation.

Chapter 3

This chapter elucidates the method to solve the Kohn-Sham equations with periodic functions, called plane waves, whose periodicity is defined by Bloch's theorem and since a periodic framework is employed Von Karman or periodic boundary conditions have to be introduced. The crystalline structure of transition metals is shown and described using Bravais' lattices. The bulk is assembled with an infinite repetition of a selected unit cell along the crystallographic axes and the lattice constant of the metals is calculated by minimizing the system total energy, checking the convergence with respect to kinetic energy cutoff and k-points. The creation of a surface is accomplished by a supercell, in which the bulk is cut, and the periodicity is lost in the direction perpendicular to the plane of the surface, where a vacuum spacing is inserted.

Criteria used to establish atomic positions within a supercell are discussed in detail; a profile of the heats of adsorption illustrates the affinity between the metal and the adsorbate. An explanation of the results is provided by the assessment of the projected density of states.

The binding energies of the chemical compounds that appear at the metal surface of the elementary steps (discussed in chapter 5) have been computed with quantum-ESPRESSO, an integrated suite of Open-Source computer codes for electronic-structure calculations and materials modeling at the nanoscale. The simulations are held on a 2x2 supecell with 3 layers of fixed atoms, surface chemistry has been examined on (111) surface and the heats of adsorption on the three metals show:

- Carbon dioxide does not considerably adsorbe at the catalytic surface,
- Carbon monoxide exhibits the largest binding energy on Nickel,
- The adsorption of atomic carbon is strongly exothermic, it displays the greatest binding energy,

- Atomic oxygen has a remarkable binding energy too, with a predilection for Nickel,
- Atomic hydrogen shows lower heats of adsorption if compared to the other atomic species, and hydrogen binding energies are little influenced by the choice of the metal,
- The heat of adsorption of the carboxylic group is very similar to the one of hydrogen, with a greater affinity with Rhodium.

	Pt	Rh	Ni
C	-6.825 eV (fcc)	-7.032 eV (hcp)	-7.027 eV (fcc)
O	-4.381 eV (fcc)	-5.010 eV (fcc)	-5.710 eV (fcc)
H	-2.740 eV (top)	-2.797 eV (fcc)	-2.905 eV (fcc)
CO	-1.797 eV (hcp)	-1.883 eV (hcp)	-2.118 eV (hcp)
CO_2	-0.053 eV (top)	-0.027 eV (top)	-0.033 eV (top)
COOH	-2.317 eV (top)	-2.510 eV (top)	-2.473 eV (top)

Table 1.1:binding energies of C, O, H, CO, CO_2, COOH computed for the most stable adsorption site on (111) surfaces

Chapter 4

The importance of heterogeneous catalysis for industrial processes has led to the implementation of the Transition State Theory also on gas-solid systems, the study of the potential energy surface is an essential prerogative to identify the Transition State that connects reactants with products, set in local minima at the end of the Minimum Energy Path. Several numerical methods have been developed for the location of the Transition State, the one adopted in this dissertation is the CI-NEB, or Climbing Image, Nudged Elastic Band, able to build up a profile of the Minimum Energy Path, and to provide a discrete profile of the MEP, placing an electronic structure exactly in correspondence of the Transition State, in agreement with the permitted tolerance. An example of CI-NEB calculations is proved in the dissociation of the hydroxyl group on Platinum (111), the energy profile of the MEP allows to identify the presence of a just one Transition State between the initial and final images, then the reaction at the metal surface actually is an elementary step.

Chapter 5

The following elementary steps have been selected as possible starting point of a detailed reaction mechanism in CO_2 activation on transition metals:

$$CO_2 \rightarrow CO + O \quad (1.1)$$

$$CO_2 + C \rightarrow 2CO \quad (1.2)$$

$$CO_2 + nC \rightarrow 2CO + (n-1)C \quad (1.3)$$

$$CO_2 + H \rightarrow COOH \quad (1.4)$$

Reaction (1.1) has been chosen since it entails the direct reduction of carbon dioxide at the metal surface, giving birth to gaseous carbon monoxide, that is a more reactive intermediate and which can be turned into methane through the methanation reaction with hydrogen. Reaction (1.2) has been selected since carbon monoxide may be further reduced to elements, by overlaying the metal surface with carbon; CO_2, that is the most abundant reactant, is able to gasify the coke at the metal surface. According to the operative conditions, a higher coverage of coke can occur at the metal surface (1.3). On the other hand, the co-fed reactants of the methanation reactor, that are molecular hydrogen and carbon dioxide, may be involved in the same elementary step (1.4), with hydrogen that first experiences a dissociative adsorption.

When different chemical compounds are simultaneously adsorbed on the catalytic surface the adsorbate-substrate interaction is modified because of the altered distribution of electronic states, and the adsorption site of greatest energetic stability may change. Therefore a combined search is required in order to assess the most stable configuration for reactants and products of the 4 elementary steps, such as:

- Carbon monoxide and atomic oxygen,
- Carbon dioxide and atomic carbon,
- Two molecules of carbon monoxide,
- Carbon monoxide and atomic hydrogen,
- Two molecules of carbon monoxide with carbon covered surface.

12 NEB calculations have been performed since the above-mentioned elementary steps have been studied on Platinum, Rhodium and Nickel. A 2x2 supercell with 3 fixed layers has been used; then, activation energy calculations have been refined by introducing a further layer. Moreover the outer layer has been allowed to relax in the direction perpendicular to the plane of the surface.

The computation of activation energies brought to the classification of the Transition State according to both geometrical and electronic structures. As consequence, the Transition State has been defined "early" if it shares the geometrical structure and electron density of the reactants, and thus the same chemical properties, whereas the Transition State has been declared "late" if it strongly resembles the products.

- By considering the dissociation reaction of CO_2:

  - Both forward and backward activation energies depend on the binding energy of a product of reaction, that is the atomic oxygen,
  - An Evans-Polanyi relations exists, and this presupposes the Transition State to be "late",
  - According to geometry and PDOS it is possible to confirm that the Transition State is "late".

- By considering the Boudouard reaction:

  - Forward activation energy slightly varies from metal to another as well as the binding energy of the atomic carbon,
  - An Evans-Polanyi relations is found, and this suggests the Transition State to be "early",
  - Geometry and PDOS confirm the "early" character of the Transition State.

- By considering the Boudouard reaction in cocking conditions:

  - Forward and backward activation energies are respectively correlated with high coverage atomic carbon binding energy, the former, and low coverage atomic carbon binding energy, the latter,
  - Evans-Polanyi theory cannot provide crucial information about the nature of the Transition State,
  - Only geometry and PDOS are capable to establish that the Transition State is "early".

- By considering the hydrogenation of CO_2 to carboxyl group:

  - The binding energy of atomic hydrogen affects both forward and backward activation energies,
  - Evans-Polanyi theory cannot be employed to explain the properties of the Transition State,
  - PDOS is a fundamental tool to understand that the Transition State is "early", instead the geometrical analysis is in disagreement with PDOS. Nevertheless geometrical investigation does not represents a decisive criterion since chemical properties are dominantly due to the electronic configuration that states if electros are actually shared into orbitals or not.

The NEB calculations for the estimation of the activation energies of the examined elementary steps have shown that:

- In the presence of coke carbon dioxide tends to easily produce two molecules of carbon monoxide, one adsorbed on the metal surface and the other is in gas phase,
- If a charge that does lead to limited production of coke is treated, on Platinum CO_2 activation occurs by hydrogenation to carboxyl species, while Rhodium and Nickel tend to dissociate the molecule into carbon monoxide and atomic oxygen, both adsorbed on the catalyst surface.

	$CO_2 \rightarrow CO + O$		$CO_2 + C \rightarrow 2CO$		$CO_2 + nC \rightarrow 2CO + (n-1)C$		$CO_2 + H \rightarrow COOH$	
E_{act} [eV]	$E_{forward}$	$E_{backward}$	$E_{forward}$	$E_{backward}$	$E_{forward}$	$E_{backward}$	$E_{forward}$	$E_{backward}$
Platinum	1.62	0.76	1.43	2.93	0.47	1.45	0.89	0.84
Rhodium	0.77	1.15	1.41	3.13	0.72	2.07	1.07	1.11
Nickel	0.53	1.19	1.55	3.53	0.35	1.61	1.46	1.31

Table 1.2: forward and backward activation energies of four elementary steps on a (111) 2x2 4 layers slab of Pt, Rh, Ni

According to these considerations, the next step of this modern approach leads to the theoretical formulation of the recipe of the catalyst whose electronic structure has been selected on the basis of a numerical modeling of the solid matter:

- With an active phase and composition that ensure the realization of the optimal reactive pathway,
- With the lowest activation energy,
- With the absence of intermediate species excessively stable and maximum conversion rate,
- By reducing the experimental laboratory research, on the one hand, and also allowing the evaluation of specific properties of matter not investigable with existing analysis tools.

1.3 State of The Art

Renewable, stable and almost emission-free energy systems are fundamental to allow the production of fossil fuel free energy, in this context the "Power to Gas" technology has been developed. The importance of methanation is related to the production of hydrogen and methane with short contact time reactor while reverse water gas shift reaction is subject to mechanistic study.

Several formulations of catalysts, with various active phases and supports have been experimentally investigated; however, Nickel is the industrial metal for methanation reaction, because it combines high activity and selectivity towards methane and low cost.

Several oxides have been tested as possible support: TiO_2,SiO_2,Al_2O_3,CeO_2,ZrO_2 [1-3].

Perkas, Aksoylu et al. investigated Nickel based catalysts, supported by Al_2O_3 and ZrO_2, and they discovered the support to be active for CO_2 methanation [4, 5]. Cai et al. [2] selected Ni/ZrO_2-Al_2O_3 supported catalysts and they brought to light the better properties with respect to the single oxide. Seo et al. [6] scrutinized the role of zirconia and identified its capability to act as a spacer or barrier, or as a structural promoter, which prevented the aggregation of nickel species for fine dispersion. They also compared catalytic activity related to three different methods of preparation. When the support is synthesized with the impregnation-precipitation method higher activity and stability appeared, because of the best dispersion of Nickel active phase, and the highest reducibility and chemisorption capacity.

Choudhary et al. [7] correlated the performance of the catalyst with the basicity and strength of active sites, whereas Ocampo et al. [8] studied Nickel activity on $Ce_{0.72}Zr_{0.28}O_2$ mixed oxides, proving that high performances were due to the high oxygen storage capacity and high Nickel dispersion.

Also the effects on adsorption produced by a La_2O_3 support have been scrutinized by Zhao et al. [9], this kind of support enhances Ni dispersion, while Inui proposed a Ni- La_2O_3-Ru catalyst that can favor CO_2 adsorption through the slight basicity of La_2O_3, while H_2 adsorption is highly promoted by Ru [10].

Rhodium based catalysts were subject to a detailed study which showed their very high activity, because of a lower attitude to deactivation, and a strong dependence on activity on metal-support

interaction. Experiments with $Rh/\gamma\text{-}Al_2O_3$ give evidence that at room temperature and at atmospheric pressure, a feed of CO_2 and H_2 can be turned into methane with 100% of selectivity [11, 12]. Karelovic and Ruiz studied the carbon dioxide methanation mechanism on Rh/TiO_2, focusing on the particle size of metal and learned that by increasing the particle size up to 7 nm intrinsic activity of Rh/TiO_2 catalysts increases [12], whereas if larger particle are employed, the activation energy does not change.

Titania nanotube Pt supported catalysts have been analyzed by Yu et al. [13]. Pt particles on the TiO_2 induce a certain extent of the CO_2 adsorption, the high CO_2 adsorption capacity was ascribed to the synergetic effect of the high surface area tubular morphology and the mixed-valence Pt nanoparticles. Moreover a selectivity of 100% towards methane has been found, and these catalysts were very active even at low temperatures (180°C). Thus the authors identified the Platinum based supported catalyst to be a potential catalyst for CO_2 recycling and methane production.

Kusmierz [14] studied another transition metal, Ruthenium based catalysts on $\gamma\text{-}Al_2O_3$. They found it to be extremely active for carbon dioxide methanation, and performances are directly affected by the metal dispersion and a minimum is reached if ruthenium dispersion is equal to 0.5.

E.W. McFarland and J. Park [15] have studied bi-functional catalysts ($Pd\text{-}Mg/SiO_2$), that sum up positive aspects of traditional Pd/SiO_2 and Mg/SiO_2, enhancing methane selectivity, achieving a high methane selectivity and carbon dioxide conversion (at 723K 95% CH_4 selectivity, 59% CO_2 conversion).

However, it is necessary to study in details surface chemistry to explain the experimental evidences and investigate the reactive paths that involve CO_2 on these metals. In particular Platinum, Rhodium and Nickel base catalysts have been examined in this work.

Nowadays DFT and first-principles approach appear to be a successful tool capable to describe the actual behavior of heterogeneous reactive systems and a new interest is growing in the desire to develop a better knowledge of surface chemistry.

Silvestrelli, Hütter et al. [16] in 1997 studied the dissociation of CO_2, to give CO and O, on a (111) Pt surface with a pseudopotential code, LDA and GGA correction were used. The supercell was made by a three layers slab, and the Transition State was located. A Langmuir-Hinshelwood mechanism was identified.

Andreas Eichler [17] in 2001 applied DFT to simulate the oxidation reactions of CO over Platinum, Palladium and Rhodium (111) and (100) surfaces with “VASP” code and RPBE GGA

pseudopotential. The Transition State was detected through NEB calculations, vibrational frequencies were computed to evaluate the prefactor of the rate constant.

Morikawa and Nakamura et al. [18] in 2004 examined the CO_2 adsorption and activation on low index surfaces of a copper cluster, the DFT pseudopotential periodic package "STATE" was applied in the adsorption problem.

Christian Minot [19] in 2004 described the effects due to high pressure and low coverage on (111) and (100) Platinum surfaces for the initial and final states of the Boudouard reaction by including in the vacuum spacing gas phase carbon monoxide.

Gajdoš, Eichler and Hafner in 2004 discussed trends from ab-initio calculations about CO adsorption on transition and noble metals. They tested the capability of PW91 and RPBE pseudopotentials to reproduce lattice constant experimental data and they also evaluated the strongest adsorption site for CO on the metals of 8-10 groups, and 4-5 periods. PDOS is adopted to analyze electronic structure and to explain the variation in adsorbate-substrate interaction.

Pedersen and Anderrson [20] in 2007 compared PW91 and RPBE pseudopotentials, furthermore they proposed a correction in the computation of the binding energy of CO when high coordination occurs at the metal surface.

Gokhale, Dumesic and Mavrikakis [21] in 2008 weighed the elementary steps of the redox and of the carboxyl mechanism of Low-Temperature Water Gas Shift reaction that occurs on a (111) Cu surface.

Grabow, Gokhale, Evans, Dumesic and Mavrikakis [22] in 2008 realized a first-principles microkinetic modeling of the Water Gas Shift reaction on a (111) Pt surface, considering carbon dioxide decomposition (in carbon monoxide and atomic oxygen) and the carboxyl group production, neglecting the capability of carbon dioxide to react with atomic carbon.

Flaherty, Henkelman et al. [23] in 2011 inspected the possible deactivation mechanisms involved in the Water Gas Shift reaction on Platinum.

Liu, Cundari and Wilson [24] in 2012 worked over CO_2 reduction to CO and C, in comparison with homogeneous catalysis. The CI-NEB method has been used to compute the activation energy on (100) surfaces of Fe, Co, Ni and Cu based catalysts, an Evans-Polanyi dependence has been identified.

Catapan, Vlachos et al. [25] in 2012 inquired over coke formation mechanism on Ni(111) and Ni(211) surfaces. The DFT approach with the package "SIESTA" allowed to study the chemistry of H_2 and H_2O, moreover three different pathways for CO oxidation to CO_2, the direct path, the carboxyl path and the formate path have been scrutinized.

However, the detailed research of trends and correlations among the different metals and their relationship with electronic structure has not been performed yet, so this Thesis work aims to provide a deeper understanding of heterogeneous catalysis process.

CHAPTER 2

2 Fundamentals of Density Functional Theory

2.1 The Schrödinger Equation

The description of a system requires some basic features to be defined as:

- How many and what kind of particles compose the system,
- Where are the particles,
- Which is the velocity of the particles,
- What kind of chemical and physical interaction exists among the above mentioned particles,
- How to describe the dynamical evolution of the system in time.

If the subjects of interest are atoms, molecules or condensed matter, whose properties need to be studied at nano/micro scale, atomic nuclei and electrons can be chosen as building block. This choice affects what can be described and what cannot. Since nuclei and especially electrons are small, fast-moving particles, with high velocity, comparable to the speed of light they show both wave and particle behavior that can be properly described by quantum mechanics laws, but usually electrons around atoms are not able to reach more than few percents of the speed of light, so a relativistic theory is not mandatory [Figure 2.1],[26].

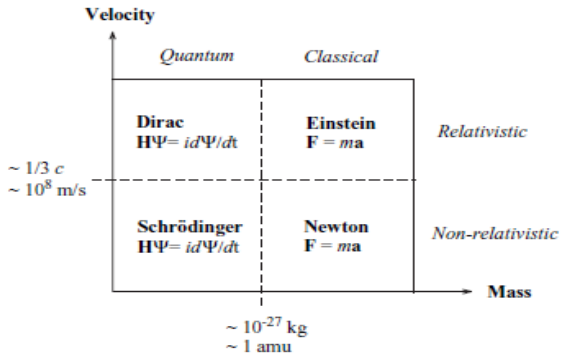

Figure 2.1: range of validity of the theory, adapted from [27]

For an isolated system of a given set of interacting electrons moving in an external potential field, generated by a set of fixed nuclei (or ions, assumed as point charges) it is fundamental to find the state of electrons with the lowest energy configuration, usually known as "ground state", function of nuclei's spatial coordinates.

The non-relativistic time-independent expression of the Schrödinger equation [28] for a system of "Ne" electrons and "Nn" nuclei is:

$$H\psi(\boldsymbol{R}_1, \dots, \boldsymbol{R}_i, \dots, \boldsymbol{R}_{Nn}, \boldsymbol{r}_1, \dots, \boldsymbol{r}_i, \dots, \boldsymbol{r}_{Ne}) = E\psi(\boldsymbol{R}_1, \dots, \boldsymbol{R}_i, \dots, \boldsymbol{R}_{Nn}, \boldsymbol{r}_1, \dots, \boldsymbol{r}_i, \dots, \boldsymbol{r}_{Ne}) \tag{2.1}$$

Where "ψ" is the global wave function, which depends on electrons' and nuclei's spatial positions (time and spin dependence is neglected).

"H" is the Hamiltonian operator, and is the sum of energies in atomic units ($m_e = e = \hbar = 4\pi\varepsilon_0 = 1$):

$$H = T_e + U_{ne} + U_{ee} + U_{nn} \tag{2.2}$$

$$H = \sum_i^{Ne} \left(-\frac{1}{2} \nabla_i^2 + v(\boldsymbol{r}_i) \right) + \frac{1}{2} \sum_{i \neq j}^{Ne} \sum_{j \neq i}^{Ne} \frac{1}{|\boldsymbol{r}_i - \boldsymbol{r}_j|} + U_{nn} \tag{2.3}$$

$$H = \sum_i^{Ne} \left(-\frac{1}{2} \nabla_i^2 - \sum_j^{Nn} \frac{Z_j}{|\boldsymbol{r}_i - \boldsymbol{R}_j|} \right) + \frac{1}{2} \sum_{i \neq j}^{Ne} \sum_{j \neq i}^{Ne} \frac{1}{|\boldsymbol{r}_i - \boldsymbol{r}_j|} + \frac{1}{2} \sum_{i \neq j}^{Nn} \sum_{j \neq i}^{Nn} \frac{Z_i Z_j}{|\boldsymbol{R}_i - \boldsymbol{R}_j|} \tag{2.4}$$

"T_e" refers to the kinetic energy of the electrons, "U_{ne}" instead is the potential energy due to electrons interaction with nuclei, "U_{ee}" accounts for electrostatic interactions between electrons' couples, and finally "U_{nn}" stands for electrostatic potential energy between nuclei.

2.2 Born-Oppenheimer Approximation

The electronic wave function appears to be simultaneously function of "3Ne + 3Nn" spatial coordinates, this means that a large system may involve the resolution of a very complex problem, with an enormous number of variables.
Because of proton's and neutron's mass is more than 1800 times the electron's mass it is possible to assume that the nuclei are infinitely heavier than the electrons, indeed electrons are able to respond more rapidly to change. Thus the electronic problem can be solved for a certain set of stationary nuclei, reducing the total number of independent variables form "3Nn + 3Ne" to "3Ne", giving birth to a parametric "3Ne" surface, function of the nuclear coordinates, that represents the form of the electronic energy.

This is commonly called Born-Oppenheimer approximation [29] :

$$H\psi(\boldsymbol{R}_e, \boldsymbol{R}_n) = E\psi(\boldsymbol{R}_e, \boldsymbol{R}_n) \tag{2.5}$$

$$[H_e + T_n]\psi = E\psi(\boldsymbol{R}_e, \boldsymbol{R}_n) \tag{2.6}$$

$$[E_e(\boldsymbol{R}_n) + T_n]\psi_n(\boldsymbol{R}_n)\psi_e(\boldsymbol{R}_e, \boldsymbol{R}_n) = E\,\psi_n(\boldsymbol{R}_n)\psi_e(\boldsymbol{R}_e, \boldsymbol{R}_n) \tag{2.7}$$

$$[E_e(\boldsymbol{R}_n) + T_n]\psi_n(\boldsymbol{R}_n) = E\,\psi_n(\boldsymbol{R}_n) \tag{2.8}$$

As consequence it will become possible to solve the problem splitting it in two separate problems.

First the electron motion's equation are solved, with fixed nuclei, in order to find the "ground state" for electrons, that is the total energy of the system, only function of nuclei positions, E($\mathbf{R}_1$,…, $\mathbf{R}_i$,…, $\mathbf{R}_{Nn}$), because electrons are able to instantaneously update their wave function.
The electron wave function is written as a parametrical function of the positions of the nuclei, and then the motion of the nuclei on the "3Ne" surface can be solved subsequently.

$E(\mathbf{R}_1,\ldots, \mathbf{R}_i,\ldots, \mathbf{R}_{Nn})$ is called "adiabatic potential energy surface", and thanks to this function it is possible to understand the energy dependence on atomic positions [30].

Looking For a Solution

Schrödinger equation is an eigenvalue equation, dealing with a wavefunction related to a many body system. This wavefunction depends on "3Ne" spatial coordinates, because nuclei are considered as fixed. "ψ" is a set of eigenstates of the Hamiltonian operator, and for each eigenstates "ψ_n" (complex numbers) exist an eigenvalue, "E_n", that is a real number.

The solution may be expressed as:

$$\psi = \sum_{n}^{K} \alpha_n \phi_n \tag{2.9}$$

Where "ϕ_n" are a set of orthonormal eigenfunctions, and "α_n" are the corresponding eigenvalues.

It is also possible to approximate the wave function "ψ" as a product of each electron wave functions, commonly known as Hartree product, which is not antisymmetric:

$$\psi = \psi_1 \psi_2 \ldots \psi_{Ne} \tag{2.10}$$

Because of the complexity of Hamiltonian operator that particularly lies in the electron-electron contribution, it is unrealistic to find each electron wave function, one by one, so Schrödinger equation has to be solved as a many body problem, considering all electrons' wave functions at the same time.

$\psi = \psi[\mathrm{Ne}, v(\mathbf{r})]$, so the solution is merely determined by Ne and the external potential "$v(\mathbf{r})$", therefore is called "functional".

2.3 Hartree-Fock Approximation

Hartree-Fock methods are grounded in the wish to solve Schrödinger equation by directly finding the electron wave function "ψ", but the computational effort is remarkable because the solution to the problem is an effective unknown function, with "3Ne" independent variables [31]. Since no explicit form exists the solution has to be built with a set of guess functions able to satisfy particular properties.

Since it is impossible to find the ground state searching among all the allowed "Ne" electron wave functions it is mandatory to look for the best approximation to the exact wave function belonging to a subset that grants a physically sensible estimate. The subset chosen by Hartree and Fock consists of all antisymmetric products of "Ne" one electron wave functions "$\chi_i(r_i)$".
The product is the "Slater determinant" and represents a successful model able to describe the electron's behavior. The electron is a constituent particle of matter commonly called by physicists "Fermion" whose properties are:

- Being antisymmetric,
- Having half spin number,
- Obeying to Pauli's exclusion principle.

From a mathematical point of view Slater determinant is a matrix of single electron wave functions [32]:

$$\psi \cong \Phi_{SD} = \frac{1}{\sqrt{Ne!}} \begin{bmatrix} \chi_1(\boldsymbol{r}_1) & \cdots & \chi_{Ne}(\boldsymbol{r}_1) \\ \vdots & \ddots & \vdots \\ \chi_1(\boldsymbol{r}_{Ne}) & \cdots & \chi_{Ne}(\boldsymbol{r}_{Ne}) \end{bmatrix} \tag{2.11}$$

The one electron wave functions "$\chi_i(r_i)$" are referred to as the spin orbitals, with a spatial function "$\phi_i(\mathbf{x})$" and an orthonormal spin function, "$\sigma(s)$" that is represented by "$\alpha(s)$" or "$\beta(s)$".

$$\chi_i(\boldsymbol{r}) = \phi_i(\boldsymbol{x})\sigma(s) \tag{2.12}$$

$$\int \chi_i^*(\boldsymbol{r})\chi_i(\boldsymbol{r})d\boldsymbol{r} =< \chi_i|\chi_j >= \delta_{i,j} \tag{2.13}$$

The Slater determinant is effectively antisymmetric because if two rows or columns are exchanged the sign of the determinant changes, it fulfills Pauli's principle and includes the exchange part, but not the correlation one. From a physical perspective this property means that if two electrons are permutated the wave function's sign is modified, and this is in full agreement with the concept of Fermion.

$$\psi(\boldsymbol{r}_1, \dots, \boldsymbol{r}_i, \boldsymbol{r}_j, \dots, \boldsymbol{r}_{Ne}) = -\psi(\boldsymbol{r}_1, \dots, \boldsymbol{r}_j, \boldsymbol{r}_i, \dots, \boldsymbol{r}_{Ne}) \tag{2.14}$$

This wave function property represents Pauli's exclusion principle in a quantum mechanical perspective.

The variational principle is used to determine the best Slater determinant:

$$E_{HF} = \min_{\Phi_{SD} \to Ne} E[\Phi_{SD}] \tag{2.15}$$

Where "Φ_{SD}" is an evaluation of the true "ψ", and is an allowed "Ne" electron wave function, continuous everywhere and quadratic integrable.

$$E_{HF} =< \Phi_{SD}|H|\Phi_{SD} >= \sum_i^{Ne}(i|h|i) + \frac{1}{2}\sum_i^{Ne}\sum_j^{Ne}\big((ii|jj) - (ij|ji)\big) \tag{2.16}$$

The contribution due to kinetic energy and electron-nucleus interaction:

$$(i|h|i) = \int \chi_i^*(\boldsymbol{r})\left\{-\frac{1}{2}\nabla^2 - \sum_k^{Nn}\frac{Z_k}{|\boldsymbol{r} - \boldsymbol{r}_k|}\right\}\chi_i(\boldsymbol{r})d\boldsymbol{r} \tag{2.17}$$

The Coulomb integral:

$$(ii|jj) = \frac{1}{2}\int\int |\chi_i(\boldsymbol{r})|^2 \frac{1}{|\boldsymbol{r}-\boldsymbol{r}'|} |\chi_j(\boldsymbol{r}')|^2 \, d\boldsymbol{r}d\boldsymbol{r}' \tag{2.18}$$

The index i = j is allowed, as consequence the unphysical self interaction contribution is introduced. The exchange integral:

$$(ij|ji) = \int\int \chi_i(\boldsymbol{r})\chi_j^*(\boldsymbol{r}) \frac{1}{|\boldsymbol{r}-\boldsymbol{r}'|} \chi_j(\boldsymbol{r}')\chi_i^*(\boldsymbol{r}')d\boldsymbol{r}d\boldsymbol{r}' \tag{2.19}$$

This term takes care of the self interaction contribution and deletes it, giving birth to the same expression for i = j but with opposite sign.

The condition of orthonormality of the spin orbitals is satisfied through the constrained minimization which introduces the Lagrangrian multipliers, which are the eigenvalues of the "Ne" equations but can also be interpreted as the orbital energies.

$$\hat{f}\chi_i = \varepsilon_i\chi_i \tag{2.20}$$

During the energy minimization which leads to the calculation of the Slater determinant able to best approximate the "Ne" electron wave function spin orbitals remain orthonormal.

$$\hat{f}_i = -\frac{1}{2}\nabla_i^2 - \sum_k^{Nn} \frac{Z_k}{|\boldsymbol{r}-\boldsymbol{r}_k|} + V_{HFi} \tag{2.21}$$

"V_{HFi}", the Hartree-Fock potential, replaces the two electron repulsion with a single electron operator, that describes the average electron repulsion that the i-th electron feels, because of the others "Ne – 1" electrons.

$$V_{HF}(\boldsymbol{r}) = \sum_j^{Ne} \left(\hat{J}_j(\boldsymbol{r}) - \hat{K}_j(\boldsymbol{r})\right) \tag{2.22}$$

"J" is the Coulomb local operator and considers the potential experienced by an electron in **r** due to the charge distribution of the j-th electron, in "χ_j" spin orbital.

$$\hat{J}_j(\boldsymbol{r}) = \int \chi_j^2(\boldsymbol{r}') \frac{1}{|\boldsymbol{r} - \boldsymbol{r}'|} d\boldsymbol{r}' \tag{2.23}$$

"K" instead is the exchange contribution to the Hartree-Fock potential, this operator is non local because the result depends on "χ_i", function of **r**', the new variable on which the integration is done.

To practically solve the single electron Schrödinger equation a description of the spin orbitals has to be provided. A finite set of functions (of "K" elements) are added to approximate the exact spin orbitals.

$$\chi_j(\boldsymbol{r}) = \sum_i^K \alpha_{i,j} \phi_i(\boldsymbol{r}) \tag{2.24}$$

This set of "ϕ_i" functions is called basis set; a lager basis set, obtained by increasing "K", on one hand increases the accuracy of the calculation and on the other the numerical effort to solve the Schrödinger equation itself. "$\alpha_{i,j}$"are instead the expansion coefficients.

As a whole Hartree-Fock model provides a good estimation of the total energy, and if the basis set is sufficiently large to state that convergence on total energy is achieved according to the basis set itself, the computed energy is the "Hartree-Fock limit", that accounts for almost 99% of the total energy, but omits the correlation contribution that plays a fundamental role since the remaining 1% is very important for accurately describing a chemical process.
The resolution of Hartree-Fock problem requires a particular technique of the Self Consistent Field because Hartree-Fock potential itself depends on the spin orbitals that can be determined only through the resolution of the single electron equations. The exact solution of the problem is a Slater determinant that correctly describes "Ne" non interacting electrons that experience the Hartree-Fock potential.

The self consistent approach requires:

- An initial guess of the spin orbitals,
- The definition of the electron density, realized using the spin orbitals,
- The solution of the single electron equations for the spin orbitals,
- The update of spin orbitals, until convergence criteria are satisfied.

2.4 Density Functional Theory Approach

The problem to obtain the correct ground state for a many body wave function, given an external potential, appears extremely hard even if the problem itself is totally defined by the total number of "Ne" particles and by the external potential "$v(\mathbf{r})$". The high complexity rises up as the size of the considered system increases because of the many body nature of the problem. Thus a new theory called "Density Functional Theory" was developed. The aim of this theory, and the important contribution that it gives to quantum mechanics, lies in possibility to reduce the size of the problem:

$$3Ne \rightarrow 3\ independent\ varibles$$

by rewriting the many body problem in terms of the electron density, defined as the integral over all the spin electrons' coordinates and over all but one electrons' spatial coordinates:

$$n(\boldsymbol{r}) = Ne \int |\psi(\boldsymbol{r}_1, \dots, r_{Ne})|^2 d\boldsymbol{r}_1 \dots d\boldsymbol{r}_{Ne} \tag{2.25}$$

From a mathematical perspective a "3Ne" dimensional problem is converted into another of only 3 independent variables, realizing a notable improvement and reducing the computational complexity.

Other important electron density's properties besides being a three dimensional function are listed [32]:

$$n(\boldsymbol{r}) > 0 \tag{2.26}$$

$$Ne = \int n(\boldsymbol{r}) d\boldsymbol{r} \tag{2.27}$$

$$\lim_{\boldsymbol{r}_{ik}\to 0} \left[\frac{\partial}{\partial r} + 2Z_k\right] n(\boldsymbol{r}) = 0 \tag{2.28}$$

The electron density shows a various number of maxima and cusps, that are usually found at $\mathbf{r}_k$ where the nucleus with charge "Z_k" is located.

The aim to capitalize the density functional approach, replacing the complicated wave functions with simpler quantity as electron density, led to several attempts to refocus the search on the ground state charge density, and the first successful effort gave birth to the so called Thomas-Fermi model [33].

This quantum statistical model treats electron-electron interaction in a classical way and reduces nuclear-electron interaction to the Coulomb electrostatic energy. The kinetic energy expression instead is based on the uniform electron gas, using a local density approximation, thus the functional is:

$$E_{TF}[n(\boldsymbol{r})] = T_{TF}[n(\boldsymbol{r})] + E_{ne}[n(\boldsymbol{r})] + E_{ee}[n(\boldsymbol{r})] \tag{2.29}$$

$$E_{TF}[n(\boldsymbol{r})] = \frac{3}{10}(3\pi^2)^{2/3} \int n^{5/3}(\boldsymbol{r}) d\boldsymbol{r} - Z \int \frac{n(\boldsymbol{r})}{\boldsymbol{r}} d\boldsymbol{r} + \\ + \frac{1}{2} \int \int \frac{n(\boldsymbol{r}_1) n(\boldsymbol{r}_2)}{|\boldsymbol{r}_1 - \boldsymbol{r}_2|} d\boldsymbol{r}_1 d\boldsymbol{r}_2 \tag{2.30}$$

Where **r** is the vector of the three spatial coordinates.

This model is only historically significant because the total energy is actually expressed as a density functional, even though no explicit expression of electron density is provided.

The rough approximation of the true kinetic energy and the total absence of exchange and correlation effects make the model able to uniquely describe isolated atoms, but on the other hand it dramatically fails in providing sensible qualitative prediction.

Although an essential issue has been ignored, if Schrödinger equation is no longer solved with respect to electron wave function but the solution leads to the evaluation of an electron density, the ground state energy computed could be different, in the early 1900 Thomas-Fermi model totally neglected this feature. It took about 40 years after Thomas and Fermi to develop the current "Density Functional Theory", when in 1964 a pivotal paper [34] by Hohenberg and Kohn highlighted the existence of a theorem that proves that electron density uniquely determines the Hamiltonian operator and all the other ground state properties of the system.

2.5 The Hohenberg-Kohn Theorems

These theorems are the origin/starting point of a new, exact reformulation of Schrödinger's problem and legitimate the use of the charge density as basic variable in terms of what is called Density Functional Theory. Charge density thus covers a main role in the research of the ground state; in fact it is possible to tackle the problem form a new perspective, easier and less demanding.
Now, thanks to Hohenberg-Kohn theorems, it is possible to point out that a CO molecule has 14 electrons, and 42 independent variables, that can be decreased to 3 if Schrödinger equation is rewritten in terms of electron density.

- The first theorem of Hohenberg and Kohn states:

"The ground state energy of a many body system is a unique functional of the electron density"

The external potential is a functional of electron density, and since it fixes the Hamiltonian of the system, the full many particle ground state is a functional of electron density itself.

This demonstration is based on reduction ad absurdum.

If two different external potentials $V_{ext1} \neq V_{ext2}$, which differ by more than a constant, produce the same electron density and non-degenerate ground states, the two Hamiltonian operators, as well as electron ground state wave functions and ground state energies will not be the same:

$$H_1 = T + V_{ee} + V_{ext1} \tag{2.31}$$

$$H_2 = T + V_{ee} + V_{ext2} \tag{2.32}$$

$$H_1 \psi_1 = E_{01} \psi_1 \tag{2.33}$$

$$H_2 \psi_2 = E_{02} \psi_2 \tag{2.34}$$

$$\psi_1 \neq \psi_2 \;\&\&\; E_{01} \neq E_{02} \tag{2.35}$$

If "ψ_2" is used as a trial wave function for "H_1", according to variational principle, the energy computed with the guess function must be greater than the ground state energy:

$$E_{01} < \langle \psi_2 | H_1 | \psi_2 \rangle = \langle \psi_2 | H_2 | \psi_2 \rangle + \langle \psi_2 | H_1 - H_2 | \psi_2 \rangle \tag{2.36}$$

$$E_{01} < E_{02} + \langle \psi_2 | V_{ext1} - V_{ext2} | \psi_2 \rangle \tag{2.37}$$

$$E_{01} < E_{02} + \int n(\boldsymbol{r})[V_{ext1} - V_{ext2}]d\boldsymbol{r} \tag{2.38}$$

If instead "ψ_1" is used as a trial wave function for "H_2", according to variational principle and repeating the previous steps, the final equation is:

$$E_{02} < E_{01} - \int n(\boldsymbol{r})[V_{ext1} - V_{ext2}]d\boldsymbol{r} \tag{2.39}$$

By adding the two equations it is possible to fall in contradiction:

$$E_{02}+E_{01} < E_{02}+E_{01} \tag{2.40}$$

This is the evidence that two different external potentials cannot bring to the same ground state electron density, thus in conclusion the ground state energy is a unique functional of electron density.

Even if the theorem confirms the existence of a tight/narrow correlation between ground state electron density and ground state wave function Hohenberg-Kohn theorem does not explain what kind of shape should have the functional that can solve the Schrödinger equation.

- The second theorem of Hohenberg and Kohn states:

"The energy of the overall functional is minimized only by the true electron density which matches/suites the full solution of the Schrödinger equation".

The theorem asserts that only the true ground state electron density "n_0" can be used to return the correct ground state energy.

According to variational principle, for any trial electron density "n_{trial}", the ground state energy still represents the lowest energy admitted by the system:

$$E_0 \leq E[n_{trial}(\boldsymbol{r})] \tag{2.41}$$

Any trial density must be positive and must integrate to the total number of electrons, but even though all the trial electron densities satisfy these constraints they define their own Hamilitonian operator.

$$T[n_0(\boldsymbol{r})] + V_{ee}[n_0(\boldsymbol{r})] + V_{ne}[n_0(\boldsymbol{r})] \leq T[n_{trial}(\boldsymbol{r})] + V_{ee}[n_{trial}(\boldsymbol{r})] + V_{ne}[n_{trial}(\boldsymbol{r})] \tag{2.42}$$

For an isolated system of "Ne" interacting electrons, once formulated the expression of the external potential "$v(\mathbf{r})$", electron density is completely specified, but not in an explicit way. If the true functional formula were available it would be possible minimize the total energy of the system in order to find the ground state, but the lack of knowledge forces to make use of the variational

principle to develop approximations of the true functional. Thus a trial function is built and its variational parameters are calculated by use of the minimization of the total energy, but the quality of the model undergoes the choice of the initial trial functions, an example is provided by the famous Hartree and Fock which propose to search the solution to Schrödinger equation by means of the product of single particle orbitals/wave function, and single Slater determinant to satisfy the antisymmetric property of wave function.

The energy functional, written by use of single electron wave functions "ψ_i" is:

$$E[\{\psi_i\}] = E_k[\{\psi_i\}] + E_{XC}[\{\psi_i\}] \tag{2.43}$$

"E_k" is the known part, but it is not a universal functional of the charge density because it depends on the external potential for the electrons:

$$E_k[\{\psi_i\}] = T_e[\{\psi_i\}] + U_{ne}[\{\psi_i\}] + U_{1e1e}[\{\psi_i\}] + U_{1n1n}[\{\psi_i\}] \tag{2.44}$$

$$\begin{aligned} E_k[\{\psi_i\}] = -\frac{\hbar^2}{m}\sum_i^{Ne}\int \psi_i^* \nabla^2 \psi_i d^3\boldsymbol{r} + \int V(\boldsymbol{r})n(\boldsymbol{r})d^3\boldsymbol{r} + \\ + \frac{e^2}{2}\int\int \frac{n(\boldsymbol{r})n(\boldsymbol{r}')}{|\boldsymbol{r}-\boldsymbol{r}'|} d^3\boldsymbol{r}\, d^3\boldsymbol{r}' + U_{1n1n}[\{\psi_i\}] \end{aligned} \tag{2.45}$$

The following terms are electron kinetic energy, Coulomb nucleus-electron interaction in which appears the external potential, Coulomb one electron - one electron interaction called Hartree potential, Coulomb one nucleus - one nucleus interaction.

It is possible to notice that the total energy is written as a function of electron density:

$$n(\boldsymbol{r}) = Ne\int |\psi(\boldsymbol{r}_1, \dots, r_{Ne})|^2 d\boldsymbol{r}_1 \dots d\boldsymbol{r}_{Ne} \tag{2.46}$$

"E_{XC}" is the unknown part, called exchange - correlation energy, and it is the very heart of problems in which lies the ability to guarantee a good description of the system.

"E_{XC}" considers the contribution to the interaction energy among electrons due to exchange between electrons and correlation among them.

Even if the exchange - correlation functional were explicit the minimization of the total energy functional can still be very difficult as the resolution of Schrödinger equation for the wave function.

The ground state many body problem can be reformulated in terms of a variational problem, introducing the universal functional, whose name wants to underline the independence from the external potential "V".

$$F[n(\boldsymbol{r})] = T_e[n(\boldsymbol{r})] + U_{1e1e}[n(\boldsymbol{r})] + E_{XC}[n(\boldsymbol{r})] \tag{2.47}$$

$$\delta\left[F[n(\boldsymbol{r})] + \int V(\boldsymbol{r})\, n(\boldsymbol{r}) d\boldsymbol{r} - \lambda\left(\int n(\boldsymbol{r}) d\boldsymbol{r} - Ne\right)\right] = 0 \tag{2.48}$$

"λ" is the Lagrangian multiplier, that multiplies the difference between total electron "Ne" and the charge density integrated over **r**, but when "n(**r**)" is the true ground state density:

$$Ne = \int n(\boldsymbol{r}) d\boldsymbol{r} \tag{2.49}$$

The variational equation is properly differentiated, and this operation leads to the equivalent differential equation:

$$\frac{\delta F[n(\boldsymbol{r})]}{\delta n(\boldsymbol{r})} + V(\boldsymbol{r}) - \lambda = 0 \tag{2.50}$$

2.6 Kohn and Sham Approach

Kohn and Sham proposed to by-pass the problem connected to the resolution of the total functional, splitting Schrödinger equation for a many body system into a set of one electron equations, that permits to reach the right electron density [35]. Thus the attention will be focused on a reference system of non interacting electrons.

The Kohn-Sham equations are:

$$\left[-\frac{\hbar^2}{2m}\nabla^2 + V(\boldsymbol{r}) + V_H(\boldsymbol{r}) + V_{XC}(\boldsymbol{r})\right]\psi_i(\boldsymbol{r}) = \varepsilon_i\,\psi_i(\boldsymbol{r}) \tag{2.51}$$

The i-index runs from 1 to "Ne", there are as many equations as many electrons.
Each equation is function of only 3 spatial variables that describe the electron's position.
Four contributions are shown:

- Kinetic energy (2.52), that is a one body operator and requires a constrained minimization over all Slater determinants/antisymmetric wave functions of order "Ne" that integrates to "n(**r**)",

$$T_s[n(\boldsymbol{r})] = \min_{\psi_{S\to n}}\left[-\frac{\hbar^2}{2m}\sum_i^{Ne}\int \psi_i^*(\boldsymbol{r})\,\nabla^2\psi_i(\boldsymbol{r})d\boldsymbol{r}\right] \tag{2.52}$$

- Potential energy of one electron-nuclei interaction,
- Hartree potential (2.53) which represents the Coulomb repulsion between the electron considered in the Kohn-Sham equation and the total electron density. Total electron density is calculated considering the contribution of all electrons belonging to the system, this way the unphysical so called self-interaction contribution is introduced.

$$V_H[n(\boldsymbol{r})] = e^2\int\frac{n(\boldsymbol{r}')}{|\boldsymbol{r}-\boldsymbol{r}'|}d^3\boldsymbol{r}' \tag{2.53}$$

- Functional derivative of exchange correlation energy (2.54), for the single electron, tries to describe the energetic contribution caused by electron exchange and correlation and considers the necessity to erase the self-interaction contribution generated by the Hartree potential and to estimate the difference between the true kinetic energy and the one (T_s) of "Ne" non interacting electrons.

$$V_{XC}[n(\boldsymbol{r})] = \frac{\delta E_{XC}(\boldsymbol{r})}{\delta n(\boldsymbol{r})} \tag{2.54}$$

As shown before, the differential equation will be:

$$\frac{\delta T_s[n(\boldsymbol{r})]}{\delta n(\boldsymbol{r})} + V_{KS}(\boldsymbol{r}) - \lambda = 0 \tag{2.55}$$

But this time:

$$V_{KS}(\boldsymbol{r}) = V(\boldsymbol{r}) + V_H(\boldsymbol{r}) + V_{XC}(\boldsymbol{r}) \tag{2.56}$$

The difference between Hartree-Fock method and Kohn-Sham one is related to the lack of the exchange correlation potential that appears in Kohn-Sham equations. Although Kohn-Sham equations require an iterative approach to be solved, as well as for Hartree-Fock method, because the functional depends on the electron density itself:

- A trial electron density is specified,
- By use of the electron density is possible to compute the kinetic energy, the Hartree and exchange-correlation potential, and then to solve Kohn-Sham equations; at this step single electron wave functions are estimated,
- It is now possible to evaluate a new value of the electron density,
- This value is compared with the old electron density, if the convergence criteria are satisfied the electron density is the ground state electron density, otherwise the new electron density has to be up-to-date.

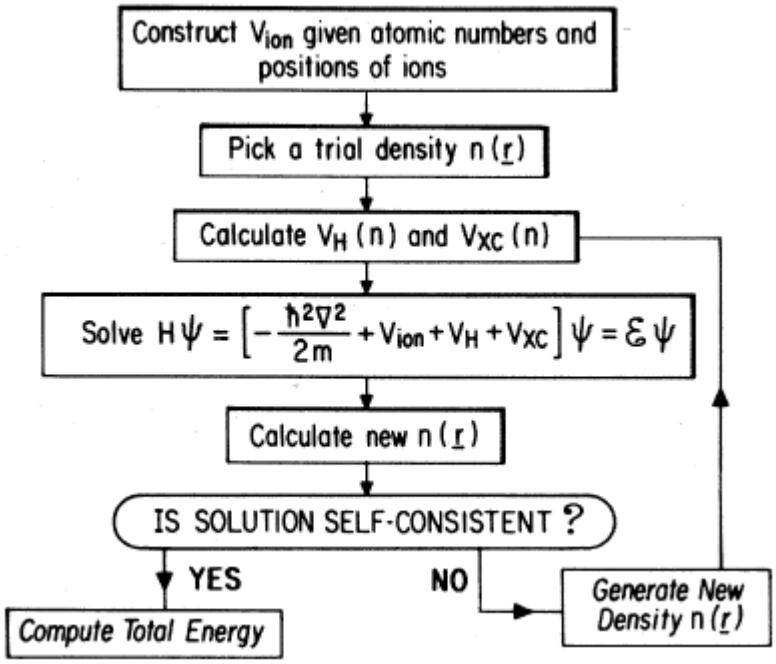

Figure 2.2: self consistent approach, adapted from [36]

The solution is said to be self consistent [Figure 2.2], and for "Ne" non interacting electrons may be expressed by a single Slater determinant:

$$\psi_s = \frac{1}{\sqrt{Ne!}} det\left[\psi_1, \psi_2, \dots, \psi_{Ne}\right] \tag{2.57}$$

Even though this new approach appears to be an elegant intuition the main issue is always the incapability to provide an exact and explicit mathematical expression to completely write down the total energy as a known functional of electron density. In fact the ground state is reached when the total energy is minimized with respect to the electron density, made up by all allowed "Ne" electron wave functions:

$$E_0 = \min_{n(\boldsymbol{r})\to Ne} (F[n(\boldsymbol{r})] + E_{ne}[n(\boldsymbol{r})]) \tag{2.58}$$

"F" is the "universal functional", and contains the contribution of the kinetic energy of the real, full interacting system (T), the classical Coulomb interaction (J) and the non classical (ncl) electron exchange and correlation part.

$$F[n(\boldsymbol{r})] = T[n(\boldsymbol{r})] + J[n(\boldsymbol{r})] + E_{ncl}[n(\boldsymbol{r})] \tag{2.59}$$

Although only "J" is really completely defined, indeed kinetic energy is an unknown portion of the functional because interactions among particles are not described according Kohn-Sham approximation, thus a better reformulation of the "universal functional" is:

$$F[n(\boldsymbol{r})] = T_s[n(\boldsymbol{r})] + J[n(\boldsymbol{r})] + E_{XC}[n(\boldsymbol{r})] \tag{2.60}$$

Where the known expression of the kinetic energy, of a non interacting system, is provided by "T_s" and the unknown part is now represented by the exchange-correlation functional conveniently built as a sum of members that satisfy the identity (2.61) (2.62).

$$\begin{aligned} E_{XC}[n(\boldsymbol{r})] = T[n(\boldsymbol{r})] - T_s[n(\boldsymbol{r})] + E_{ee}[n(\boldsymbol{r})] - J[n(\boldsymbol{r})] = \\ = T[n(\boldsymbol{r})] - T_s[n(\boldsymbol{r})] + E_{ncl}[n(\boldsymbol{r})] \end{aligned} \tag{2.61}$$

$$\begin{aligned} F[n(\boldsymbol{r})] = T_s[n(\boldsymbol{r})] + J[n(\boldsymbol{r})] + T[n(\boldsymbol{r})] - T_s[n(\boldsymbol{r})] + E_{ncl}[n(\boldsymbol{r})] = \\ = T[n(\boldsymbol{r})] + J[n(\boldsymbol{r})] + E_{ncl}[n(\boldsymbol{r})] \end{aligned} \tag{2.62}$$

2.7 Electron Correlation

The single Slater determinant is not the true wave function, but it is capable to include several important physical properties, although the total energy computed appears to be greater than the effective ground state.

The difference between the real value of the ground state and the energy computed by Hartree-Fock is defined as correlation energy:

$$E_C^{HF} = E_0 - E_{HF} \tag{2.63}$$

$$E_C^{HF} < 0;\ E_0 < 0;\ E_{HF} < 0 \tag{2.64}$$

$$|\,E_0| > |\,E_{HF}| \tag{2.65}$$

The Hartree-Fock potential doesn't account for instantaneous electrons' repulsion, this purpose is sought introducing the concept of correlation (E_C^{HF}), which has a dynamical part (short range effects), because it is related to the individual electrons' motion, and another non-dynamical contribution due to the possible co-existence of different ground state Slater determinant with similar energies.

2.7.1 Pair Density

The concept of pair density is related to the probability of finding simultaneously two electrons with spin "σ_1", "σ_2", inside two volumes of space d$\mathbf{x}_1$, d$\mathbf{x}_2$, and it contains the proper information to describe correlation's effect.

$$n_2(\boldsymbol{r}_1, \boldsymbol{r}_2) = Ne(Ne-1)\int \dots \int |\psi(\boldsymbol{r}_1, \dots, \boldsymbol{r}_{Ne})|^2 \, d\boldsymbol{r}_3 \dots d\boldsymbol{r}_{Ne} \tag{2.66}$$

($\mathbf{r}_i$ is the vector of spatial and spin variables of the i-th electron)

As the model assumes electrons as ideal particles and punctual masses, two electrons may be found in the same volume element, thus the pair density becomes:

$$n_2(\boldsymbol{r}_1, \boldsymbol{r}_2) = \frac{Ne-1}{Ne} n(\boldsymbol{r}_1) n(\boldsymbol{r}_2) \tag{2.67}$$

Electrons are charged particles and show a Coulomb repulsion, they are also fermions and posses the antisymmetry property of the wave functions.

After introducing the reduced density matrix "γ", that has a double set of independent variables, ($\mathbf{r}_1$, $\mathbf{r}_2$; $\mathbf{r}_1$', $\mathbf{r}_2$'), it is possible to point out what happens if two electrons are interchanged, according to wave function's antisymmetry property:

$$\gamma_2(\boldsymbol{r}_1, \boldsymbol{r}_2; \boldsymbol{r}_1', \boldsymbol{r}_2') = Ne(Ne-1)\int \dots \int \psi(\boldsymbol{r}_1, \boldsymbol{r}_2, \dots, \boldsymbol{r}_{Ne}) \psi^*(\boldsymbol{r}_1', \boldsymbol{r}_2', \dots, \boldsymbol{r}_{Ne}) \, d\boldsymbol{r}_3 \dots d\boldsymbol{r}_{Ne} \tag{2.68}$$

$$\gamma_2(\boldsymbol{r}_1, \boldsymbol{r}_2; \boldsymbol{r}_1', \boldsymbol{r}_2') = -\gamma_2(\boldsymbol{r}_2, \boldsymbol{r}_1; \boldsymbol{r}_1', \boldsymbol{r}_2') \tag{2.69}$$

If $\mathbf{r}_1 = \mathbf{r}_1'$ and $\mathbf{r}_2 = \mathbf{r}_2'$ the matrix returns the pair density, and in the particular situation that exhibits two electrons at the same spatial and spin coordinates the probability "n(**r**)" is found to be exactly zero:

$$n_2(\boldsymbol{r}_1, \boldsymbol{r}_1) = -n_2(\boldsymbol{r}_1, \boldsymbol{r}_1) = 0 \tag{2.70}$$

Electrons of same spin do not move independently from each other, this effect is known as Fermi correlation, different from the electrostatic effects accounted in the Coulomb correlation term.
At the Hartree-Fock level electrons of different spin (antiparallel) have an uncorrelated motion and Coulomb correlation is not present, but pair density is actually affected by Coulomb and Fermi correlation, so it is built starting from simple electron density:

$$n_2(\boldsymbol{r}_1, \boldsymbol{r}_2) = n(\boldsymbol{r}_1)n(\boldsymbol{r}_2)[1 + f(\boldsymbol{r}_1, \boldsymbol{r}_2)] \tag{2.71}$$

A correlation factor "f" can be introduced.

A better insight into the correlation concept can be provided by the consideration of the conditional probability, linked to the possibility to find an electron located at $\mathbf{r}_2$ when another electron is already at $\mathbf{r}_1$.

$$\Omega(\boldsymbol{r}_1, \boldsymbol{r}_2) = \frac{n_2(\boldsymbol{r}_1, \boldsymbol{r}_2)}{n(\boldsymbol{r}_1)} \tag{2.72}$$

That integrates to "Ne – 1", where 1 is the reference electron at $\mathbf{r}_1$.

$$\int \Omega(\boldsymbol{r}_1, \boldsymbol{r}_2) d\boldsymbol{r}_2 = Ne - 1 \tag{2.73}$$

The difference between the correlated and uncorrelated probability to find an electron at $\mathbf{r}_2$ is the exchange correlation hole, that is usually negative:

$$h_{XC}(\boldsymbol{r}_1, \boldsymbol{r}_2) = \frac{n_2(\boldsymbol{r}_1, \boldsymbol{r}_2)}{n(\boldsymbol{r}_1)} - n(\boldsymbol{r}_2) = n(\boldsymbol{r}_2) f(\boldsymbol{r}_1, \boldsymbol{r}_2) \tag{2.74}$$

$$\int h_{XC}(\boldsymbol{r}_1, \boldsymbol{r}_2)\, d\boldsymbol{r}_2 = \int \left\{ \frac{n_2(\boldsymbol{r}_1, \boldsymbol{r}_2)}{n(\boldsymbol{r}_1)} - n(\boldsymbol{r}_2) \right\} d\boldsymbol{r}_2 = Ne - 1 - Ne = -1 \tag{2.75}$$

2.7.2 Fermi and Coulomb Holes

The description of the electron-electron repulsion term in the Hamiltonian is written considering how Coulomb and exchange correlation affect the electron distribution in the considered system.
The electrostatic repulsion of electrons depends on the distance between two electrons and the probability to find the two electrons at that distance.

$$E_{ee} = \frac{1}{2}\int\int \frac{n_2(\boldsymbol{x}_1, \boldsymbol{x}_2)}{|\boldsymbol{x}_1 - \boldsymbol{x}_2|} d\boldsymbol{x}_1 d\boldsymbol{x}_2 \tag{2.76}$$

Where "$n_2(\mathbf{x}_1, \mathbf{x}_2)$" is the spin independent equivalent of pair density (**x** is the vector of spatial coordinates, the spin variable is neglected)

$$n_2(\boldsymbol{x}_1, \boldsymbol{x}_2) = n(\boldsymbol{x}_1)n(\boldsymbol{x}_2) + n(\boldsymbol{x}_1)h_{XC}(\boldsymbol{x}_1, \boldsymbol{x}_2) \tag{2.77}$$

$$E_{ee} = \frac{1}{2}\int\int \frac{n(\boldsymbol{x}_1)n(\boldsymbol{x}_2)}{|\boldsymbol{x}_1 - \boldsymbol{x}_2|} d\boldsymbol{x}_1 d\boldsymbol{x}_2 + \frac{1}{2}\int\int \frac{n(\boldsymbol{x}_1)h_{XC}(\boldsymbol{x}_1, \boldsymbol{x}_2)}{|\boldsymbol{x}_1 - \boldsymbol{x}_2|} d\boldsymbol{x}_1 d\boldsymbol{x}_2 \tag{2.78}$$

The first term in (2.78) is the classical electrostatic energy of a charge distribution with itself, and therefore it contains the unphysical self interaction contribution.
The second term instead represents the energy due to the interaction between the electron density and the charge distribution of the exchange correlation hole, and therefore it contains the correction to the unphysical self interaction contribution.

The exchange correlation hole is usually split:

$$h_{XC}(\boldsymbol{x}_1, \boldsymbol{x}_2) = h_X^{\sigma_1=\sigma_2}(\boldsymbol{x}_1, \boldsymbol{x}_2) + h_C^{\sigma_1,\sigma_2}(\boldsymbol{x}_1, \boldsymbol{x}_2) \tag{2.79}$$

The former in (2.79) is the Fermi hole, it is the dominant part of the total hole. It has a direct relationship with Pauli's principle and wave function antisymmetry. No self interaction is produced because this formulation considers the interaction of a reference electron with all other.

This operator applies only to electrons with same spin, and integrates to -1 as the total hole:

$$\int h_X(\boldsymbol{x}_1, \boldsymbol{x}_2)\, d\boldsymbol{x}_2 = \int \left\{ \frac{n_{2\sigma}(\boldsymbol{x}_1, \boldsymbol{x}_2)}{n_\sigma(\boldsymbol{x}_1)} - n_\sigma(\boldsymbol{x}_2) \right\} d\boldsymbol{x}_2 = Ne_\sigma - 1 - Ne_\sigma = -1 \tag{2.80}$$

And the Fermi holes becomes equal to the opposite of the charge density if $\mathbf{x}_1 = \mathbf{x}_2$, (2.81), according to Pauli's principle that avoids two electrons of same spin to coexist at the same spatial position.

$$h_X(\boldsymbol{x}_1, \boldsymbol{x}_1) = -n(\boldsymbol{x}_1) \tag{2.81}$$

The latter in (2.79) has contributions for electrons of either spin, and is the Coulomb hole. It integrates to zero to satisfy the property of the total hole:

$$\int h_C(\boldsymbol{x}_1, \boldsymbol{x}_2)\, d\boldsymbol{x}_2 = Ne_\sigma - 1 - Ne_\sigma = 0 \tag{2.82}$$

The probability of finding an electron of spin "σ" everywhere in the space is the total number of the electrons with spin "σ" if the reference electron has a spin σ'≠σ.
Because no electrons of parallel spin can occupy the same point in the space, the cusp condition occurs for $\mathbf{x}_1 = \mathbf{x}_2$.

This splitting of the total hole is particularly useful for Hartree-Fock methods, in which Fermi holes is accounted by Slater determinant, instead the Coulomb hole is totally neglected.

The exchange contribution, connected with wave function's antisymmety, consists in the interaction between electron density of spin "σ" and Fermi hole of the same spin:

$$E_X = \frac{1}{2} \int \int \frac{n(\boldsymbol{x}_1) h_{XC}(\boldsymbol{x}_1, \boldsymbol{x}_2)}{|\boldsymbol{x}_1 - \boldsymbol{x}_2|} d\boldsymbol{x}_1 d\boldsymbol{x}_2 \tag{2.83}$$

Slater constructed the Fermi hole assuming that it is spherically symmetric and centered around the reference electron at $\mathbf{x}_1$, it is also constant inside the sphere and zero outside.

The Fermi hole contains exactly one elementary charge, and has a spherical radius, known as Wigner-Seitz radius:

$$r_S = \left(\frac{3}{4\pi}\right)^{1/3} \frac{1}{n^{1/3}(\boldsymbol{x}_1)} \tag{2.84}$$

The potential of a uniformly charged sphere is proportional to $n^{-1}(\mathbf{x}_1)$ and so the exchange energy can be represented by:

$$E_X \cong C_X \int n^{4/3}(\boldsymbol{x}_1)\, d\boldsymbol{x}_1 \tag{2.85}$$

The non local exchange term of Hartree-Fock theory (2.83) is converted to a local function of electron density and adjusted with the numerical constant "C_X".
This formula was originally expressed as an approximation of the Hartree-Fock method, but is now a density functional representation of the exchange energy.

2.8 The Adiabatic Connection

The hole functions debated before contain all the essential information to describe the non-classical electron-electron interaction (E_{ncl}), although in the Kohn-Sham framework theory "E_{XC}" must also account for the difference between the kinetic energy of the real, interacting system (KT) and the reference non-interacting one (KT_S).

$$E_{XC}[n] = (KT[n] - KT_S[n]) + E_{ncl}[n] \tag{2.86}$$

The real and the reference system are connected by the coupling strength parameter "λ":

- λ=0 non interacting system,
- λ=1 real interacting system.

$$H_\lambda = T + V_{ext}^{\lambda} + \lambda \sum_{i}^{Ne} \sum_{j>i}^{Ne} \frac{1}{|\boldsymbol{x}_i - \boldsymbol{x}_j|} \tag{2.87}$$

Assuming that the two end points (reference and real system) can be linked by a continuous function of the coupling strength parameter the adiabatic connection leads to the following expression:

$$E_{\lambda=1} - E_{\lambda=0} = \int_0^1 f(\lambda) d\lambda \tag{2.88}$$

"f(λ)dλ" has to be explicated to obtain the energy as the expected value of the Hamiltonian operator.

$$\begin{aligned} f(\lambda)d\lambda = \int n(\boldsymbol{x}) dV_{ext}^{\lambda} d\boldsymbol{x} + \frac{1}{2} d\lambda \int\int \frac{n(\boldsymbol{x_1}) n(\boldsymbol{x_2})}{|\boldsymbol{x_1} - \boldsymbol{x_2}|} d\boldsymbol{x_1} d\boldsymbol{x_2} + \\ + \frac{1}{2} d\lambda \int\int \frac{n(\boldsymbol{x_1}) h_{XC}^{\lambda}(\boldsymbol{x_1}, \boldsymbol{x_2})}{|\boldsymbol{x_1} - \boldsymbol{x_2}|} d\boldsymbol{x_1} d\boldsymbol{x_2} \end{aligned} \tag{2.89}$$

$$E_{\lambda=1} - E_{\lambda=0} = \int n(\boldsymbol{x})\left(V_{ext}^{\lambda=1} - V_{ext}^{\lambda=0}\right)d\boldsymbol{x} + \frac{1}{2}\int\int \frac{n(\boldsymbol{x}_1)n(\boldsymbol{x}_2)}{|\boldsymbol{x}_1 - \boldsymbol{x}_2|} d\boldsymbol{x}_1 d\boldsymbol{x}_2 + \\ + \frac{1}{2}\int\int\int_0^1 \frac{n(\boldsymbol{x}_1)h_{XC}^{\lambda}(\boldsymbol{x}_1, \boldsymbol{x}_2)}{|\boldsymbol{x}_1 - \boldsymbol{x}_2|} d\boldsymbol{x}_1 d\boldsymbol{x}_2 d\lambda \tag{2.90}$$

The electron density appears to be "λ" independent, and replacing $V_{ext}^{\lambda=1}$ with "V_{eff}" and $V_{ext}^{\lambda=0}$ with "V_S" it will be possible to express the energy of the fully interactive system by using the non-interactive system's kinetic energy:

$$E_{\lambda=1} - E_{\lambda=0} = E_{\lambda=1} - \left\{T_S + \int n(\boldsymbol{x})V_S d\boldsymbol{x}\right\} \tag{2.91}$$

$$E_{\lambda=1} = \int n(\boldsymbol{x})V_{eff} d\boldsymbol{x} + \frac{1}{2}\int\int \frac{n(\boldsymbol{x}_1)n(\boldsymbol{x}_2)}{|\boldsymbol{x}_1 - \boldsymbol{x}_2|} d\boldsymbol{x}_1 d\boldsymbol{x}_2 + \\ + \frac{1}{2}\int\int\int_0^1 \frac{n(\boldsymbol{x}_1)h_{XC}^{\lambda}(\boldsymbol{x}_1, \boldsymbol{x}_2)}{|\boldsymbol{x}_1 - \boldsymbol{x}_2|} d\boldsymbol{x}_1 d\boldsymbol{x}_2 d\lambda \tag{2.92}$$

With:

$$E_{XC} = \frac{1}{2}\int\int\int_0^1 \frac{n(\boldsymbol{x}_1)h_{XC}^{\lambda}(\boldsymbol{x}_1, \boldsymbol{x}_2)}{|\boldsymbol{x}_1 - \boldsymbol{x}_2|} d\boldsymbol{x}_1 d\boldsymbol{x}_2 d\lambda \tag{2.93}$$

The integration over the coupling strength parameter transfers the difference between "T" and "T_S" in the exchange correlation energy. The expression of the kinetic energy is therefore simpler, but the hole expression, that is actually unknown, gets further complication. If the hole were known also the exchange correlation is totally defined.

2.9 Exchange Correlation Functionals

In the exchange correlation functionals are inserted all those quantum mechanical aspects that are neglected in the explicit parts of the Kohn-Sham equations. The Hohenberg-Kohn theorem assures the existence of the true form of "Exc" functional, but there is no way to get the exact explicit expression.
It is just possible to derive the correct "Exc" form for a particular system, the uniform electron gas, whose electron density appears as a constant. This model is known as LDA, Local Density Approximation.
This statement can be considered as a limitation, but on the other side the LDA can give back good first trial results. At the same time the results according with LDA are not the true solution of the Schrödinger equation that describes the system, in fact the true nature of the exchange correlation part is actually unknown.

The concrete aim is to represent the real nature of the exact functional, and to implement it in an efficient algorithm.
Several functional are now developed, but it is crucial to understand the similarities and the differences among them.
A useful classification, referred to a biblical verse from Genesis, is provided by John Perdew:

Genesis 28 "...had a dream ...a ladder was set on the earth with its top stretching to heaven ...
and the angels of God were ascending and descending on it."

Jacob's ladder establishes a list of functionals of increasing accuracy climbing the ladder itself, due to a greater amount of physical information [Figure 2.3].

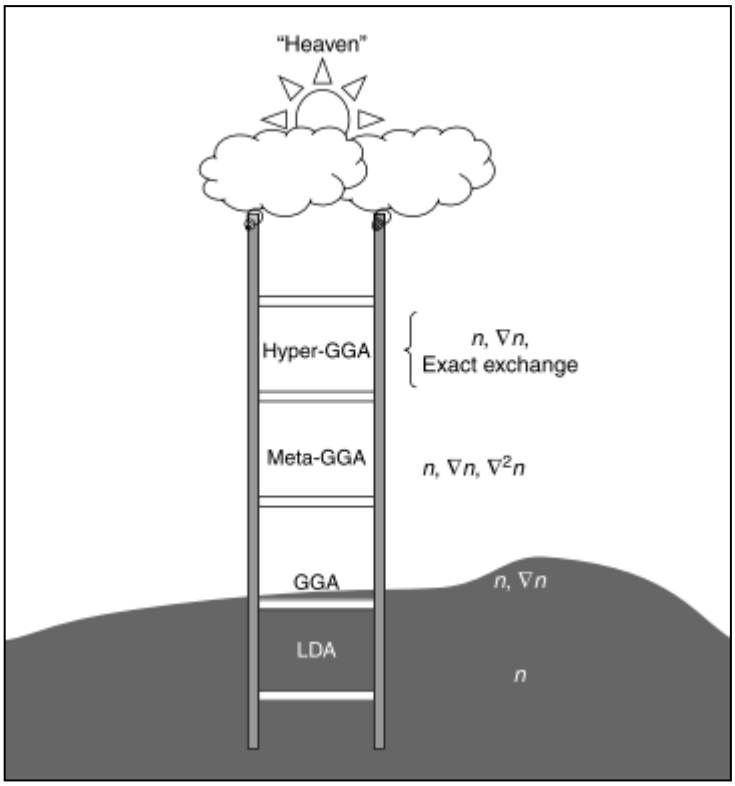

Figure 2.3: Jacob's ladder, adapted from [30]

For each of the rungs generally exists:

- Non empirical functionals
- Semi empirical functionals
- Emipirical functionals

The simplest and widespread functionals are LDA and GGA, they are often used because of their capability to reproduce experimental data with good agreement by requiring a restricted number of information to characterize the functional expression. Although these functionals may be mistaken and lose their capability to properly provide a good description of the electronic structure and to generate a reliable potential that affects inter-atomic interactions and thus all chemical and physical properties of matter. The main features of the different kinds of functionals are following declared.

The LDA is employed as assumption to build the corresponding pseudopotential.
In the LDA approximation the exchange correlation potential selected is the one of spatially uniform electron gas, whose density is the local electron density.
In this reference system electrons move on a positive background charge, so that the total charge is zero. Electron density represents a constant value everywhere, and this gives a good physical description of a perfect metallic crystal, where the positive charge is produced by the ions (nuclei and core electrons), unfortunately atoms and molecules often possess variable density.

$$E_{XC}^{LDA}[n(\boldsymbol{r})] = \int n(\boldsymbol{r})\varepsilon_{XC}[n(\boldsymbol{r})]d\boldsymbol{r} \tag{2.94}$$

If the spin densities are considered:

$$n(\boldsymbol{r}) = n_{\alpha}(\boldsymbol{r}) + n_{\beta}(\boldsymbol{r}) \tag{2.95}$$

$$E_{XC}^{LSDA}[n(\boldsymbol{r})] = \int n(\boldsymbol{r})\varepsilon_{XC}\left[n_{\alpha}(\boldsymbol{r}), n_{\beta}(\boldsymbol{r})\right]d\boldsymbol{r} \tag{2.96}$$

Where "ε_{XC}" is the exchange correlation energy per particle, it is weighted with the probability n(**r**) to find an electron in **r**, and is composed by:

$$\varepsilon_{XC}[n(\boldsymbol{r})] = \varepsilon_{X}[n(\boldsymbol{r})] + \varepsilon_{C}[n(\boldsymbol{r})] \tag{2.97}$$

"ε_X" is the exchange energy, usually named Slater exchange:

$$\varepsilon_{X}[n(\boldsymbol{r})] = -\frac{3}{4}\sqrt[3]{\frac{3n(\boldsymbol{r})}{\pi}} \tag{2.98}$$

"ε_C" instead is not explicit but accurately estimated by Monte Carlo simulations of the homogeneous electron gas, however various authors have proposed analytical expressions based on interpolation's procedures.

LDA often fails in accurately describing atoms and molecules whose electron density varies rapidly, so most of the applications in chemistry require a greater accuracy than the one that LDA can assure, as consequence an extension of LDA has been developed, it is the Generalized Gradient Approximation, and is widely employed in solid state physics problems.
GGA considers much information than LDA, it computes not only n(**r**) at a particular position **r**, but also takes account of the information about the gradient ∇n(**r**):

$$E_{XC}^{GGA}[n(\boldsymbol{r})] = \int n(\boldsymbol{r})\varepsilon_{XC}[n_\alpha(\boldsymbol{r}), n_\beta(\boldsymbol{r})]d\boldsymbol{r} + \\ + \sum_{\sigma,\sigma'} \int C_{XC}^{\sigma,\sigma'}[n_\alpha(\boldsymbol{r}), n_\beta(\boldsymbol{r})] \frac{\nabla n_\sigma(\boldsymbol{r})}{n_\sigma(\boldsymbol{r})^{2/3}} \frac{\nabla n_{\sigma'}(\boldsymbol{r})}{n_{\sigma'}(\boldsymbol{r})^{2/3}} d\boldsymbol{r} \tag{2.99}$$

With σ and σ' referred to either α or β spin.
GGA functional is commonly a local operator in a mathematical sense because its value at **r** only depends only on n(**r**) and ∇n(**r**) and is totally independent of n(**r**') and ∇n(**r**').

The desired improvement of accuracy is unfortunately not reached because of the loss of many physical properties of LDA, thus new constrains have to be added, in fact, if some parts of GGA violate the negative property of the exchange holes the former are set to zero.
As for LDA, even GGA is made up of two contributions:

$$E_{XC}^{GGA} = E_X^{GGA} + E_C^{GGA} \tag{2.100}$$

It is possible to build the exchange energy starting from the exchange part of the LDA:

$$E_X^{GGA} = E_X^{LDA} - \sum_\sigma \int F[S_\sigma(\boldsymbol{r})] n_\sigma(\boldsymbol{r})^{4/3} d\boldsymbol{r} \tag{2.101}$$

S_σ is a dimentionless function, intended as a local inhomogeneity parameter, and is set to zero for the homogeneous electron gas:

$$S_\sigma(\boldsymbol{r}) = \frac{|\nabla n_\sigma(\boldsymbol{r})|}{n_\sigma(\boldsymbol{r})^{4/3}} \tag{2.102}$$

This statement allows non-empirical GGA functionals to satisfy the uniform density limit, and several exact properties of the exchange-correlation hole, two examples are provided by PW91 and PBE functionals. Even if GGA functionals are able to provide a correct description of several properties of the matter they are also extremely ineffective if particular aspects of certain materials want to be investigated, in fact van der Waals interactions are not properly described by GGA, which uses to underestimate binding energies if the intermolecular attraction is not accounted for. Furthermore, GGA approximately characterizes transition metals, in particular it miserably fails if a transition metal oxide wants to be studied in terms of electrical conductivity, in fact an oxide, with a band gap, is described by both LDA and GGA like a metal that has no gap.

Thus more refined functionals have to be built in order to provide a better description of a large amount of physical aspects and to be able to well define disparate systems.

To provide a sensible qualification of the most complex atomic systems upper rungs are needed. Meta GGA functionals are positioned at the third rung of the Jacob's ladder and include the second order derivative of the charge density, instead the fourth rung is occupied by Hyper GGA functionals that evaluate the exact exchange energy but also possess a critical part that is non local and requires to know the electron density to be properly calculated. Hyper GGA are by far much more computationally demanding, they are built as a mixture of the exact exchange and a GGA exchange functional.

2.10 Density of States and Projected Density of States

PDOS is the acronym for "Projected Density of States", that is a portion of the Total Density of States (DOS) used to describe the electronic state of a material:

$$Total\ Number\ of\ States = \int_{-\infty}^{+\infty} DOS(E)\, dE \tag{2.103}$$

As for PDOS, DOS is a function of the energy of the system, and is usually expressed with arbitrary units [A.U.]. The total number of states represents the number of the electrons included in the system, these electrons can be found to fill particular energetic levels, that can be associated with orbitals, and thus chemical bonds. Usually, only some states can be effectively occupied, in fact the calculation of the Fermi Energy is fundamental since it defines the highest occupied electronic state at T = 0 K (at the ground state), thus DOS and PDOS are not plotted in terms of an absolute energy but instead relative to the Fermi Energy itself. Metals are characterized by a non null DOS at the Fermi Level, but DOS itself cannot be used to define which levels are filled by a particular valence state. Thus the PDOS is used, in fact it turns useful to select individual atomic orbitals or groups of atomic orbitals as localization functions (ϕ_α) upon which to project the electron density.

$$PDOS(\alpha, \varepsilon) = \sum_{i=1}^{\infty} \left|\langle \phi_\alpha | \varphi_i \rangle\right|^2 \delta(\varepsilon - \varepsilon_i) \tag{2.104}$$

The projections of all the Kohn-Sham states onto a particular molecular orbital (α) are computed and added up as a function of the energy "ε". PDOS describes the electronic structure, thus can be used as a fundamental tool to explain the chemical reactivity and the substrate-adsorbate interaction, in terms of occupied and unoccupied states, and it also can define on a quality level the strength of a chemical bond according to the distribution of the states and the overlapping among substrate's and adsorbate's states.

CHAPTER 3

3 Modeling Extended Surfaces: Fundamentals and Chemisorption

3.1 Localized and Spatially Extended Functions

DFT, according to Kohn-Sham approximation, deals with the resolution of "N" single particle equations, thus no longer Schrödinger equation, that is a "many-body" model, is considered.
Even though it was demonstrated that a many body problem can in principle be solved by use of a three dimensional observable, that is the electron density, and that can in practice be treated as a single particle problem, handling a great number of non interacting electrons sill represents a demanding task. In addition to the mathematical effort towards the research of the solution of Kohn-Sham equations, an effort to correctly describe the chemical and physical behavior of the system is required, since Schrödinger equation is not completely known, the unknown member of the equation is what makes the difference between a coarse approximation of reality and a reliable one.
The solution of the Kohn-Sham equations usually leads to the explicit expression of the electron wave function or electron density. These expressions can be represented by different classes of functions, spatially localized or spatially extended.
Spatially localized functions are built around each atom of the system, they are centered on the single atomic species, and originate an efficient framework often used in the description of isolated molecules, with functions that decay to zero far away from the molecule itself. However, if the system has some kind of periodicity, or is spatially extended as a bulk material or a surface it can still be described by localized functions, that are added up to describe all the atoms of the solid state, but this is not the only way to give a representation of the Kohn-Sham equations.
A useful alternative suggests operating with periodic functions in fact for perfect bulk materials the electron density and wave function are spatially periodic function.

3.2 Reciprocal Space and K Points

Considering a crystal of a pure metal, the crystal structure can be defined only if the locations of all the atomic species are identified. A crystal is a three dimensional solid that can be included in a finite volume of space, and if the crystal is flawless and thus perfect, the volume can be divided into smaller identical units that contain a certain number of atoms. If this volume is translated along the crystal vectors (depending on the shape of the volume elements selected) the full crystal structure is thus created.

The smaller volume that contains a single atom allows to reproduce the full structure and is referred to as "primitive cell".

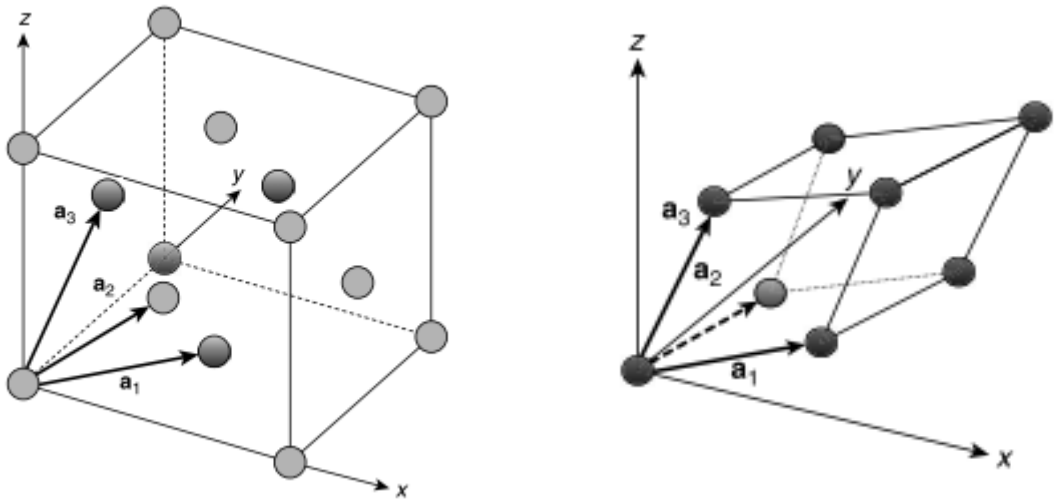

Figure 3.1: two different primitive cells of a fcc material, adapted from [30]

The primitive cell for a face-centered-cubic (fcc) metal can be defined by the three crystal vectors [Figure 3.1]:

$$\boldsymbol{a}_1 = a\left(\frac{1}{2},\frac{1}{2},0\right) \qquad \boldsymbol{a}_2 = a\left(0,\frac{1}{2},\frac{1}{2}\right) \qquad \boldsymbol{a}_3 = a\left(\frac{1}{2},0,\frac{1}{2}\right) \tag{3.1}$$

The vectors are used as parameters to fix the position of an atom of the crystal structure at **r**, with n_1, n_2, n_3, integers.

$$\boldsymbol{r} = n_1\boldsymbol{a}_1 + n_2\boldsymbol{a}_2 + n_3\boldsymbol{a}_3 \tag{3.2}$$

For a fcc structure the geometry of the crystal is fully defined by a single parameter "a", that is the "lattice constant" and is the side of the cube in Figure 3.1, with which the space is filled.

If Kohn-Sham equations are solved for a crystalline periodic system the solution will satisfy the Bloch theorem that states:

"In a periodic solid, each electronic wave function that is a physically acceptable solution of the Kohn-Sham equations can be written as the product of a cell-periodic part and a plane-wave part".

The solution can be made up of two parts [37], [30]:

$$\psi_i(\boldsymbol{r}) = exp(i\boldsymbol{k}\cdot\boldsymbol{r})u_i(\boldsymbol{r}) \tag{3.3}$$

Where the exponential part is due to the plane wave's contribution and the u-function is the cell-periodic part (3.3).
The resolution of the problem leads to a **k**-independent wave function, this means that Kohn-Sham equations can be solved for each **k** value, and because of considerable mathematical problems it is convenient to solve in terms of **k** and no longer in terms of **r**. A transition from real space to k-space or reciprocal space is done, and the reciprocal lattice vectors of the crystal are defined:

$$\boldsymbol{b}_1 = 2\pi\frac{\boldsymbol{a}_2 \times \boldsymbol{a}_3}{\boldsymbol{a}_1 \cdot (\boldsymbol{a}_2 \times \boldsymbol{a}_3)} \qquad \boldsymbol{b}_2 = 2\pi\frac{\boldsymbol{a}_3 \times \boldsymbol{a}_1}{\boldsymbol{a}_2 \cdot (\boldsymbol{a}_3 \times \boldsymbol{a}_1)} \qquad \boldsymbol{b}_3 = 2\pi\frac{\boldsymbol{a}_1 \times \boldsymbol{a}_2}{\boldsymbol{a}_3 \cdot (\boldsymbol{a}_1 \times \boldsymbol{a}_2)} \tag{3.4}$$

The cell-periodic part (3.6) is expanded using a discrete basis set of plane waves whose wave vectors (3.5) are the reciprocal lattice vectors, with m_1, m_2, m_3 integers:

$$\boldsymbol{G} = m_1\boldsymbol{b}_1 + m_2\boldsymbol{b}_2 + m_3\boldsymbol{b}_3 \tag{3.5}$$

$$u_i(\boldsymbol{r}) = \sum_G c_{i,G}\ exp(i\boldsymbol{G}\cdot\boldsymbol{r}) \tag{3.6}$$

$$\psi_i(\boldsymbol{r}) = \sum_G c_{i,k+G}\ exp(i(\boldsymbol{k}+\boldsymbol{G})\cdot\boldsymbol{r}) \tag{3.7}$$

Just a limited set of k points, chosen according to the boundary conditions applied to the bulk solid, contain non-empty electronic states. In fact an infinite number of k points exists and, although an infinite number of electrons is contained in the periodic bulk, only a finite number of electronic states are occupied at each k point. Bloch turns the problem and calculates a finite number of wave functions at an infinite number of k points instead of computing an infinite number of wave functions.

If k points are very close the wave functions will be very similar, and this allows to use a single k point to describe the electronic wave functions over a region of k space, so just a finite number of k points is considered.

Like in real space, to define a primitive cell is fundamental, even in reciprocal space, because the primitive cell has several special properties, special k points, and so a special name: "Brillouin zone" (BZ). A typical way to map the grid of k point is given by the Monkhorst and Pack method (1976) [38].

By using a sparse grid the evaluation of integrals over k space requires less computational time but on the other hand a reduction of the solution accuracy is observed. A suitable extension of the grid has to be found by means of convergence test of the total energy against the number of k points.

According to Bloch theorem, at each k point the wave functions can be expanded using a discrete set of plane-waves, even if an infinite number of waves should be used to represent a periodic function as the electronic wave function. This approach is essential to solve Kohn-Sham equations with the aid of a calculator, that has a finite memory; fortunately the coefficients "$c_{i,k+G}$" (3.7) for the plane waves with small kinetic energy are the most important, and the basis set is thus cut to contain the plane waves with less kinetic energy than a reference value, commonly called "cutoff" of the kinetic energy.

$$E_{Kin} = \frac{\hbar^2}{2m}|\boldsymbol{k}+\boldsymbol{G}|^2 \tag{3.8}$$

$$\psi_i(\boldsymbol{r}) = \sum_{G}^{|\boldsymbol{k}+\boldsymbol{G}|<G_{cut}} c_{i,k+G}\, exp(i(\boldsymbol{k}+\boldsymbol{G})\cdot\boldsymbol{r}) \tag{3.9}$$

The truncation of the basis set introduces an error in the total energy value, this error decreases with higher cutoff as long as numerical effort increases.

3.3 Pseudopotential Approach

The solution of Kohn-Sham equations shows several technical difficulties among which the need of a great number of plane waves appears. Although, according to Bloch's theorem, electronic wave functions can be expanded with a finite set of plane waves but the basis set is usually not well suited to expanding wave functions, in particular the number of plane waves rapidly rises up if the "core" region wants to be described in detail. The core region is inhabited by electrons that are strongly localized in the neighborhood of the atomic nucleus. Here the potential due to nucleus-electron interaction is particularly strong and introduces broad oscillations [Figure 3.2], electrons have an important kinetic energy to balance the strong Coulomb interaction. To properly describe these oscillations becomes necessary to rapidly extend the wave functions' summation and a large cutoff is required [36].

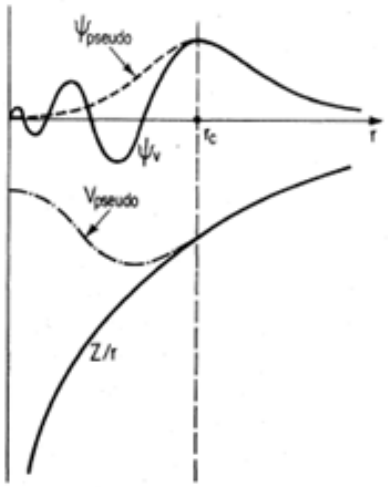

Figure 3.2: illustration of all-electron (solid lines) and pseudoelectron (dashed lines) potentials, and corresponding wave functions, adapted from [36]

This complex system may be reduced to another, of lower mathematical intricacy, by replacing the Coulomb potential for the core electrons with a useful approximation. The core potential is replaced by a weak potential named "pseudopotential". The pseudopotential, besides describing all the salient features of a valence electron that moves through the solid including relativistic effects, also produces a regular non-fluctuating wave function near the nucleus, and it needs a serial expansion of the plane wave functions that extends the summation to a lower upper index thus the pseudopotential itself makes the solution of the Kohn-Sham equations simpler.

This idea was introduced in 1934 by H. Hellman [39] who first understood the utility to treat simultaneously the atom kernels (closed shell electrons and nucleus) according to Thomas-Fermi theory, and the valence electrons according to Schrödinger.

Thus the pseudopotential substitutes the all electron potential (AE) eliminating the core states and describing the valence electrons with smooth pseudo wave functions.

The success of the pseudopotential method lies in the capability to reproduce the real potential in the valence region, where valence electrons determine several chemical properties such as bond strength and they have a basic role in chemical reactivity. Core electrons are instead treated as chemically inert, and considered together with the nuclei as a rigid non polar ion core, and in this case is usual to talk about "frozen core".

The advantages of the pseudopotential method can be summarized:

- The number of electrons to be described is reduced,
- Oscillations in the neighborhood of the nucleus are not accounted for,
- Less wave functions are required to reach the convergence to the solution.

These advantages are translated into less computational effort and thus a reduction of the machine time needed to solve the model that describes the system. Just few decades ago the modeling capability of this method was restricted to describe few atoms system, now the number of atoms is grown up to thousands, and keeps on growing thanks to the increasing computational efficiency of the "ab-initio"/"first-principles" pseudopotential methods. Since the calculations require considerable amounts of CPU, it is essential to use and develop more and more efficient numerical algorithms. A compromise has to be reached because if the size of the system gets too large quantum-mechanical calculations become unfeasible, more cost effective than experiment, and fail to determine the desired chemical-physical properties.

Two important properties the pseudopotential has to honor are:

- The pseudopotential has to be transferable,
- The pseudopotential has to be norm-conserving.

The mathematical version of the first term implies to reproduce the scattering properties of the true potential in a certain range of energies, instead the second term is linked to potentials derived from an atomic reference state, evaluated by all electron calculations; it requests that pseudo and all electron valence eigenstates have the same energies and amplitude outside a selected cutoff radius. The larger is the cutoff radius the softer is said the pseudopotential, softer pseudopotentials converge more rapidly, but are less transferable, that is to say less accurate and able to reproduce the true atomic behavior in different environments.

Ultrasoft pseudopotentials are widespread and very popular among scientific community because of their large cutoff radius and the fast convergence in fact they relax the norm-conserving constraint to reduce the basis set size. An example is provided by Vanderbilt pseudopotentials that substantially reduce the cutoff energy if the majority of the weight of the wave function is not kept within the core by relaxing the norm conserving rule. Although the wave function needs to be projected back to the correct pseudovalence wave function before normalization and this leads to define an energy dependent pseudopotential.

3.4 Crystallography, Bulk Crystal Structures

At the microscopic level materials can be considered as a collection of atoms that can give birth to an amorphous or a crystalline structure. Crystal structures are made up of a collection of atoms neatly arranged into a framework, which is symmetrically reproduced on a long range of space. The fundamental box that contains all the essential information to create the whole material is usually called "unit cell", with an own shape, fully defined by the "lattice parameters".

Seven crystal systems can be identified:

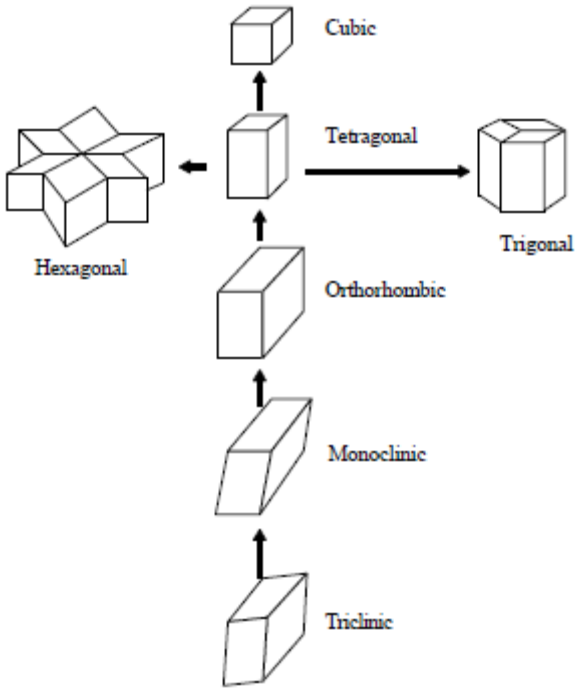

Figure 3.3: possible 3D crystal systems, by S. Garret

Only seven lattice systems exist to describe the bulk fashion of a condensed matter, and these systems can be divided into 14 "Bravais' Lattices" that exhaust the possibilities to describe all distinct cases [Figure 3.5], [Figure 3.6].

Bravais' lattices allow to specify the periodic array in which the repeated units of the crystal are arranged and represent themselves an array of discrete points positioned and orientated in a such way that appears exactly the same, independently from the chosen point of view. The location of the points that belong to a particular Bravais' lattice can be determined by the following rule:

$$\boldsymbol{r} = n_1\boldsymbol{a}_1 + n_2\boldsymbol{a}_2 + n_3\boldsymbol{a}_3 \tag{3.10}$$

$\mathbf{a}_1$, $\mathbf{a}_2$, $\mathbf{a}_3$, are three non planar vectors and $\mathbf{n}_1$, $\mathbf{n}_2$, $\mathbf{n}_3$, are integer values.
The vectors are called "primitive vectors" and they span the lattice. Although, for any given Bravais' lattice, the set of primitive vectors is not unique, that is to say a crystal structure can be described by the use of different kinds of primitive vectors.

A volume of space that is able to fulfill all the space without overlaps or voids is referred to as "primitive unit cell", and different primitive cells can be chosen to describe a given Bravais' lattice. The whole space can also be covered by cells that are not unit cells, generally bigger, whose size is specified as a multiple of the unit cell's lattice constant.

A list of all the possible structures is provided [37]:

- Cubic: there are three kind of cubic structures, simple cubic (cs), body centered cubic (bcc) and face centered cubic (fcc). The structure is defined by three perpendicular lattice vectors of the same length.

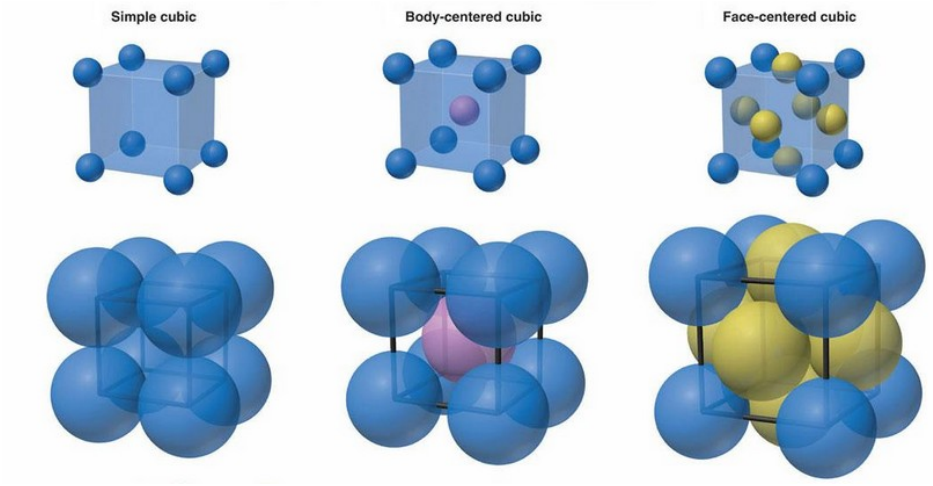

Figure 3.4: cubic structures, cs, bcc, fcc, by P. J. Brucat

Several metals show a cubic crystalline structure such as Palladium, Rhodium and Nickel.

- Tetragonal: the strong symmetry of the cube is reduced by pulling on two opposite faces, stretching the simple cubic lattice to get a rectangular prism with a square base. The corresponding Bravais' lattice is generated by three mutually perpendicular primitive vectors, only two vectors have the same length, and the third vector of different modulus is oriented along the so called "c-axis". As for cubic structures also tetragonal structures are simple or centered.

- Orthorhombic: this structure can be created by deforming the square face of a cube into a rectangular one, and stretching the "c-axis", thus the Bravais' lattice will be described by use of three lattice vectors of different length.

- Monoclinic: if the orthorhombic structure is distorted by changing the shape of the rectangular faces perpendicular to the "c-axis" into a general parallelogram, the monoclinic structure is drawn. Two lattice vectors belong to the same plane but are not mutually perpendicular, instead the third one will be perpendicular to the previous plane.

- Triclinic: the cube is completely destructed if the monoclinic structure experiences a tilt of the "c-axis". Now the three vectors are mutually non-perpendicular.

- Tridiagonal: this structure can be thought as a cubic structure that sees a stretching along the cube's diagonal, the primitive vectors are of equal length and creates equal angles with one another.

- Hexagonal: is a framework that cannot be related with cubic structure, in fact it is a regular prism with a hexagonal base.

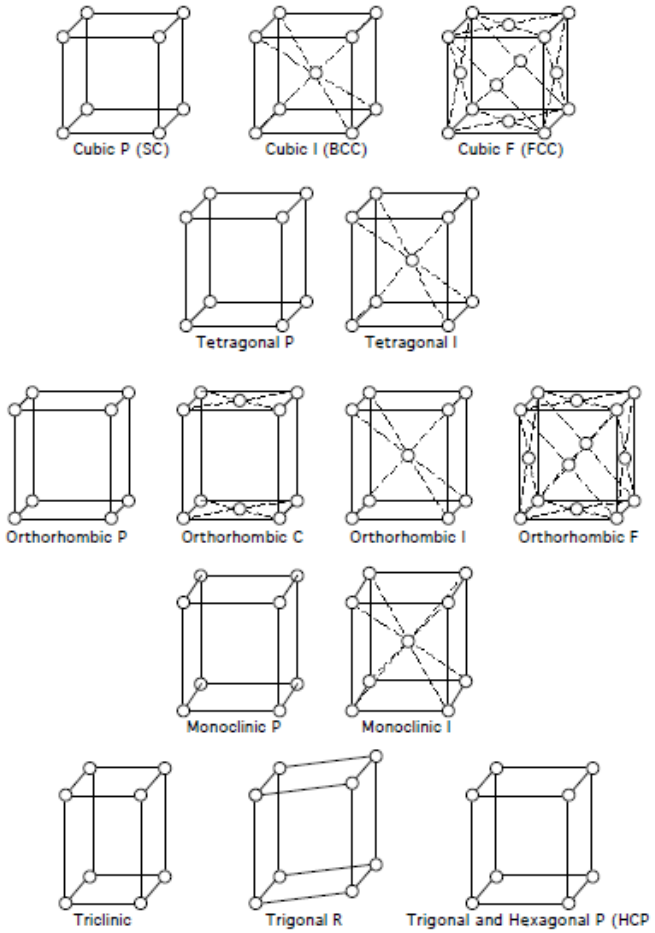

Figure 3.5: expansion of the 7 crystal systems into 14 Bravais' lattices, by S. Garret

Triclinic	$a\neq b\neq c$, $\alpha\neq\beta\neq\gamma$	P (primitive)
Monoclinic	$a\neq b\neq c$, $\alpha=\gamma=90°\neq\beta$	P (primitive) I (body centered)
Orthorhombic	$a\neq b\neq c$, $\alpha=\beta=\gamma=90°$	P (primitive) C (base centered) I (body centered) F (face centered)
Tetragonal	$a=b\neq c$, $\alpha=\beta=\gamma=90°$	P (primitive) I (body centered)
Cubic	$a=b=c$, $\alpha=\beta=\gamma=90°$	P (primitive) I (body centered) F (face centered)
Trigonal	$a=b=c$, $120°>\alpha=\beta=\gamma\neq90°$	R (rhombohedral primitive)
Hexagonal	$a=b\neq c$, $\alpha=\beta=90°$, $\gamma=120°$	R (rhombohedral primitive)

Figure 3.6: geometrical properties of Bravais' lattices, by S. Garret

3.5 Bulk Materials

Now that it is clear how a perfect crystal can be described and what kind of elemental representation is necessary to fulfill the space covered by the whole crystal, it is possible to remind the importance of the Bloch's theorem and the success of the use of plane waves that are a mathematical tool whose properties of periodicity are particularly suited to deal with a periodic framework. This concept is mathematically translated in a problem with periodic boundary conditions (PBC) also called Von Karman conditions.

A bulk material shows a 3D spatial periodicity and if a unit cell is considered [Figure 3.7], it is easy to notice that some atoms are not totally included in the cell, because a fraction of them is shared among the adjacent cells.

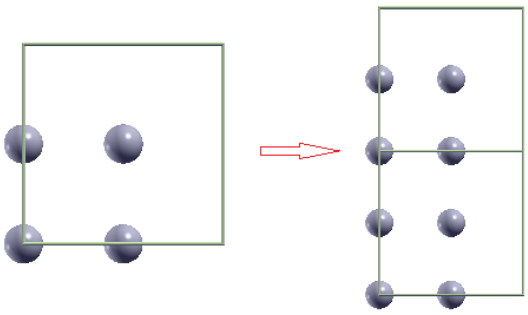

Figure 3.7: coupling of two unit cells sharing atoms

Since cells are adjacent they interact with each others. Atoms that are contained in a cell are affected by the presence of other atoms either in the same cell or in the neighboring ones, and the influence is mutual because of the symmetry and periodicity effects.

An important example may be provided referring to metals, whose central role in chemical industry is undisputed since they are usually used in a great number of technological applications as supported metal catalysts or as crystalline active phase.

Most of them only exist in one bulk structural form:

- bcc → body centered cubic (Fe, W, Mo)
- fcc → face-centered cubic (Pt, Rh, Ni, Pd)
- hcp → hexagonal close packed (Co, Zn, Ti, Ru)

Since the CO_2 activation has been studied on fcc metals as Pt, Rh and Ni, the face-centered cubic crystal structure will be examined. To have a full classification of the structure the interatomic distance that minimizes the system's total energy, the lattice constant, has to be found. If the energy is minimized this means that the most stable structure, and thus the most widespread structure in nature, is obtained.
Different kinds of unit cell can be employed:

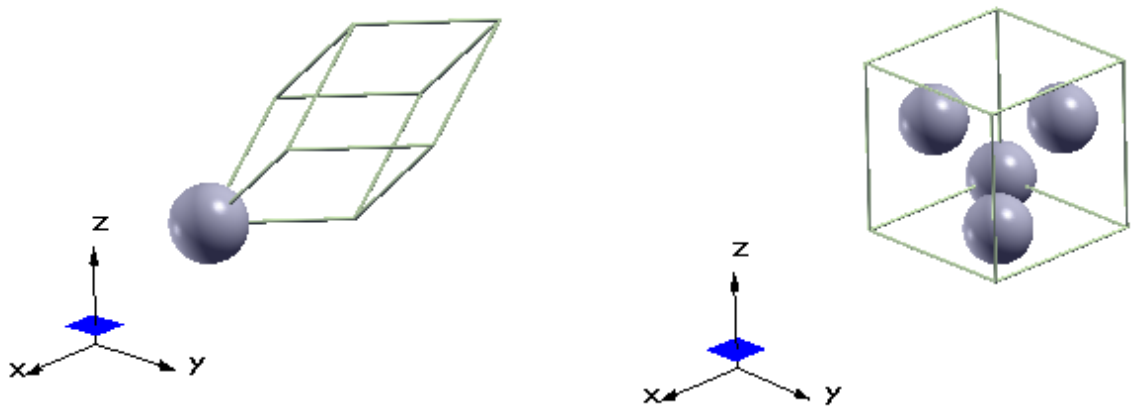

Figure 3.8: two different unit cells with 1 atom, on the left side, and with 4 atoms on the right

The total energy, $E_{TOT}(a)$, calculated as a function of the lattice constant "a", shows a single minimum that is the physical prediction of the lattice parameter of the fcc material.

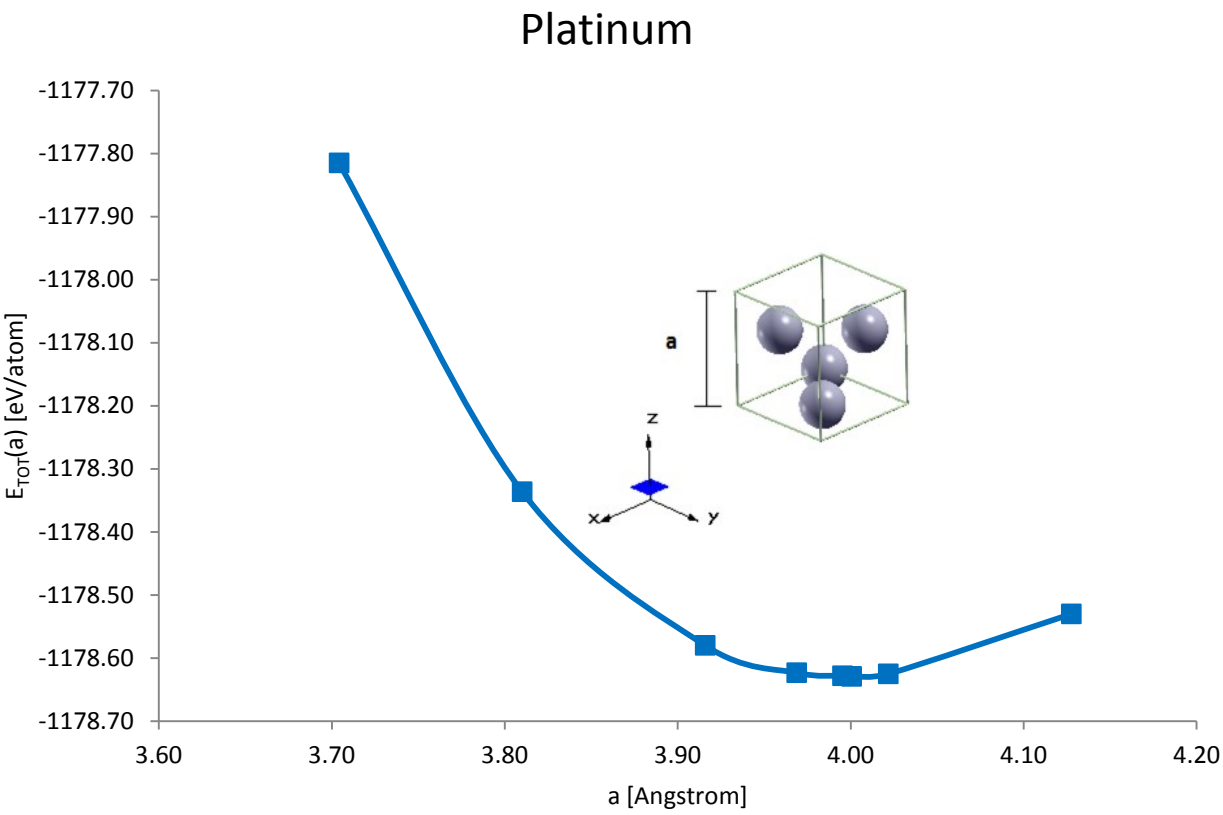

Figure 3.9: minimization of the total energy against lattice parameter of Platinum

The parametric expression of the total energy against the lattice parameter "a", shows a minimum corresponding to the lattice constant for Platinum, that is 7.56 Bohr, equal to 4.00 Angstrom, in good agreement with experimental data.

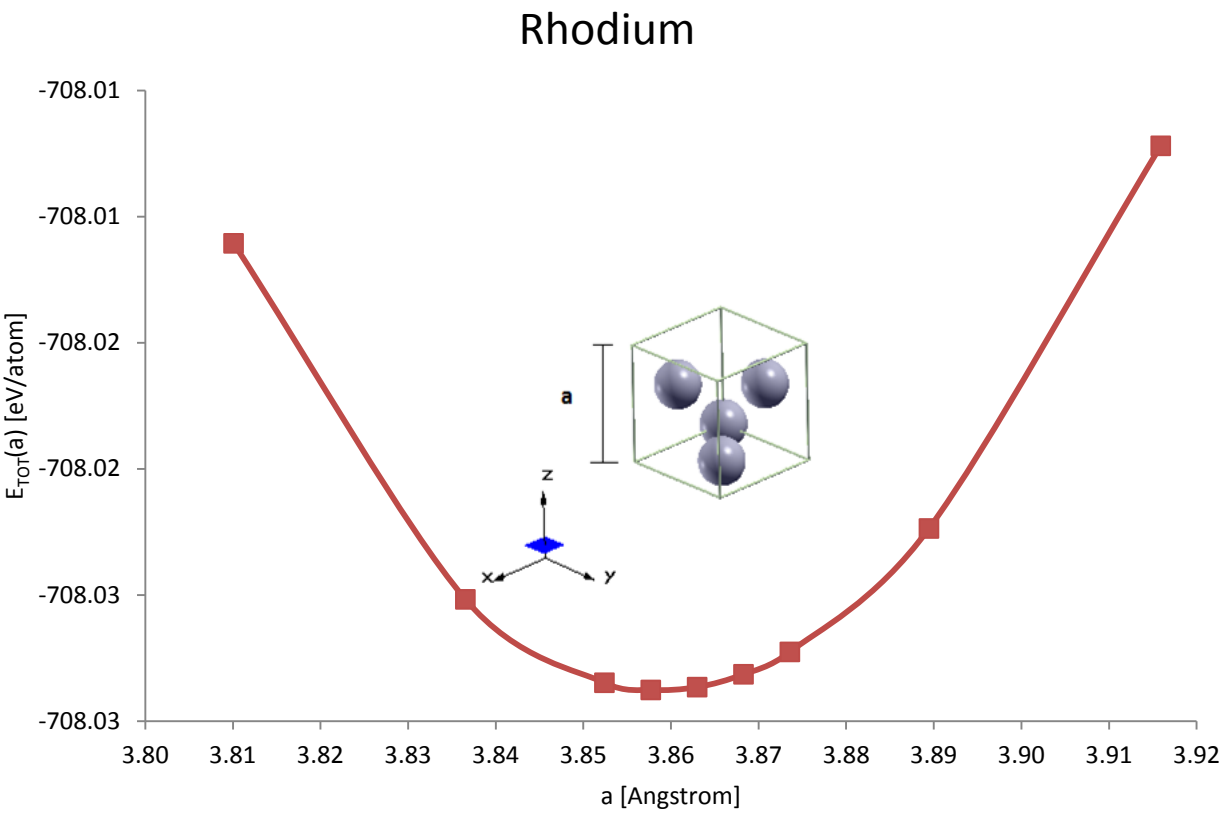

Figure 3.10: minimization of the total energy against lattice parameter of Rhodium

As for Platinum, the unit cell used to build the Rhodium bulk has its total energy minimized with respect to lattice parameter, and thus the lattice constant obtained 7.29 Bohr, that is to say 3.86 Angstrom.

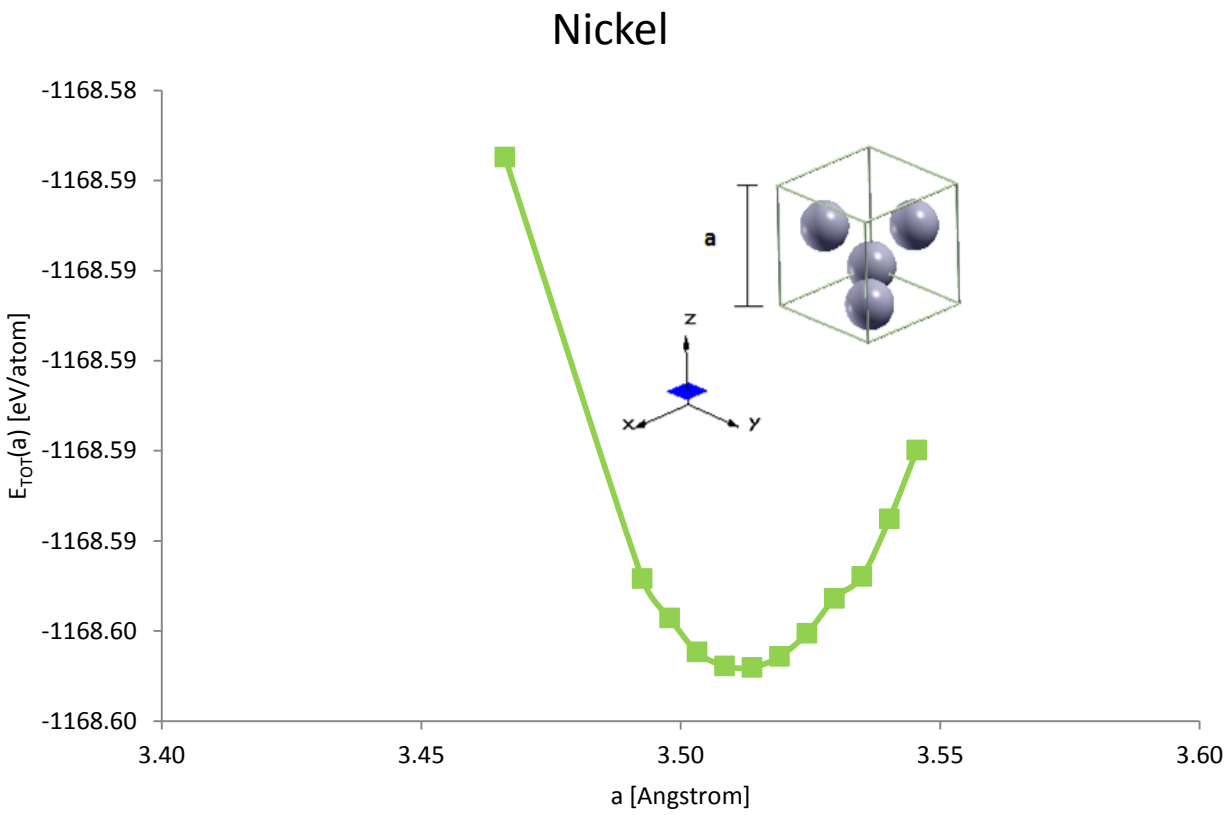

Figure 3.11: minimization of the total energy against lattice parameter of Nickel

Nickel shows the same fcc structure thus the unit cell is always the same for the three metals, but this time the minimum falls at 6.64 Bohr, otherwise 3.51 Angstrom.

The results of the energy minimization are strongly subject to:

- the cutoff energy,
- the k point sampling,
- the pseudopotential.

Thus a convergence check has to be done, instead the pseudopotential can be chosen according to its capability to best reproduce the experimental data.

The previous evaluation of the Platinum's, Rhodium's and Nickel's lattice constants was realized with:

- PBE ultrasoft Vanderbilt pseudopotential,
- Monkhorst-Pack 12x12x12 k-point grid, with 1 1 1 displacement to break symmetry,
- Energy cutoff of 40 Ry.

The choice has been done according to the following convergence analysis with respect to the cutoff and k-points for the Platinum metal [Figure 3.12], as consequence the same cutoff and k-point grid was used to estimate Rhodium and Nickel lattice constants.

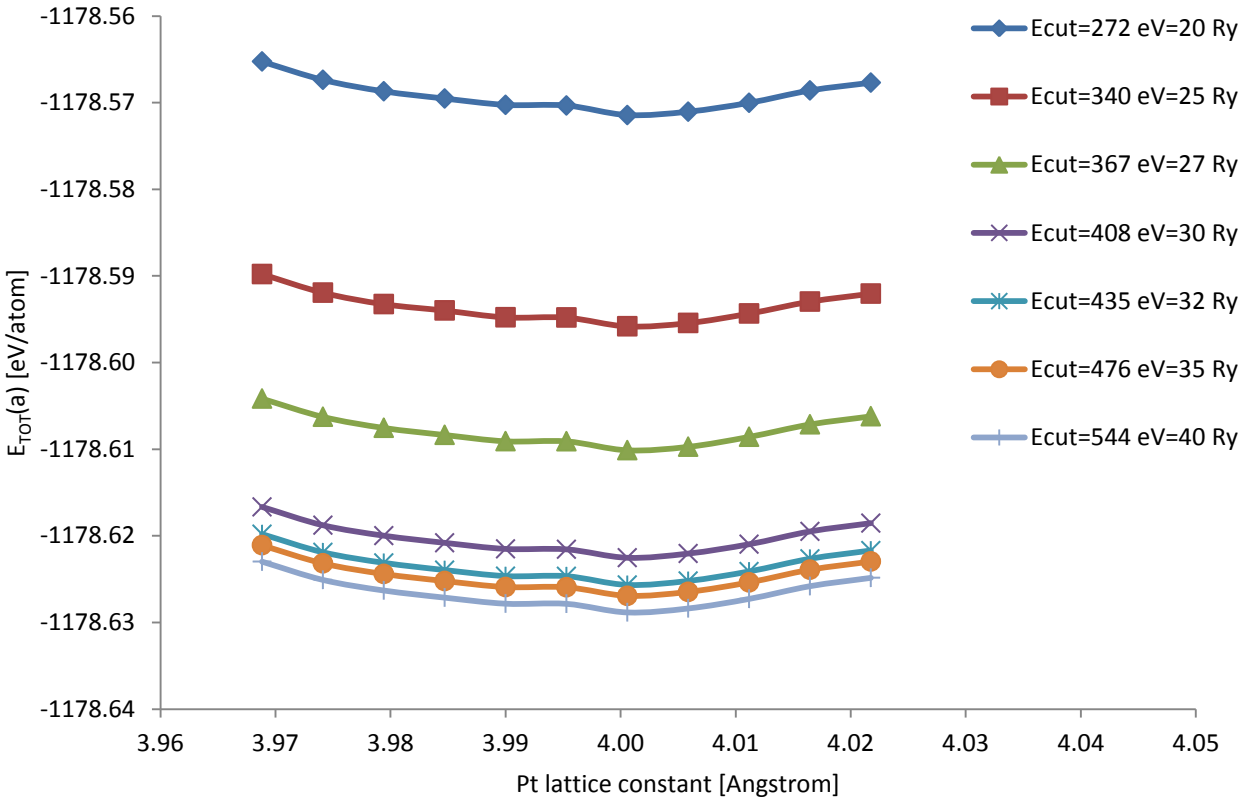

Figure 3.12: cutoff energy convergence

The total energy is a quantity that requires high cutoff energy to converge, instead the lattice parameter is found to be 4.00 Angstrom in all cases [Figure 3.13].

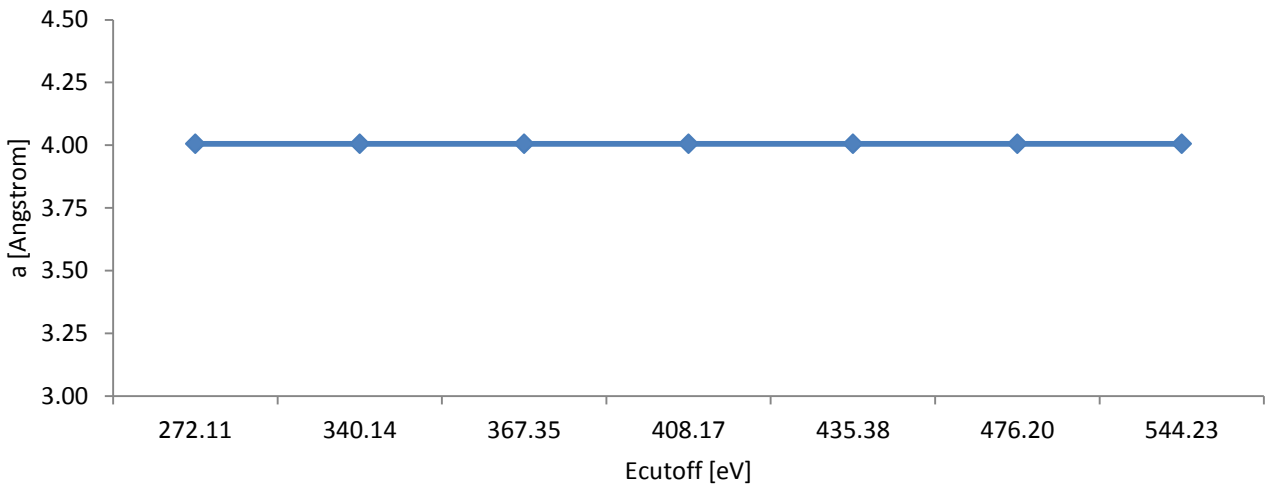

Figure 3.13: variation of the lattice constant against the cutoff energy

k-points convergence shows how the minimum of the total energy always falls at 4.00 Angstrom, even if total energy is still not converged, but the purpose of the following calculations is a geometrical optimization, that always leads to the same result.

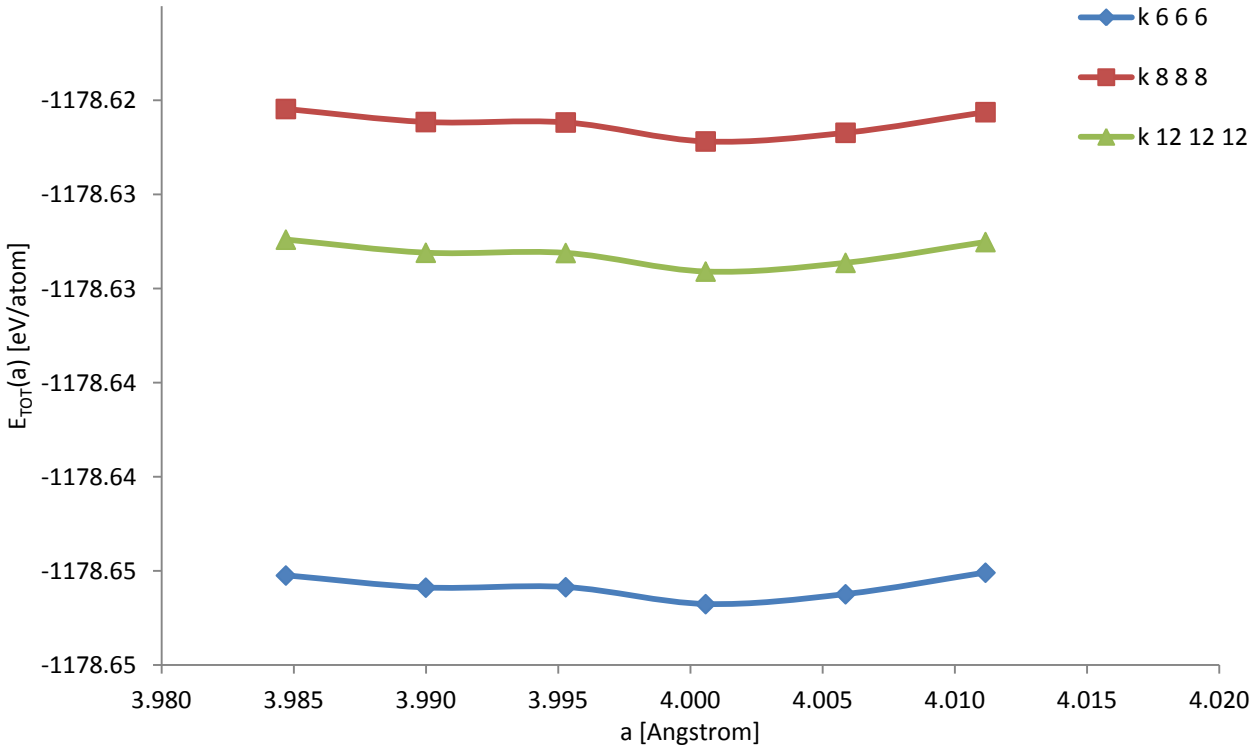

Figure 3.14: k-points convergence

Geometrical properties are little influenced by energy cutoff and by the number of k-points, instead if an appraisal of the cohesive energy value (3.11) wants to be provided high cutoff and dense k-point grid have to be used, because energy is strongly dependent on these two "parameters".

$$E_{cohesive} = E_{Me\_bulk} - E_{Me\_atom} \tag{3.11}$$

That is the energy gain that the system feels when an isolated Metallic atom (Me) is brought inside a bulk structure, since it is a negative number the Metallic atom is more stable when it belongs to a crystal structure rather that when it is surrounded by vacuum.

Metal	**Platinum**	**Rhodium**	**Nickel**
$E_{cohesive}$ [eV/atom]	-5.43	-5.55	-4.66

Table 3.1: Cohesive energies

3.6 Surfaces Classification

The bulk structure is the inner core of a material, but since materials as crystals are three dimensional finite bodies the bulk is in some way physically cleaved. There are many planes along which the crystal may be cleaved, and different directions of cleavage lead to different kinds of surfaces, which expose to the external environment their atoms in a different arrangement, acting on:

- Surface atom coordination,
- Surface symmetry,
- Physical properties,
- Chemical reactivity.

In fact surface chemistry is crucially dependent upon the nature and type of the exposed surface of these crystals. Thus appears remarkable to define which surface is accounted for and the amount of each type of surface exposed to have a deep knowledge of the properties of each of them.

Miller index are commonly employed.

- This method first requires to define a 3D reference system, with x,y and z axes,
- Then the atoms belonging to the conventional cell of the selected crystal structure must be positioned in the reference system,
- Now the conventional cell can be cleaved along a specified plane, defined by use of the perpendicular vector to the plane,

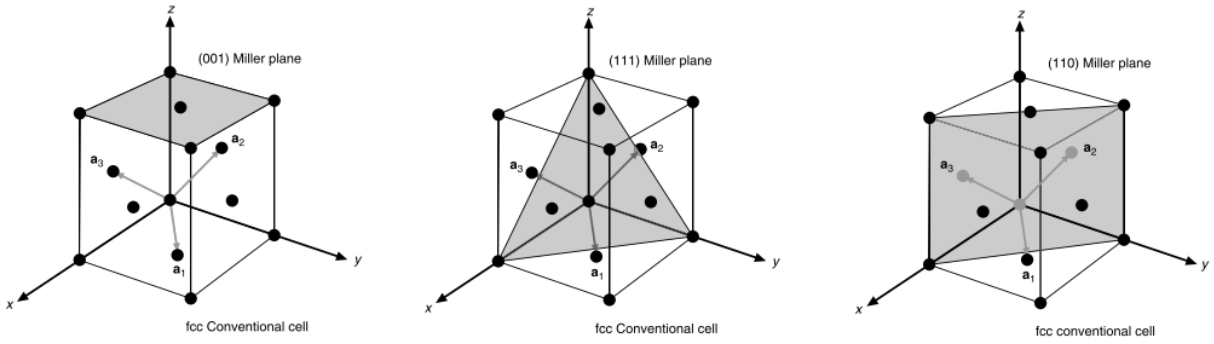

Figure 3.15: low-index planes, from fcc bulk material, (001), (111), (110), adapted from [30]

- The points at which the plane intersects the three axes of the material primitive/conventional cell are considered,
- The reciprocal of the intercepts are multiplied by a scaling factor to make each reciprocals integer,
- Each integer is divided by the smaller integer and thus the Miller indexes (hkl) are obtained.

For each of these crystal systems an infinite number of possible surfaces is admitted but in practice only a limited number of planes (called "low-index") are found to exist in any significant amount [Figure 3.16].

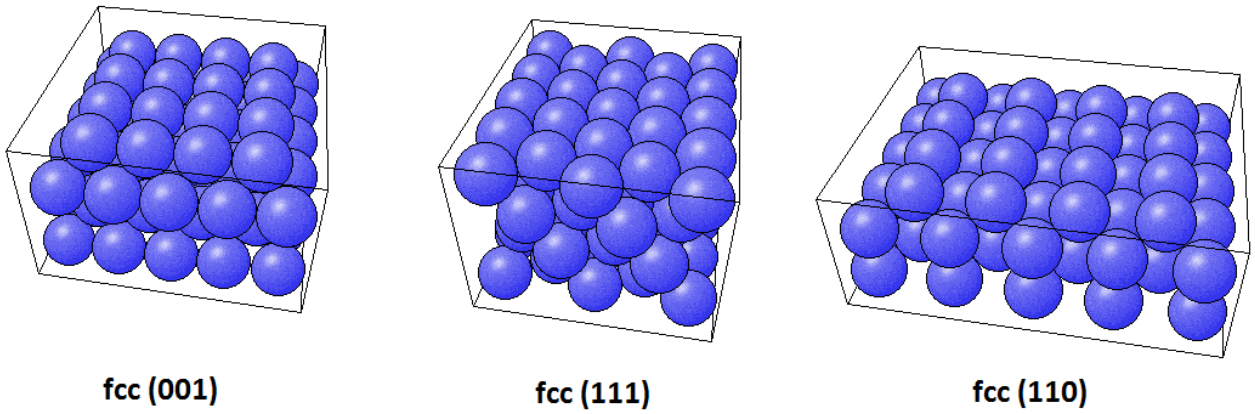

Figure 3.16: 3D view of the low-index planes, from FHI

Surfaces are no longer 3D periodic framework, but periodicity is in some way broken along z coordinate, although, if plane wave method are used an aperiodic system has to be converted into a periodic one, thus a supercell approximation has to be done.
A supercell is no longer a primitive cell, but it is a volume of space that contains a set of atoms opportunely positioned, and this volume is used as a brick to fill the real space, and is periodically reproduced by translations along the lattice vectors.

This trick allows to deal with aperiodic configurations of atoms within the framework of Bloch's theorem. If the framework is not actually periodic the problem can be by passed by studying the properties of the system for larger and larger unit cells, to gauge the importance of the induced periodicity and systematically filter it out.

Plane surfaces are not periodic systems, in a mathematical fashion a surface is a geometrical 2D function, but in a physical fashion it can be considered as portion of matter extended in x-y directions, but with a z minimal finite thickness.
If a perfect crystal is considered, it can be cleaved to get a perfect surface, this surface is spatially finite, but to describe it with plane wave models it has to be thought as spatially infinite through x-y directions, that define the plane of the surface, and this is not difficult, but even along z direction, perpendicular to the surface itself.
If the supercell contains a crystal slab and a vacuum region the purpose is thus achieved. The supercell is repeated over all space, and the total energy of an array of crystal slabs is calculated. As supercells interact with one another the surface or slab must be sufficiently far away to ensure that the results of the calculation accurately represent an isolated surface.

How far surfaces have to be, can be checked evaluating the total energy of the system, by varying the thickness of the vacuum region, and when the vacuum region is wide enough the interaction between the faces of the adjacent crystal slabs will be negligible.
The interaction between upper and lower layers has to be accounted for, although surface's effects happen on a micrometric scale and involve the first ~100 Angstrom of thickness, but so big supercell, with thousands of atoms, requires an excessive, often unaffordable, computational time. As consequence a slab can be only represented by few atomic layers [Figure 3.17].

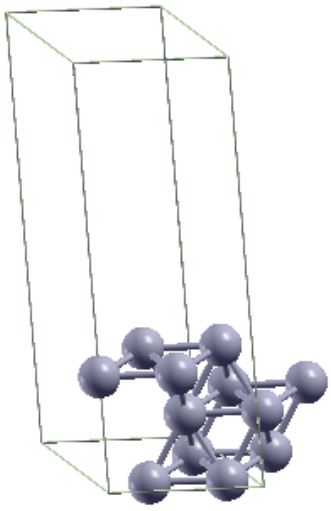

Figure 3.17: 3 layers slab in a supercell

3.7 Supercell and Slab Models

The technological importance of surfaces is considerable in many fields as catalysis, interfaces, membranes, and understanding the geometry and the electronic structure is fundamental to define the correlation between plane surfaces' structure and chemical-physical properties.

A surface can be treated with the DFT plane wave models taking advantage of the periodic boundary conditions in two directions but plane wave codes commonly apply PBC in all three dimensions. Thus the supercell will contain atoms in the lower portion, in order to fill the x and y directions, instead z direction is partially empty, in the upper side a free space, called vacuum, will be left.

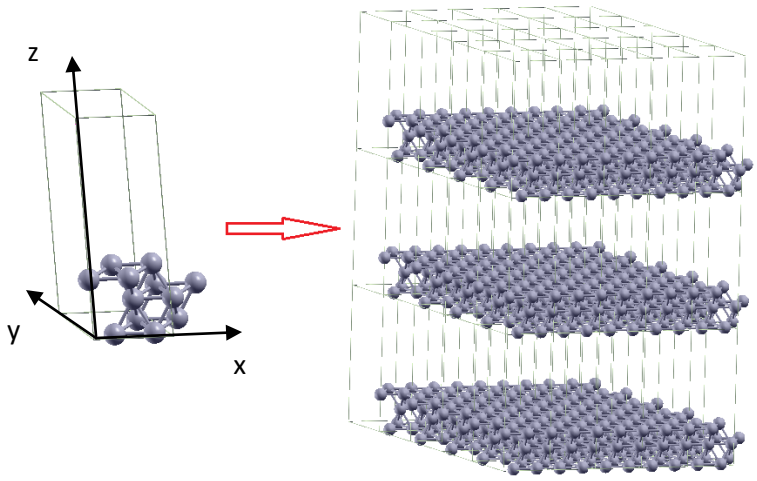

Figure 3.18: slab model in a 3D periodic system

The surface is described with a certain number of atomic layers, in a staked fashion, with a vacuum region necessary to avoid interaction among the supercell reproductions along z axis. Electron density has to decay to zero in order to prevent the tails of electron densities to overlap in the vacuum region.

A fundamental parameter that is observed to determine the surface's stability can be calculated from the total energy of the system. A surface is thought as a portion of bulk, but this time the energy per atom is not the same as for the bulk itself where atoms show the same coordination.

The actual surfaces are two, on the upper and lower side, thus the formation energy can be:

$$E_{surf} = \frac{E_{slab} - nE_{bulk}}{2A} \tag{3.12}$$

Where the difference between the total energy of the slab, made up of "n" atoms, is reduced by "n" times the bulk energy per atom, and divided by the sum of the upper and lower surfaces of area "A".

Since a work has to be done to cleave the bulk, the surface energy will be positive, thus the less is the energy requirement the less expensive is the work.

Pt	100	111	110
E slab [eV/atom]	-7068.16	-3534.61	-3533.15
E bulk [eV/atom]	-1178.63	-1178.63	-1178.63
A [Å^2]	16.00	6.93	11.32
E surf [eV/ Å^2]	28.89	4.43	15.47

Table 3.2: Platinum surface energy

Rh	100	111	110
E slab [eV/atom]	-4243.69	-2122.41	-2120.76
E bulk [eV/atom]	-708.03	-708.03	-708.03
A [Å^2]	14.88	6.44	10.52
E surf [eV/ Å^2]	33.34	5.40	17.48

Table 3.3: Rhodium surface energy

Ni	100	111	110
E slab [eV/atom]	-7008.13	-3504.46	-3503.21
E bulk [eV/atom]	-1168.60	-1168.60	-1168.60
A [Å^2]	12.35	5.35	8.73
E surf [eV/ Å^2]	21.28	3.56	11.25

Table 3.4: Nickel surface energy

The slab construction and its energy of formation depend on:

- the type of metal,
- the number of the atomic layers,
- the thickness of the vacuum,
- the kind of plane selected.

The type of metal imposes the value of the lattice constant "a", this influences the interlayer distance and the length of the cell along x-y directions, as a multiple of this parameter. It is usual to refer to the x-y size as a multiple of the elementary cell, in x-y direction, thus are reported the following supercell:

Slab 1x1:

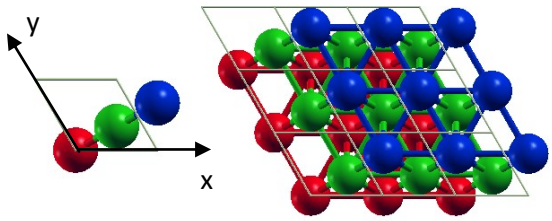

Figure 3.19: (111) 1x1 slab translated three times along the crystal vectors

Slab 2x2:

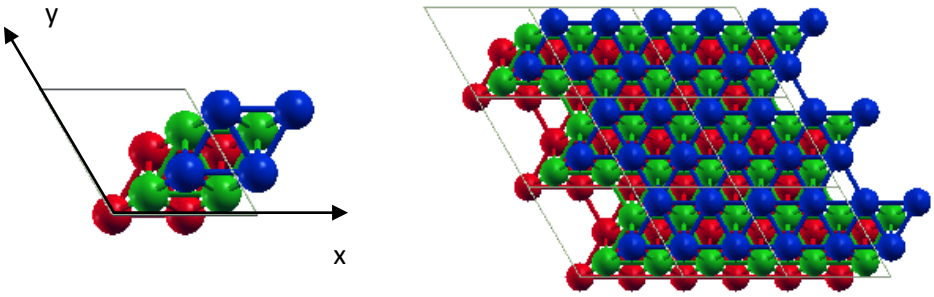

Figure 3.20: (111) 2x2 slab translated three times along the crystal vectors

Slab 3x3:

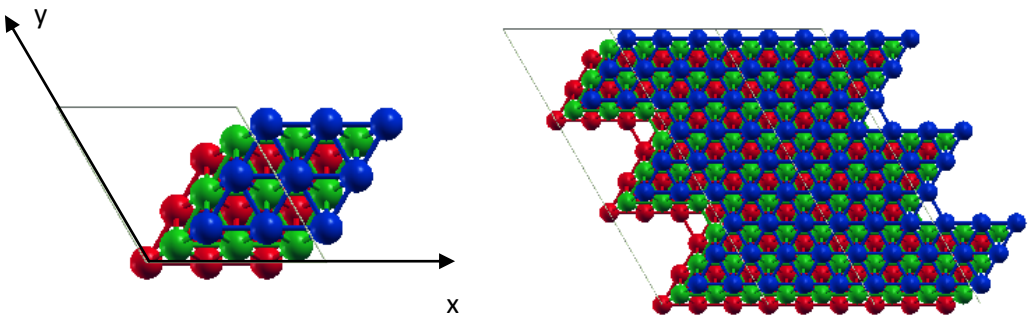

Figure 3.21: (111) 3x3 slab translated three times along the crystal vectors

The number of the atomic layers conditions the overall z length of the supercell, the greater is the number of the atomic layers and the more representative is the slab model, thus it will be able to mimic the important characteristics of a real surface, but since computational time scales cubically with the number of atoms included in the supercell the time required to solve the Kohn-Sham equations grows rapidly, till becoming unbearable. A compromise between computational cost and physical accuracy has to be found, usually a 3-4 layers slab assures a good convergence with respect to the surface energy of formation [Figure 3.22].

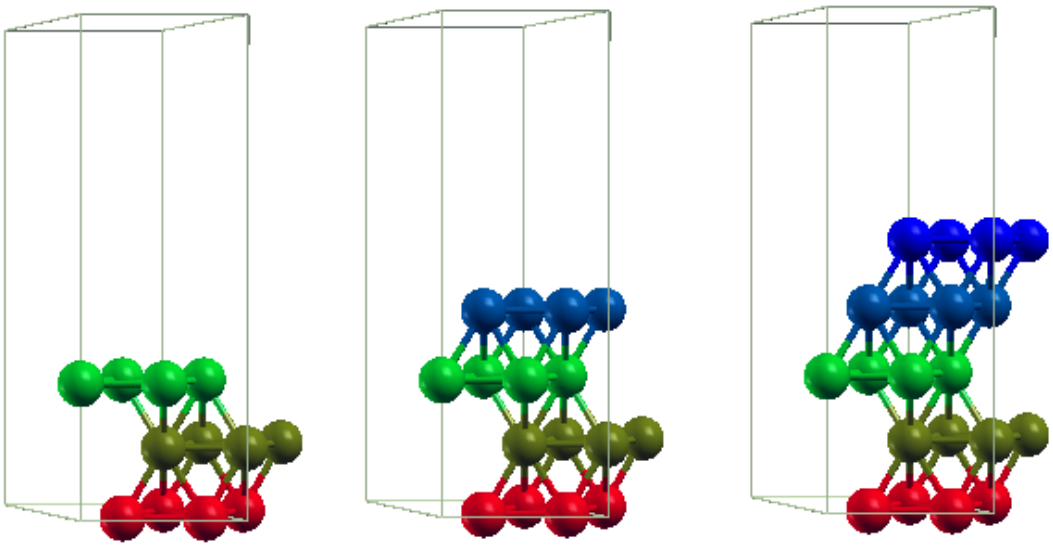

Figure 3.22: increasing thickness of the slab, with fixed supercell's volume

The thickness of the vacuum has to be large enough to avoid electron density overlapping but a larger vacuum spacing also means more computational effort is needed. The grater is the distance between facing surfaces and the better is the slab model, since interactions between the surfaces only represent a physical phenomenon whose origin is exclusively due to the periodic framework that is needful to mathematically solve the Kohn-Sham equations with the aid of periodic plane waves [Figure 3.23].

Several calculations should be done by increasing the vacuum spacing until the plane surface's energy of formation becomes quite constant, according to the convergence criteria. Often a vacuum of 10-15 Angstrom is large enough to allow electron density to tail off.

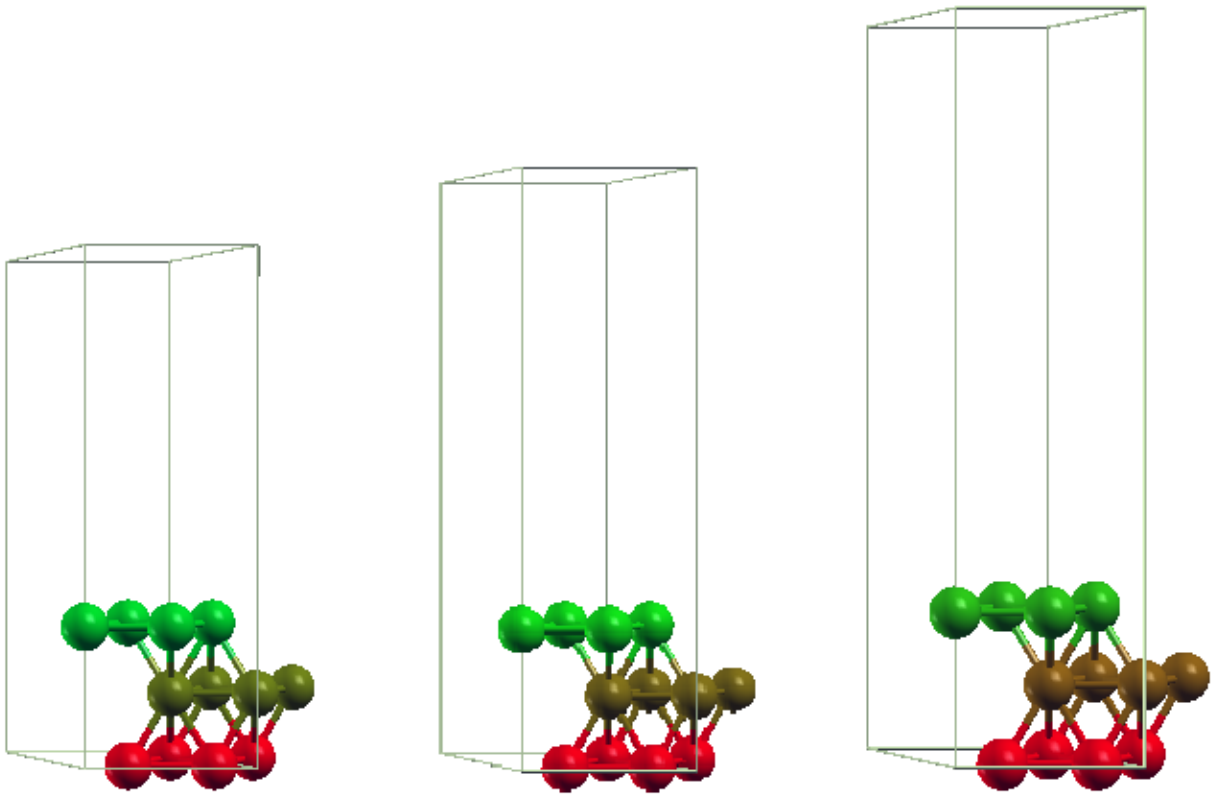

Figure 3.23: three layers slab model with larger vacuum

The kind of plane affects the interatomic distance along z axis and the number of atoms that have to be used to build the monolayer, it also affects the length of the x-y lattice vectors.

3.8 Methods to Geometrically Build a Slab

If a certain surface of a face centered cubic metal needs to be reproduced, by placing atoms inside a reference coordination system it's clearly necessary to know where atoms are positioned at least in the elemental cubic framework.

Inside the fcc cell the plane with Miller index (100) is drawn.

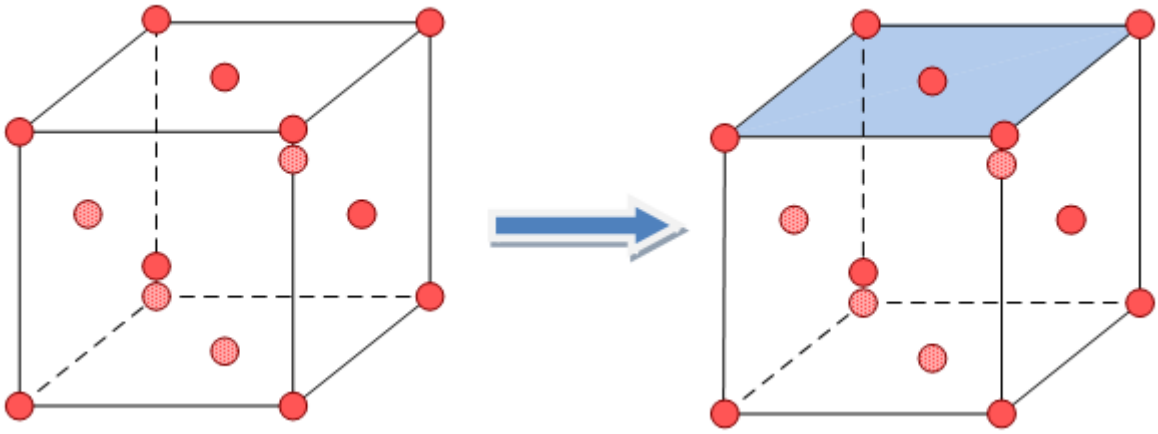

Figure 3.24: cleavage of the bulk to create a (100) surface

The blue square is seen from an upper point of view, and inserted in a reference system with x-y-z axes mutually orthogonal.

The crystal vectors are:

$$\boldsymbol{v}_1 = a(1,0,0) \tag{3.13}$$

$$\boldsymbol{v}_2 = a(0,1,0) \tag{3.14}$$

$$\boldsymbol{v}_3 = a(0,0,c/a) \tag{3.15}$$

"a" is the usual lattice parameter, instead "c" is the total height of the supercell.

These vectors define the Bravais' tetragonal unit cell and allow to move from an atom of the same layer of the 100 plane to another (3.13), (3.14), thus the position of the other atoms can be spanned by the vector:

$$\boldsymbol{r} = n_1\boldsymbol{v}_1 + n_2\boldsymbol{v}_2 \tag{3.16}$$

With n_1 and n_2 scalar integers.

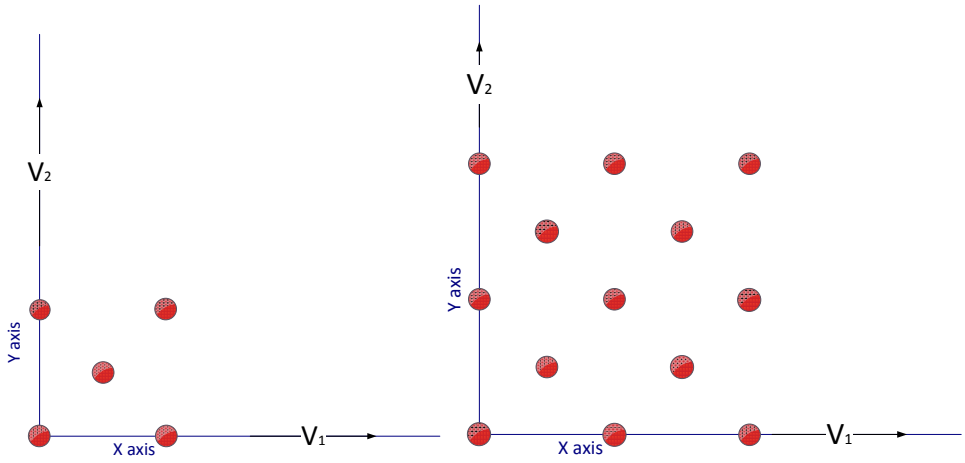

Figure 3.25: upper view of the (100) layer, and periodic system

An upper view in Figure 3.26 shows how each atom is organized in a square framework, but some atoms belong to the first layer of the cubic cell, others to the second, and the remaining to the third atomic level.

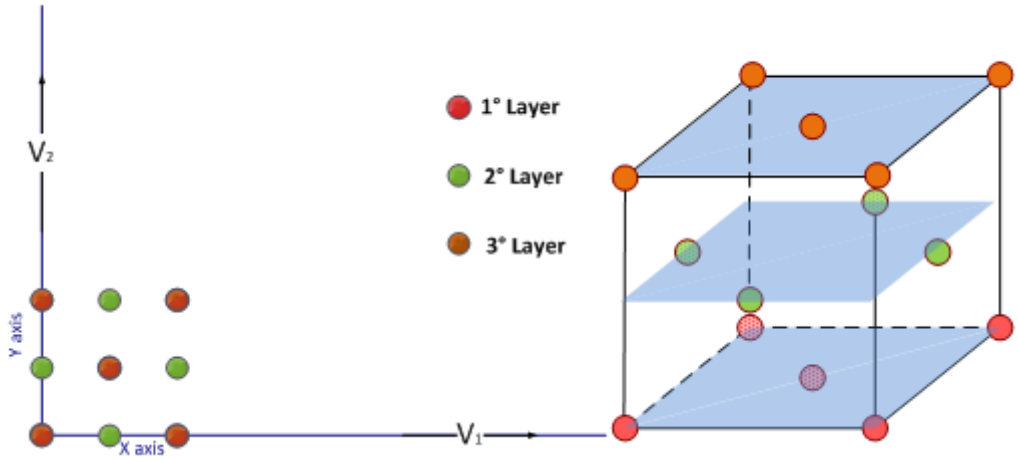

Figure 3.26: upper and lateral view of the reference cube, (100) surface

The red dots of the first layer are not visible because the x-y coordinates of the atoms that form the third layer are identical. In this case, that is surface (100) and 1x1 slab, the edge of the cubic cell is the "lattice constant" and affects the size of the whole cell, so to make a more practical methodology the atomic coordinates are written as fractional coordinates with respect to the lattice constant "a". If different metals with various lattice constants are studied, spatial coordinates of their atoms change, depending on the lattice constant parameter, instead if atoms' coordinates are rewritten in terms of fractional coordinates, where the denominator is the length of the edge of the supercell, no problem is met and no dependence on lattice parameter is found.
Since the lattice constant could be a multiple of the edge of the tetragonal cell, if 2x2 or 3x3 slabs are desired, it is common to call this edge in a more general way, "alat" [Figure 3.27]. To avoid atoms to overlap because of the periodic translation of the supercell along the crystal vectors, a remark is put on the spatial symmetry: shared atoms are not considered in the unit cell.

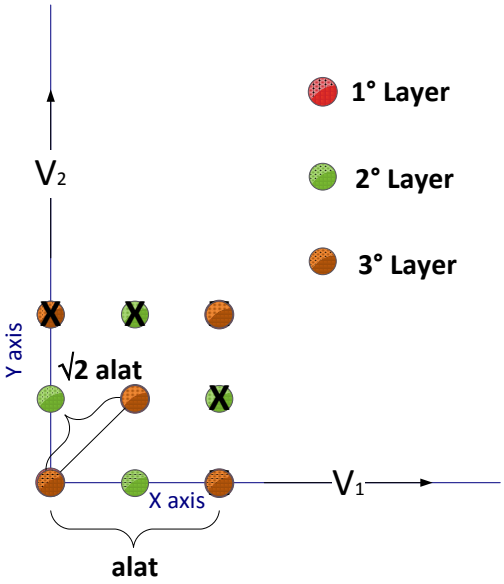

Figure 3.27: distances and geometrical properties of a (100) surface

If the slab has three layers and only two atoms per layer it is the essential brick that can reproduce a (100) surface by translation along $\mathbf{v}_1$ and $\mathbf{v}_2$, so it is a 1x1 slab.

After these considerations, atomic positions in the reference system of fractional coordinates will be easy to be defined; as reported in Table 3.5.

slab 1x1	X	Y	Z	Layer
Me	0.0	0.0	0.0	1
Me	0.5	0.5	0.0	1
Me	0.0	0.5	0.5	2
Me	0.5	0.0	0.5	2
Me	0.0	0.0	1.0	3
Me	0.5	0.5	1.0	3

Table 3.5: fractional coordinates of a (100) 1x1 slab with three layers

"Me" stands for "metal", and since x-y atomic coordinates of the first and third layers are the same, if the first layer's atoms were lifted from z = 0 to z = 1 the third layer is thus created. The same concept can be adopted to produce the fourth layer as a translation from z = 0.5 to z = 1.5 of the second layer in order to give birth to an AB-AB-AB frame.

If a 2x2 or a 3x3 or a NxN supercell is required to reach a suited level of coverage the 1x1 supercell can be used as a brick of the desired supercell:

- a 1x1 slab of M layers is considered,
- the new "alat" is a multiple of the "alat" value of the 1x1 supercell:

$$alat_{NxN} = N \cdot alat_{1x1} \tag{3.17}$$

- all fractional coordinates are multiplied by 1/N,
- then the atoms of the 1x1 supercell are translated along the crystal vectors $\mathbf{v}_1$ and $\mathbf{v}_2$.

A 2x2 supercell can be seen as a coupling of 4 1x1 supecells:

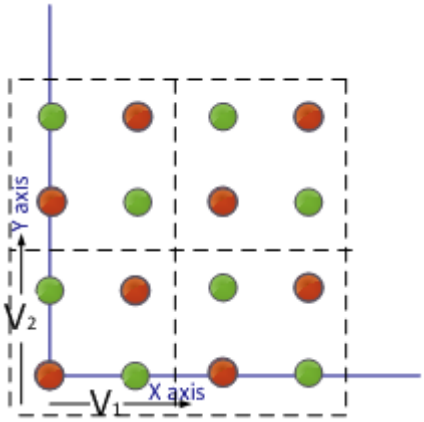

Figure 3.28: upper view of a 2x2 slab

If 3 layers are desired the fractional coordinates will be:

slab 2x2	X	Y	Z	Layer
Me	0.00	0.00	0.00	1
Me	0.25	0.25	0.00	1
Me	0.00	0.25	0.25	2
Me	0.25	0.00	0.25	2
Me	0.00	0.00	0.50	3
Me	0.25	0.25	0.50	3
TRANSLATION ALONG $\mathbf{v}_1$				
Me	0.50	0.00	0.00	1
Me	0.75	0.25	0.00	1
Me	0.50	0.25	0.25	2
Me	0.75	0.00	0.25	2
Me	0.50	0.00	0.50	3
Me	0.75	0.25	0.50	3
TRANSLATION ALONG $\mathbf{v}_2$				
Me	0.00	0.50	0.00	1
Me	0.25	0.75	0.00	1
Me	0.00	0.75	0.25	2
Me	0.25	0.50	0.25	2
Me	0.00	0.75	0.50	3
Me	0.25	0.75	0.50	3
TRANSLATION ALONG $\mathbf{v}_1 + \mathbf{v}_2$				
Me	0.50	0.50	0.00	1
Me	0.75	0.75	0.00	1
Me	0.50	0.75	0.25	2
Me	0.75	0.50	0.25	2
Me	0.50	0.75	0.50	3
Me	0.75	0.75	0.50	3

Table 3.6: fractional coordinates of a (100) 2x2 slab with three layers

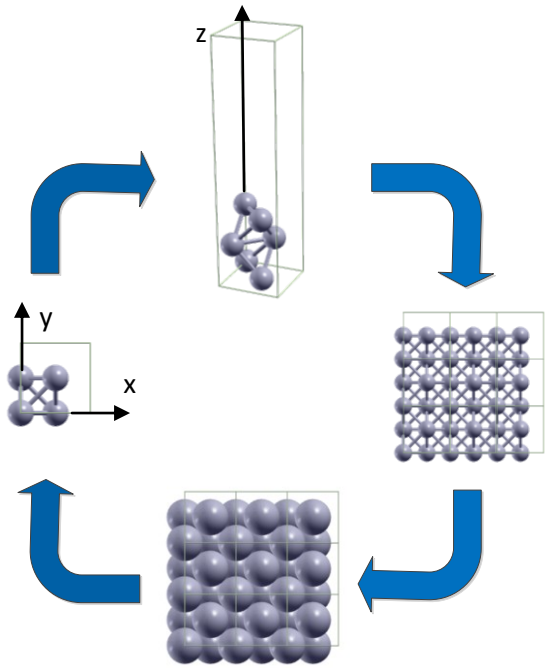

Figure 3.29: single supercell and periodic framework of a (100) surface

If (111) surface needs to be created the steps are the same, first the fcc cube is opportunely cleaved:

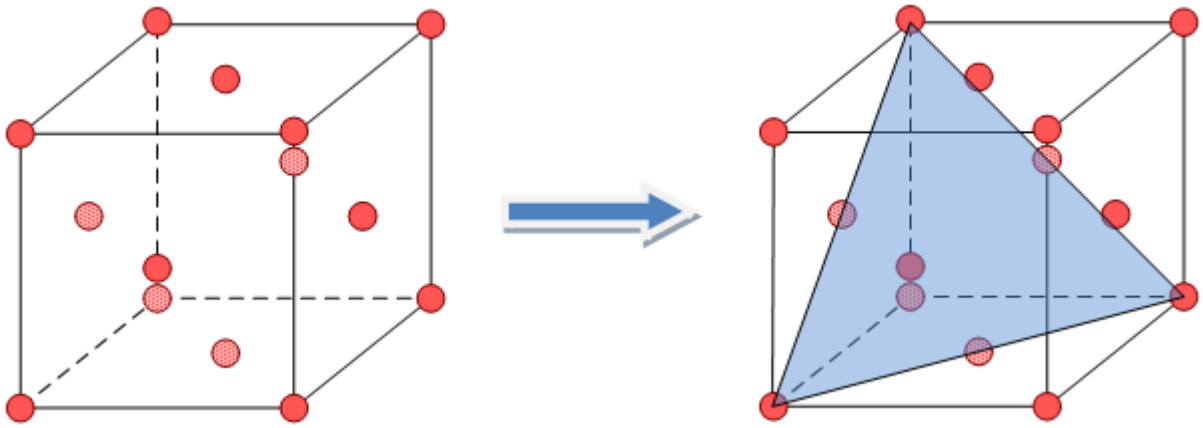

Figure 3.30: cleavage of the bulk to create a (111) surface

This time crystal vectors are:

$$\boldsymbol{v}_1 = a(1,0,0) \tag{3.18}$$

$$\boldsymbol{v}_2 = a(\cos(60°), \sin(60°), 0) \tag{3.19}$$

$$\boldsymbol{v}_3 = a(0,0,c/a) \tag{3.20}$$

These new vectors define the Bravais' trigonal unit cell, and if three layers are represented the upper view is the following:

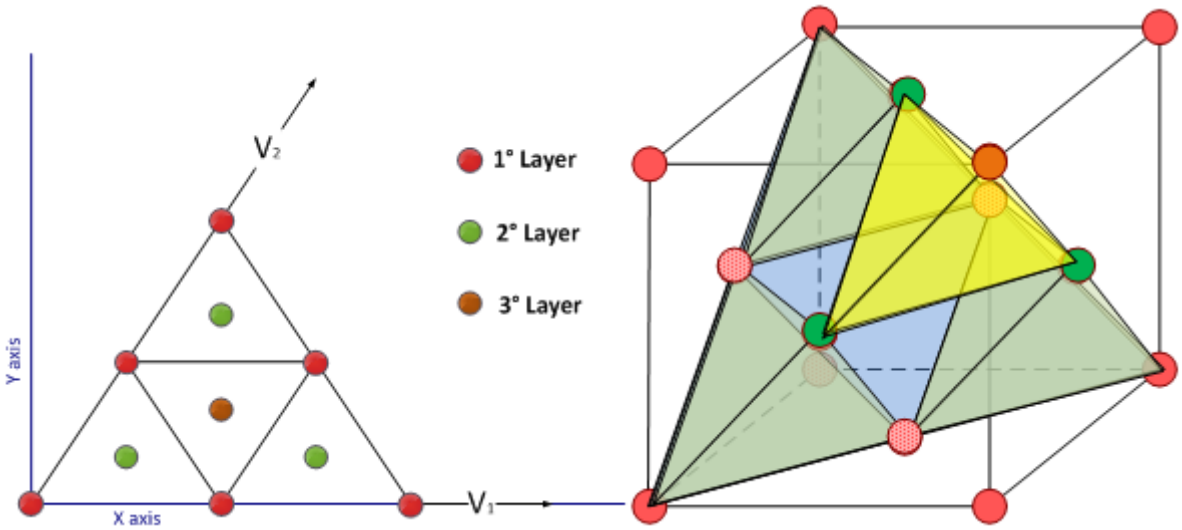

Figure 3.31: upper and lateral view of the reference cube, (111) surface

To make a 1x1 supercell and to prevent atoms from overlapping some atoms are erased:

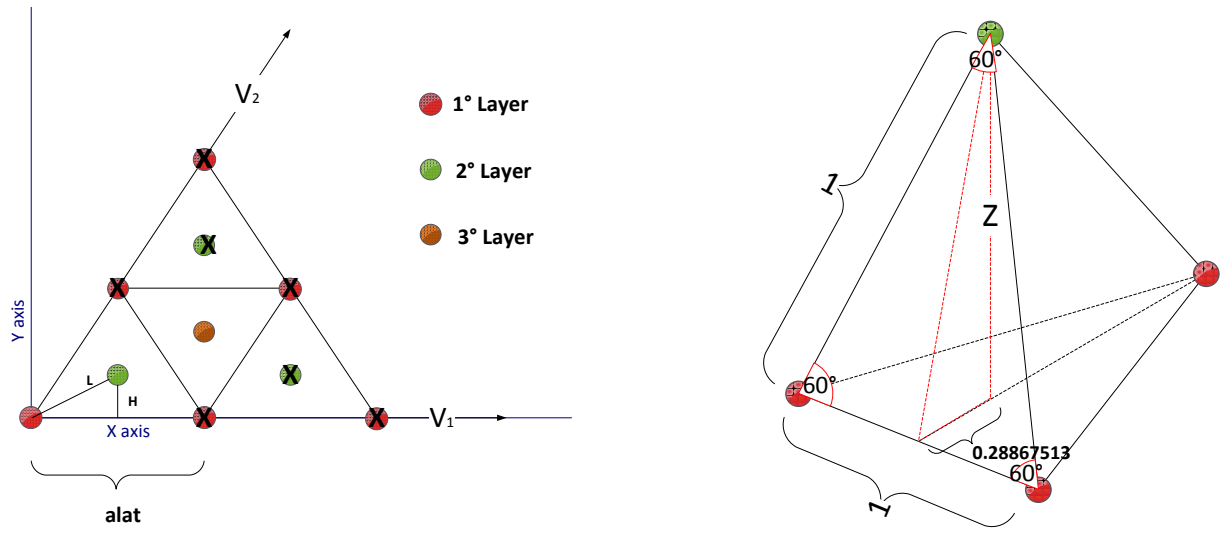

Figure 3.32: distances and geometrical properties of a (111) surface

This time the geometrical definition of the atomic positions appears less intuitive:

- "alat" is the half part of the diagonal of the cube's face:

$$alat = lattice\ constant \cdot \frac{\sqrt[2]{2}}{2} \tag{3.21}$$

- L and H are determined by the following formula:

$$H + L = alat \cdot \sin(60°) \rightarrow H' + L' = \sin(60°) \tag{3.22}$$

$$L' \cdot \sin(30°) + L' = \sin(60°) \rightarrow L' = \frac{L}{alat} = \frac{\sqrt[2]{3}}{3} = 0.57735027 \tag{3.23}$$

$$H' = \sin(60°) - L' = 0.28867513 \tag{3.24}$$

- The interlayer distance is the height of the tetrahedron:

$$z = \sqrt[2]{(\cos(30°))^2 - (L' \cdot \sin(30°))^2} = 0.816496581 \tag{3.25}$$

As well as the previous example the atomic coordinates of a 1x1 slab of three layers are listed in the following table:

slab 1x1	X	Y	Z	Layer
Me	0.0	0.00000000	0.000000000	1
Me	0.5	0.28867513	0.816496581	2
Me	1.0	0.57735027	1.632993162	3

Table 3.7: fractional coordinates of a (111) 1x1 slab with three layers

Each layer can be characterized by just one atom, and further layers can be added by lifting the previous in an ABC-ABC-ABC fashion.

slab 1x1	X	Y	Z	Layer
Me	0.0	0.00000000	0.000000000	1
Me	0.5	0.28867513	0.816496581	2
Me	1.0	0.57735027	1.632993162	3
Me	0.0	0.00000000	0.000000000+0.816496581	4
Me	0.5	0.28867513	0.816496581+0.816496581	5
Me	1.0	0.57735027	1.632993162+0.816496581	6

Table 3.8: fractional coordinates of a (111) 1x1 slab with six layers

If the creation of a greater supercell is desired, as well as (100) surface, the problem may be always handled with a general NxN supercell, built by N^2 1x1 supercells, translated N times along $\mathbf{v}_1$ and $\mathbf{v}_2$.

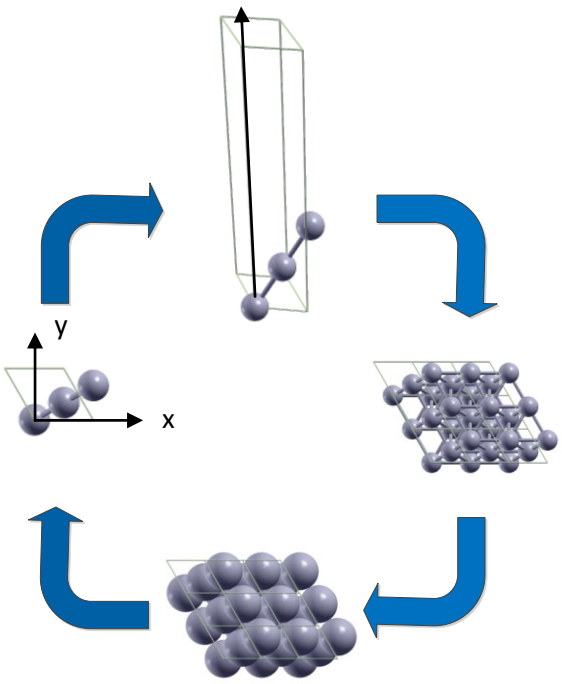

Figure 3.33: single supercell and periodic framework of a (111) surface

The last low-index surface one should refer to is the one defined by (110) Miller index, by cleaving the bulk the blue square stands out six atoms:

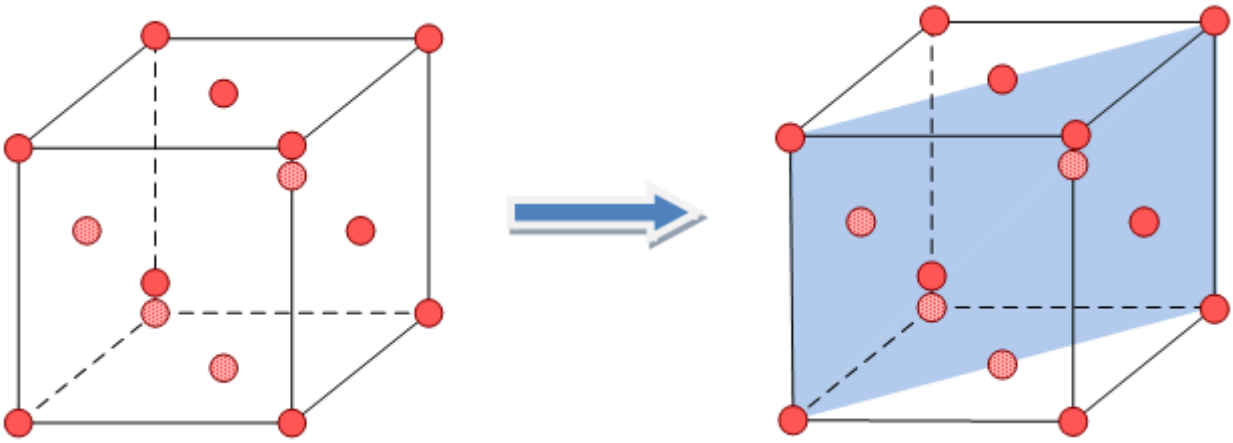

Figure 3.34: cleavage of the bulk to create a (110) surface

This time crystal vectors are:

$$\boldsymbol{v}_1 = a(1,0,0) \tag{3.26}$$

$$\boldsymbol{v}_2 = a(0, \mathrm{b/a}, 0) \tag{3.27}$$

$$\boldsymbol{v}_3 = a(0,0,c/a) \tag{3.28}$$

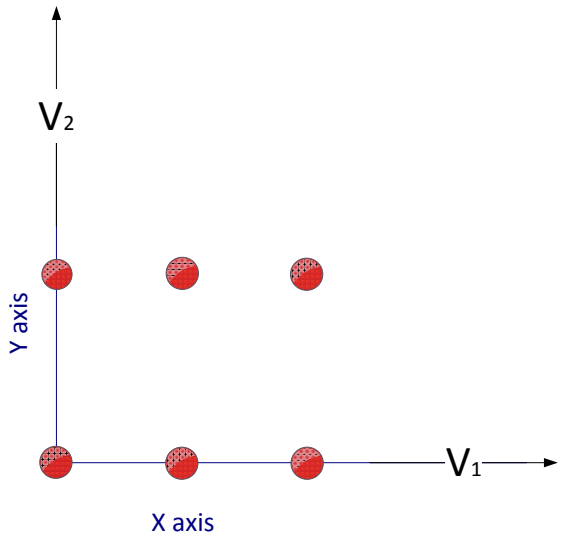

Figure 3.35: upper view of the (110) layer

These new vectors define the Bravais' orthorhombic unit cell, and if three layers are represented the upper view is reported in Figure 3.36:

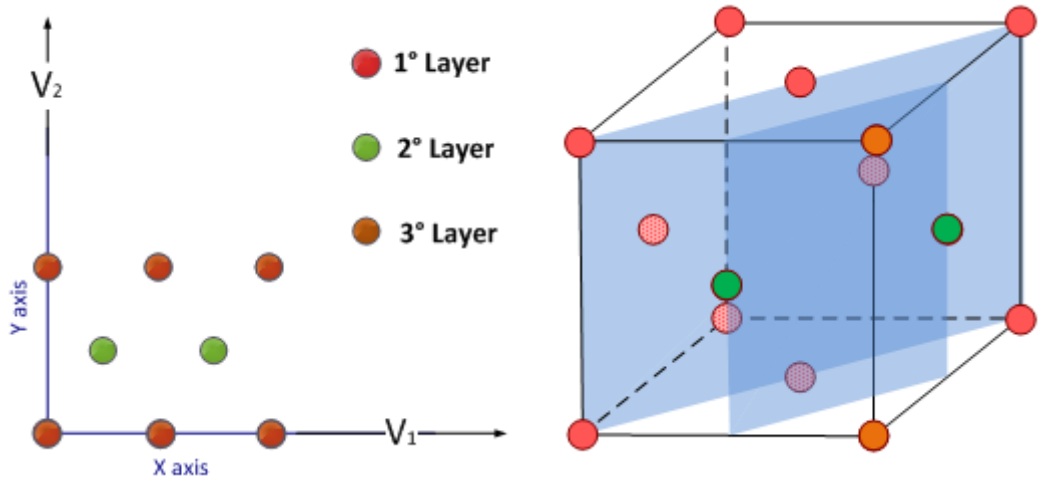

Figure 3.36: upper and lateral view of the reference cube, (110) surface

The first and the third layer are composed by atoms that experience the same x-y coordinates, since they seem completely overlapped from an upper point of view [Figure 3.36].
Now a 1x1 supercell is going to be built, opportunely eliminating redundant atoms:

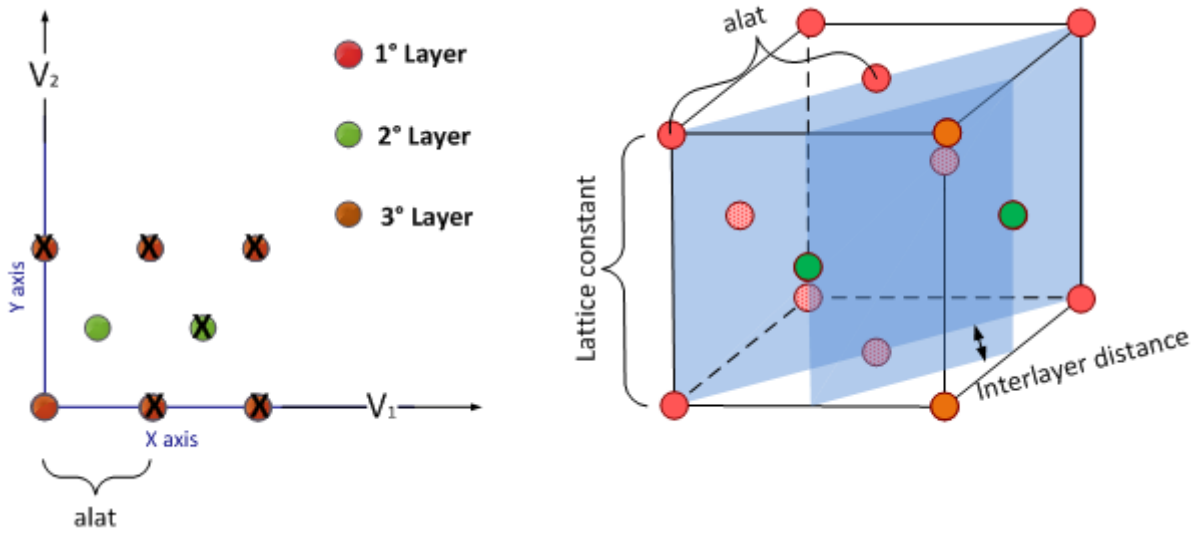

Figure 3.37: distances and geometrical properties of a (110) surface

Fractional coordinates are easy to define, starting from geometrical peculiarities of the square, as identical sides and right-angles:

- "alat" is half time the diagonal of the square, thus:

$$alat = lattice\ constant \cdot \frac{\sqrt[2]{2}}{2} \tag{3.29}$$

- b, according to crystal vectors is √2.
- The interlayer distance is half time the diagonal of the square.

The atomic coordinates of a 1x1 slab of three layers are:

slab 1x1	X	Y	Z	Layer
Me	0.0	0.00000000	0.0	1
Me	0.5	0.70710678	0.5	2
Me	0.0	0.00000000	1.0	3

Table 3.9: fractional coordinates of a (110) 1x1 slab with three layers

It is possible to notice that a (110) slab requires just one atom per layer, and as previously illustrated, layers can be added by lifting the first and the second level (AB-AB-AB), instead the amplitude of the unit cell can be varied generating atomic coordinates of a generic NxN, starting from a 1x1, revised by normalizing fractional coordinates by 1/N, and translating the unit cell along the orthorhombic crystal vectors.

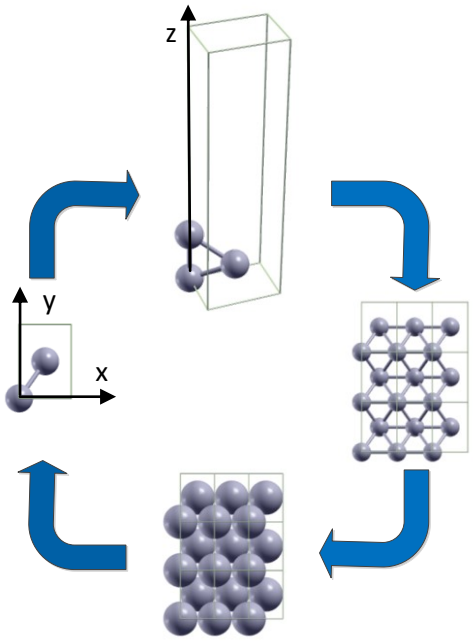

Figure 3.38: single supercell and periodic framework of a (110) surface

3.9 Surface Relaxation

Up to now, the ionic positions have been held fixed while relaxing the electronic configuration to its ground state. In fact, atoms are placed inside the supercell to build a slab whose atomic positions are the ideal bulky-like positions for the material where the distance between any two adjacent layers is always identical. Although, if the bulk continuity is interrupted there is no guarantee that the layers of the slice of surface must preserve the same spacing, atomic coordination of the superficial atoms in reduced indeed, and a phenomenon called relaxation may occur.
Relaxed atomic structure performs an alteration of the first layer, facing to the vacuum space; the atomic structure remains the same as in the bulk, but the interatomic and relative distance between the first and the second layer changes.
In most cases the abrupt termination of a surface in the direction of the surface normal leads to a dramatic change in coordination of the atoms and this leads to a decrease in the distance between the first and second atomic layer [40]. Smoluchowski smoothing at metal surfaces explains how the charge density will be redistributed such the charge is moved from the regions directly above the atom cores to the regions between the atoms, in fact atoms in the surface layer feel a charge imbalance that produces an inward electrostatic force.

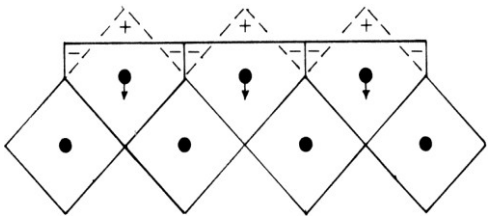

Figure 3.39: redistribution of the electron charge density, from [40]

Instead the deviation from the bulk interlayer distance decreases with depth for deeper layers, since the material shows a chemical and physical behavior that is strictly linked to the bulk structure.

Atoms allowed to relax to equilibrium actually move, therefore the relaxation is a full dynamical simulation of the ionic system, where the path from the initial state towards the final state is

uninteresting. The relaxed surface has a lower energy than the original, ideal surface, and its geometry can be found by performing an energy minimization.
The degree of relaxation physically depends on:

- The nature of the solid matter (metals, alloys, oxides or salts),
- The crystallographic structure,
- The kind of surface relaxed.

Oxides use to behold important displacement, up to 10-20% of the interplanar distance, so if a surface of oxide of aluminum wants to be studied this important behavior has to be accounted for, unless the mathematical model won't be able to properly trace the surface's capability to participate in the substrate-adsorbate interaction. This interaction due to the outward relaxation is less felt if a metal is involved, in fact in the following lines are reported the percentage of vertical relaxation for a slab model 2x2 4 layers (111) surface:

	Pt	Rh	Ni
Z4i-Z3i [Angstrom]	2.3097359	2.227245	2.028657
Z4f-Z3f [Angstrom]	2.3286737	2.194311	2.018434
Variation %	0.8199123	-1.478710	-0.503920

Table 3.10: z-relaxation of the 4th layer of a (111) 2x2 slab, with 3 x-y-z fixed layers

Where Z4i-Z3i is the bulk interlayer spacing and Z4f-Z3f is the interlayer spacing between layers 3 and 4 after relaxation. The "Variation %" is:

$$Variation\ \% = 100 \cdot \frac{(Z4f - Z3f) - (Z4i - Z3i)}{(Z4i - Z3i)} \tag{3.30}$$

Forces affected by atoms of the first layer are not zero since the surface is a simply bulk-truncated surface, but after the minimization they are set to zero whilst forces acting on the lower atoms are still non zero since their positions are fixed in a bulkylike fashion.
No displacement in Figure 3.40 can be seen with naked eye since metals sense very little relaxation, in particular closed surface with low index and high atomic coordination.

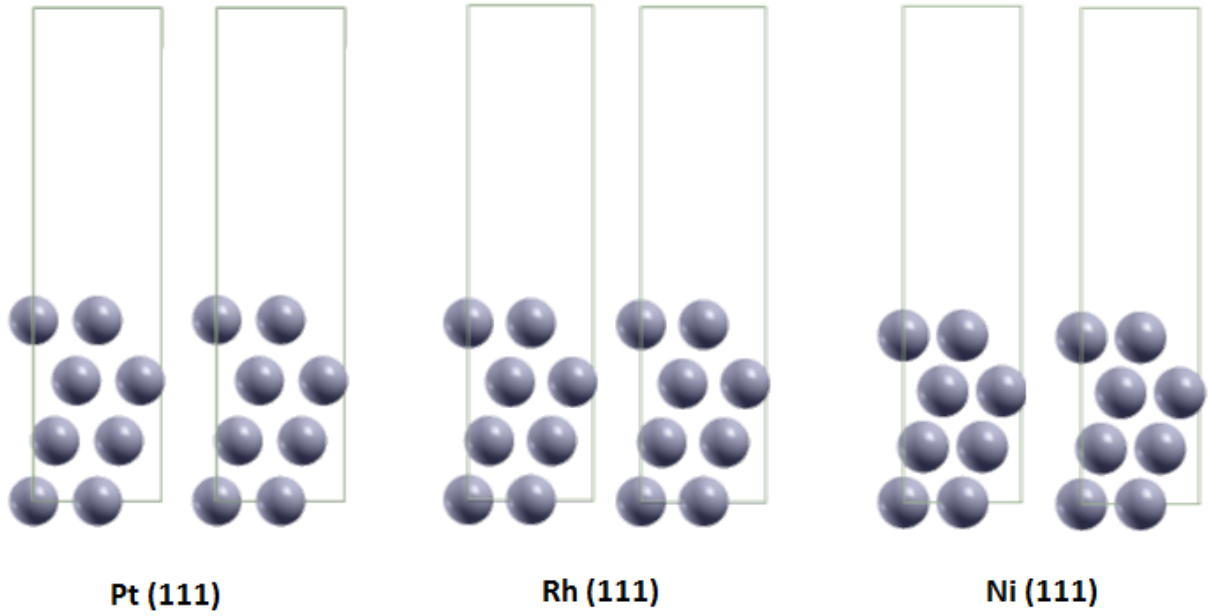

Figure 3.40: imperceptible relaxation of the upper layer of Platinum, Rhodium and Nickel

3.10 Chemical Adsorption

Chemical or physical adsorption appears to be the fundamental issue of heterogeneous catalysis because a reaction path starts from a configuration that often sees atoms or molecules bound with the atoms of the catalyst, thus an optimum design of it requires a deep understanding of the surface geometry and chemistry [41]. A solid material, even if it is considered having a perfect structure, reveals an heterogeneous distribution of the surface energy, with different kinds of active sites of adsorption, some stronger and others weaker. A chemical bond is formed between the adsorbate and the adsorbent, and the binding energy can be calculated in order to state the stability of the whole electronic structure and the effective strength of the active site. The larger is the binding energy and the more stable is the atomic configuration considered, since nature tends to minimize the energy expense the structure with lower energetic content will also be the most likely one.

Different surfaces characterized by Miller index are provided with different atomic disposition and thus various kind and uneven density of active sites. The coordination number and the number of

atoms per unit surface's area affects the geometry of the adsorbate and may provoke a weak interaction because of steric hindrance or an intense bound due to a multisite adsorption. A weak chemisorption bond can lead to the desorption of the molecule instead a too strong bond can prevent the release of the product and the regeneration of the site, with consequences on the kinetic of reaction and possible deactivation of the catalyst.

DFT allows to determine the value of the binding energy by calculating the total energy of the system, first of all some particular sites can be identified thanks to their special symmetry and appealing geometry as:

- on top site,
- bridge site (long/short),
- fcc site (threefold),
- hcp site (threefold),
- hollow site (fourfold).

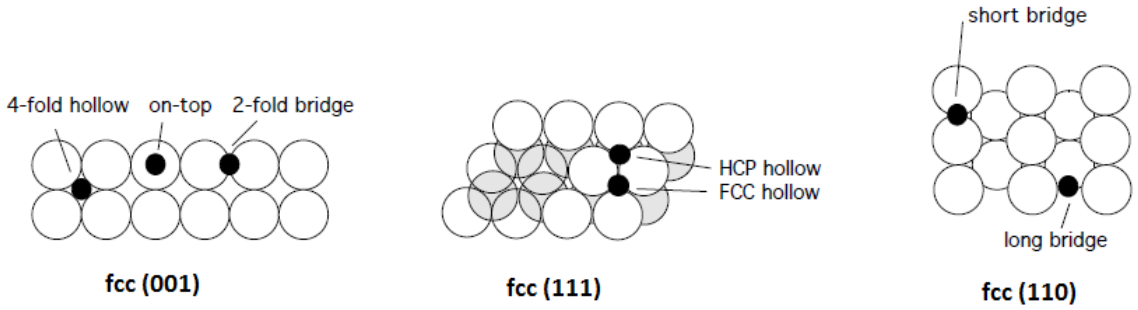

Figure 3.41: important symmetric sites of adsorption, adapted from [41]

With periodic boundary conditions in plane wave methods, it is impossible to model any kind of truly random arrangement of adsorbates, although in nature adsorbates on crystal surfaces often exhibit long-range ordering, especially at low temperatures, so it is possible for calculations to mimic real systems in many cases. A further issue is that the size of the supercell is limited and thus it defines the distance between neighboring adsorbates, in fact putting one adsorbate in a supercell means that each adsorbate feels a copy of itself in each of the neighboring supercells, and if the distance is very low the binding energy will be deeply subject to adsorbate-adsorbate interaction. Therefore an important contribution to the adsorption energy lies into the surface coverage effect which is quantified by the monolayer fraction.

The coverage θ is defined as:

$$\theta = \frac{Number\ of\ occupied\ adsorption\ sites}{Number\ of\ adsorption\ sites} \tag{3.31}$$

A monolayer of coverage means that all the adsorption sites of the x-type existing in the supercell are no longer available, that is to say θ = 1, thus:

- 0.50ML only half of the x-type sites interact with an adsorbate,
- 0.25ML only one quarter of x-type sites interact with an adsorbate,
- 0.10ML only one tenth of x-type sites interact with an adsorbate.

Reducing the coverage the size of the cell will increase to contain a greater number of active sites on the portion of surface that is periodically repeated in the space. Greater supercells need more atoms and as consequence the computational time increases, thus the determination of coverage effects may require notable effort and time machine.

- To define a 1ML supecell a 1x1 slab is sufficient,
- To create a 0.25ML supercell a 2x2 slab is required,
- By decreasing to a 1/9ML a 3x3 slab has to be built.

To calculate the binding energy the adsorbate has to be spatially located inside the supercell, where only the positions of the atoms belonging to the slab are well defined. Since the adsorbate geometry may be unknown the adsorbate's structure has to be relaxed to a local minimum, even the slab structure can be simultaneously relaxed, but as remembered before, the greater is the number of the moving atoms and harder becomes the minimization of the system's total energy.

Since different local minima are eligible it is of good practice to avoid symmetry-induced trap by deliberately breaking the symmetry of atom's coordinates, in fact the OH group when adsorbed on a Pt (111) surface, on a top site, appears to be tilted, but if the hydroxyl is initially perfectly vertical the system will relax to a different local minimum, with a higher energy, thus less stable, due to the lack of forces acting on both H and O atoms, parallel to the plane surface.

The calculation of the binding energy referred to a new example, that involves carbon monoxide, requires determining:

- The total energy of the CO molecule that is positioned inside a big enough cell to avoid self interaction with the neighboring copies,
- The total energy of the supercell containing the slab's atoms,
- The total energy of the system slab+CO adsorbed.

The binding energy can be expressed by the following formula:

$$E_{bind} = BE = E_{slab}^{adsorbate} - [E_{slab} + E^{adsorbate}] \tag{3.32}$$

This quantity is the amount of energy required to pull an adsorbate off the surface into the gas phase, and it can be a negative number if the adsorption process is lower in total energy compared to the bare surface, thermodynamically this means that the adsorption is favorite because the energy associated with the sum of the isolated gas phase species and the slab energy is greater than the total energy of the system in which the adsorption occurs.

It is quite obvious that calculations have to be performed with the same cutoff energy, and the same k-point grid, at least for the slab and slab+CO supercell, since the spatial volume and the reciprocal one are the same, in addition the fixed and moving atoms belonging to the surface must be identical both in the slab and slab+CO supercell, otherwise the total energy cannot be compared in a rational way.

Binding energies have been computed on the three reference metals, Pt, Rh and Ni for the following species: C, O, H, CO, CO_2, COOH, H_2O. The binding energy is the one related to the most stable site for the selected adsorbate on a certain metal whose bulk is cleaved to exhibit (111) surface.

The selected model uses:

- A 2x2 slab,
- Vacuum of 12 Angstrom,
- 3 fixed layers,
- Coverage 0.25 ML,
- Energy cutoff of 40 Ry,
- Monkhorst-Pack 8x8x1 k-point grid.

	Pt	Rh	Ni
C	-6.825 eV (fcc)	-7.032 eV (hcp)	-7.027 eV (fcc)
O	-4.381 eV (fcc)	-5.010 eV (fcc)	-5.710 eV (fcc)
H	-2.740 eV (top)	-2.797 eV (fcc)	-2.905 eV (fcc)

Table 3.11: BE, binding energy of atomic and molecular species, C, O, H, on Pt, Rh, Ni and in the most stable adsorption site

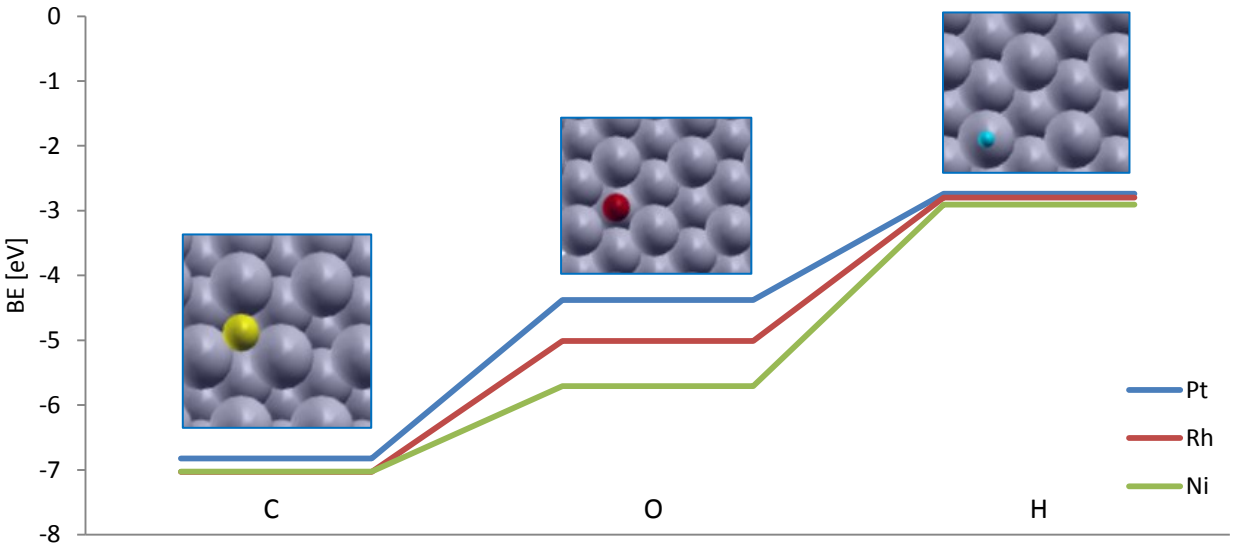

Figure 3.42: BE of atomic and molecular species, C, O, H; the four pictures are referred to Platinum

The chemisorption of carbon (yellow atom) on the metallic surfaces is very strong, the bond length is almost 1 Å for all the three metals, instead the binding energy of the oxygen chemisorptions (red atom) is strongly metal-dependent, the vertical distance from the upper layer is 1.1 (Pt, Ni)-1.3 (Rh) Å.

Hydrogen (blue atom) interacts with metals in a very similar way, its heats of adsorption vary smoothly on the slab surface in fact H has a considerable mobility, the vertical distance is almost 1 (Rh, Ni)-1.5 (Pt) Å. Even carboxyl binding energy does not show a substantial metal dependence, its stable geometry is the trans configuration, with H pointing at a top site, and the carbon bonded with a top at 1.8 (Ni)-2 (Pt, Rh) Å distance.

	Pt	Rh	Ni
CO	-1.797 eV (hcp)	-1.883 eV (hcp)	-2.118 eV (hcp)
CO_2	-0.053 eV (top)	-0.027 eV (top)	-0.033 eV (top)
COOH	-2.317 eV (top)	-2.510 eV (top)	-2.473 eV (top)

Table 3.12: BE, binding energy of molecular species, CO, CO_2, COOH, on Pt, Rh, Ni and in the most stable adsorption site

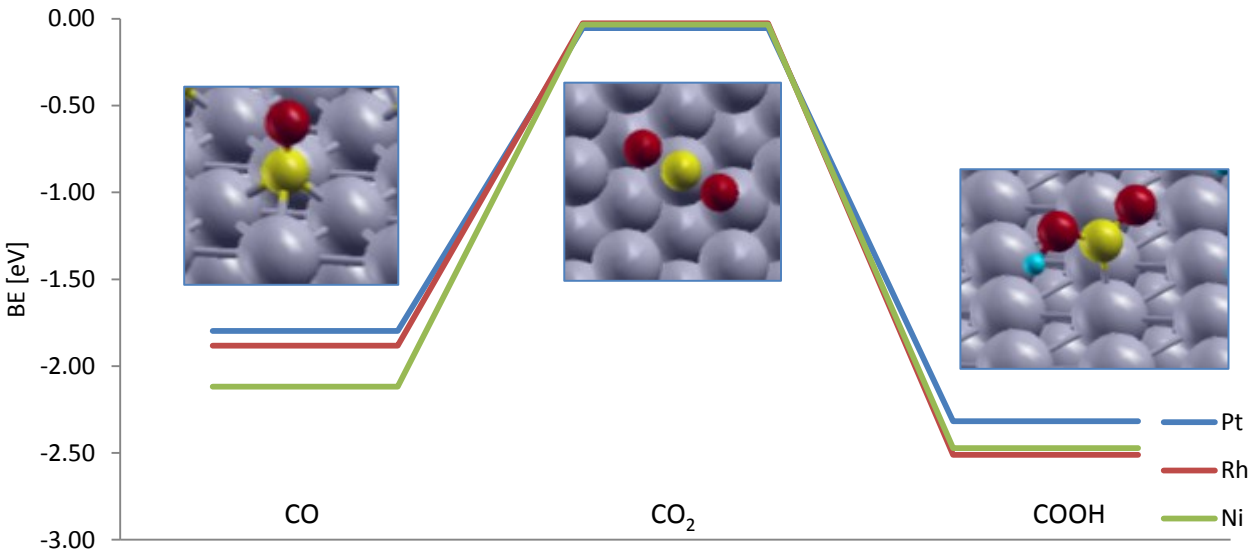

Figure 3.43: BE of molecular species (CO, CO_2, COOH) show different substrate-adsorbate affinity, the three pictures are referred to Platinum

The binding energy of CO depends on the different substrate-adsorbate interaction, the C-O bond length is 1.19 Å in all cases, instead the z distance from the surface is 1.3 (Ni)-1.4 (Pt, Rh). CO_2 instead has a very weak feeling with the substrates, in fact it is a closed shell molecule, with all molecular orbitals doubly occupied. CO_2 remains at almost 4.00 Å far above the surface, and the C-O bond length is 1.17 Å either on Pt, or Rh or Ni, carbon dioxide does not interact with surface and as consequence the C-O bond is the same of a CO_2 gas phase molecule. The CO_2 closed shell structure prevents the molecule to establish a chemical bond with the metal surface, although the real adsorbate-substrate interaction is due to van der Waals forces that are not accurately described by GGA functionals, thus the binding energy is actually underestimated.

Although, the search of the lowest energy configuration may be not so easy, if two or more chemical species are co-adsorbed, the larger is the supercell, the more abundant is the number of kinds of sites and the many more are the adsorbates, as consequence the greater are the possible combinations to be evaluated. It has been observed by experimental evidences that intermolecular interactions frequently lead to the formation of ordered layers strongly dependent on the level of coverage, in fact at medium coverage most adsorbates begin to order themselves, so that the adsorbate exhibits a unit cell. Ordered adsorbate layers are normally described in relation to the substrate's elementary cell and are usually called "adlayers".

3.11 Investigation of the Substrate-Adsorbate Interaction with PDOS

A chemical bond exists if the spacing between two atoms becomes so small that the electron wave functions overlap, as consequence the energy level of an isolated atom splits into bonding and antibonding molecular orbitals with lower and higher energy than the original level. The bonding molecular orbital is more stable than the atomic orbital and encourages the bonding whereas the antibonding is less stable and hinders the bond formation.
If electrons of atomic species are shared with the atoms of the metal surface and if electronic states overlap in order to create sharp peaks, evidence of bonding or antibonding molecular orbitals appears.

The metal-adsorbate interaction can be examined by the analysis of the PDOS of atomic carbon, atomic oxygen, atomic hydrogen, carbon monoxide, carbon dioxide and carboxyl group to provide an explanation to the trends in binding energies depicted in Figure 3.42, Figure 3.43.

Atomic Carbon

If the density of states is projected onto the "p" orbitals of an atom of carbon, in gas phase, just a sharp peak appears [Figure 3.44 (A)], this peak is split in bonding and antibonding when the "p" valence sates feel the d-bands of the substrate [Figure 3.44 (B-C-D)]. The peak of bonding states is below the Fermi Energy (FE), instead the antibonding states are shifted through the Fermi level, as consequence the antibonding states are empty and the metal-adsorbate interaction is always strong, and slightly affected by the choice of the metal.

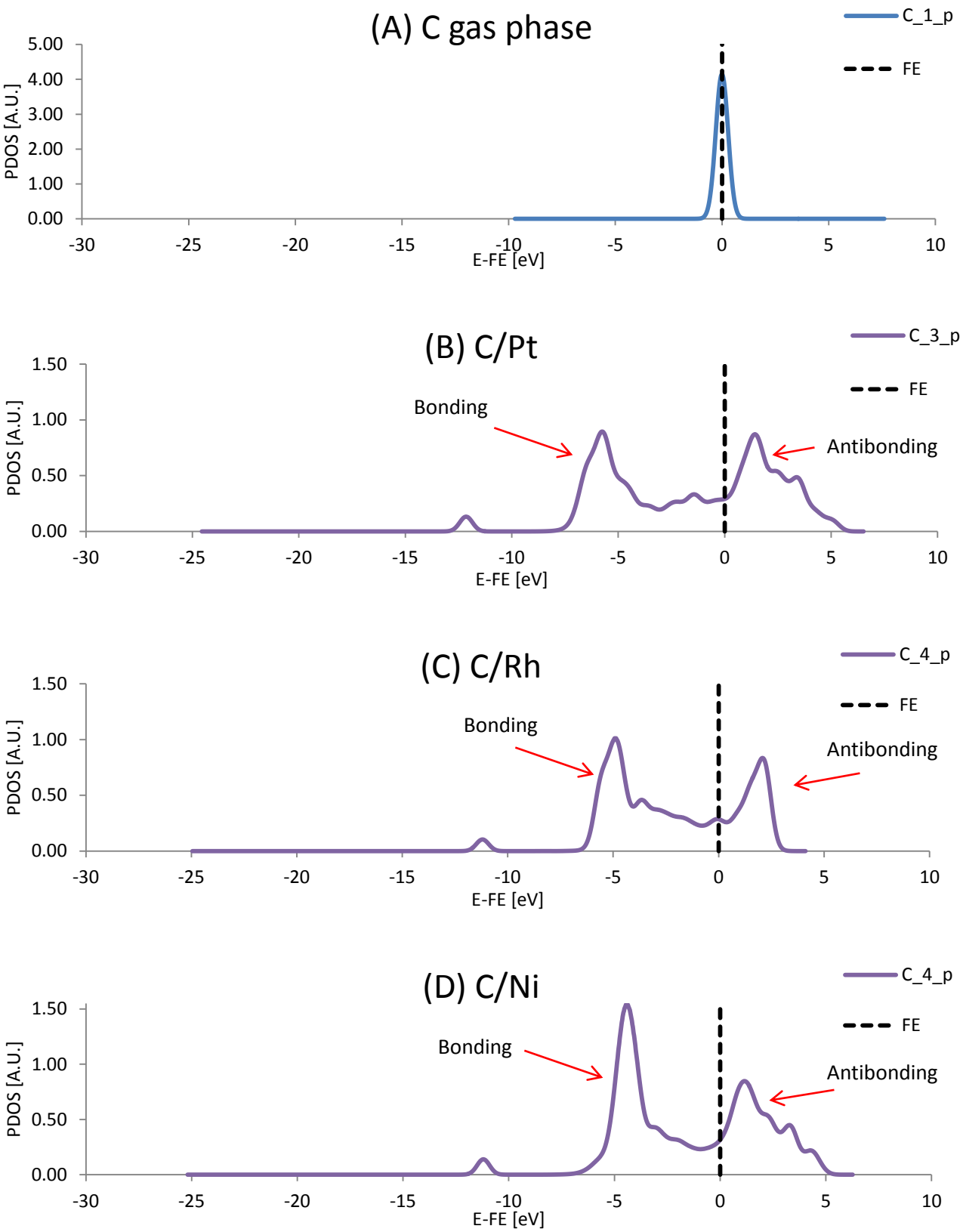

Figure 3.44: PDOS of atomic carbon in gas phase (A), on Pt (B), on Rh (C) on Ni (D); FE = Fermi Energy (reference level); X_n_v means X = atomic type, n = label of the atom, v = valence orbital

Atomic Oxygen

The same approach is used to explain the strong binding energy of the atomic oxygen [42].

The oxygen peaks in Figure 3.45 (A) due to the valence "p" states are split in bonding and antibonding when they feel the d-states of the metal. The bonding states are still represented by narrow bands, the peak is higher moving from Platinum to Rhodium and Nickel, this trend reflects the increase of the binding energy of O on Pt, Rh and Ni. Antibonding states with higher energy produce broad and low bands. Some of the antibonding states are allocated above the Fermi Energy (FE) thus they are empty and the bond becomes increasingly stronger as the number of empty antibonding states increases. The more the bonding states are shifted down through the Fermi level and the more narrow are the d-bands of the metal, the stronger is the chemical bond, in fact d-bands of Ni are sharper than d-bands of Pt and Rh.

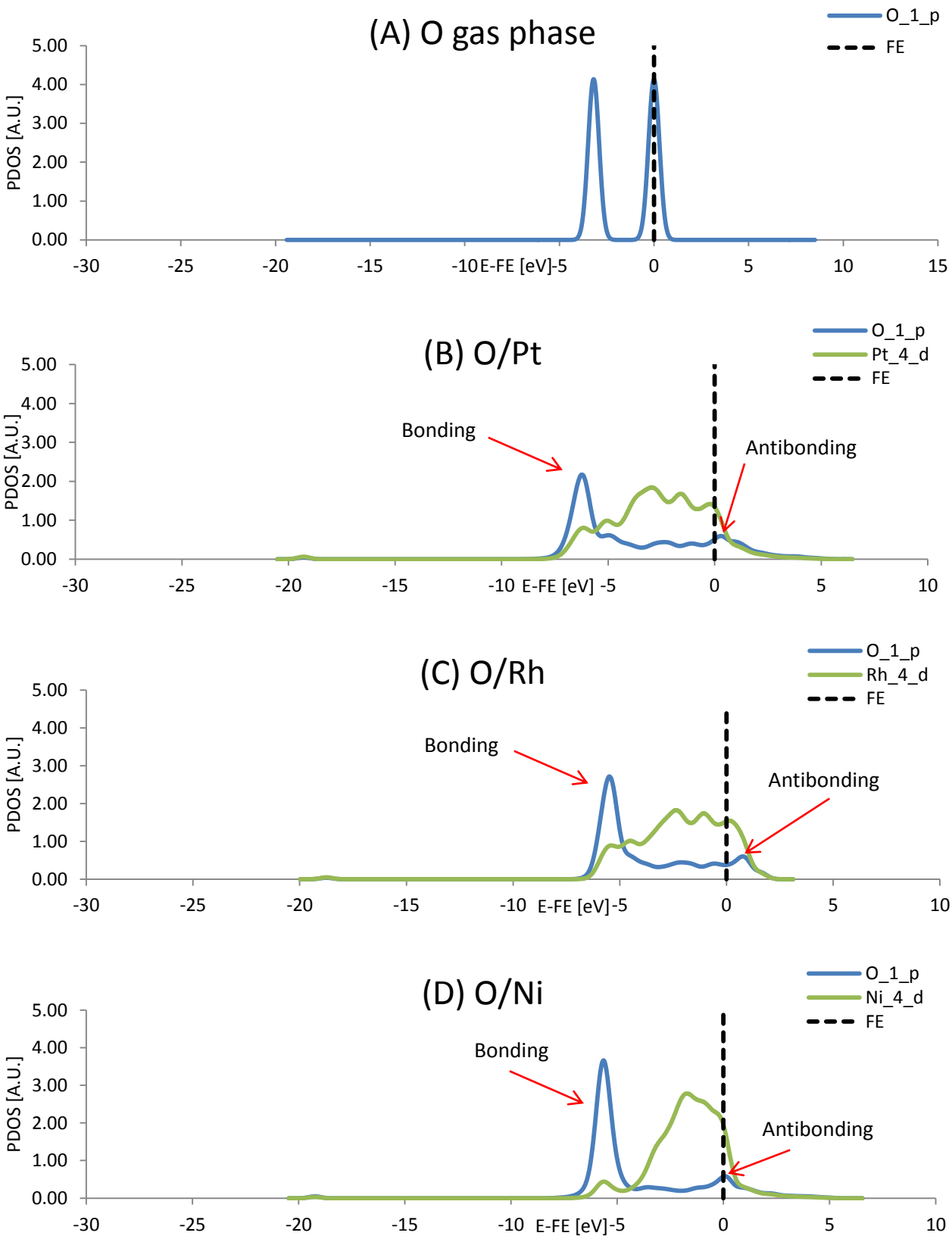

Figure 3.45: PDOS of atomic oxygen in gas phase (A), on Pt (B), on Rh (C) on Ni (D); FE = Fermi Energy (reference level); X_n_v means X = atomic type, n = label of the atom, v = valence orbital

Atomic Hydrogen

Hydrogen has one single electron that can easily be used to produce a chemical bond, but this bond is stronger if 3d bands are involved (Ni).

The one electron state of the atom of hydrogen is initially represented by a sharp band [Figure 3.46 (A)]. Then, when its $1s^1$ state interacts with all the "d" valence states of the surface atoms, the adsorbate state broadens. No peaks due to antibonding states are detected in fact the electron that belongs to the hydrogen prefers to fill the bonding state that is lower in energy than the "1s" atomic orbital. The shape of hydrogen PDOS does not considerably change if this atom is adsorbed on Platinum or Rhodium, rather than Nickel, as consequence hydrogen binding energy is quite the same on the three metals. On the other hand, the metal PDOS is completely overlapped with the adsorbate PDOS if Platinum is considered, whereas Rhodium and Nickel d-bands do not overlap the bonding peak of hydrogen, which appears to be sharper if the "4d" and "3d" metals are involved. As Rhodium and Nickel d-bands are shifted up through the Fermi Energy these bands become more narrow and produce a stronger metal-substrate chemical bond [Figure 3.46 (D)].

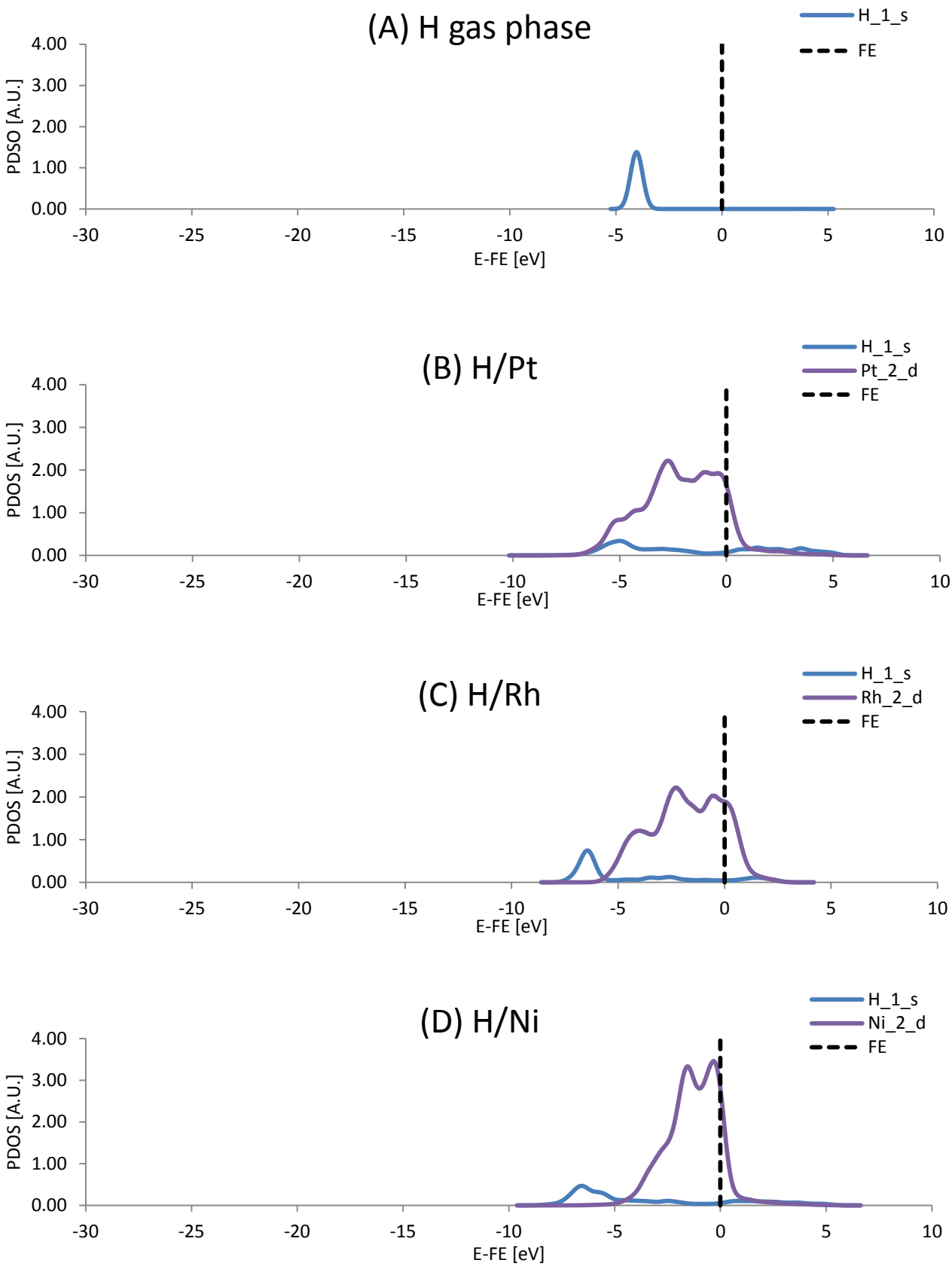

Figure 3.46: PDOS of atomic hydrogen in gas phase (A), on Pt (B), on Rh (C) on Ni (D); FE = Fermi Energy (reference level); X_n_v means X = atomic type, n = label of the atom, v = valence orbital

Carbon Monoxide

Carbon monoxide shows a moderate variation in its binding energy that grows moving from Platinum to Rhodium and Nickel [20].

An explanation can be produced if the electronic configuration of the system is inspected, the density of states is projected onto the "p" and "d" valence orbitals of the atomic species to define which states are filled and which are empty, and how adsorbate and substrate peaks overlap to produce interactions among the metal and the carbon or oxygen states.

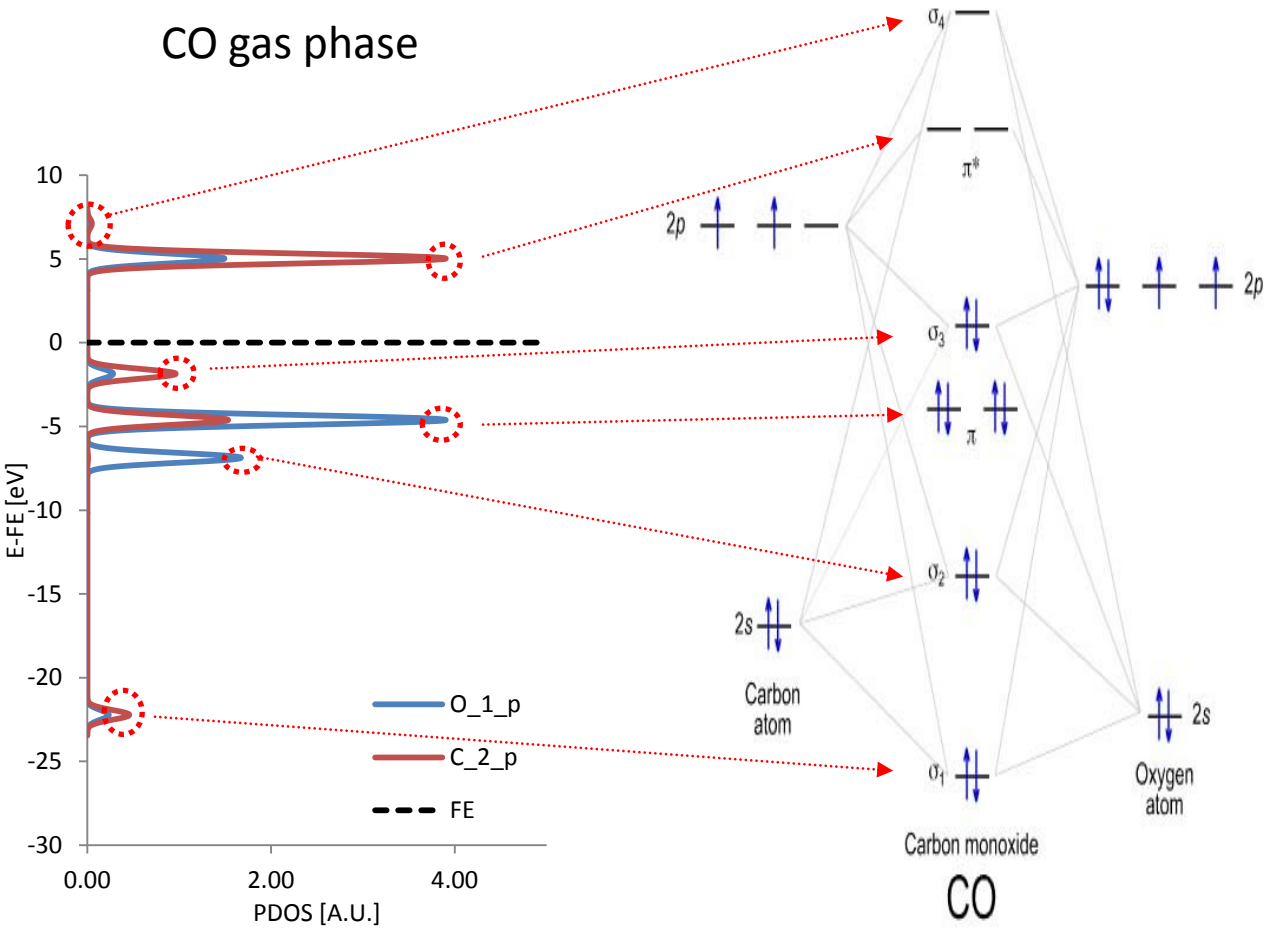

Figure 3.47: PDOS of carbon monoxide in gas phase and Molecular Orbitals

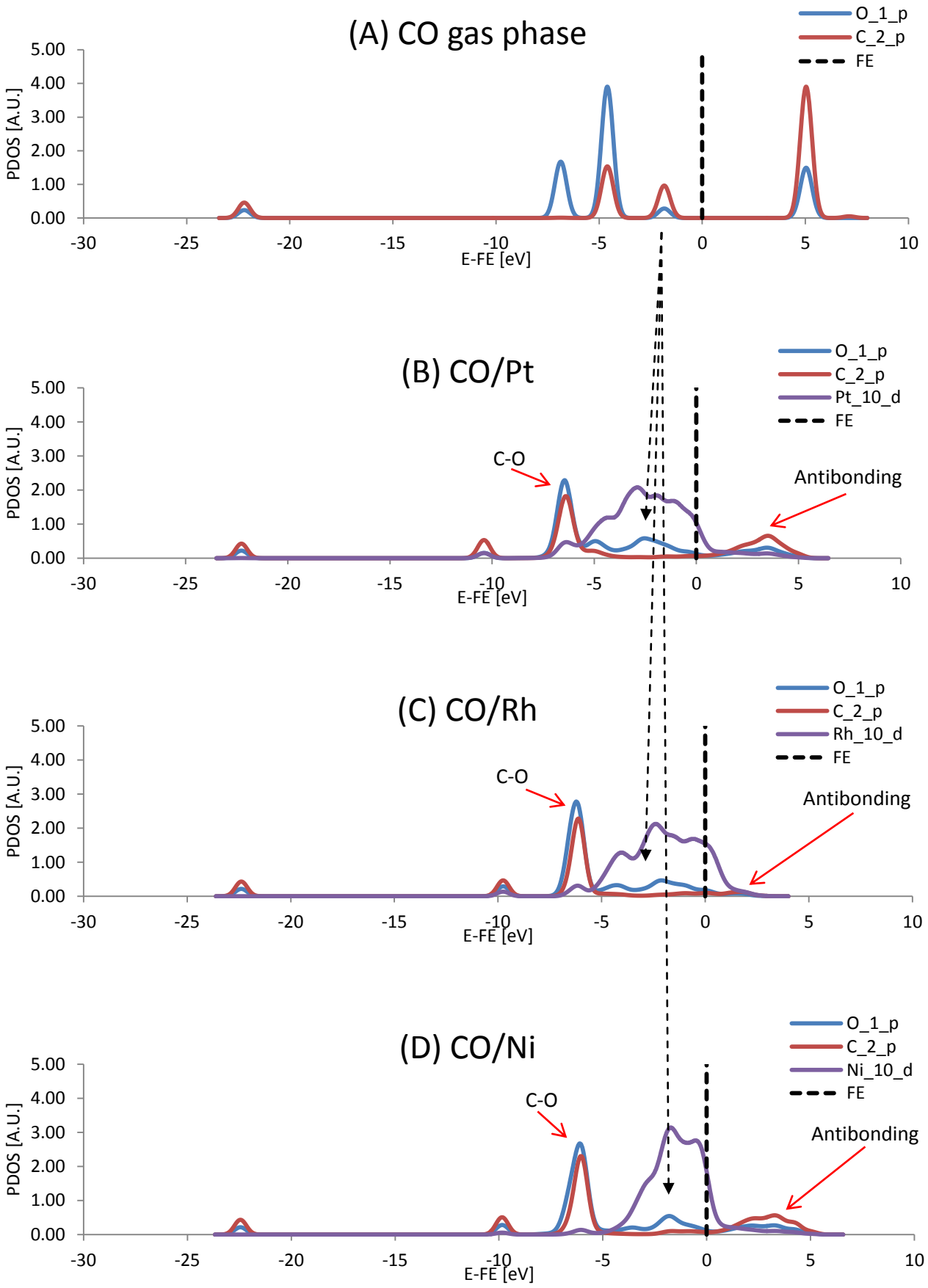

Figure 3.48: PDOS of carbon monoxide in gas phase (A), on Pt (B), on Rh (C) on Ni (D); FE = Fermi Energy (reference level); X_n_v means X = atomic type, n = label of the atom, v = valence orbital

When the adsorbate feels the electrons of d-bands this interaction produces an alteration in electronic structure during CO chemisorption [Figure 3.48].

The sharp states of CO in vacuum are seen to broaden, the bonding and antibonding states move below the two original states, and the overlapping among d-bands and antibonding states of CO (fourth peaks of C and O, PDOS for the CO in gas phase) appears [42, 43].

A portion of the antibonding states are above the Fermi level and are empty, the more are the empty antibonding states and the stronger becomes the bond, as consequence, if the antibonding states are shifted up the Fermi Energy the intensity of the bond increases. Narrow d-bands can be expected to give rise to a strong substrate-adsorbate interaction.

Nickel d-bands are more sharp than Platinum and Rhodium d-bands [Figure 3.48], and a considerable number of states is shifted towards the Fermi Energy, as consequence a considerable amount of antibonding states may be empty. The analysis of electronic structure explains how Nickel creates a stronger bond with CO rather than Platinum or Rhodium, that possess broad d-bands with lots of antibonding states fully occupied.

Carbon Dioxide

The density of states is projected over the valence orbitals of the atomic species to obtain a deeper insight into electronic configuration. The line describing the projected density of states of the oxygen 1 over the "p" orbital resembles the line of the oxygen 2 since the C-O interaction is the same for the two oxygens of CO_2 in gas phase [Figure 3.50 (A)].

Figure 3.50 (B,C,D) describe the density of states of CO_2 when it is on a surface of Platinum, Rhodium and Nickel. The same peaks due to CO_2 molecular orbitals appear in the three examples:

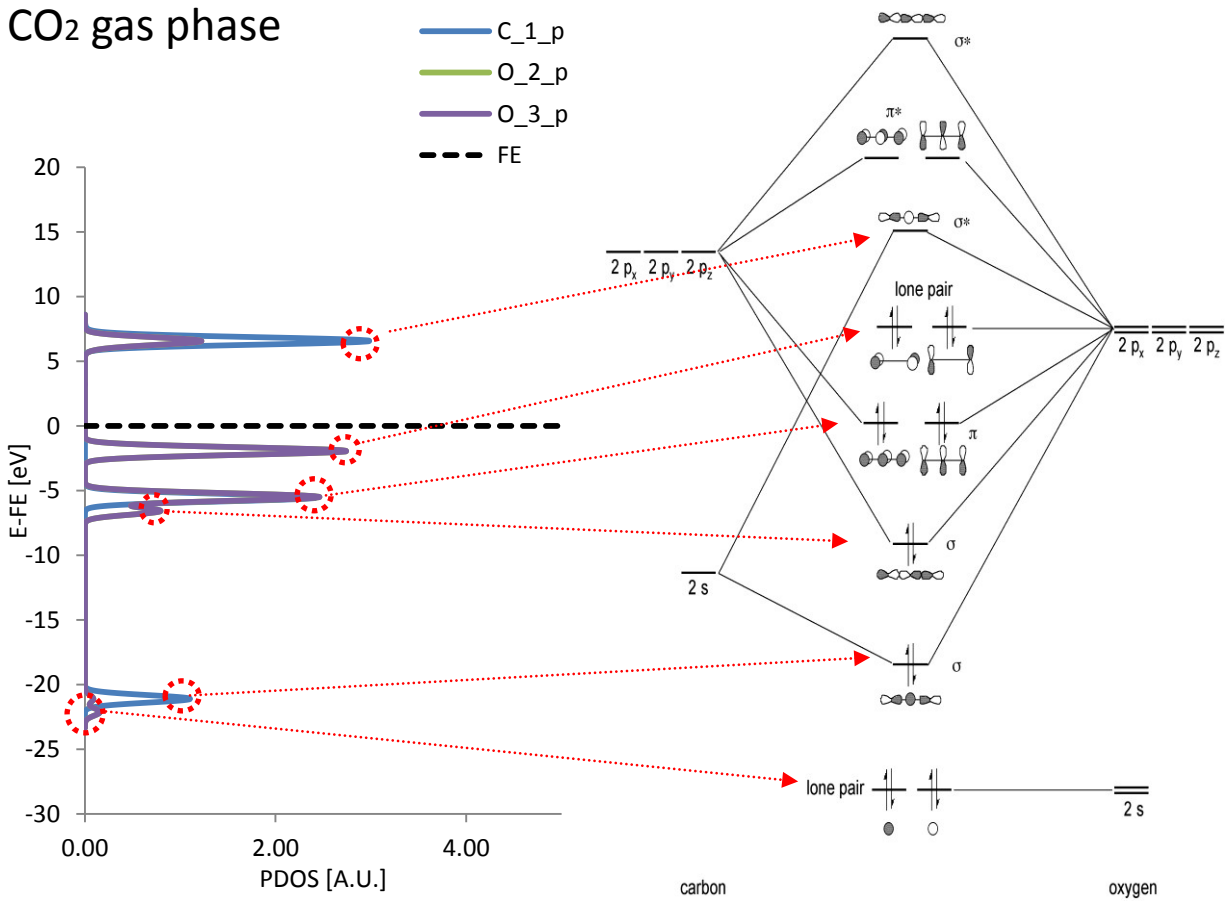

Figure 3.49: PDOS of carbon dioxide in gas phase and Molecular Orbitals

All bonding states are doubly occupied by carbon dioxide electrons [Figure 3.49], this molecule is said to be closed shell and has no available electrons to share with the metal catalyst. As consequence, d-bands states of the metal do not change the shape of the valence states of CO_2 and no substrate-adsorbate interaction can be detected.

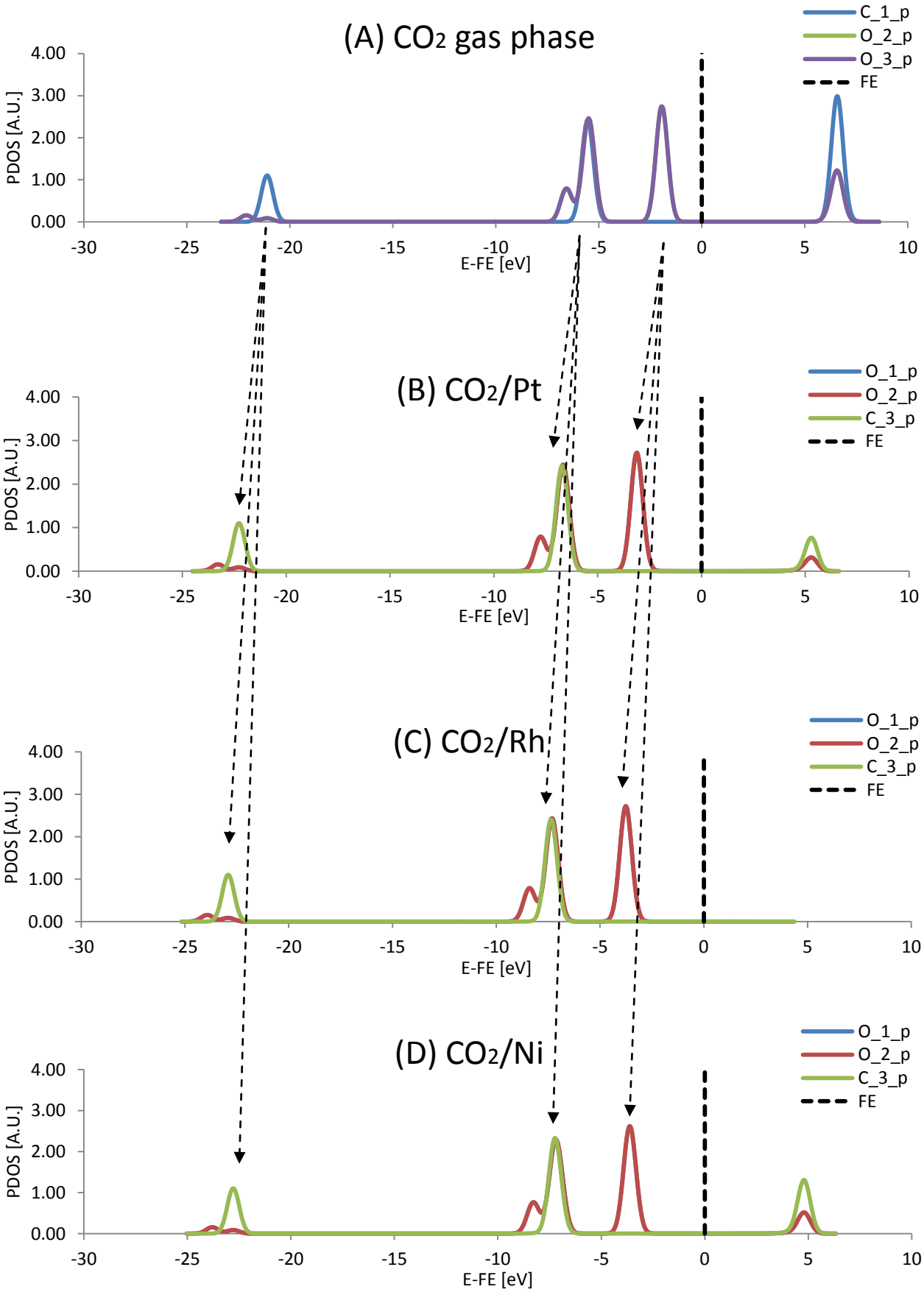

Figure 3.50: PDOS of carbon dioxide in gas phase (A), on Pt (B), on Rh (C) on Ni (D); FE = Fermi Energy (reference level); X_n_v means X = atomic type, n = label of the atom, v = valence orbital

Carboxyl Group

The PDOS of the carboxyl group is inquired, since more atoms and more bonds are considered the shape of the projected density of states is more complex, and a considerable number of peaks can be noticed.

When the carboxyl group is adsorbed on the surface two peaks, involving oxygen and carbon "p" states, are split in bonding and antibonding, and the overlapping of d-bands can be seen [Figure 3.51]. Nickel d-bands are still more narrow than Platinum and Rhodium d-bands, thus the first is expected to be the metal that exhibits the strongest adsorbate-substrate interaction, although this prevision is actually incorrect because the binding energy of COOH on Rhodium is larger. Probably steric effects on Nickel cause a reduction in the absolute value of the binding energy and produce repulsive forces acting between nearby COOH groups adsorbed at the surface.

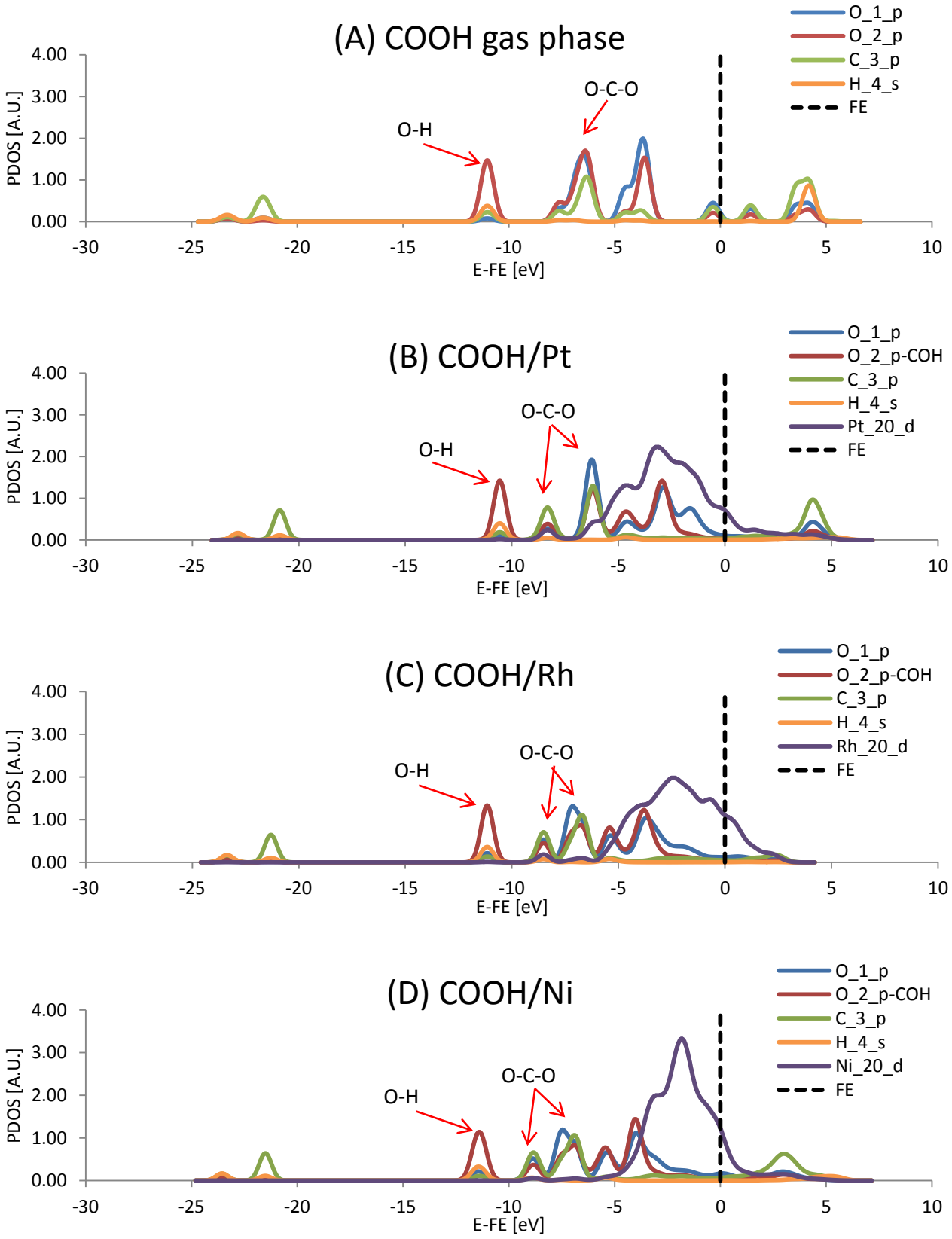

Figure 3.51: PDOS of carboxyl group in gas phase (A), on Pt (B), on Rh (C) on Ni (D); FE = Fermi Energy (reference level); X_n_v means X = atomic type, n = label of the atom, v = valence orbital

CHAPTER 4

4 Finding the Transition State for Elementary Steps

4.1 Transition State Theory

Chemical reactivity is a non trivial aspect of a great number of industrial processes whose goal is to convert different kinds of reactants into products. To maximize the production of a particular molecule the rate of generation of that species has to be very fast but in typical operative conditions of temperature and pressure the reaction rate is very slow, thus a catalyst is often required.

A catalyst is a substance that increases the rate of a chemical reaction by reducing the activation energy, but it doesn't affect thermodynamics and is left unchanged by the reaction.

Heterogeneous and homogeneous catalysis can be weighted:

Homogeneous catalysis		Heterogeneous catalysis	
PROS	**CONS**	**PROS**	**CONS**
• Fast transport phenomena	• Difficult separation of products from the catalyst	• Easy separation of products from the catalyst	• Only the surface is reachable by reactants
• Catalyst uniformly reachable by reactants	• Corrosive acid catalysts	• No notable corrosion occurs	• The surface may be poisoned
• High selectivity	• Only at low temperature	• Possibility to operate at high temperature	• Less selectivity
• Easy temperature control for very exothermic reactions	• Considerable separation and purification costs		• Difficult heat removal
			• Possible diffusion limitations
			• High mechanical resistance required

Table 4.1:homogeneous vs. heterogeneous catalysis

Notable chemical processes adopt heterogeneous catalyst of different and usually very complex composition that assures good selectivity and conversion, but no explanation is provided because the reaction mechanism is actually unknown. A rationalization of the performance of a catalyst is usually difficult because the structure of the catalyst under reaction conditions and the mechanism of reaction are not well known at the atomic level.

Homogeneous processes usually can be studied in details since the whole reaction mechanism can be experimentally determined and a catalytic cycle is thus developed. If a certain molecule appears to change the reaction rate the chemical and physical properties of the same molecule can be investigated in depth, and are an intrinsic characteristic of the chemical species. Instead heterogeneous processes are difficult and quite expensive to be examined, the whole reaction rate is strongly dependent on surface chemistry, and since the exposed surfaces may differ in terms of Miller index, density (m^2/m^3) a particular particle of catalyst may have different effects on chemical reactivity, since all particles are different and affected by surface inhomogeneity, as vacancies, kinks, terraces randomly delivered.

As consequence a catalyst's behavior can be understood by collecting reaction kinetics data at various process conditions as temperature, pressure, concentration, and by building a kinetic model starting from the data analysis.

In the early 1920s 1930s mechanistic models based on Langmuir's findings were developed. The kinetics used were often grounded on Langmuir lattice model of a surface ideally consisted of identical non interacting adsorption sites. In the 1940s -1950s Langmuir kinetics were improved by Hinshelwood, and then by Hougen and Watson to essentially provide a rate equation capable to fit experimental data. Even if the rate equation is able to reproduce the exact trend of compositions in the range of validity, nothing can be said outside this range since the mechanism used to establish the rate equation is only assumed and can be far different from the real sequence of reaction steps.

Almost 30 years later spread out microkinetic models where no "a priori" assumptions are to be made about Rate Determining Step or Quasi-Equilibrium Steps and MARI or NES. All steps are assumed to be reversible and a good esteem of the kinetic parameters can be obtained by Density Functional Theory [44].
The aim of microkinetic modeling is to yield a more detailed study of the reaction kinetics, performing simulations that take account of molecular properties and structure sensitivity [45], thus key features of the surface chemistry that controls catalysts performances can be elucidated.

Combining microkinetic modeling with a traditional experimental approach will enable to understand reactions at microscale and will allow fast catalyst development.

The microkinetic model describes the catalytic process on a surface as a sequence of elementary reactions involving adsorbed reactants, products, and reaction intermediates, although just some steps are said "kinetically significant" and only these steps need accurate kinetic parameters.

An elemental step can involve a bond formation or breaking, but it isn't necessarily related to a chemical reaction, in fact the diffusion of an atom on a plane surfaces is an elemental step, but doesn't represent the formation of a new molecular species. Thus the step is the evolution of the system from an initial state to a final one, where these states are two local minima since they are actually permitted. During a step the nuclei move on a potential energy surface, in principle an infinite number of trajectories are allowed, but one plays a special role in understanding the rate of transition, which is the path having the lowest energy. This path is commonly called "Minimum Energy Path" and links two minima, without passing through any other minima, but coming up to a saddle point, that is the highest energy configuration along the path and is a bottleneck for the transition from the initial to the final state.

Mathematically the first-order saddle point on the potential energy surface is a maximum in the reaction coordinate direction and a minimum along all other coordinates, so methods for finding saddle points invariably involve some kind of maximization of one degree of freedom and minimization in other degrees of freedom. It has also the physical meaning of barrier, a surplus of energy to overcome to reach the final state, and is worldwide known as "Transition State" (TS). It is the configuration that divides the reactant and product parts of the surface, while the geometrical configuration of the energy maximum along the reaction path is called the Transition Structure.

Energies of the initial, final and Transition State can be computed via DFT calculations, but a criticism appears since DFT evaluates properties of the materials in which the atoms are set at minimum energy positions, and this information is referred to a particular temperature, that is 0 Kelvin.

The "Transition State Theory" [46], is a statistical approach that does not account for dynamical effects, is founded on two essential hypotheses that are usually satisfied, and on three additional restrictive hypotheses that define the limits and the level of approximation of the theory:

1- The validity of Born-Oppenheimer approximation allows to solve Schrödinger equation considering electrons in a minimum of energy during the nuclei's translation,
2- The velocity of molecules follows the Maxwell-Boltzmann distribution, the rate is slow enough that a Boltzmann distribution is established and maintained in the reactant state,
3- Once passed the TS no re-crossings occur for a given temperature,
4- At the TS the motion along the reaction coordinate that links initial and final states is treated as a translation,
5- The molecules at the TS are in equilibrium with the reactants.

These hypotheses provide an idealization of the real environment, on a real surface energy is continually exchanged among atoms in the system by collisions that induce instantaneous forces, thus the atoms gain more energy than the equilibrium thermal energy, and this exact supply of energy enables the crossing of the energy barrier.

The rate constant that is built according to the previous statements represents an upper limit to the true rate constant:

$$k_r = \frac{k_B T}{h} e^{-\frac{\Delta G^{\neq}}{RT}} \tag{4.1}$$

$$\Delta G^{\neq} = G^{TS} - G^{reactant} \tag{4.2}$$

Where k_r is the macroscopic rate constant, "k_B" is the Boltzmann's constant, h is the Plank's constant, T is the temperature in Kelvin, and ≠ stands for "Transition State" [30].
Since the path that links the initial and the final states can be travelled either from the begin to the end, or from the end to the begin, a forward and backward reaction rate can be defined, and since the total energies of the first and last states do not depend on the reaction path, forward and backward activation energies have to be connected to honor thermodynamic consistency.

If the process is referred to as A→B:

$$\Delta H_f^{\neq} + \Delta H_b^{\neq} = \Delta H_{prod-react} \tag{4.3}$$

$$\Delta H_{A\to B}^{\neq} + \Delta H_{B\to A}^{\neq} = \Delta H_{A\to B} \tag{4.4}$$

$$\Delta S_f^{\neq} + \Delta S_b^{\neq} = \Delta S_{prod-react} \tag{4.5}$$

$$\Delta S_{A\to B}^{\neq} + \Delta S_{B\to A}^{\neq} = \Delta S_{A\to B} \tag{4.6}$$

The Transition State Theory defines the reaction rate (4.7) as the product between the average thermal velocity (v) of crossing the barrier (TS) and the probability (p) of finding the system at the Transition State. This product is forerun by the factor of one-half that reminds the possible crossing of the barrier towards two opposite ways:

$$k_{A\to B} = \frac{1}{2} vp \tag{4.7}$$

If total energy can be written as a function of the reaction coordinate that links initial and final states, and if the reaction coordinate is monodimentional, the average velocity of atoms, according to Maxwell-Boltzmann distribution, will be:

$$v = \sqrt[2]{\frac{2}{\beta \pi m}} \tag{4.8}$$

Where "m" is the atomic mass (kg/mol) and $\beta = (k_B T)^{-1}$.

The probability of finding the system at the Transition State is:

$$p = p(x) \propto exp\left(-\frac{E(x)}{k_B T}\right) \tag{4.9}$$

But this formula can be written as the ratio between the energy of the Transition State and the energy of all allowable states:

$$p(x = x^{\neq}) = \frac{e^{-\beta E(x^{\neq})}}{\int_A^{+\infty} e^{-\beta E(x)}\, dx} \tag{4.10}$$

The main issue lies in the integral that is taken over all positions within the minimum A, thus an approximation has to be introduced. The evaluation of the integral can be easily done if atoms with thermal energy near to the minimum configuration only perform slight oscillation around the minimum. Since atoms in crystals are usually tightly packed, this approximation to TST can be used in studies of reactions at crystal surfaces. As consequence total energy is expanded using a Taylor series.

$$E(x) \cong E_A + \frac{k}{2}(x - x_A)^2 \tag{4.11}$$

Where "k" is related to the vibrational frequency.

$$\int_A^{+\infty} e^{-\beta E(x)}\, dx \cong e^{-\beta E_A} \int_A^{+\infty} e^{-\beta \frac{k}{2}(x-x_A)^2}\, dx \cong e^{-\beta E_A} \int_{-\infty}^{+\infty} e^{-\beta \frac{k}{2}(x-x_A)^2}\, dx =$$

$$= e^{-\beta E_A} \int_{-\infty}^{+\infty} e^{-\beta \frac{k}{2}(x-x_A)^2}\, dx = e^{-\beta E_A} \sqrt{\frac{2\pi}{\beta k}} \tag{4.12}$$

The integral is extended to - ∞ since it rapidly decays to zero, and if the two formulas (4.8) (4.12) are joined the final kinetic expression (4.13) will remark the dependency on the difference between the total energy of the Transition State and the total energy of the initial state A, that is the activation energy of the process:

$$k_{A \to B} = \frac{1}{2} \sqrt{\frac{2}{\beta \pi m}} \sqrt{\frac{\beta k}{2\pi}} \cdot e^{-\beta (E(x^{\neq}) - E_A)} = \upsilon \cdot e^{\left[-\frac{(E(x^{\neq}) - E_A)}{k_B T}\right]} \tag{4.13}$$

This is the "Harmonic Transition State Theory", and the pre-exponential "υ" is a frequency of oscillation, a very usual frequency is around 10^{12}-10^{12} Hz, and thus the pre-actor can be roughly determined without performing any calculation with a good level of precision.
It seems to be that no need to high accuracy is required on the pre-exponential factor, and this is true because the effect of pre-factor on the reaction rate is by far less crucial than the effect that can rise as a consequence of an inaccurate evaluation of the activation energy.

However, up to now a 1D Transition State has been examined, but such a type of TS exists only for very simple systems, as gas phase molecules breaking a single bond and preserving the geometrical structure of the molecule itself, or a superficial diffusion of an adsorbed atom, from a certain adsorption site to the next one. In most of cases the reaction coordinate can't be represented by a straight line or rather a one dimensional energy path that links two states, a more general version of the Transition State Theory faces the multidimensional complexity of a system composed by multiple atoms moving and interacting each others, thus energy has to be integrated over an hyperspace defined by all relevant particle coordinates (**r**), and x is one coordinate chosen to define the reaction coordinates.

If "N" atoms are considered, "3N" are the relevant coordinates, and thus the total energy is written as a function of "3N" coordinates itself. Since the Transition State energy is defined when all atoms are positioned at "$3N^{\neq}$ ", it is possible to define "3N" monodimensional Transition States, one for each coordinate.

$$k_{A\to B} = \frac{1}{2}\sqrt{\frac{2}{\beta\pi m}}\frac{\int_{x=x^{\neq}} e^{-\beta E(\mathbf{r})}\, d\boldsymbol{r}}{\int_{A}^{+\infty} e^{-\beta E(\mathbf{r})}\, d\boldsymbol{r}} \qquad (4.14)$$

This multidimensional rate expression can be transformed as the previous monodimensional one (4.13) into the Arrhenius formula:

$$k_{A\to B} = \upsilon \cdot e^{\left[-\frac{(E(x^{\neq})-E_A)}{k_B T}\right]} = \frac{\upsilon_1 \cdot \upsilon_2 \cdot \ldots \cdot \upsilon_M}{\upsilon_1^{\neq} \cdot \upsilon_2^{\neq} \cdot \ldots \cdot \upsilon_{M-1}^{\neq}} \cdot e^{\left[-\frac{(E(x^{\neq})-E_A)}{k_B T}\right]} =$$

$$= \frac{\prod_{i=1}^{M} \upsilon_i}{\prod_{i=1}^{M-1} \upsilon_i^{\neq}} \cdot e^{\left[-\frac{(E(x^{\neq})-E_A)}{k_B T}\right]} \qquad (4.15)$$

If the system has "M" degrees of freedom at the initial configuration A, the total degrees of freedom are reduced to "M-1" at the TS, since one vibrational degree of freedom is physically turned into a translational one, the system indeed is assumed to translate along the reaction coordinate. Mathematically the vibrational frequency associated with the Transition State has an imaginary component, but if more than one, or no imaginary frequencies are found, the selected configuration is not a Transition State.

The necessary but not sufficient condition requires that just one imaginary frequency exists.

To connect properties of microscopic and macroscopic systems, where temperature is no longer 0 Kelvin, and molecules are no longer in their ground state energy, the use of statistical mechanics is necessary. All the possible energy states are allocated according to Boltzmann distribution, thus the maximum of the probability to find a molecule in a certain state is no longer located at the minimum of energy. An extremely important role is performed by the "Partition Functions" that are essential to determine all thermodynamic functions in statistical mechanics [27].

A single molecule partition function is an infinite sum over all possible quantum energy states ε_i:

$$Q = \sum_{i=states}^{\infty} e^{-\frac{\varepsilon_i}{K_B T}} \tag{4.16}$$

If a collection of "N" non interactive particles is considered the total partition function is:

$$Z = Q^N \tag{4.17}$$

If there are "N" distinguishable particles the previous expression properly describes the partition function of the system, instead if the "N" particles are identical the following formula accounts for degeneracy:

$$Z = \frac{Q^N}{N!} \tag{4.18}$$

But systems are dominantly made of interacting bodies, thus if "N" interactive particles are considered the summation will run up to "E_i", that are all energy states for the whole system, and no longer for the single particle:

$$Q = \sum_{i=states}^{\infty} e^{-\frac{E_i}{K_B T}} \tag{4.19}$$

As consequence, by determining the partition function "Q", all thermodynamic functions as Internal, Helmholtz and Gibbs free energy can be explicitly defined and computed, but also observables such as pressure and heat capacity can be calculated.

Although the main issue lies in the lack of knowledge of the expression of the total energy:

$$\varepsilon_i = \varepsilon_i^{trans} + \varepsilon_i^{rot} + \varepsilon_i^{vib} + \varepsilon_i^{elec} \tag{4.20}$$

That is the sum of different contributions due to translational, rotational, vibrational and electron degrees of freedom, thus approximations have to be introduced to provide their explicit formula.

Thanks to thermodynamic functions kinetic rate equation can be built, if the reaction (4.21) is considered:

$$A + B \leftrightarrow TS^{\neq} \rightarrow C + D \tag{4.21}$$

The equilibrium constant is:

$$K_{eq} = \frac{C_{TS^{\neq}}}{C_A C_B} = \frac{Q_{TS^{\neq}}}{Q_A Q_B} \tag{4.22}$$

The rate equation of an elementary step is defined as:

$$R = \upsilon \cdot C_{TS^{\neq}} = \frac{\nu_{\Delta}}{2\Delta} \cdot \frac{Q_{TS^{\neq}}}{Q_A Q_B} \cdot C_A C_B \tag{4.23}$$

Where "υ" is the frequency of crossing the Transition State, considered as the rate between the crossing velocity and the length of the translation along the reaction coordinate.
As said before one of the internal modes, which would be classically described as a vibrational mode, degenerates in a translational mode, treated with the "Particle In a Box Approximation".

$$k_r = \frac{v_\Delta}{2\Delta} \cdot \frac{Q_{TS^{\neq}}}{Q_A Q_B} = \frac{1}{2\Delta} \cdot \sqrt[2]{\frac{2k_B T}{\pi m}} \cdot \frac{Q_{TS^{\neq}}^{trasl} \cdot Q_{TS^{\neq}}^{rot} \cdot Q_{TS^{\neq}}^{trasl1D} \cdot Q_{TS^{\neq}}^{vib3N-7} \cdot Q_{TS^{\neq}}^{el}}{Q_A Q_B} \tag{4.24}$$

$$k_r = \frac{1}{2\Delta} \cdot \sqrt[2]{\frac{2k_B T}{\pi m}} \cdot \sqrt[2]{\left(\frac{2\pi m k_B T}{h^2}\right)} \cdot \Delta \cdot \frac{Q_{TS^{\neq}}^{trasl} \cdot Q_{TS^{\neq}}^{rot} \cdot Q_{TS^{\neq}}^{vib3N-7} \cdot Q_{TS^{\neq}}^{el}}{Q_A Q_B} \tag{4.25}$$

$$k_r = \frac{k_B T}{h} \cdot \frac{Q_{TS^{\neq}}^{trasl} \cdot Q_{TS^{\neq}}^{rot} \cdot Q_{TS^{\neq}}^{vib3N-7} \cdot Q_{TS^{\neq}}^{el}}{Q_A Q_B} = \frac{k_B T}{h} \cdot \frac{Q_{TS^{\neq}}}{Q_R} \tag{4.26}$$

$$k_r = \frac{k_B T}{h} \cdot \frac{Q_{TS^{\neq}}}{Q_R} = \alpha \cdot e^{\left[-\frac{\Delta G_{TS^{\neq}}^0}{k_B T}\right]} = \beta \cdot e^{\left[-\frac{\Delta E_{TS^{\neq}}^0}{k_B T}\right]} \tag{4.27}$$

4.2 Identification of the Transition State

The shape of the "Potential Energy Surface" is actually unknown, but sometimes it is possible to guess a physical path, according to symmetry considerations, but if the system involves a considerable number of moving atoms the guess may not be so easy to define, and so it is essential to be able to find the correct Transition State without suggesting any reasoned initial path. Thus numerical methods have to be implemented to carry out a blind research of the Transition State, but this research requires expensive computational effort, in fact since a saddle point has to be found, the Hessian matrix, made up of second derivatives, needs to be evaluated. Although DFT plane wave methods readily provide first order derivative, that are the forces acting on atoms (F = -∇E), but not second derivative, as consequence methods that follow low curvature directions from energy minima can't be simply implemented.

Various minimization methods have been proposed [27, 47], but all are founded on the idea that the MEP is a certain continuous function that describes the spatial motion of atoms, if "N" atoms are considered the MEP will be defined by "N" functions, where x-y-z are the spatial independent variables that define the position of each atom. Although a continuous function can't be properly represented with a calculator since a finite budget of memory is available. Thus the MEP, which can be thought as a movie, is reduced to a discrete number of snapshots or images, and each image is linked to the next and belongs to the MEP. The more are the images and the better is the description of the MEP, but the more intensive is the computational resources consumption. In fact intermediate images are actually unknown, and they have to be brought on the MEP, thus more images ask more time to converge and find the correct MEP.

The simplest method is called the "Drag" method, but different names exist since various editions have been proposed. One of the total "N" degrees of freedom of the system, the drag coordinate, is held fixed while the energy of the system is minimized with respect to the others "N-1". Step by step the drag coordinate is increased in order to bring the system from the initial state, to the final configuration, and the highest computed energy represents the Transition State, although a good guess is required to define the drag coordinate since it is unknown. The identification of a reasonable drag coordinates may be arcane, and so a liner interpolation of the atomic positions, between the initial and final configuration, is done. The problem lies both in the assumed reaction coordinate and into the straight linear interpolation that can lead to a bad initial path, in fact the reaction coordinate should be the one that provides an imaginary normal mode at the "Transition State", and then a minimization of the total energy of the system with respect to the other degrees of freedom is reasonable, otherwise the system will not pass through the "Transition State", in fact if the reaction coordinate differs from the exact drag coordinate the drag method miserably fails and produces a discontinuous path.

The "Chain-of-State" method instead can work with more than two images connecting the initial and final states. If intermediate images are properly relaxed the method provides an approximation of the whole path and the location of the TS, but intermediate images guide the search in a particular way. The energy of each image, placed with regular spacing along a suitable reaction coordinate, is computed; the highest energy image is relaxed along a particular direction defined by the gradient component orthogonal to the line connecting two neighboring images. The image with major energy can change during the research, but when the orthogonal component of the gradient becomes near to zero (within a certain threshold), no forces act on images to make them slide away

from the current path, that is the MEP. When all images are on the MEP the highest one is no longer relaxed but moved uphill the path towards the saddle point.

The "Elastic Band" method builds the initial path between the two minima by evenly spacing atoms along the path with variable spring constants and by linking the initial and final states with elastic bands [30]. Atomic coordinates of the intermediate images are initialized by use of an easy linear interpolation (4.28), if "Q + 1" images, composed by "N" atoms are considered:

i=0 : Q
j=1 : N
k=1 : 3

$$r_{i,j,k} = r_{0,j,k} + \left(r_{Q,j,k} - r_{0,j,k}\right) \cdot \left(\frac{i}{Q}\right) \tag{4.28}$$

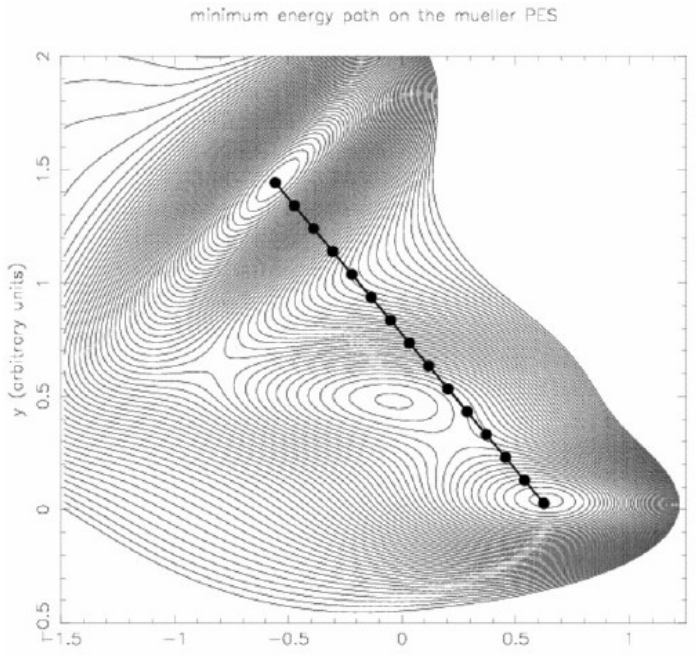

Figure 4.1: initial guess of the MEP

Intermediate images have to be brought along the MEP [Figure 4.1, Figure 4.2], they are effectively located on the MEP only if forces defined by any images are oriented along the path.

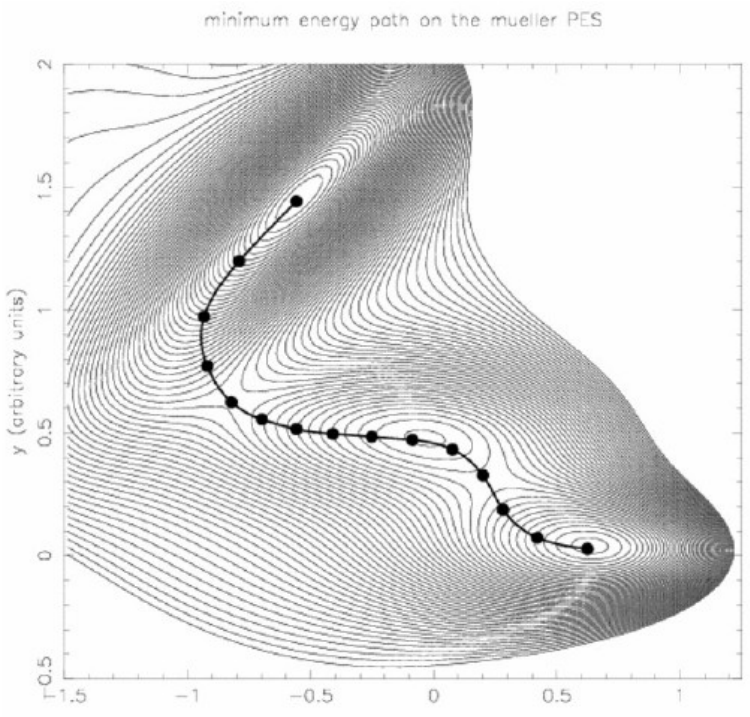

Figure 4.2: converged MEP

To move images along the desired path an objective function is used, if "Q + 1" images are selected to define the path, the function adopted by the Elastic Band method is:

$$f(\boldsymbol{r}_0, \dots, \boldsymbol{r}_Q) = \sum_{i=1}^{Q-1} E(\boldsymbol{r}_i) + \sum_{i=1}^{Q} \frac{K_i}{2} (\boldsymbol{r}_i - \boldsymbol{r}_{i-1})^2 \tag{4.29}$$

Where the label "0" is referred to the initial state, and the label "Q" to the final state.
The total energy of each image, by neglecting the initial and final optimized structures, is added, with the elastic part that has the purpose of joining neighboring images by harmonic springs, called elastic bands, of "K_i" stiffness, and acting on the intermediate images' distance.

If springs are very stiff a good resolution can be obtained because images are moved around the saddle point, but this method can fail because of two notable causes:

- The sliding down problem,
- The corner cutting problem.

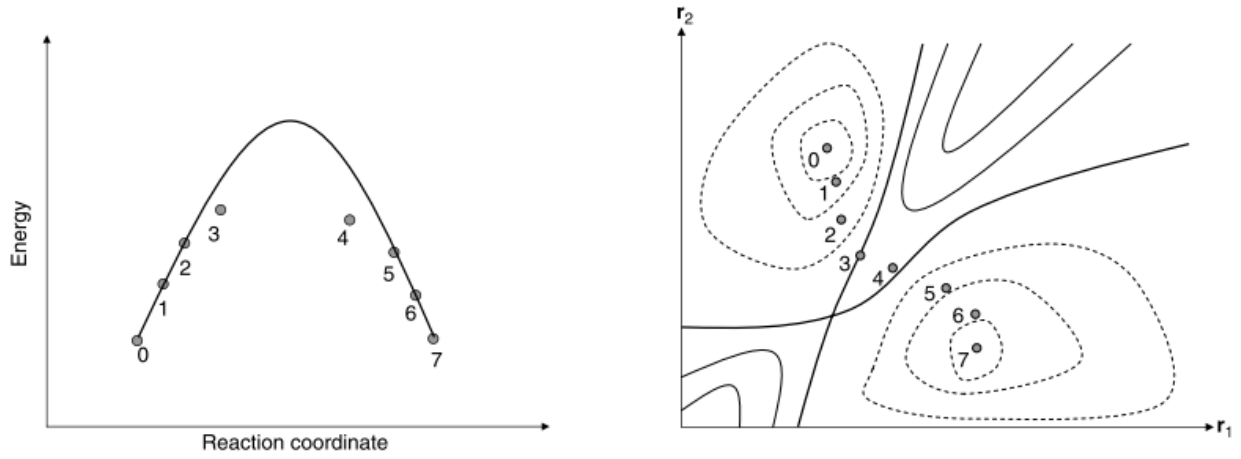

Figure 4.3: sliding down problem (on the left) and corner cutting (on the right), adapted from [30]

The slope of the MEP changes from image to image, thus moving a particular image along the path may lead to a low or strong spring stretching, if a unique stiffness "K" is used springs that link images set near the Transition State are low stretched, and tend to slide downhill, instead images near to the initial and finial configuration, that are local minima, are compressed and thus inclined to approach to the path's double end. Unfortunately the most interesting portion of the path is the one near the TS, where no images are found.
The corner cutting is instead a phenomenon due to the choice of a bad initial path, that produces a final shorter path unable to pass through the Transition State. As consequence the activation energy computed will be smaller than the exact one.

A solution to the sliding problem is provided by "Nudged Elastic Band" method, which can be considered as an improvement of the basic Elastic Band method.
If the i-th image is considered, the path direction is defined by the unit vector τ_i:

$$\boldsymbol{\tau}_i = \frac{\boldsymbol{r}_{i+1} - \boldsymbol{r}_{i-1}}{|\boldsymbol{r}_{i+1} - \boldsymbol{r}_{i-1}|} \tag{4.30}$$

This image will exactly belong to the MEP only if no force perpendicular to the path acts upon the image itself:

$$\boldsymbol{F}_i = \boldsymbol{F}_i^{\perp} + \boldsymbol{F}_i^{||} = \boldsymbol{F}_i^{\perp} + (\boldsymbol{F}_i \cdot \boldsymbol{\tau}_i)\boldsymbol{\tau}_i = (\boldsymbol{F}_i \cdot \boldsymbol{\tau}_i)\boldsymbol{\tau}_i \tag{4.31}$$

In additional the downhill motion of the images is adjusted by considering the spring forces that keep images spread out along the path:

$$\boldsymbol{F}_i^{\perp \mathrm{S}} = \boldsymbol{F}_i^{\perp} + \boldsymbol{F}_i^{\mathrm{Spring}} = \boldsymbol{F}_i^{\perp} + (K_{i+1}|\boldsymbol{r}_{i+1} - \boldsymbol{r}_i| - K_i|\boldsymbol{r}_i - \boldsymbol{r}_{i-1}|) \tag{4.32}$$

The interesting component of the real forces is the one perpendicular to the MEP, instead the interesting component of the spring forces is the one that points along the direction of the MEP.
As consequence only the projection of the spring forces is accounted for:

$$\boldsymbol{F}_i^{\mathrm{Nudged}} = \boldsymbol{F}_i^{\perp} + \left(\boldsymbol{F}_i^{\mathrm{Spring}} \cdot \boldsymbol{\tau}_i\right)\boldsymbol{\tau}_i \tag{4.33}$$

In such a way the true force does not affect the distribution of images along the path, but if this scheme is not used the spring forces prevent the band from following the MEP and cause the corner cutting phenomenon, instead the true force along the path provokes the images to slide towards the initial and final states.
Even if the perpendicular force to the path acting on each image is less that a selected threshold no guaranty exists that any of the images in the NEB calculation lies precisely at the Transition State, as consequence the computed activation energy slightly underestimates the true one.

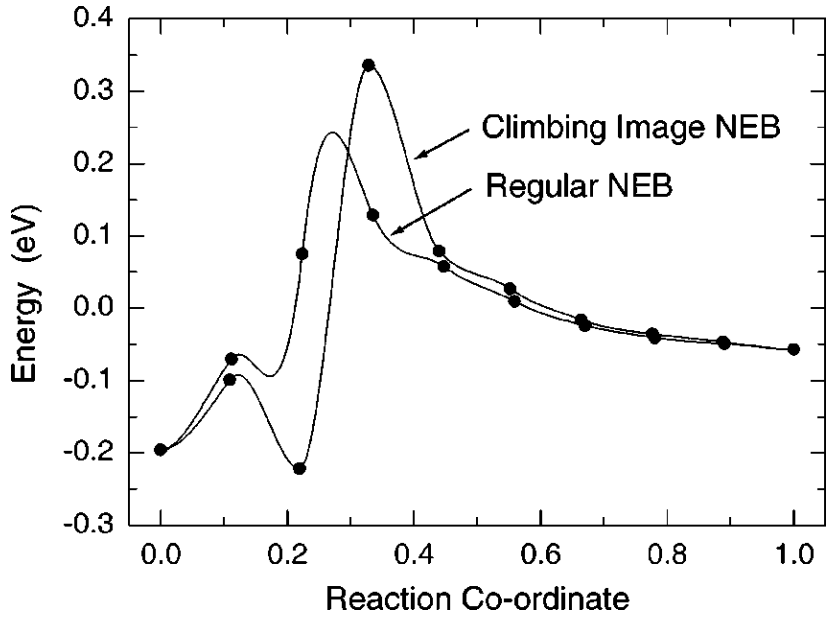

Figure 4.4: NEB vs. CI-NEB, adapted from [48]

To resolve this problem Henkelman et al. [48] proposed a modification of the NEB method, called "Climbing Image NEB", developed in order to allow the image with the highest energy to move uphill in energy along the elastic band till the TS is reached. The CI-NEB method provides, in addition to the saddle point, an idea of the shape of the whole MEP, that's essential to determine whether more than one saddle points are present, and then which one is highest in order to get a good estimate of the rate.

This method as well as NEB, has been used in conjunction with electronic structure calculations, in particular plane wave based DFT calculations, all movable images are adjusted simultaneously and only the positions of adjacent images are needed for each step, thus no significant additional effort is required.

Usually a few iterations with NEB are performed, in order to define the image with the highest energy, then the force on this image is no longer the one given by (4.32), but by the following expression:

$$\boldsymbol{F}_{i_{MAX}} = -\nabla E\left(\boldsymbol{R}_{i_{MAX}}\right) + 2\nabla E\left(\boldsymbol{R}_{i_{MAX}}\right) \cdot \boldsymbol{\tau}_{i_{MAX}} \cdot \boldsymbol{\tau}_{i_{MAX}} \tag{4.34}$$

$$\boldsymbol{F}_{i_{MAX}} = \boldsymbol{F}^{||}_{i_{MAX}} + \boldsymbol{F}^{\perp}_{i_{MAX}} - 2 \cdot \boldsymbol{F}^{||}_{i_{MAX}} = \boldsymbol{F}^{\perp}_{i_{MAX}} - \boldsymbol{F}^{||}_{i_{MAX}} \tag{4.35}$$

The spring forces don't affect the maximum energy image and the spacing between images will be different since on one side of the saddle point images are compressed, instead on the other side they are stretched out. Variable spring constants can be used to settle interimage spacing, in particular more resolution close to the saddle point is necessary to have a more accurate estimate of the tangent to the MEP and thus stronger springs are used near the saddle point. Actually spring forces do not interfere with the true forces and the choice of the stiffness of the spring that links two images doesn't affect the convergence of the band to the MEP.

A very common practice to choose the spring constant inside a selected range lies in linearly varying the stiffness of the springs proportionally to the energy of the image.

$$k_i = \begin{cases} k_{MAX} - \Delta k \left(\dfrac{E_{MAX} - E_i}{E_{MAX} - E_{ref}} \right) & if\ E_i > E_{ref} \\ k_{MAX} - \Delta k & if\ E_i > E_{ref} \end{cases} \tag{4.36}$$

Where:

- k_{MAX}/k_{MIN} and is the maximum/minimum value of the spring constant,
- $\Delta k = k_{MAX} - k_{MIN}$,
- E_{MAX} is the maximum value of E_i,
- E_{ref} is the energy of the higher energy endpoint of the MEP,
- $E_i = \max[E_i, E_{i-1}]$.

As a whole the CI-NEB method turns out to be the one of the most efficient method.

4.3 NEB Show-Case

An example of the CI-NEB method is expounded in this section of the chapter, a very simple system is investigated. The dissociation of the hydroxyl group is studied on a (111) surface of Platinum [21, 44].

$$OH \rightarrow O + H \tag{4.37}$$

The NEB method requires the atomic coordinates of the initial and final states of the elementary step to be known, thus a criterion to establish the configuration of reactants and products has to be defined. Several relaxations are performed to bring reactants and products at the local minima, then the local minima are screened and the lowest in energy is selected as best electronic structure. In principle all the local minima can be used as possible electronic structures of reactants or products, but the lowest minimum is chosen since this configuration defines the strongest adsorption site on the Platinum (111) surface when OH is adsorbed at the initial state, and when O and H are co-adsorbed at the final state.

The electronic structure calculations are performed using the quantum-ESPRESSO code, based on DFT method in a plane wave pseudopotential implementation. The unit cell employed to built the (111) slab is a 2x2 supercell with 3 fixed layers, 12 Angstrom of vacuum are left between slabs. Only two atoms (O and H) are allowed to move thus no expensive computational effort is required during the research of the relaxed electronic structure and of the energy of the local minimum.
PBE ultra-soft Vanderbilt pseudopotentials are employed, the plane wave cutoff used during electronic structure's relaxation is 40 Ry (544 eV) for the wave function and 400 Ry (5440 eV) for the electron density. An 8x8x1 Monkhorst-Pack grid is chosen to map the Brillouin zone, with Marzari-Vanderbilt cold smearing of 0.01 Ry.

The binding energies of the system are computed by making reactants and products to adsorbe on various combinations of allowable active sites.

$$B.E.reactants = E_{OH/slab} - (E_{slab} + E_{OH}) \tag{4.38}$$

$$B.E.products = E_{O+H/slab} - (E_{slab} + E_O + E_H) \tag{4.39}$$

Figure 4.5 displays the binding energy of OH with a snapshot of the relaxed electronic structure (O red dot, H blue dot). The preferred site of adsorption of the hydroxyl group on a (111) Pt surface is the top.

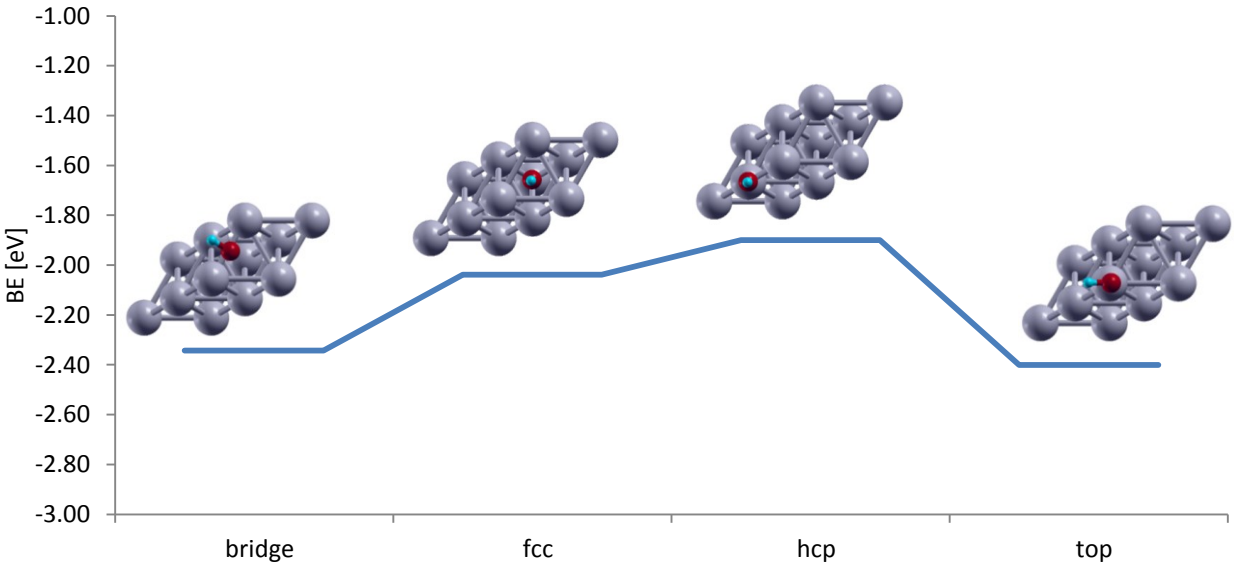

Figure 4.5: binding energies of OH on a 3 layers, 2x2 (111) Pt slab

OH	BE [eV]
Bridge	-2.343
Fcc	-2.038
Hcp	-1.900
Top	-2.401

Table 4.2: binding energies of OH on a 3 layers, 2x2 (111) Pt slab

Figure 4.6 shows the binding energy of O and H when they are co-adsorbed, a snapshot of the relaxed structure is provided. Atoms can be found at different sites if compared with the initial positions filled before the research of the stable configuration.

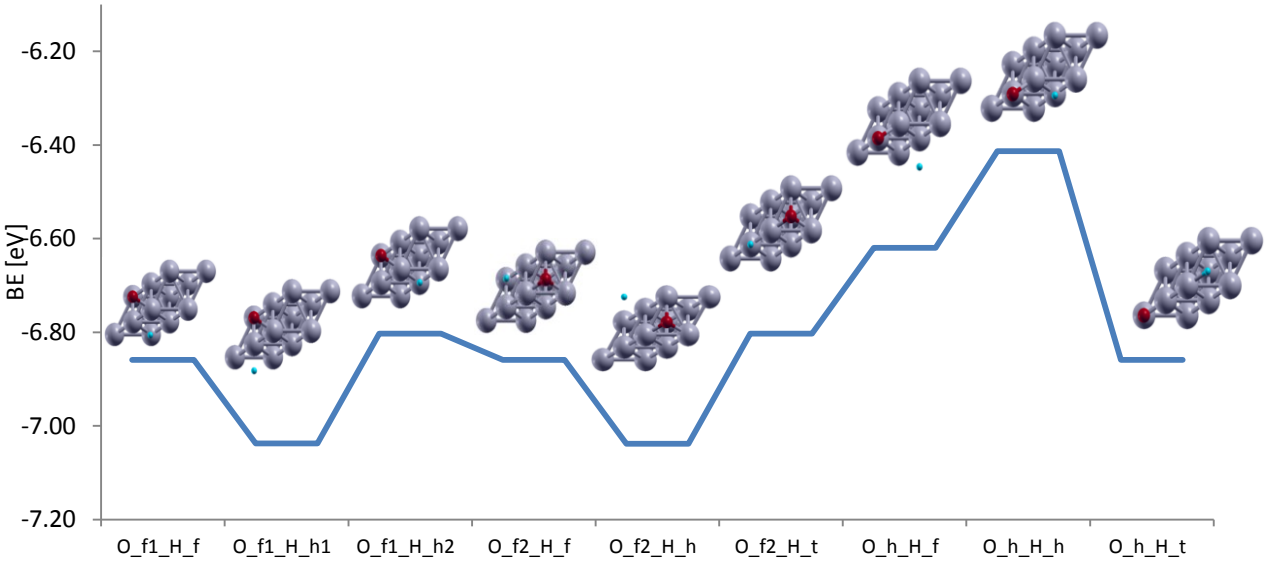

Figure 4.6: binding energies of O and H co-adsorbed at different sites on a 3 layers, 2x2 (111) Pt slab

O	H	BE [eV]
Fcc1 (f1)	**Fcc (f)**	-6.859
Fcc1 (f1)	**Hcp1 (h1)**	-7.038
Fcc1 (f1)	**Hcp2 (h2)**	-6.803
Fcc2 (f2)	**Fcc (f)**	-6.859
Fcc2 (f2)	**Hcp (h)**	-7.038
Fcc2 (f2)	**Top (t)**	-6.803
Hcp (h)	**Fcc (f)**	-6.620
Hcp (h)	**Hcp (h)**	-6.413
Hcp (h)	**Top (t)**	-6.859

Table 4.3: binding energies of O and H co-adsorbed at different sites on a 3 layers, 2x2 (111) Pt slab

The lowest binding energy (highest if the absolute value is considered) is computed when the atomic oxygen adsorbes at the fcc site, while H is at the hcp site before relaxing the system, but after the relaxation the atom of hydrogen is adsorbed on a top site.

Once the initial and final states are completely defined, the NEB calculations can be initialized, in fact the NEB code requires to know the start and the end of the Minimum Energy Path.
A complex unit cell with a great number of atomic layers, relaxed along x-y-z directions, and large vacuum could be adopted to provide a better esteem of the binding energy, but the larger is the supercell and the greater is the time required to find the relaxed electronic structure, because a considerable number of atoms can move on the Potential Energy Surface. Although the real problem lies in the NEB calculations, where the hours of CPU needed to find the Transition State directly depends on the kind of unit cell selected and the number of relaxed atoms. In fact the total number of iterations necessary to make calculations to converge is directly dependent on the number of relaxed (or allowed to move) atoms:

$$N° \; iterations \; \propto N° \; images \; x \; moving \; atoms \; x \; 3 \tag{4.40}$$

Convergence is reached when the forces acting on each image, perpendicular to the MEP, are below the selected threshold, which is 0.2 eV/ Å.

Thus a simple unit cell is selected to allow the NEB code to easily converge to the MEP and to rapidly find the Transition State. The kinetic energy cutoff is reduced to 25 Ry (344 eV) and a less

dense 6x6x1 k-point grid is used in order to speed up the research of the Transition State. 12 images are used to describe the MEP, the intermediate images (10) are initially built with a linear interpolation of the atomic positions between the initial and final state, then the shape of the 10 intermediate images is adjusted in order to bring them on the MEP. The greater is the number of the images and the better is the description of the MEP, and the evaluation of the tangent to the MEP, but, since DFT calculations are performed on each image every iteration of the NEB code, the greater is the total number of iteration required to make NEB to converge, according to (4.40), and the computational time.

NEB calculations are very tricky to converge, the first 20 iterations are performed with low spring constants (k_{min} = 0.1 ; k_{max} = 0.7) in order to allow the intermediate images to easily move on the PES, a wide "ds" that is the "optimization step length" is used. Then, when a suitable shape of the MEP is obtained (forces are below 2 eV/Å) and the image with the highest energy can be univocally determined, the Climbing Image method can be turned on, in order to allow the selected image to climb up, by following the MEP and to exactly reach the Transition State. Spring constants are increased to k_{min} = 0.2; k_{max} = 2.7, in order bring the images surrounding the Transition State closer to it and to provide a better esteem of the tangent to the MEP, instead the optimization step length is shrunk to ds = 0.5 to allow forces to satisfy the convergence criterion.

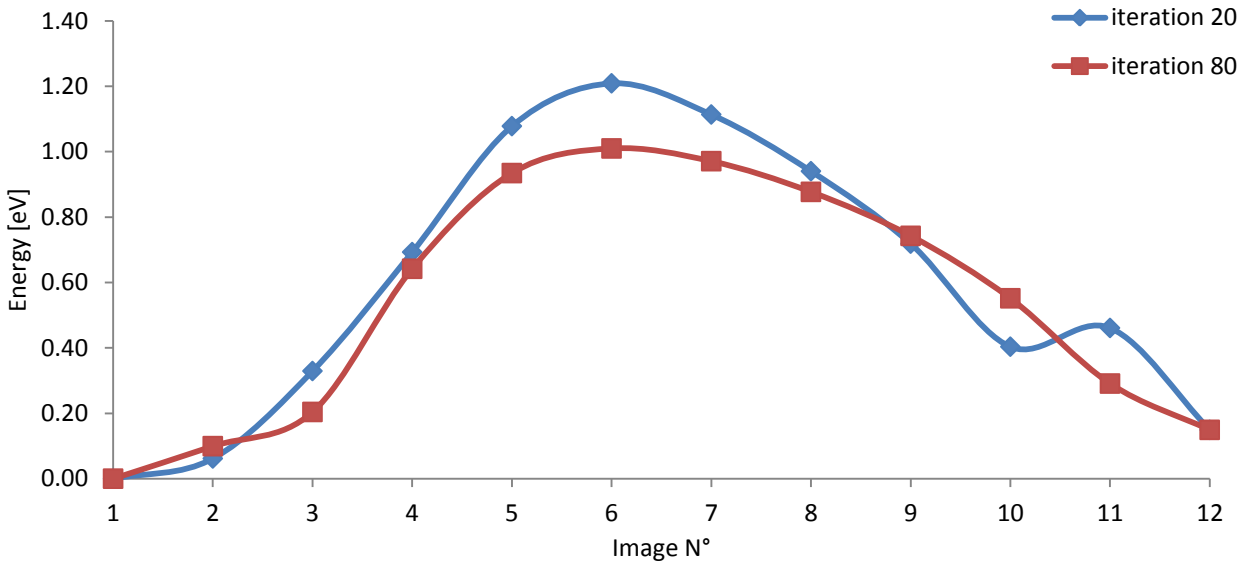

Figure 4.7: levels of energy of each image used to map the MEP after 20 iterations and after 80

The relative energy, referred to the energy of the initial state, that's the first image, is displayed for all the 12 images [Figure 4.7], after 20 iterations the image with the highest energy appears to cut the MEP, in fact image 6th doesn't lie on the MEP (0.57 eV/Å > 0.2 eV/Å), instead after 80 iterations the CI-NEB method satisfies the convergence criterion, and all the forces acting on each image are below 0.2 eV/Å.

Forward and backward activation energies are the interesting output of the various levels of energy calculated, thus an esteem of the barrier the reactants have to overcome is provided.

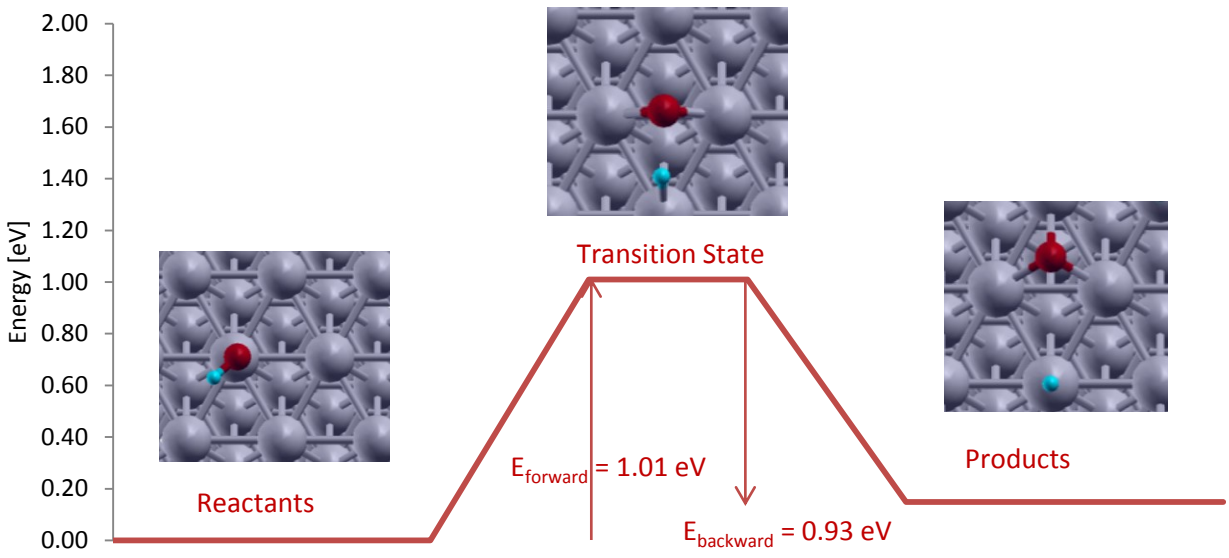

Figure 4.8: initial, transition and final state of OH dissociation on a 3 layers, 2x2 (111) Pt slab

CHAPTER 5

5 DFT Analysis of CO_2 Activation Pathways

5.1 CO_2 Activation on Metals

Carbon dioxide reactivity has been studied in order to understand its affinity with catalysts and thus to evaluate the activation energy of elementary steps that are probably involved as the initial step of a more complex further series of steps collected to build a reactive pathway.

Previous studies [49-51] led to the selection of these elementary steps, involving carbon dioxide decomposition (4.41), the Boudouard reaction (4.42), the Boudouard reaction with higher coverage of carbon species (4.43) and the carbon dioxide hydrogenation to carboxyl species (4.44):

$$CO_2 \rightarrow CO + O \tag{4.45}$$

$$CO_2 + C \rightarrow 2CO \tag{4.46}$$

$$CO_2 + nC \rightarrow 2CO + (n-1)C \tag{4.47}$$

$$CO_2 + H \rightarrow COOH \tag{4.48}$$

Now the main purpose lies in the calculation of the activation energies of these elementary steps on different catalysts to establish which one sees the lower activation energy for the forward reaction, and as consequence which step requires the lowest energy barrier to overtake the saddle point and to hop from the reactants to the products. Since the choice of the metal and the Miller index define the properties of the catalyst they also affect the surface chemistry by determining changes in chemisorptions heats, that is to say in binding energies. The selected metallic substrate acts on binding energies of the reactants and products, the larger is the binding energy and the greater is the thermodynamic stability of the chemical compounds involved in the reactive step. Since the energy

associated with the Transition State is referred to a saddle point the system is not located at a stable local minimum, the energy of the Transition State, its geometry and electronic structure can be compared with reactants' or products' chemical and geometrical properties.

The selected catalyst at a solid surface is a nanomaterial-based catalyst made up with a transition metal, belonging to the d-block of the periodic table. Transition metal activity is due to the ability to adopt multiple oxidation states, the substrate involves the formation of bonds between reactant molecules and atoms of the surface of the catalyst that use "d" and "s" electrons for bonding:

- Pt electron configuration: [Xe] $4f^{14}$ $5d^{9}$ $6s^{1}$
- Rh electron configuration: [Kr] $5s^{1}$ $4d^{8}$
- Ni electron configuration: [Ar] $4s^{2}$ $3d^{8}$

The valence electrons are delocalized and metals can be thought as a framework of atomic nuclei immersed in sea of electrons. The valence orbitals are partially empty, and thus are available to dwell another electron of adsorbate species to produce a chemical bond.

The gas phase species see a catalytic surface that possess a precise atomic spatial distribution, according to the Miller index, different kinds of adsorption sites with particular geometry and coordination of the first layer's atoms; generally an heterogeneous catalyst shows defects, kinks, terrace and numerous surfaces with different Miller index, each surface is characterized by its own surface chemistry and modifies adsorption heats, activation energies and Transition State geometry. In this work only the (111) surface has been studied, since it is the most common surface and the most abundant, in fact the energy of formation of the (111) surface is lower that the energy used to cleave the bulk along (100) and (110) Miller index.

5.2 Calculations: Technical Aspects

The electronic structure and Transition State calculations are carried out using DFT with CI-NEB method in a plane wave pseudopotential implementation, using the quantum-ESPRESSO code. PBE ultra-soft Vanderbilt pseudopotentials are employed, the plane wave cutoff in the calculations is 25 Ry (340 eV) for the wave function and 250 Ry (3400 eV) for the electron density. A k-points sampling of 6x6x1 Monkhorst-Pack is chosen, with Marzari-Vanderbilt smearing of 0.001 Ry [52].

To model the systems and represent the fcc (111) metal surface a 2x2 unit cell is chosen, the slab thickness is 3 layers, with surface atoms held at fixed positions, a vacuum spacing of 12 Angstrom is left between the slabs.

The Nudged Elastic Band method is used to find the Transition State, 12 images are used to map the MEP (including initial and final states). A linear interpolation represents the initial guess of the MEP, after few iterations, when a good approximation of the shape of the MEP is obtained and the image with the highest energy is identified the CI method is applied. Convergence is achieved when the projection normal to the MEP of the force acting on each image is less than a selected threshold, 0.2 eV/Angstrom.

Then calculations are newly performed considering a slab 4 layers thick, the upper layer, composed by 4 atoms, is relaxed along the direction defined by the lattice vector perpendicular to the surface's plane. The same vacuum spacing is maintained. The CPU consumption required to converge NEB calculations with the new supercell is much larger, since the number of the atoms used to build the slab increases from 12 to 16, and because 4 of these 16 atoms are relaxed. Each iteration requires 12 calculations of electronic structure, the greater is the number of images and the better is the mapping of the MEP, but more time consuming is the simulation. 12 images are sufficient to map the MEP in the examined cases since the intermediate image's distance is less than 0.5 Angstrom.

To overcome the great difficulties due to the higher complexity of the unit cell the MEP found as result of the converged NEB calculation over 3 layers slab is used, in fact the number of iterations asked by the CI-NEB method is strongly dependent on the initial guess. As the previous case, convergence is achieved when the projection normal to the MEP of the force acting on each image is less than 0.2 eV/Angstrom.

5.3 Elementary Step: $CO_2 \rightarrow CO + O$

The elementary step involving the dissociation of the carbon dioxide is studied on the (111) surface of the three selected metals, Platinum, Rhodium and Nickel.

Platinum (111)

Platinum is the first metal, and we first searched for the most stable adsorption sites to understand which are the most probable initial and final configuration of the reaction step.

CO_2	BE [eV]
Bridge	-0.022
Fcc	-0.023
Hcp	-0.021
Top	-0.024

Table 5.1: binding energy of carbon dioxide at different adsorption sites on Pt

CO	O	BE [eV]
Fcc	**Fcc**	-5.342
Hcp	**Fcc**	-5.588
Hcp2	**Fcc**	-5.334
Top	**Fcc**	-5.588
Fcc	**Hcp**	-5.122
Fcc	**Top**	-4.382

Table 5.2: binding energy of carbon monoxide and atomic oxygen at different combinations of adsorption sites on Pt

As shown in Table 5.1 and Table 5.2 the initial state is defined by carbon dioxide on a top site, instead at the final state a portion of surface shows a CO adsorbed on a top site, while O binds with the surface at a fcc site [22]. CI-NEB calculations are performed to identify the saddle point, which affects the activation energy of the process.

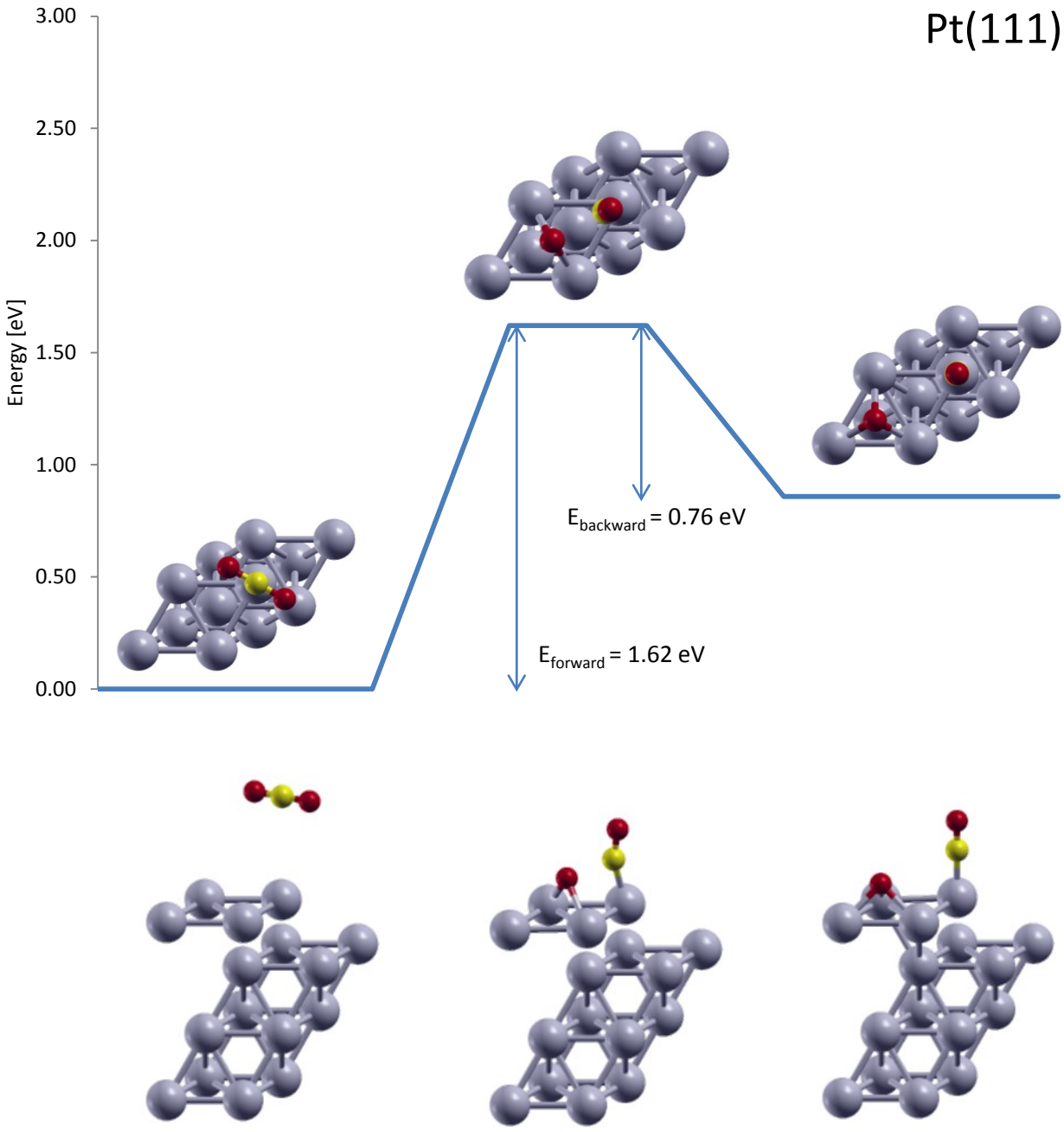

Figure 5.1: forward and backward activation energy of carbon dioxide decomposition on Pt

The upper and lateral view of the initial, transition and final state are provided by the previous pictures [Figure 5.1]. CO_2 weakly interacts with the surface, it is possible to notice [Table 5.1] that CO_2 experiences no relationship between the adsorption site and binding energy, the C atom is 4 Angstrom far away from the Platinum surface, thus no chemical bond is actually formed. The CO_2 molecular structure is very similar to the gas phase CO_2 structure, the C-O bond is 1.17 Å and the O-C-O angle is 179.90°.

At the Transition State CO_2 lands on the surface and bends the C-O bond while interacting with the Platinum, the atom of carbon is now near the atoms of the metal surface, and a C-Pt bond of 1.92 Å appears. The C-O distance is different since one oxygen is still bound to the C atom, with a C-O length of 1.15 Å instead of 1.17 Å, the monoxide molecular structure can be distinguished, but CO on the top site is tilted with a Pt-C-O angle of 157.00°. The other oxygen is instead on a bridge site, moving on the MEP towards the fcc site, the C-O distance is almost 2.02 Å, thus the original C-O bond is completely broken. The oxygen is strongly attached to the surface, the Pt-O distance is 2.07 Å, but if this distance is computed perpendicularly to the surface, only 1.50 Å are available between the Pt and O atoms' centers.

At the final state the CO molecule is no longer tilted but the Pt-C-O angle is exactly 180.00°, the C-O bond length is 1.15 Å, as for the Transition State geometry [43]. The Pt-C interaction leads to a reduction of the length from 1.92 to 1.87 Å, and the atomic oxygen falls in a threefold symmetric hollow (fcc site) interacting with the three neighboring Pt atoms. The O at fcc site is in a local minimum position, with a distance from the plane surface of 1.25 Å, against 1.50 Å of the bridge site, that is not a local minimum.

As shown in Figure 5.1 the surface reaction appears to be endothermic, according to (4.49), but if a thermodynamic cycle, with reactants and products in gas phase, is built, the reaction with gaseous reactants and products produces a larger, positive (endothermic), heat of reaction [Figure 5.2]. The first step of the cycle is referred to gaseous CO_2. CO_2 is adsorbed on the metal surface at the second step although little binding energy is computed so a very small gap exists between the first and second steps. CO_2 reaches the Transition State (step 3) and then is turned into products (step 4). CO and O are in the same supercell (step 4) so they are brought to infinite distance to do not interact with one another. This purpose is reached by using two supercells, where one dwells CO and the other includes O (step 5). At sixth step CO and O desorbe from the metal surface and are carried in gas phase.

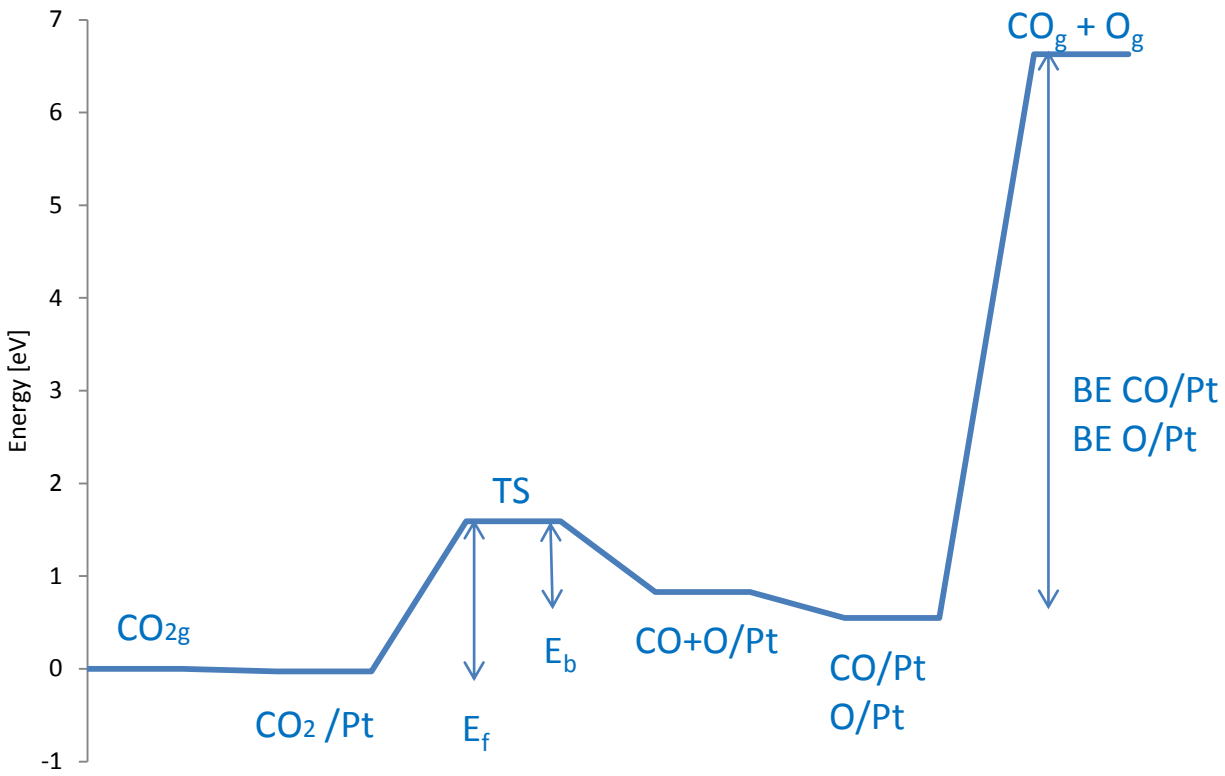

Figure 5.2: thermodynamic cycle of carbon dioxide decomposition on Pt

Rhodium (111)

The second metal of interest is Rhodium, the most stable adsorption sites are investigated to find the most probable initial and final configuration of the same reaction step.

CO_2	BE [eV]
Bridge	-0.022
Fcc	-0.015
Hcp	-0.022
Top	-0.027

Table 5.3: binding energy of carbon dioxide at different adsorption sites on Rh

CO	O	BE [eV]
Fcc	**Fcc**	-6.890
Hcp	**Fcc**	-6.890
Hcp2	**Fcc**	-6.709
Top	**Fcc**	-6.890
Fcc	**Hcp**	-6.596
Fcc	**Top**	-5.233

Table 5.4: binding energy of carbon monoxide and atomic oxygen at different combinations of adsorption sites on Rh

The substrate-adsorbate interaction may change, but carbon dioxide always experiences a flat potential energy surface with a small preference for the top site. If the unit cell containing CO and O co-adsorbed is relaxed CO moves from the fcc and hcp sites to the top, this is the explanation of identical binding energies in the third column and first, second and fourth rows of Table 5.4. CO and O are respectively found at top and fcc sites, and they show a stronger binding energy on Rhodium rather than on Platinum.

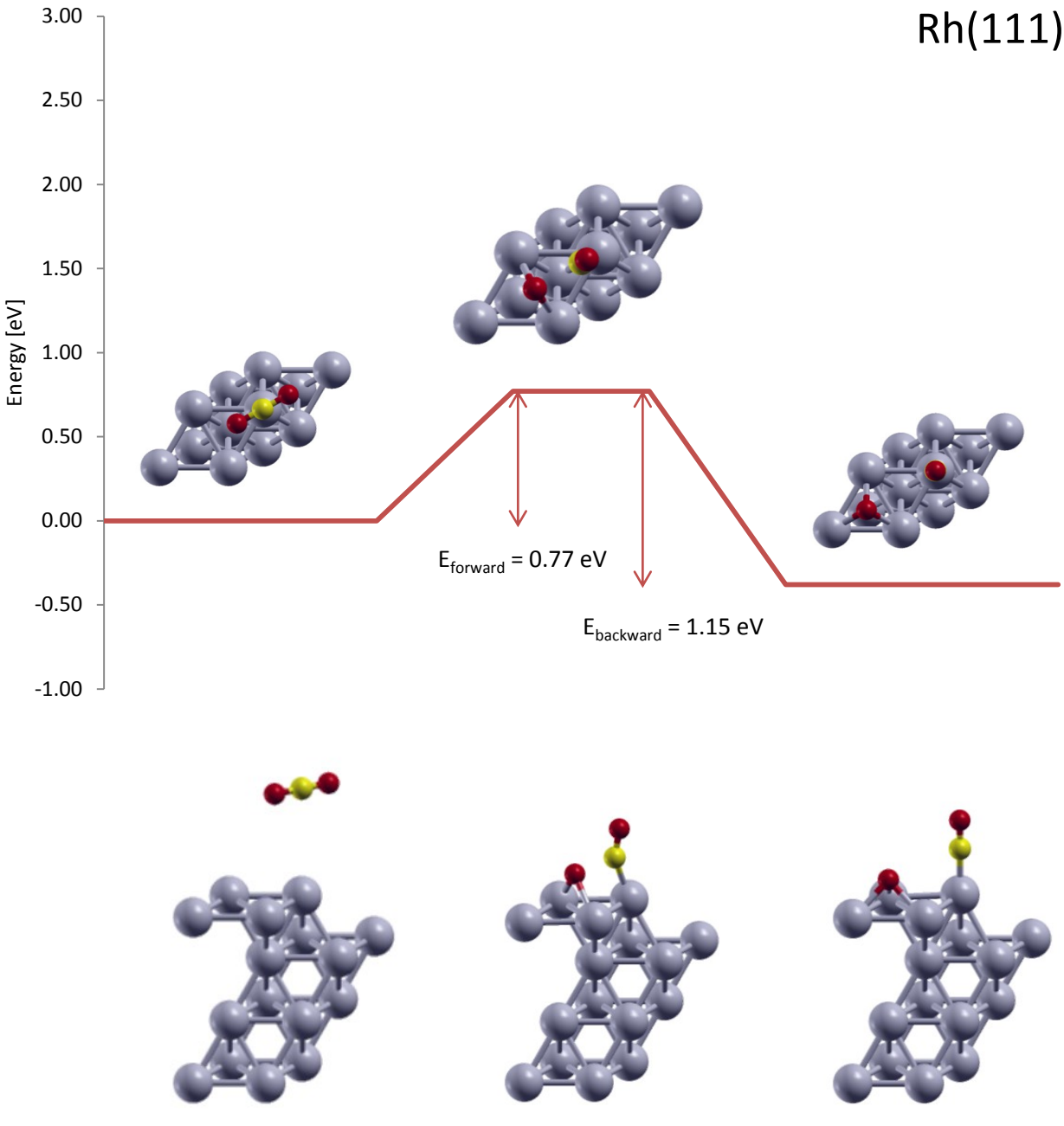

Figure 5.3: forward and backward activation energy of carbon dioxide decomposition on Rh

The initial state involves CO_2 that is weakly bound, since the heat of adsorption is almost zero no intense chemical interaction is expected, in fact CO_2 is in gas phase, the Rh-C distance is 4.30 Å, and the existence of such extended chemical bond is highly unlikely, in fact a typical bond length is 1-2 Å. CO_2 molecular structure is the gas phase structure because the substrate does not distort CO_2 shape as consequence of the negligible metal-adsorbate interaction. C-O bond length is 1.17 Å as for Pt, and the O-C-O angle 179.98°.

Then CO_2 places upon the surface, and goes on a top site with the carbon atom. At the Transition State a CO, tilted on a top site, and an atomic oxygen at a bridge site can be distinguished. The Rh-C bond distance is 1.95 Å, thus a chemical bond can be realized, the Rh-C-O angle is 150.00°. The C-O distance of the early monoxide is 1.167 Å, instead the other oxygen is dissociated, and found at a C-O distance of 1.83 Å and at 1.53 Å from the metal surface.

At the final state oxygen hops from the bridge to the fcc site, instead CO is found exactly perpendicular to the surface plane, over a top site, in fact the Rh-C-O angle is 179.98°. The Rh-C distance gets shorter, 1.86 Å, while the C-O bond length of the monoxide changes from 1.167 Å to 1.155 Å at the local minimum for CO on the slab [43]. Oxygen is at the fcc site and positioned at 1.31 Å over the Rhodium surface rather than 1.25 Å referred to a Platinum slab. The greater distance experienced by oxygen on Rhodium is probably caused by the smaller available space among the three atoms of Rhodium at the threefold site, in fact its lattice constant is smaller than the Platinum lattice constant.

As depicted in Figure 5.3, the surface reaction appears to be exothermic, according to (4.50), while it is endothermic if a Platinum catalyst is used. This opposite behavior is due to the different surface chemistry, although if the whole thermodynamic cycle is considered, with reactants and products in gas phase, the reaction appears actually endothermic as before [Figure 5.2, Figure 5.4].

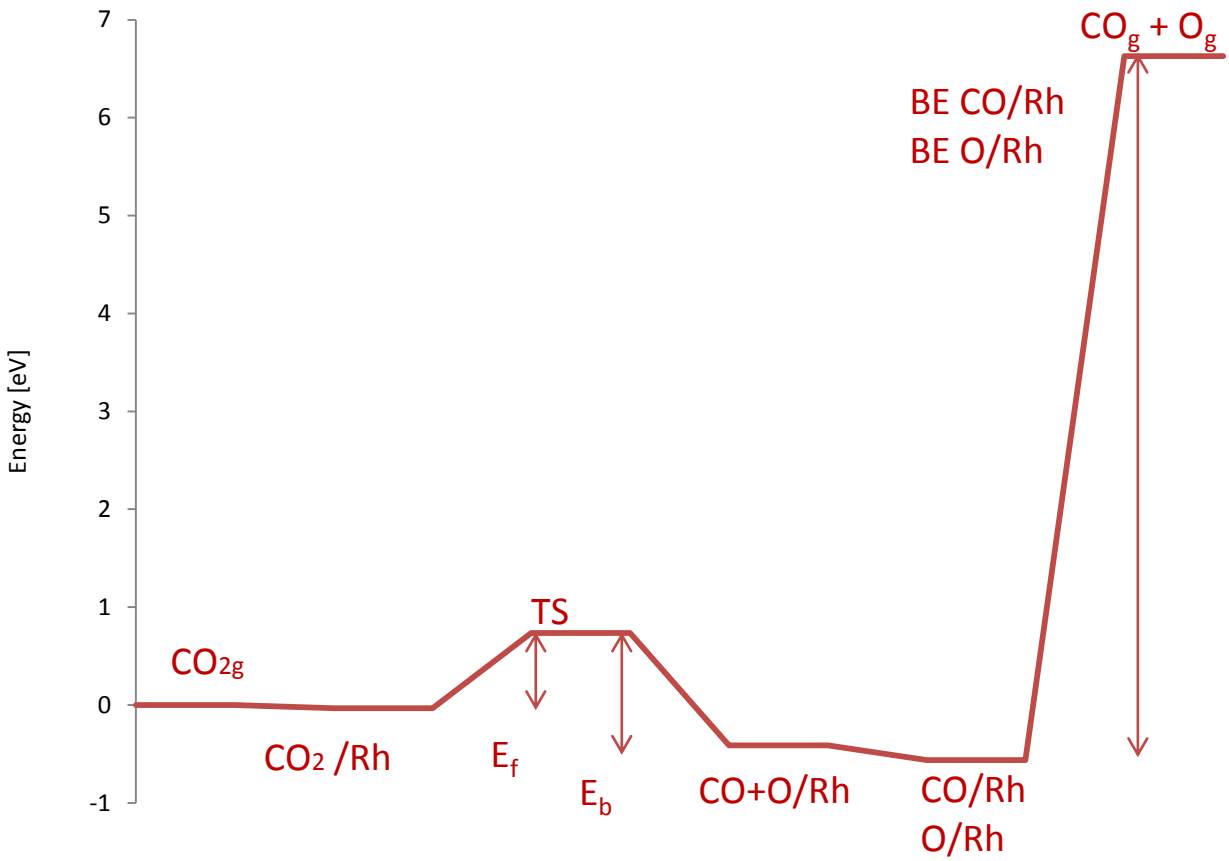

Figure 5.4: thermodynamic cycle of carbon dioxide decomposition on Rh

Nickel (111)

The third examined metal is Nickel, and always a research of the most stable adsorption sites for reactants and products is required to identify the most stable initial and final configuration of the CO_2 decomposition.

CO_2	BE [eV]
Bridge	0.235
Fcc	0.029
Hcp	0.364
Top	-0.033

Table 5.5: binding energy of carbon dioxide at different adsorption sites on Ni

CO	O	BE [eV]
Fcc	**Fcc**	-7.069
Hcp	**Fcc**	-7.171
Hcp2	**Fcc**	-7.279
Top	**Fcc**	-6.978
Fcc	**Hcp**	-7.110
Fcc	**Top**	-5.443

Table 5.6: binding energy of carbon monoxide and atomic oxygen at different combinations of adsorption sites on Ni

In line with results obtained with Platinum and Rhodium carbon dioxide experiences a flat potential energy surface even over a Ni surface. A positive value of the binding energy means that the sum of two separate systems, one containing CO_2 in gas phase, and the other representing the slab, is more stable than a single system where CO_2 and the slab coexist. However the preferred site is the top for CO_2, instead CO is found at hcp site, instead oxygen is still at fcc [24]. On the contrary the pseudo binding energy of the co-adsorbed CO and O species is greater than the binding energy experienced on a Platinum or Rhodium surfaces.

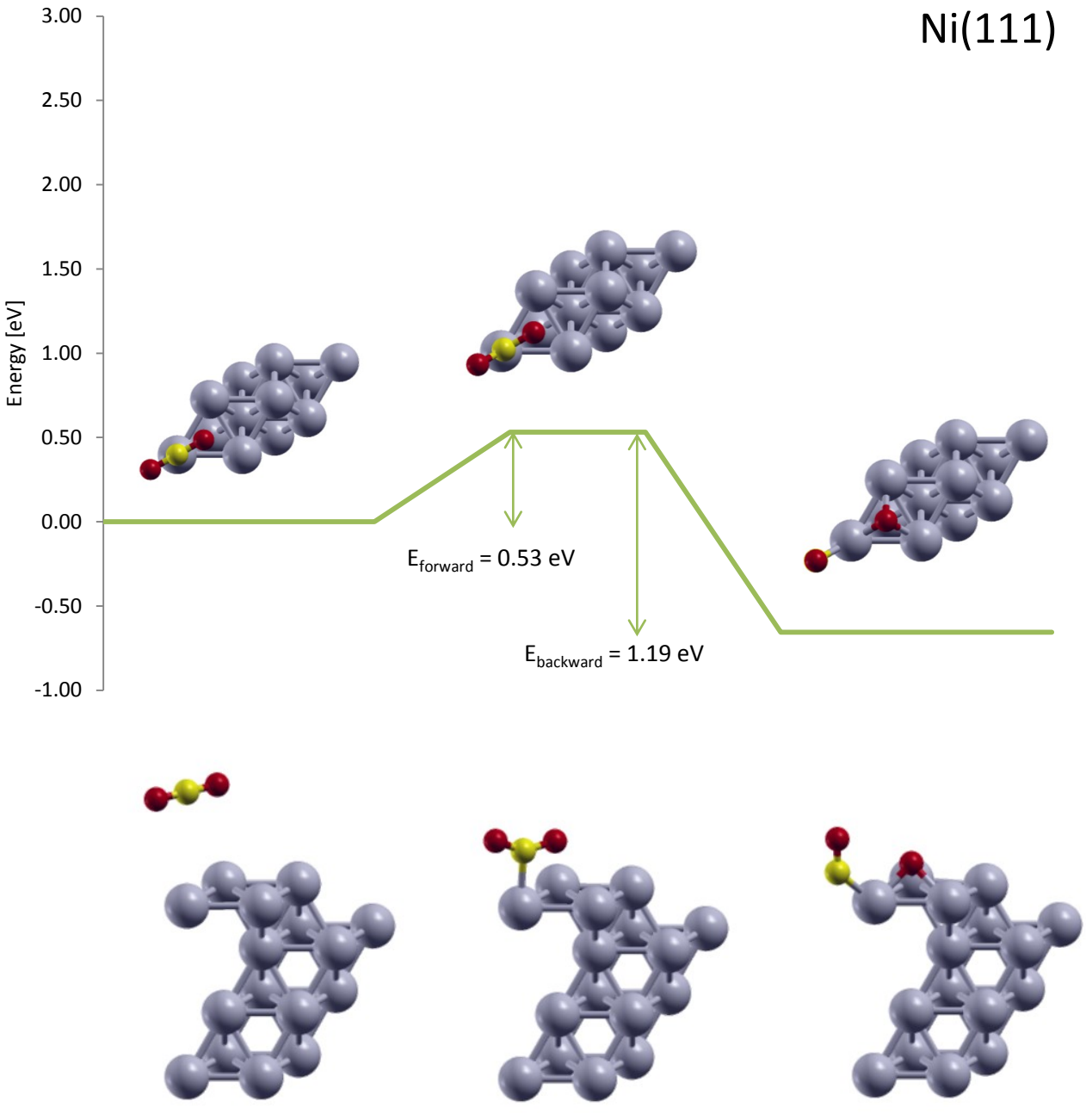

Figure 5.5: forward and backward activation energy of carbon dioxide decomposition on Ni, upper view

As for the previous substrates, CO_2 remains in gas phase even on Nickel, no chemical bond is created between Nickel and carbon, in fact the Ni-C distance is 4.04 Å, with CO_2 parallel to the surface's plane. The C-O bond length is the typical length of the gas phase CO_2, which is 1.17 Å, the substrate does not affect the CO_2 linear geometry, that shows an O-C-O angle of 179.95°.

CO_2 moves downwards the surface, this time the C-O bond is not broken yet. At the Transition State the CO_2 still exists, but it is strongly distorted. C binds to the Ni atom on a top site, the Ni-C distance is 2.01 Å, the CO_2 structure is far different from the one of the gas phase, the O-C-O angle is 147.12° against the initial 179.95°, and the Ni-C-O angle of 114.16° on one end, with a C-O bond length of 1.20 Å, and 98.72° on the other, with atomic oxygen pointing at the bridge site and a C-O spacing of 1.23 Å.

Then the oxygen pointing at the bridge does not immediately falls in the hcp site but diffuses to the fcc site, showing a structure very similar to the usual Transition State, where CO is on top, tilted. At the final state CO and O move respectively from a top to an hcp site, and O from an hcp to a fcc site. C is found to be at a 1.31 Å vertical distance from the surface, and as oxygen atom is now surrounded by three atoms of Ni, C-O bond length is 1.18 Å, greater than the same distance measured on Rhodium and on Platinum [43]. O is tightly bound to the surface with a perpendicular distance of 1.12 Å from the surface's plane. This short distance is probably due to the strong interaction of atomic oxygen with metal, in fact the oxygen binding energy is higher on Nickel rather than on Platinum or Rhodium.

The observation of Figure 5.5 leads to state that the surface reaction is exothermic, according to (4.51), thus Nickel and Platinum produce a final state with a lower total energy, although the reaction led in gas phase is endothermic, and this statement can be demonstrated with the following thermodynamic cycle. Both reactants and products are in gas phase, and difference between the initial and final state energy is independent from the intermediate states, that is from the surface reaction.

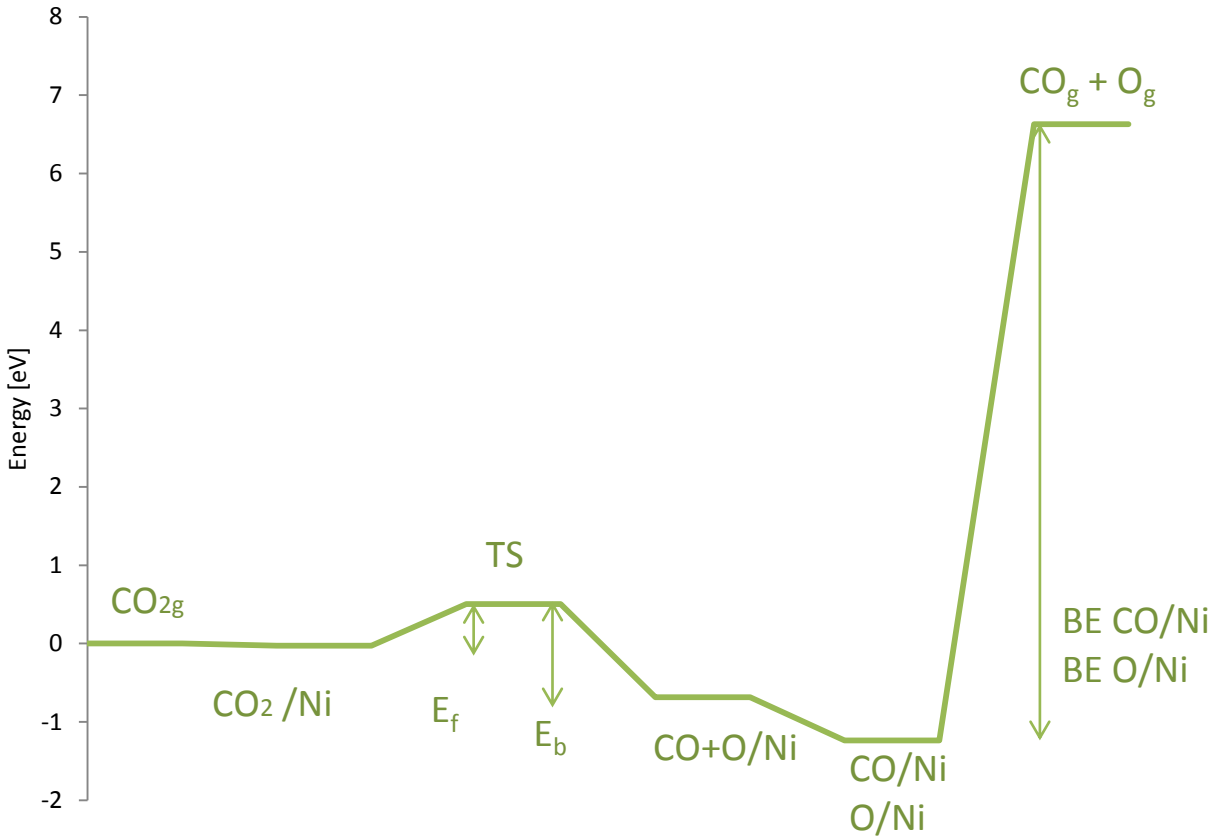

Figure 5.6: thermodynamic cycle of carbon dioxide decomposition on Ni

5.3.1 Reactivity Analysis of Metals:

$$CO_2 \rightarrow CO + O$$

The aim of this study is to identify and highlight significant trends among the three investigated metals in order to explain the influence the metals have over heats of adsorption and activation energies.

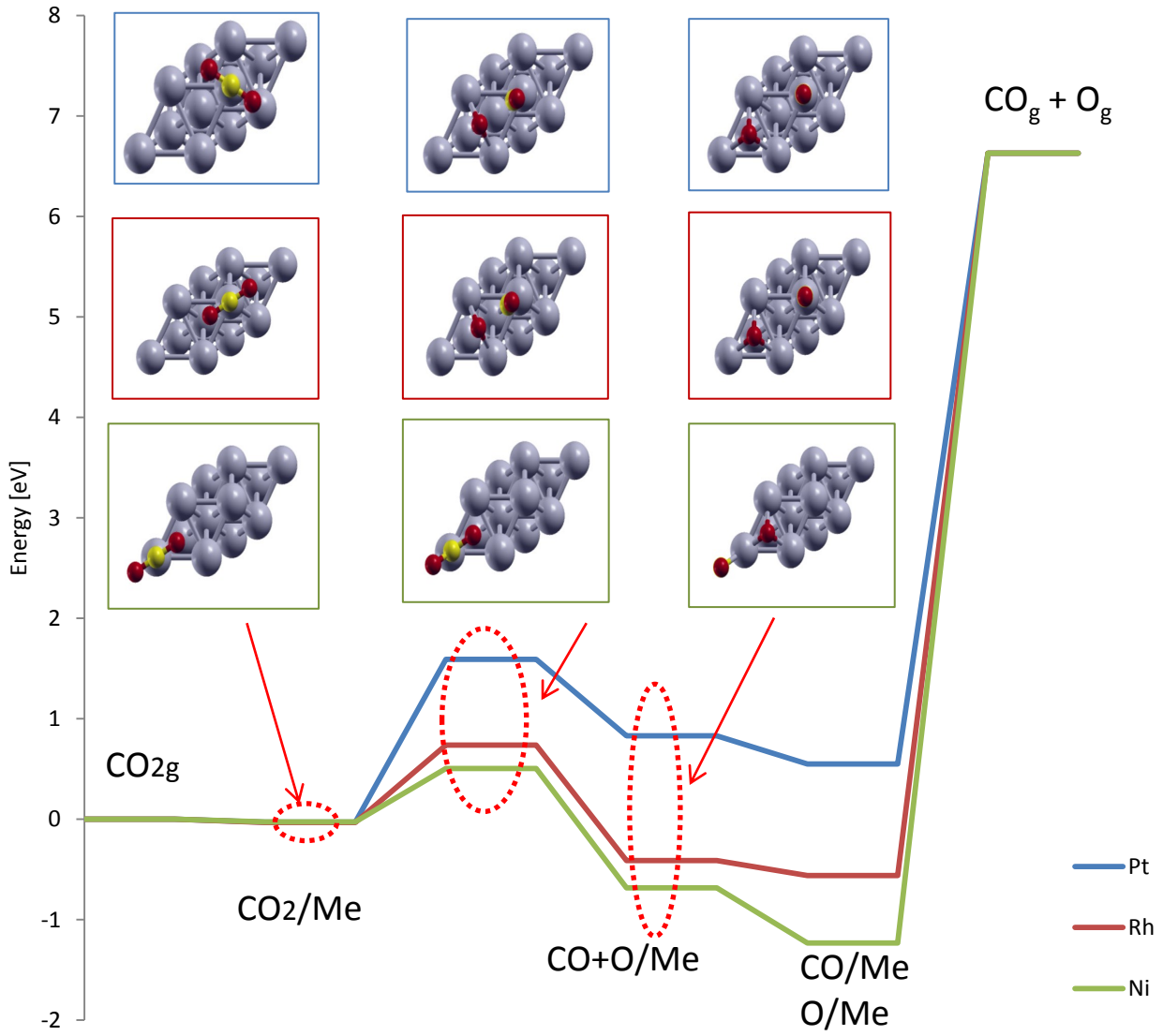

Figure 5.7: thermodynamic cycle of carbon dioxide decomposition on Pt, Rh and Ni

Figure 5.7 illustrates the thermodynamic cycle, where the first step represents CO_2 in gas phase, whose energy is considered as reference level. At second step CO_2 is no longer in gas phase but it is on the metal surface, since the binding energies due to the interaction with the metals are almost zero the lines referred to Platinum, Rhodium and Nickel are overlapped. The second step describes the initial state of reaction at the metal surface, then the Transition State of the different metals is defined by the third step, and the relative energy of products is depicted in the fourth step. The fifth step considers the effect of the co-adsorption of CO and O in the same supercell by separating the two products, then CO and O desorbe, thus the binding energy of CO and O is added to the fifth step to reach the sixth level, where CO and O are in gas phase. As consequence the difference between the energies of the first and last steps, that is the heat of reaction where both reactants and products are in gas phase, does not depend on the surface chemistry, in fact all the lines referred to the three substrates ends at the same level of energy.

The different forward and backward activation energies are provided for the three metallic substrates [Figure 5.8].

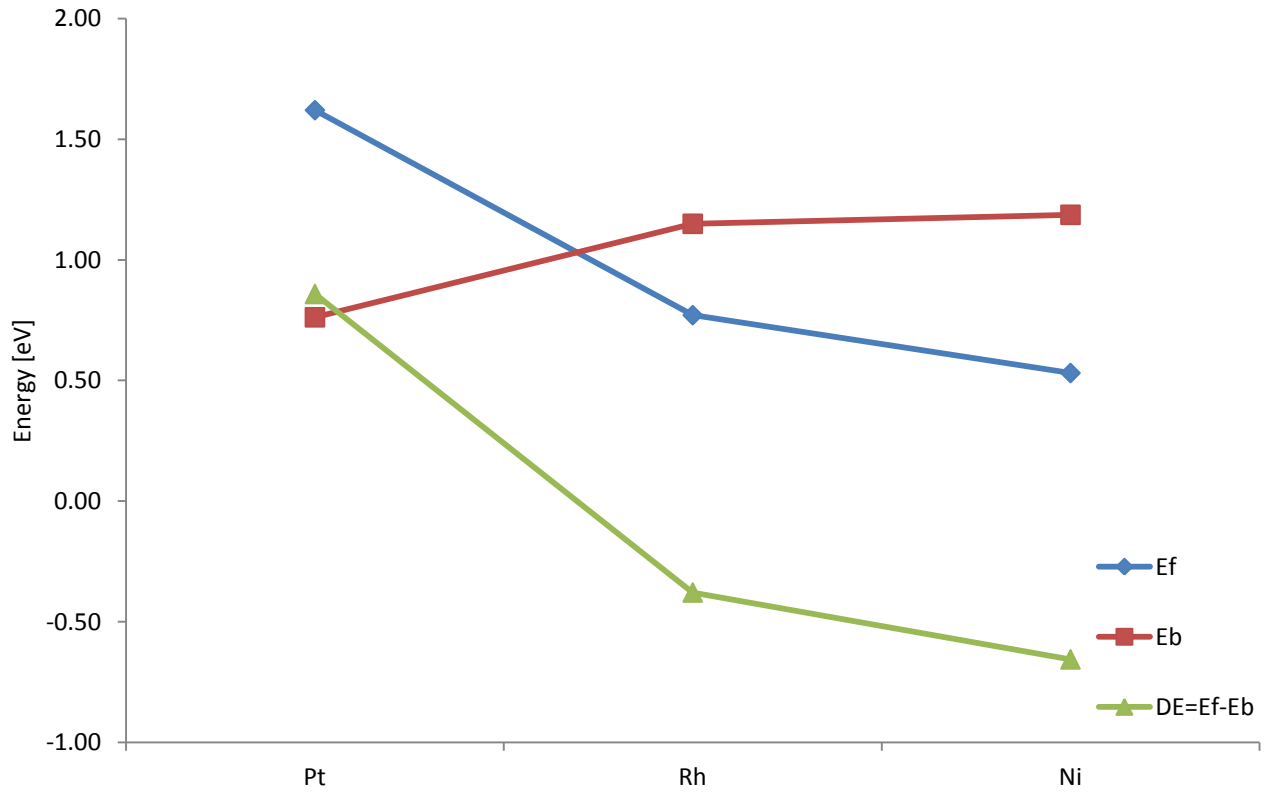

Figure 5.8: forward, backward activation energy, and heats of reaction (5.1) on the three metals

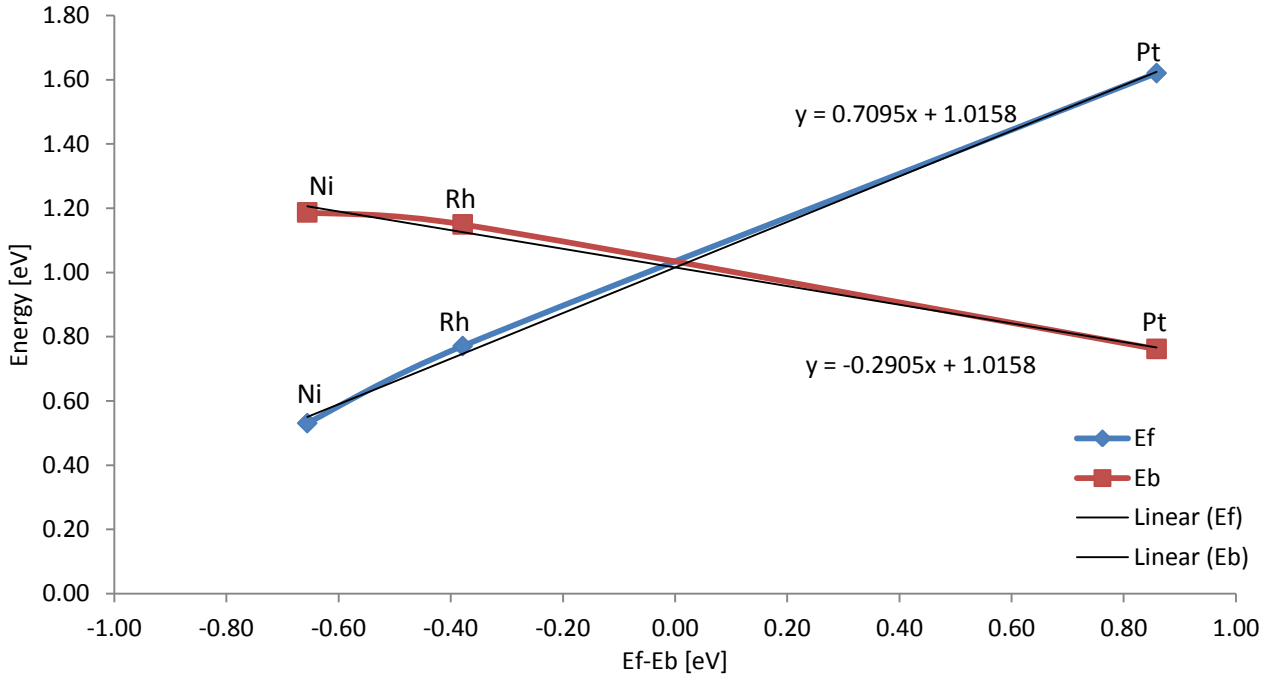

Figure 5.9: forward and backward activation energy dependence on heats of reaction (5.1)

An Evans-Polanyi dependence can be identified [53], in fact Evans-Polanyi model is a linear relationship between activation energies and heats of reactions of elementary reactive acts of the same family [Figure 5.9]. This model can be used as an efficient way to predict the activation energies of many reactions belonging to the same class.

$$E_\alpha = E_0 + \alpha \cdot \Delta E_R \tag{4.52}$$

Where "E_0" is the activation energy of a reference reaction, "ΔE_R" is the heat of reaction and "α" is the parameter that defines the position of the Transition State along the reaction coordinate.

Since the angular coefficient of the line interpolating the "Ef" curve is $\alpha = 0.71$, the Transition State is not in the middle of the path that links reactants and products ($\alpha = 0.5$), but it is shifted towards products. On the other hand if "Eb" is considered, its angular coefficient is $\alpha = 0.29$.

A notable aspect is related to the higher relative energy of the final state of the surface reaction, referred to the products of reaction adsorbed on the substrate, that occurs on Platinum [Figure 5.7]. An explanation can be sought in the adsorbate-substrate interaction [Figure 5.10].

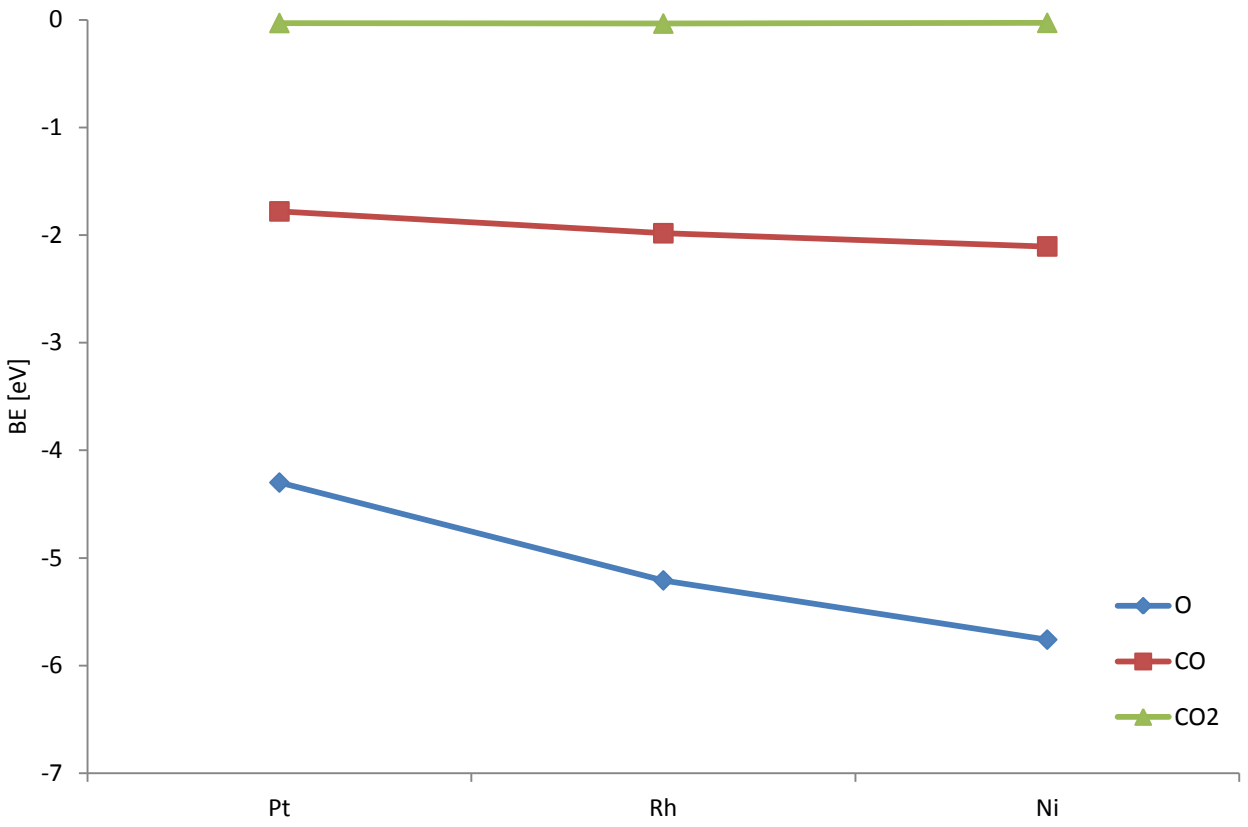

Figure 5.10: binding energies of reactants and products of reaction (5.1) on the three metals

The metal slightly affects the binding energies of CO and CO_2, instead the binding energy of oxygen is greater than the binding energy of the other compounds, and increases from Pt to Rh to Ni. Since the atom of oxygen affects the energy of the final state of the elementary step, the greater is its binding energy and the lower is the level of relative energy referred to the products at the catalytic surface as shown in Figure 5.7.

Forward activation energy should depend on the binding energy of the reactant, CO_2, but no dependence occurs, it rather increases as oxygen binding energy decreases, but oxygen is a product and not a reactant. On the other hand backward activation energy should be proportional to the binding energies of the products, but it is mainly influenced by oxygen binding energy [Figure 5.11, Figure 5.12], as explained in chapter 3 by the PDOS approach [Figure 3.45, Figure 3.48].

As a whole, atomic oxygen appears to be the chemical species that more affects the properties of the system in terms of energy, in fact both forward and backward activation energy of the process are sensitive to the binding energy of oxygen.

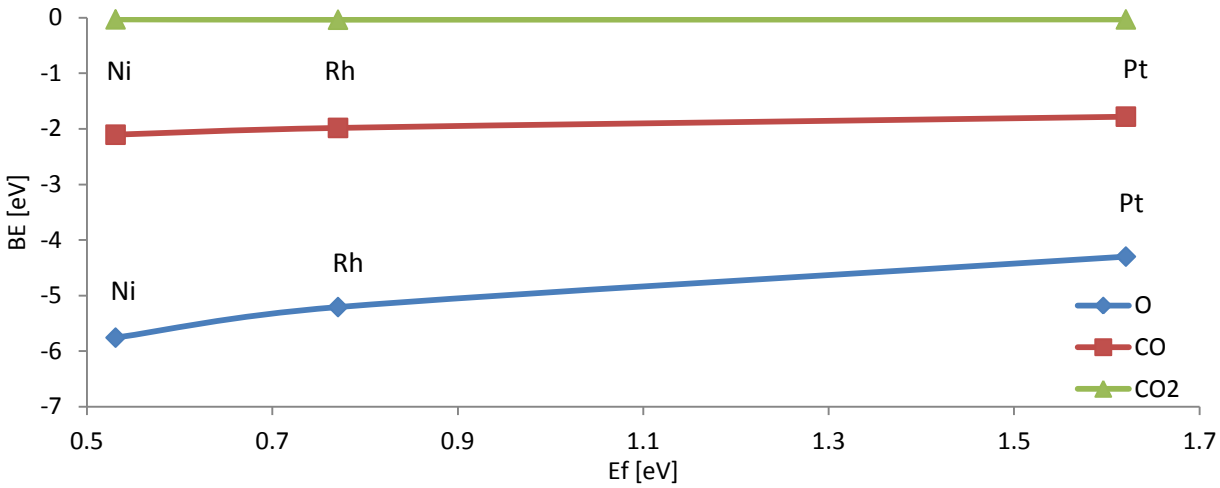

Figure 5.11: binding energies of reactants and products depending on forward activation energy, for reaction (5.1)

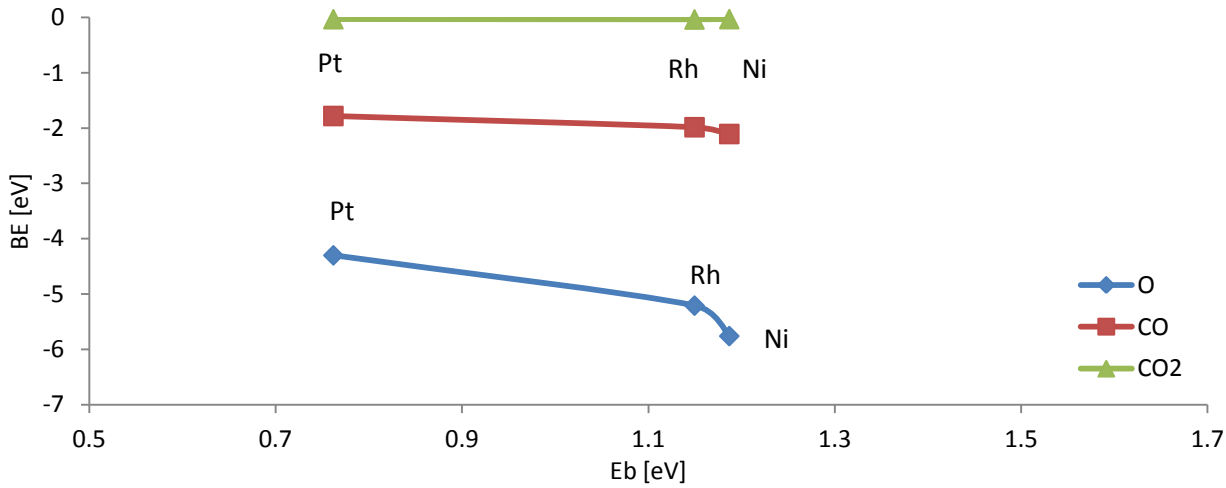

Figure 5.12: binding energies of reactants and products depending on backward activation energy, for reaction (5.1)

If the density of states is calculated for the initial, transition and final states of the surface reaction on the three different metals the electronic properties of the Transition State can be connected with the properties of reactants and products.

On Platinum:

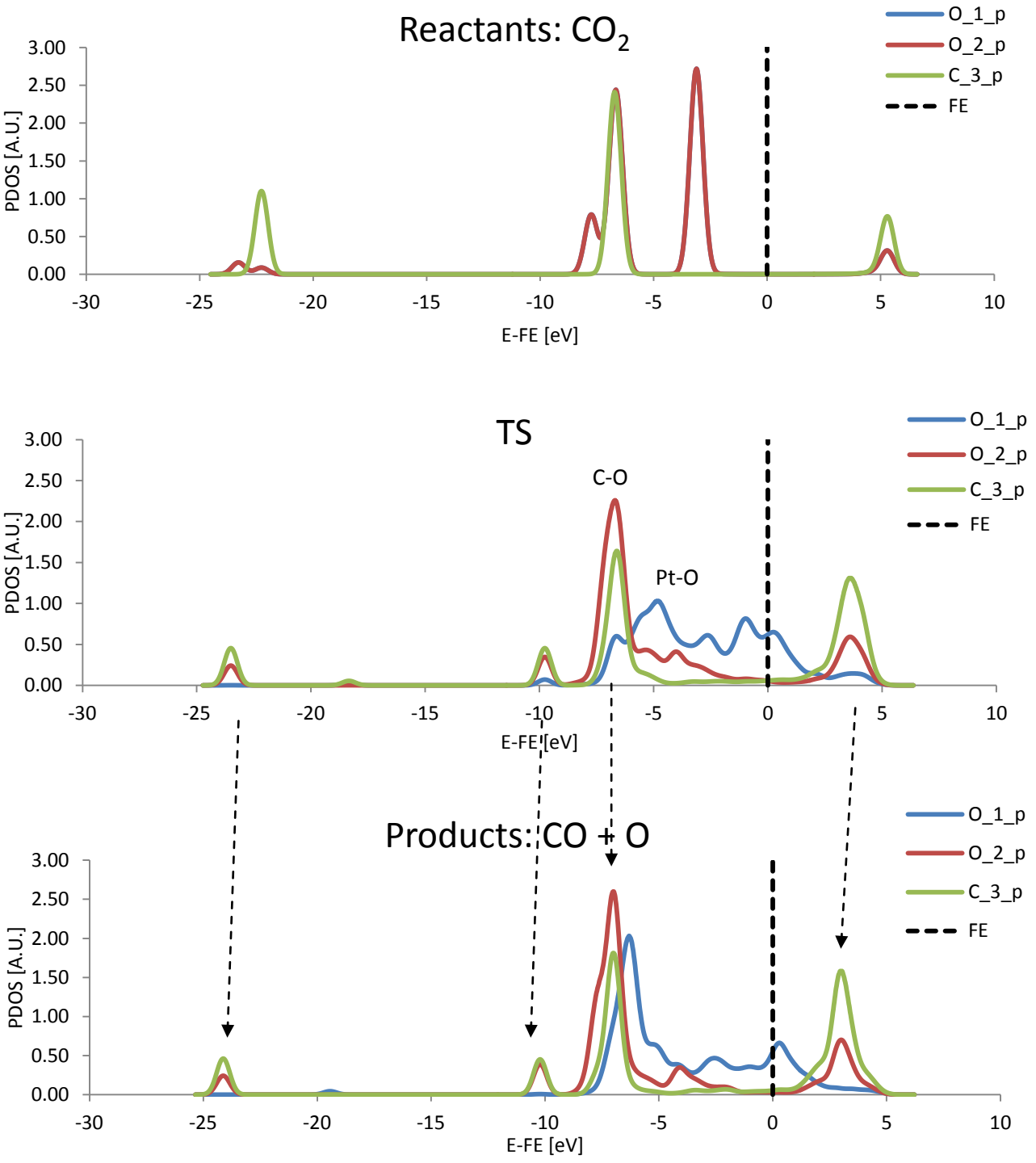

Figure 5.13: PDOS of the reactants, Transition State, and products for reaction (5.1) on Pt; FE = Fermi Energy (reference level); X_n_v means X = atomic type, n = label of the atom, v = valence orbital

On Rhodium:

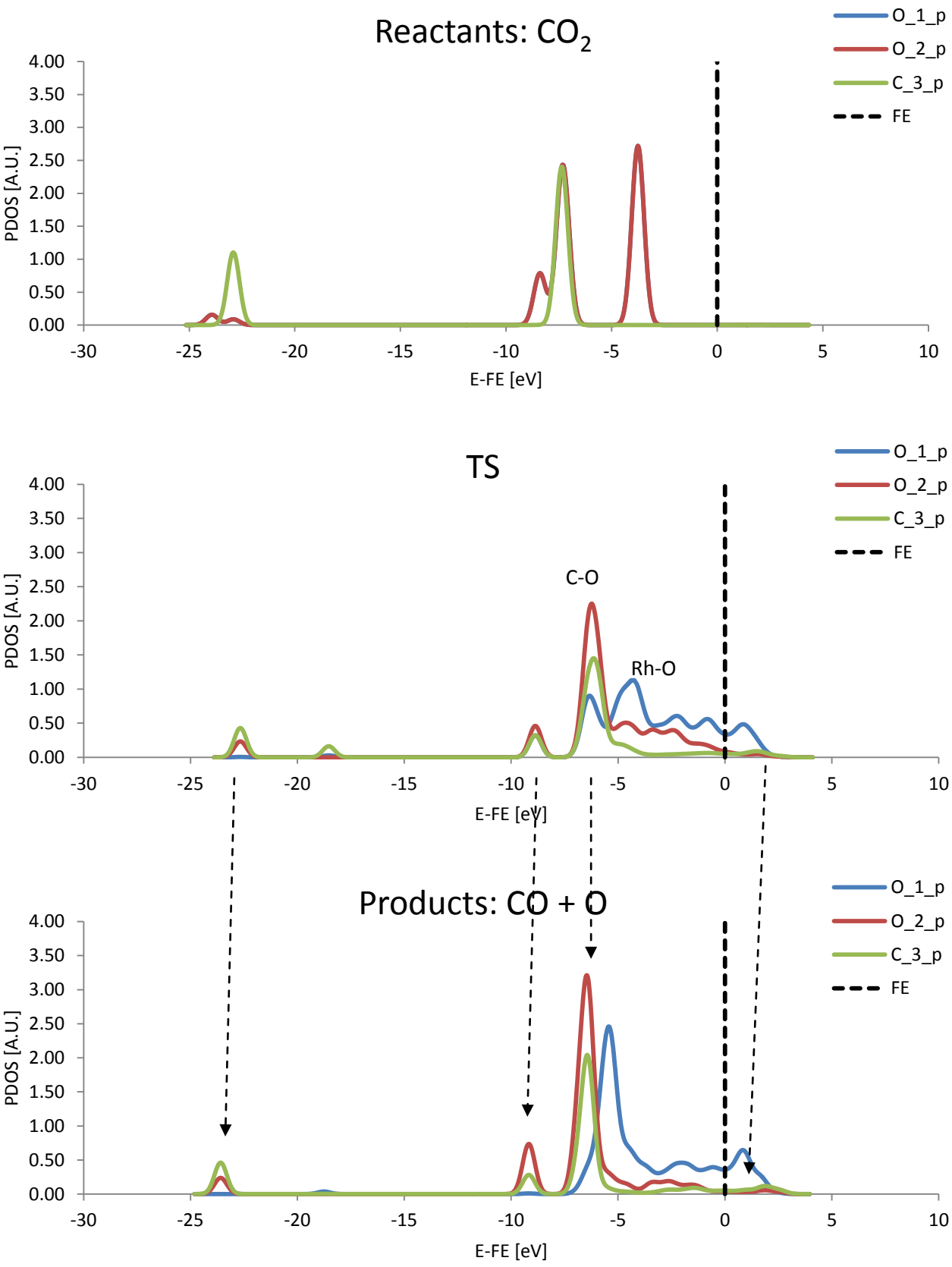

Figure 5.14: PDOS of the reactants, Transition State, and products for reaction (5.1) on Rh; FE = Fermi Energy (reference level); X_n_v means X = atomic type, n = label of the atom, v = valence orbital

On Nickel:

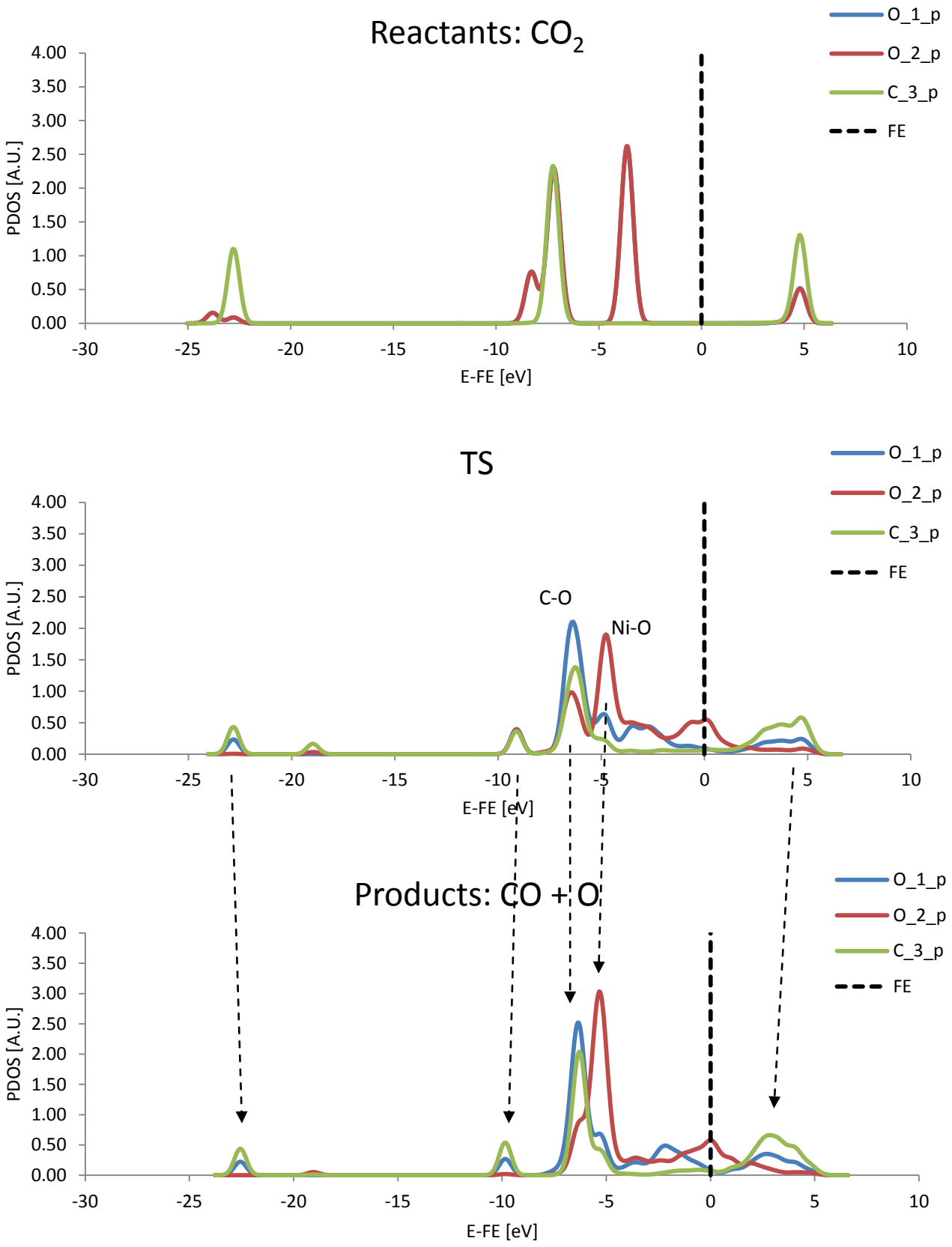

Figure 5.15: PDOS of the reactants, Transition State, and products for reaction (5.1) on Ni; FE = Fermi Energy (reference level); X_n_v means X = atomic type, n = label of the atom, v = valence orbital

The three metals give birth to a late Transition State in fact the PDOS of the TS is very similar to the PDOS of the last state, in fact at least four peaks of TS-PDOS are easily detected in the PDOS of products. Moreover the Transition State (on Platinum and Nickel) resembles the products, in fact a vertical CO is adsorbed on a top site and O is on a bridge site. As consequence the Transition State is called "late Transition State", but it is not always so easy to define, so the Transition State properties are investigated according to both geometrical and electronic properties. The results of this analysis are compared, although the Transition State geometry on Rhodium appears to be early the true nature of the late Transition State is revealed by the investigation of its electronic structure with the PDOS.

$CO_2 \rightarrow CO+O$		
	Geometry	Electronic structure
Pt	Late	Late
Rh	Early	Late
Ni	Late	Late

Table 5.7: evaluation of the Transition State for reaction (5.1)

Conclusions:

- Carbon dioxide does not affect forward activation energy,
- The Transition State is late since both backward activation energy depends on the binding energy of products,
- The activation energies are dominantly influenced by the binding energy of the atomic oxygen.

5.4 Elementary Step: $CO_2 + C \rightarrow 2CO$

The Boudouard reaction is analyzed on the (111) surface of a Platinum, Rhodium and Nickel based catalyst, in order to compute the activation energy of the process.

Platinum (111)

The Platinum is the first metal, as usual the investigation of the most stable adsorption sites is performed. The following tables illustrate the heats of adsorption computed for the initial and final states of the elementary step.

CO_2	C	BE [eV]
Top1	Fcc	-6.799
Top2	Fcc	-6.794
Top	Hcp1	-6.765
Top	Hcp2	-6.760
Top	Top	-4.662
Fcc	Fcc	-6.804

Table 5.8: binding energy of carbon dioxide and atomic carbon at different combinations of adsorption sites on Pt

CO	CO	BE [eV]
Fcc1	Fcc2	-2.879
Fcc	Hcp	-2.574
Top	Fcc1	-3.080
Top	Fcc2	-3.017
Top	Hcp1	-3.017
Top	Top	-2.519
Hcp1	Hcp2	-2.800

Table 5.9: binding energy of two monoxides at different combinations of adsorption sites on Pt

The most stable positions are the fcc site for carbon, and the fcc site for CO_2, although during the relaxation of the structure CO_2 moves from fcc to a top site, instead the two CO molecules are adsorbed on a top site and on a neighboring fcc site [19, 23].

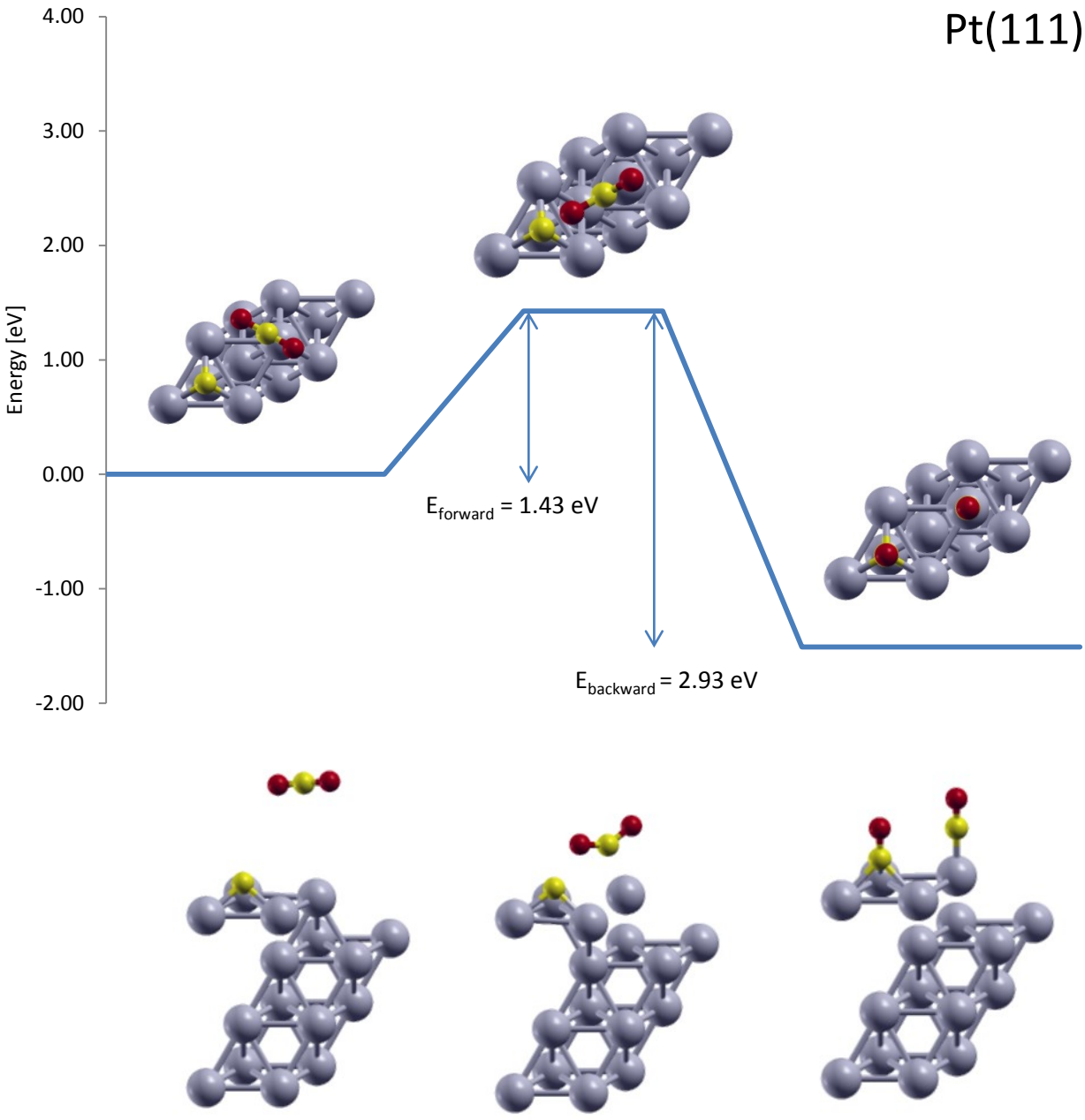

Figure 5.16: forward and backward activation energy of Boudouard reaction on Pt

Figure 5.16 shows the energy levels of the initial, transition and final state, with an upper and lateral view of the atomic disposition of these images of the MEP.

The position of CO_2 does not considerably affect the binding energy of the system, in fact the heats of adsorption related to the initial state is dominantly due to the metal-carbon interaction [Table 5.8]. As consequence the most favorite site for C is the same site that is found when CO_2 is absent, as depicted in Table 5.10, where the binding energies of the individual chemical species are calculated on a 2x2 supercell with 3 layers.

Adsorption on Platinum (111)	**Binding energy [eV]**
C	-6.825 (fcc)
CO_2	-0.053 (top)

Table 5.10: binding energy computed at the strongest adsorption site for atomic carbon on a Pt (111) 2x2 slab with 3 layers, and carbon dioxide on a Pt (111) 2x2 slab with 3 layers

At the initial state CO_2 remains 4.62 Å far from the surface, in gas phase, with a C-O bond length of 1.17 Å and an O-C-O angle of 179.99°. The C adsorbed atom is strongly bound to the surface at 1.03 Å of distance from the surface plane.

At the Transition State CO_2 experiences the surface potential and changes its linear geometry, the new O-C-O angle is 138.6°, instead the C-O initial bond length becomes 1.20 Å and 1.25 Å with the C-O bond that is stretching towards the adsorbed carbon on fcc site, that rises up from 1.03 Å to 1.1 Å, facing the neighboring oxygen.

Then CO_2 sits on the top site and one of its oxygen is shared between two atoms of carbon, the initial C-O bond breaks to make a new C-O bond. At the final state a CO is found on a top site, with a Pt-C distance of 1.87 Å, and a C-O bond of 1.149 Å, whereas the other CO is 1.33 Å far from the surface and shows a C-O distance of 1.196 Å [43].

In Figure 5.16 the energetic levels prove that the surface reaction (4.53) is exothermic, although the whole thermodynamic cycle is built starting from reactants in gas phase to products in gas phase:

- Heat of adsorption of the reactants,
- Forward and backward activation energy,
- Products' energy,
- Difference between the heat of co-adsorption of two molecules of CO on the slab and two heats of adsorption of a single CO molecule on the slab, that is called "infinite distance separation",
- Two binding energies of CO, since two molecules of product desorbe from the surface.

Even the gas phase reaction is generally endothermic [Figure 5.17].

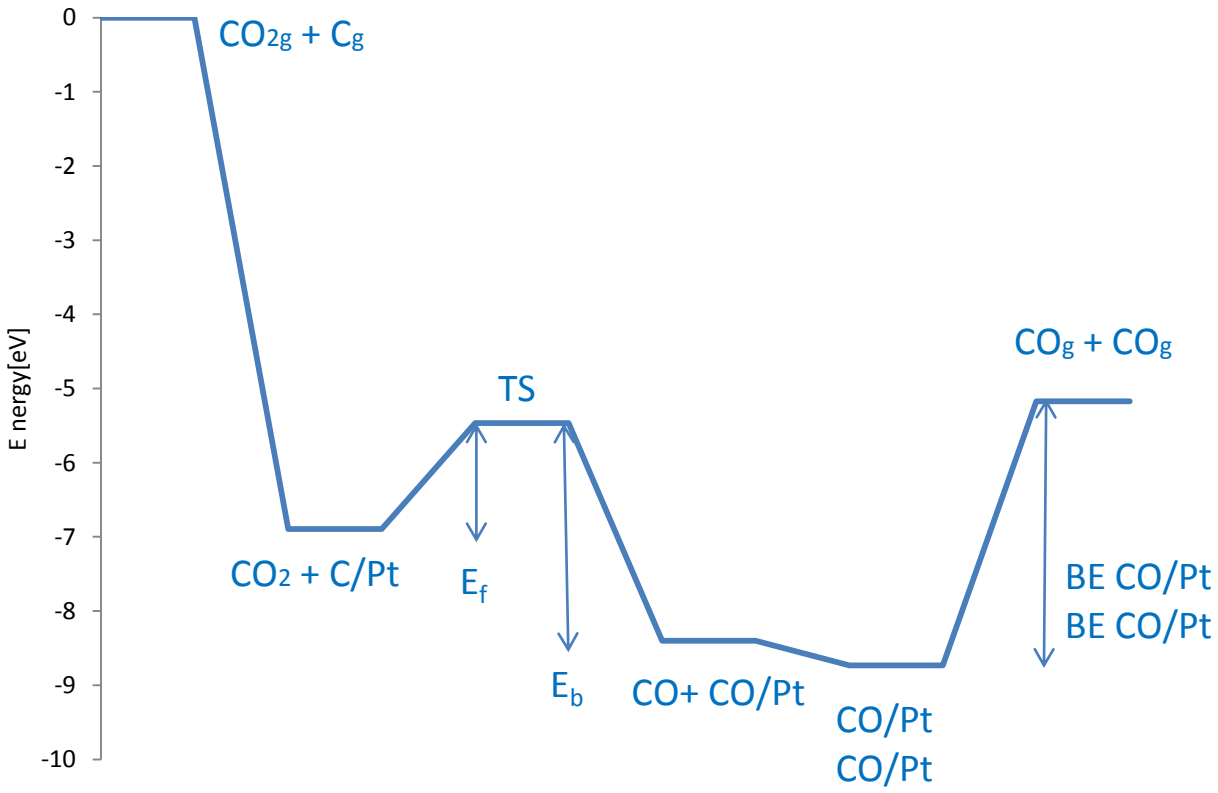

Figure 5.17: thermodynamic cycle of Boudouard reaction on Pt

Rhodium (111)

The same steps are followed for the second metal, Rhodium, the research of the most stable initial and final state is done, heats of adsorption on different sites are computed relaxing the initial electronic structure. The energies of the local minima are collected in Table 5.11.

CO_2	C	BE [eV]
Fcc	**Fcc**	-6.736
Hcp	**Fcc**	-6.719
Top	**Hcp**	-7.060
Top	**Top**	-4.948

Table 5.11: binding energy of carbon dioxide and atomic carbon at different combinations of adsorption sites on Rh

CO	CO	BE [eV]
Fcc1	**Fcc2**	-3.312
Fcc	**Hcp**	-3.164
Top	**Fcc1**	-3.407
Top	**Fcc2**	-3.519
Top	**Hcp1**	-3.519
Top	**Top**	-3.052
Hcp1	**Hcp2**	-3.311

Table 5.12: binding energy of two monoxides at different combinations of adsorption sites on Rh

The position of CO_2 produces a negligible effect on the total binding energy for the system, in fact if the first two lines of Table 5.11 are observed a variation of almost 0.2 % is caused by the displacement of CO_2 from a fcc site to an hcp site. Therefore the total binding energy will be dominantly made up by the binding energy of carbon, and as consequence the most stable configuration of the initial state of the elementary step sees the carbon on an hcp site, that is the preferred site found for the atom when no CO_2 is included in the supercell, as depicted in Table 5.13 where the binding energies of the individual compounds are shown.

Adsorption on Rhodium (111)	Binding energy [eV]
C	-7.032 (hcp)
CO_2	-0.027 (top)

Table 5.13: binding energy computed at the strongest adsorption site for atomic carbon on a Rh (111) 2x2 slab with 3 layers, and carbon dioxide on a Rh (111) 2x2 slab with 3 layers

Instead the final state has its reactants on top and hcp sites, the same binding energy is computed when the structure with CO on top and fcc sites is relaxed because a CO moves from the hcp hollow to the fcc.

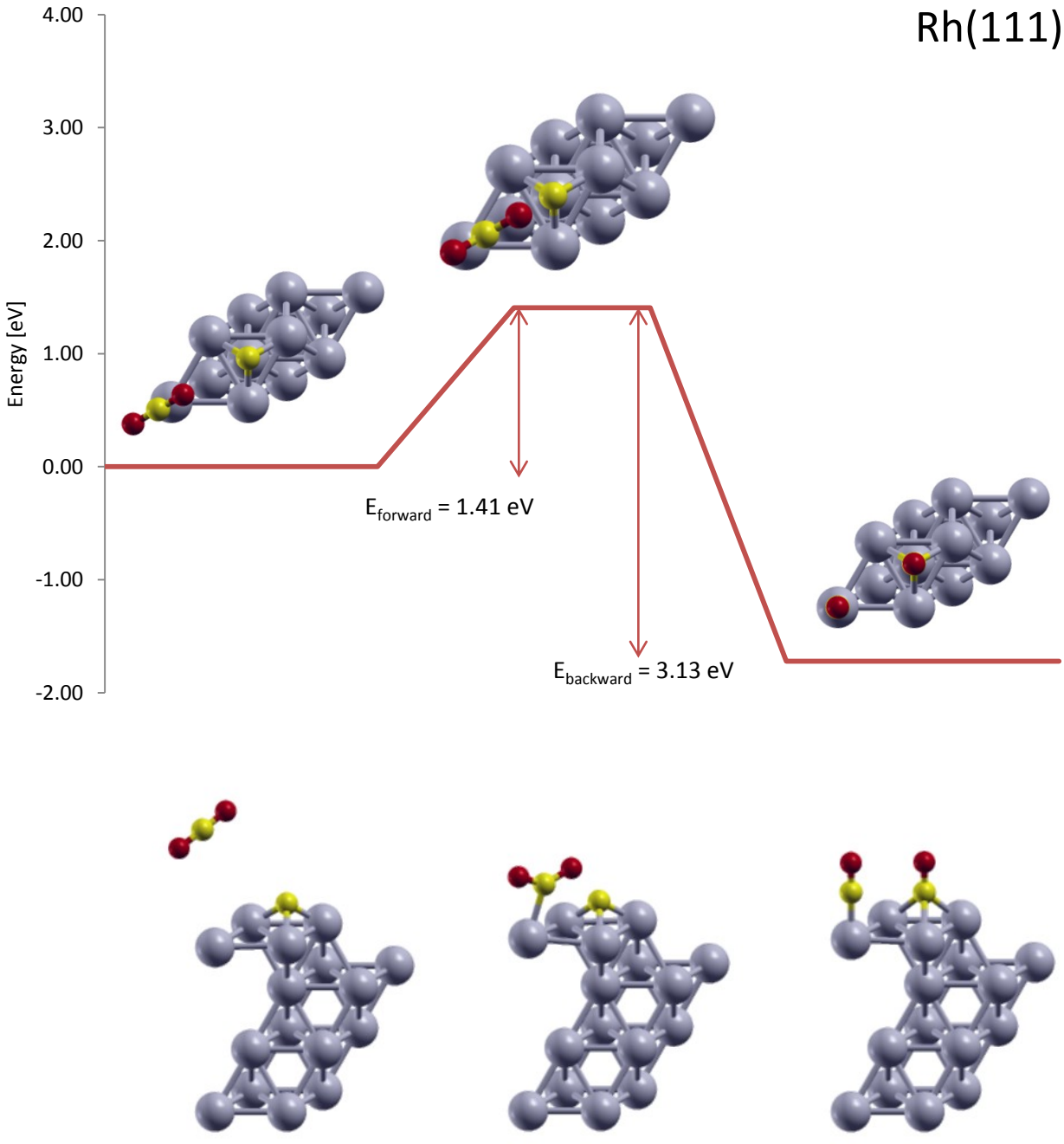

Figure 5.18: forward and backward activation energy of Boudouard reaction on Rh

NEB calculations are converged at 0.2 eV/ Å and a map of the MEP is outlined, the saddle point is the configuration highest in energy, and its energy and electronic structure are illustrated in Figure 5.18.

At the initial state, as usual, CO_2 is in gas phase, the Rh-C distance is about 4.869 Å, with the typical C-O bond length of 1.17 Å and O-C-O angle of 179.90°. The linear CO_2 is not flat over the slab, but one oxygen is pointing to the metal surface, with a vertical distance of 4.28 Å, instead the other oxygen is facing the adsorbed atom of carbon. Since a repulsion between oxygen and adsorbed carbon is experienced, that oxygen is found to have a higher z coordinate, with a distance of 5.40 Å from the surface. The adsorbed carbon is located on the hcp site at 1.09 Å from the surface plane.

CO_2 moves towards the metal, in order to react with the adsorbed carbon. At the Transition State CO_2 is bound with a Rhodium surface atom, the Rh-C distance is 2.15 Å, and the interaction with the metal produces the deformation of the CO_2 linear structure, in fact the O-C-O angle changes till reaching 136.29°. The carbon of CO_2 is slightly tilted and shifts closer the adsorbed carbon, the Rh-Rh-C angle is not 90° but 72.76°. The C-O bond length of CO_2 is 1.219 Å and 1.256 Å for the C-O bond with the oxygen put forward the carbon on the hcp site. The carbon moves downwards, the distance from the surface decreases from 1.09 Å to 1.06 Å, and C changes position from hcp to get nearer to the oxygen of CO_2, a C-O distance of 1.94 Å is calculated.

The C-O bond of carbon dioxide breaks to give birth to the new C-O bond with the adsorbed carbon, CO produced by CO_2 is on top, with a Rh-C distance of 1.865 Å and a C-O bond length of 1.15 Å, instead the other CO is 1.38 Å far from the surface, with a C-O distance of 1.192 Å. These results are very similar to the ones computed for Platinum, in fact the CO-metal interaction is the same, this statement can be confirmed by the binding energies of CO on Pt and Rh [20, 43].

The reaction (4.54) led on Rhodium is exothermic, as for Platinum, and the whole thermodynamic cycle is reported in Figure 5.19.

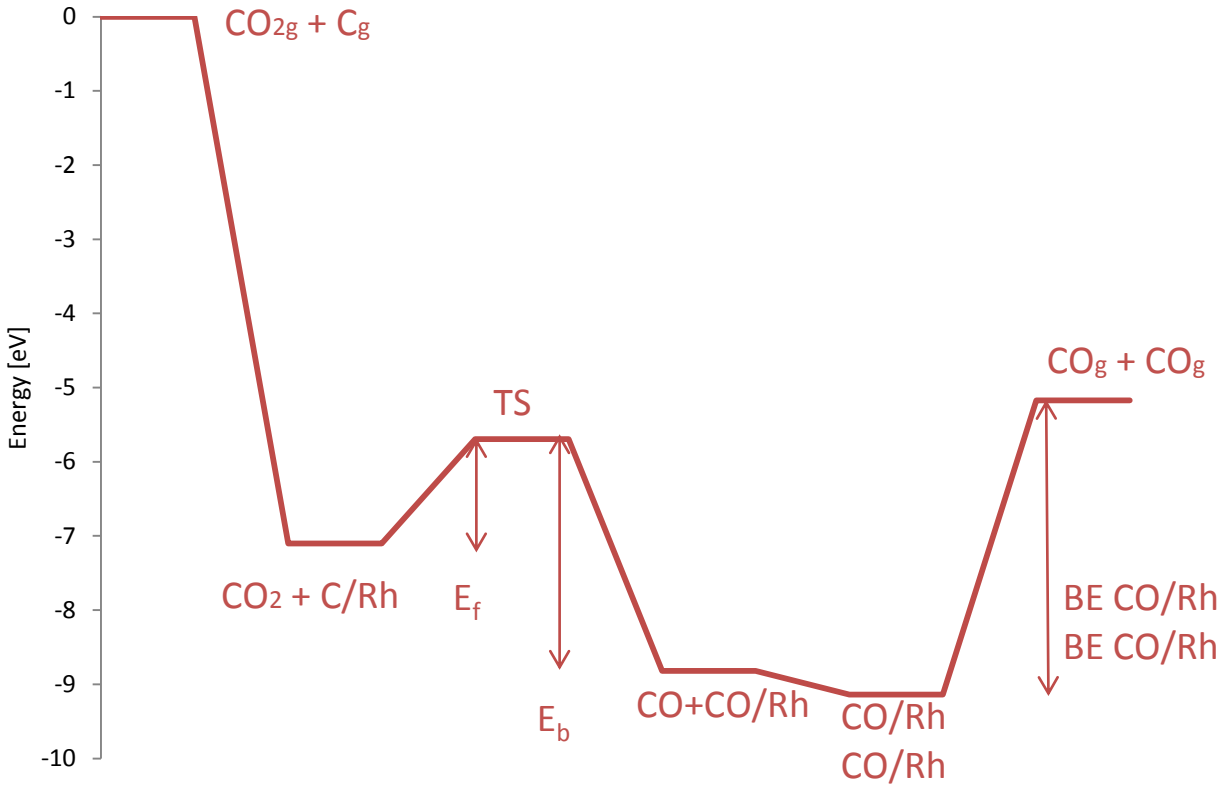

Figure 5.19: thermodynamic cycle of Boudouard reaction on Rh

Nickel (111)

The last metal subject to the analysis is Nickel, a new research has to be done since the different substrate-adsorbate interaction may change the preferred site of adsorption for reactants and products. Various allowable positions are examined, and the one that experiences the stronger binding energy is selected to define the starting or end point of the path.

CO_2	C	BE [eV]
Fcc	Fcc	-7.017
Hcp	Fcc	-7.009
Top	Hcp1	-7.081
Top	Top	-7.085

Table 5.14: binding energy of carbon dioxide and atomic carbon at different combinations of adsorption sites on Ni

CO	CO	BE [eV]
Fcc1	Fcc2	-3.20122
Fcc	Hcp	-2.97899
Top	Fcc1	-3.31563
Top	Fcc2	-3.82214
Top	Hcp1	-3.31133
Top	Hcp2	-3.82214
Top	Top	-2.20794
Hcp1	Hcp2	-3.22478

Table 5.15: binding energy of two monoxides at different combinations of adsorption sites on Ni

CO_2 does not give a relevant contribution to the total binding energy of the initial state of the elementary step. If carbon dioxide is moved from fcc to hcp (first and second rows of Table 5.14) the binding energy changes from -7.017 eV to -7.009 eV (-0.1%), if instead the adsorbed carbon changes location the binding energy of the system with C and CO_2 reflects the trend of the binding energy of a system where only C is included, as reported on Table 5.16, with the binding energies of reactants when they are individually included in a 2x2 slab model, with three layers.

Adsorption on Nickel (111)	Binding energy [eV]
C	-7.027 (fcc)
CO_2	-0.033 (top)

Table 5.16: binding energy computed at the strongest adsorption site for atomic carbon on a Ni (111) 2x2 slab with 3 layers, and carbon dioxide on a Ni (111) 2x2 slab with 3 layers

As consequence the minimum value of energy is strongly influenced by C that prefers the hcp site, in fact CO_2 is on top and C, initially positioned on top (last row of Table 5.14), shifts from the top to the fcc site. Products instead are adsorbed on top and at the fcc sites.

Once initial and final states that provide the structure of reactants and products are determined the Transition State is sought by using the CI-NEB method [Figure 5.20].

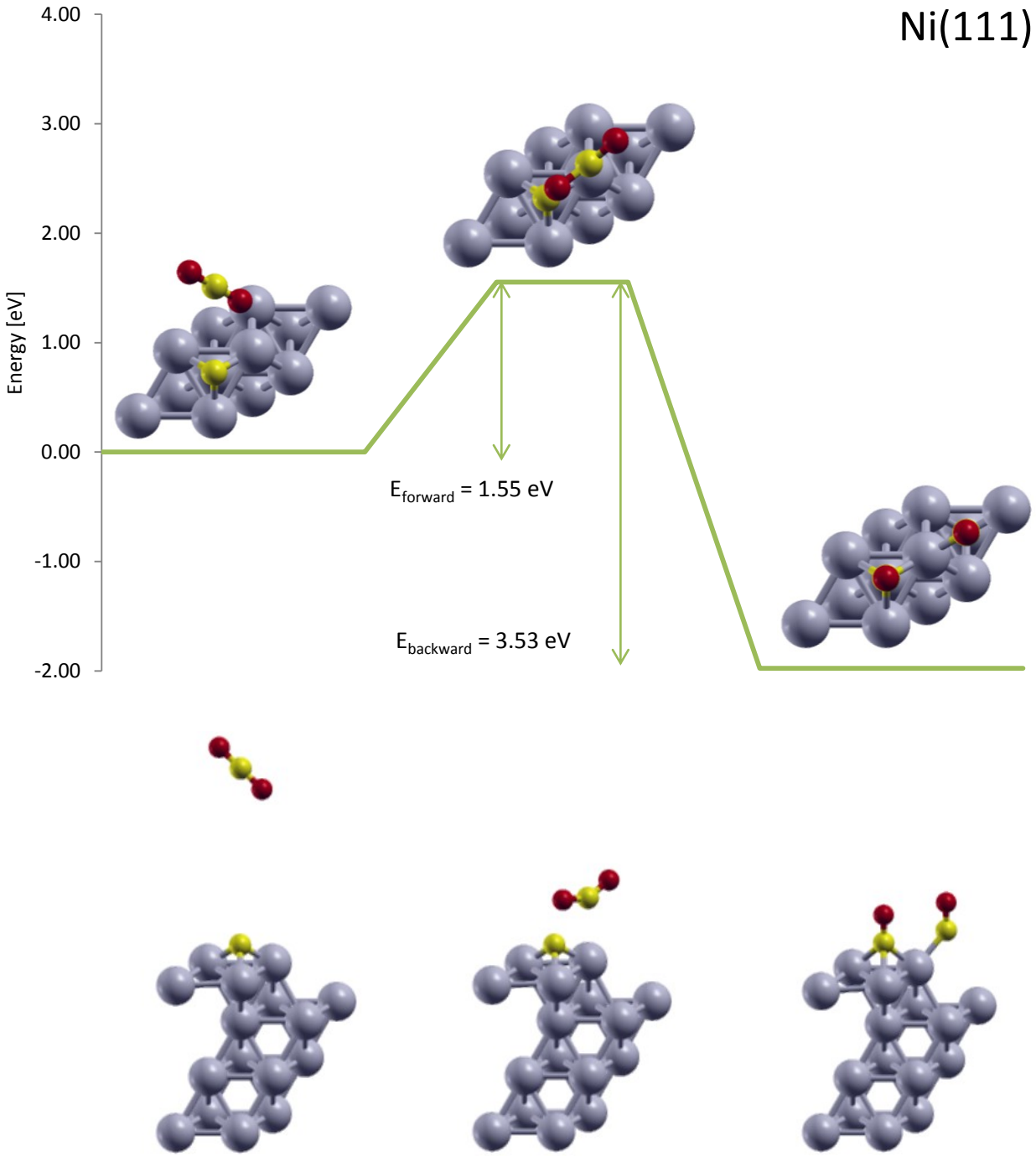

Figure 5.20: forward and backward activation energy of Boudouard reaction on Ni

The first image, used in NEB calculations, provides a geometrical description of reactants at the metal surface. The CO_2 molecule is in gas phase, with its linear structure not parallel to the surface plane. The distance of the carbon of CO_2 from the fourth layer of the slab is 7.195 Å, as consequence no chemical bond can exist among carbon dioxide and the metal of the substrate. The C-O distance is always 1.17 Å, and O-C-O angle is 179.86°. The adsorbed carbon is tightly bound at the hcp site, at 1.01 Å from the surface, the stronger is the interaction and the greater is the binding energy and the closer is the carbon to the surface, in fact the carbon experiences great binding energies on Pt, Rh and Ni surfaces, and creates short bonds.

CO_2 reaches the surface at the Transition State, the Ni-C distance is 2.513 Å, the CO_2 structure still exists but O-C-O angle is 147.29°, and the bond length of the C-O group, opposite to the adsorbed carbon, is 1.178 Å, while the other C-O bond of CO_2 is longer, 1.245 Å, in fact one of the oxygens of carbon dioxide is very near to the carbon at the hcp site, 1.785 Å.

CO_2 attaches to a top site and gives one of its oxygens to the near adsorbed carbon at the hcp site, then a CO top tilted proceeds towards the fcc site. The CO at hcp has a C-O bond length of 1.18 Å, with C 1.33 Å far from the substrate, even the CO at fcc possesses a C-O bond of 1.18 Å and is 1.33 Å over the surface [43].

As for Platinum and Rhodium, the surface reaction (4.55) on Nickel catalyst is exothermic, and even if the intermediate levels of the thermodynamic cycle change according to the catalyst selected, that affects the heats of adsorption and the activation energy of the elementary step, the initial and final states are always the same. Reactants and products are in gas phase, thus the difference in total energy only depends on their energy and not on the energy computed considering the three different metals [Figure 5.21].

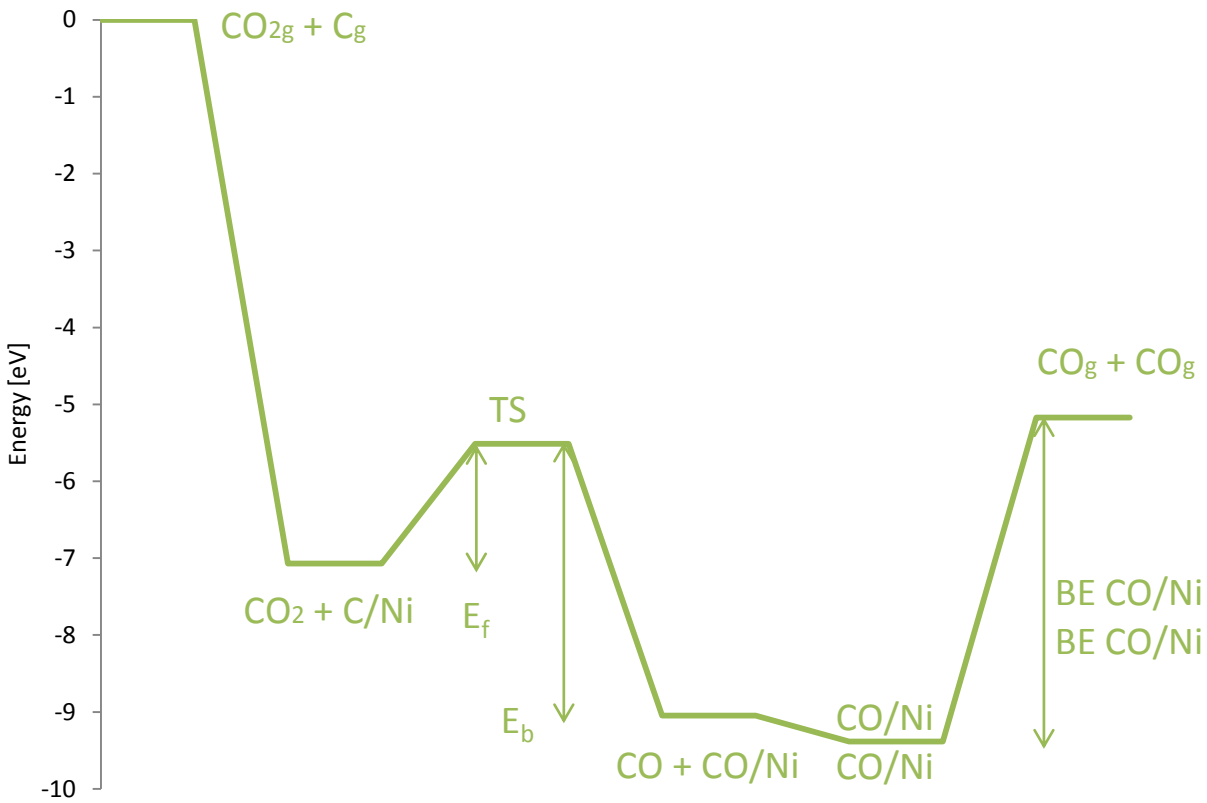

Figure 5.21: thermodynamic cycle of Boudouard reaction on Ni

5.4.1 Reactivity Analysis of Metals: $CO_2 + C \rightarrow 2CO$

This section deals with a systematic examination of energy trends to inspect relationships among binding energies, forward and backward activation energies and metal dependence. The main purpose is to provide information on surface chemistry of Platinum, Rhodium and Nickel catalysts. If Figure 5.17, Figure 5.19 and Figure 5.21 are combined to display Figure 5.22 the levels of relative energy due to the different reactivity of the metals can be compared.

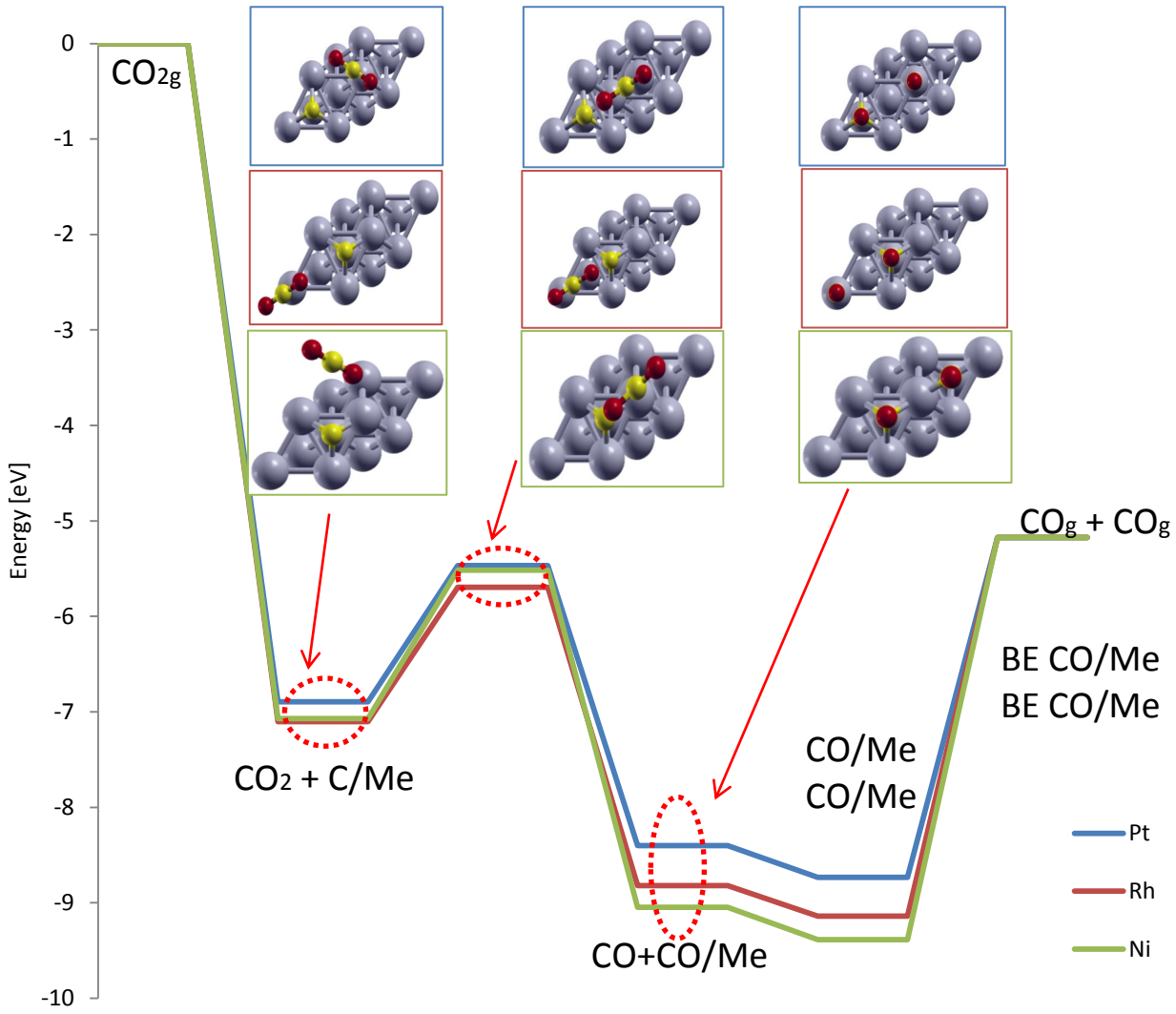

Figure 5.22: thermodynamic cycle of Boudouard reaction on Pt, Rh and Ni

The thermodynamic cycle has the same starting and end point for the three metals, that are gaseous reactants and products, and even if the different catalysts produce diverse levels of energy related to reactants and products adsorbed on the heterogeneous catalyst, the same level is reached when the products of the reaction that happens at the surface are desorbed; the binding energy of CO restores and allows the thermodynamic cycle to end at the same energetic level.

In Figure 5.23 and Figure 5.24 the dependence of activation energies on the type of metal is elucidated.

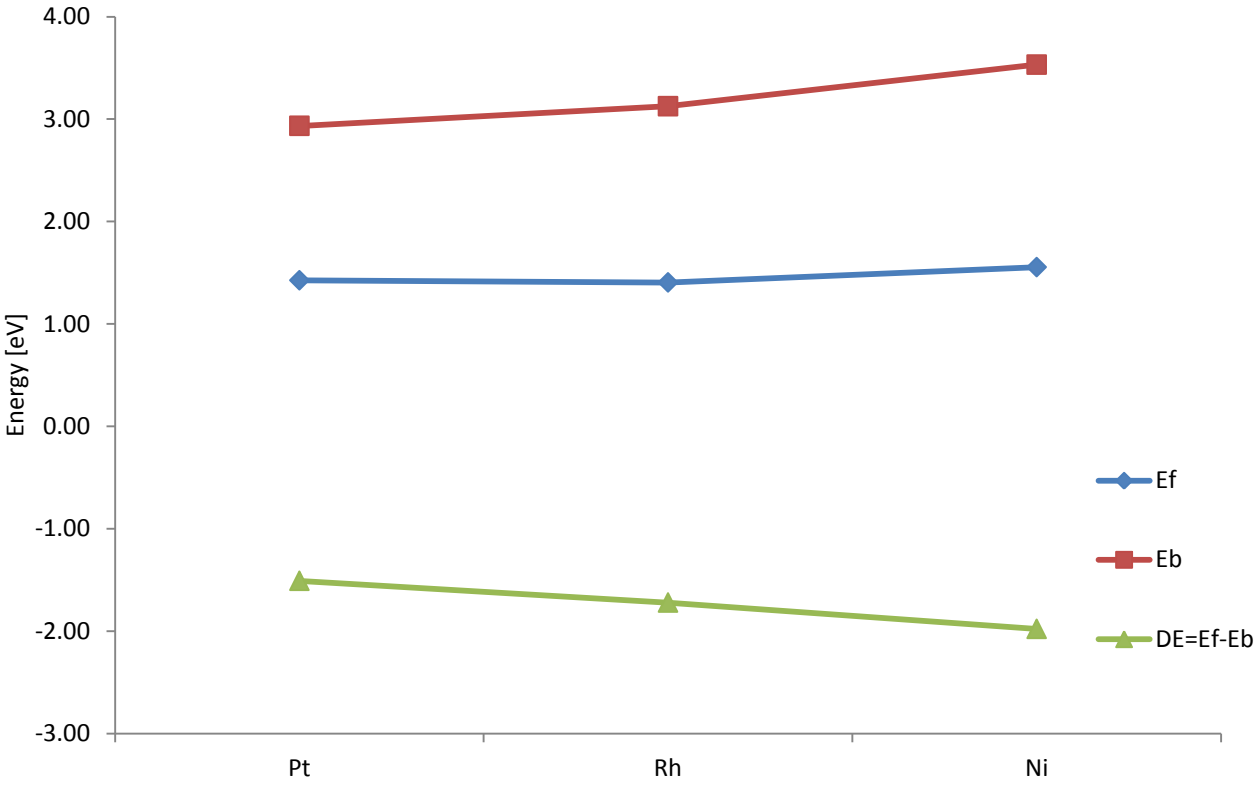

Figure 5.23: forward, backward activation energy, and heats of reaction (5.2) on the three metals

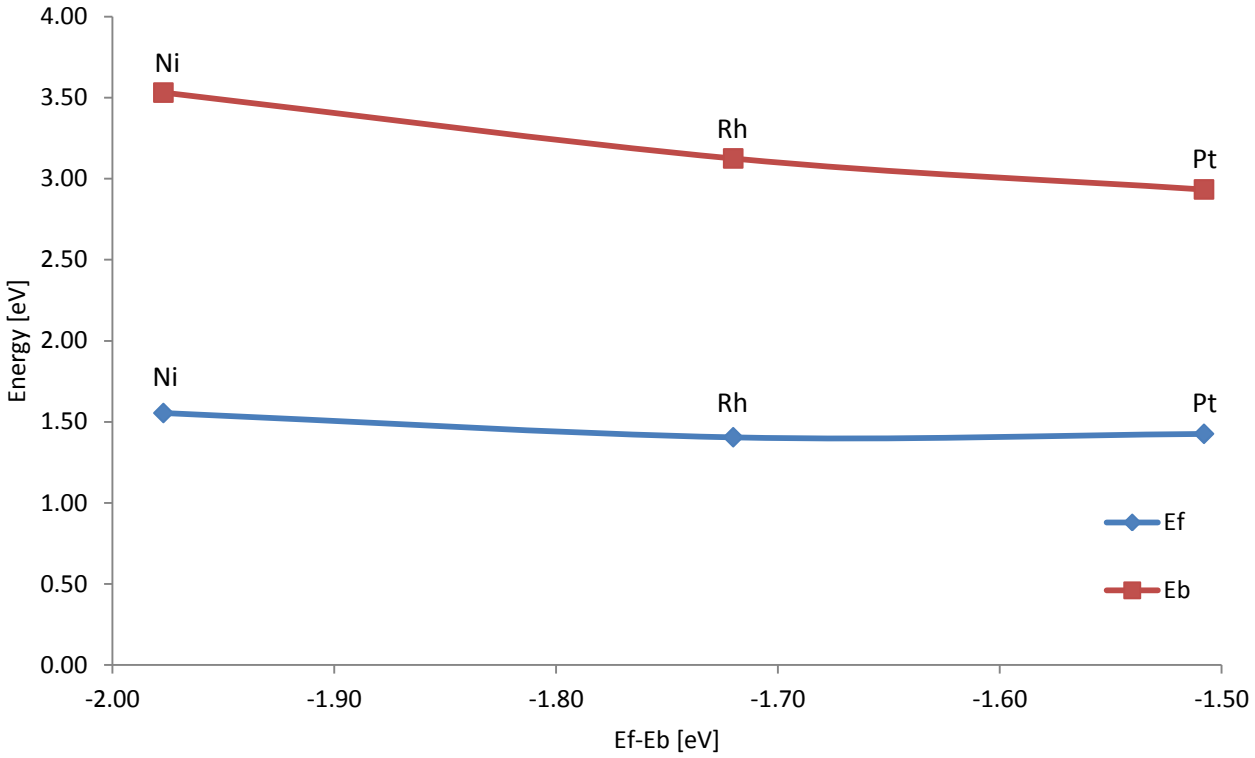

Figure 5.24: forward and backward activation energy dependence on heats of reaction (5.2)

The forward activation energy is almost the same for Pt, Rh and Ni, instead backward activation energy increases moving from Pt to Rh and Ni.

The difference in activation energy among reactions (4.56) when they are led on the three metals is proportional to the difference of the enthalpy of reaction, as consequence an Evans-Polanyi dependence exists [53].

In order to understand which chemical compound conditions the variation in energy on the different metals the binding energies of all the species involved in the elementary step are computed and collected in Figure 5.25.

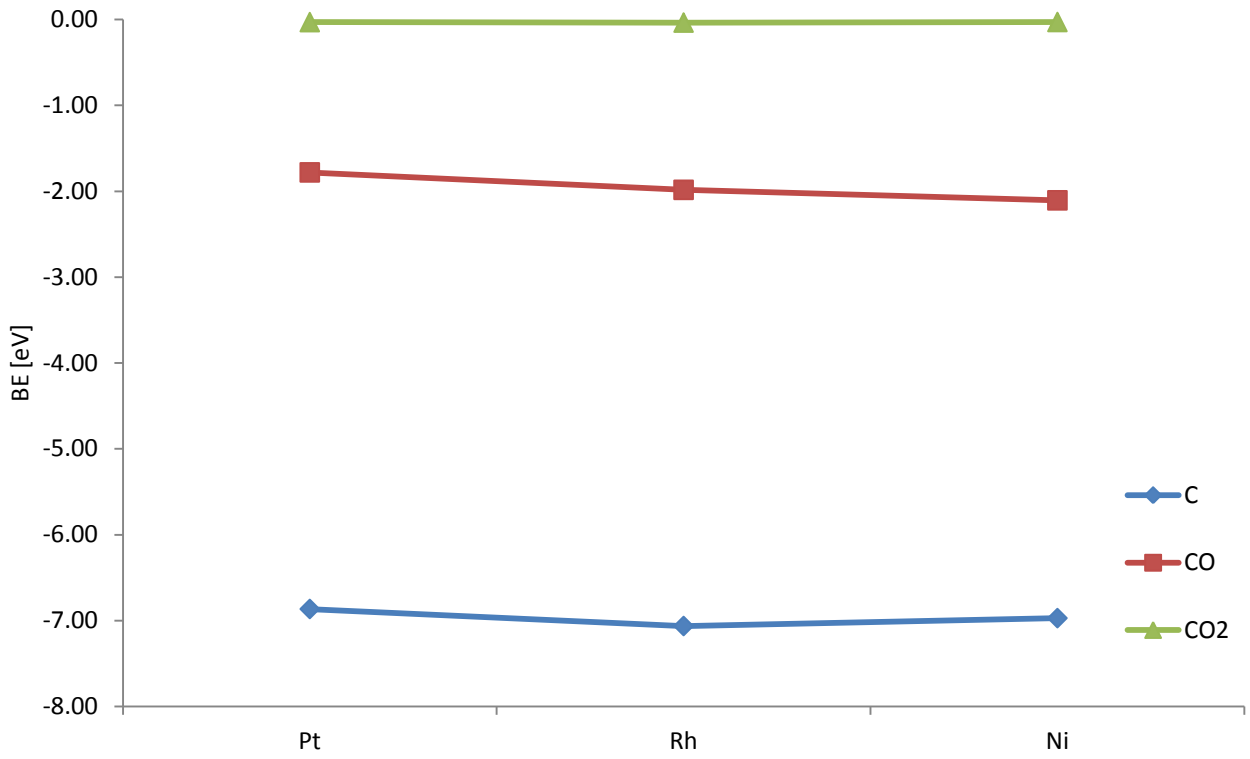

Figure 5.25: binding energies of reactants and products of reaction (5.2) on the three metals

On one end the atomic carbon produces an appreciable binding energy on the other CO_2 does not. Although Pt, Rh and Ni interact in the same way with C and CO_2, in fact no perceptible variation of the heats of adsorption is exhibited in Figure 5.25.

This behavior can be examined by the analysis of the PDOS of carbon dioxide and atomic carbon illustrated in chapter 3 [Figure 3.44, Figure 3.50].

The only chemical compound that exhibits a variation in the binding energy, even if very limited, is the carbon monoxide. Since the binding energy of CO follows this trend Ni>Rh>Pt [20], as consequence the same trend is seen if the stability of the reactants on the metal's surface is considered. The greater is the binding energy of CO and the more the products are stable, in fact the backward activation energy increases from Platinum to Rhodium and Nickel [Figure 5.23].

As a whole carbon monoxide is the chemical compound that exerts sensible influence over the backward activation energy. No relation can be defined between forward activation energy and reactants binding energies. Actually C binding energies do not vary from metal to metal, and even forward activation energies belong to a narrow range ($E_{f:Ni}$ - $E_{f:Rh}$ $\cong$ 0.15 eV), the Transition State seems to be fixed in energy as the binding energy of the atomic carbon.

On the other hand backward activation energy increases if CO binding energy becomes greater in absolute value [Figure 5.26], CO affects the stability of the final state and thus it produces a configuration where products are more strongly bound to the metal surface. The above mentioned "C-no trend" and "CO-trend" are two indicators of "early Transition State".

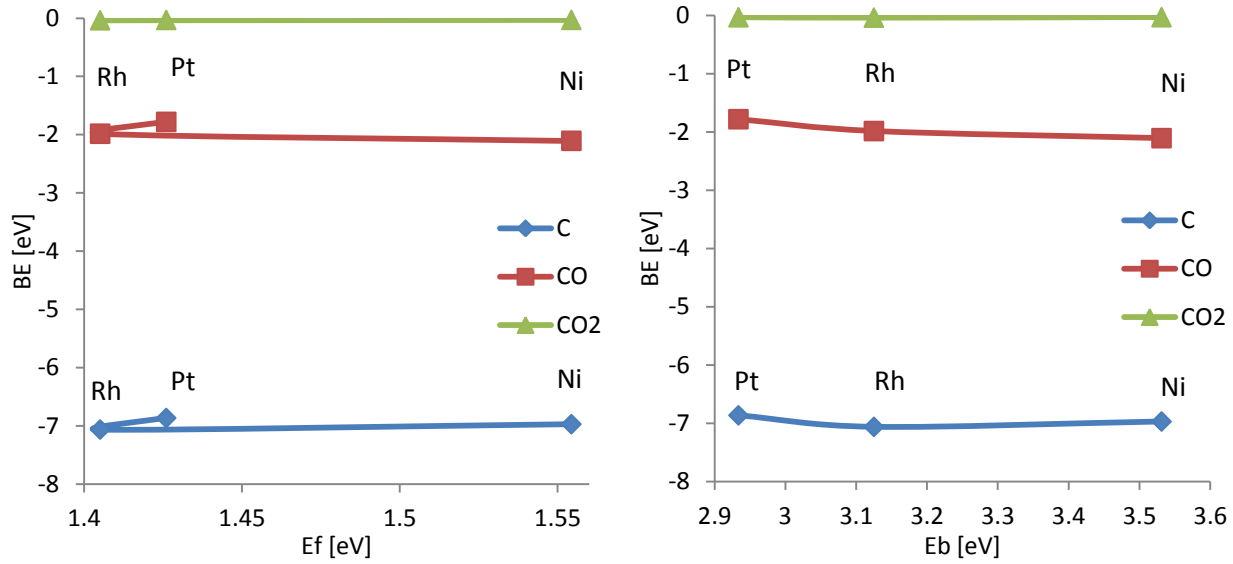

Figure 5.26: binding energies of reactants and products depending on forward and backward activation energy, for reaction (5.2)

If the density of states is calculated for the initial, transition and final states of the surface reaction on the three different metals the electronic properties of the Transition State can be related to the properties of reactants and products.

On Platinum:

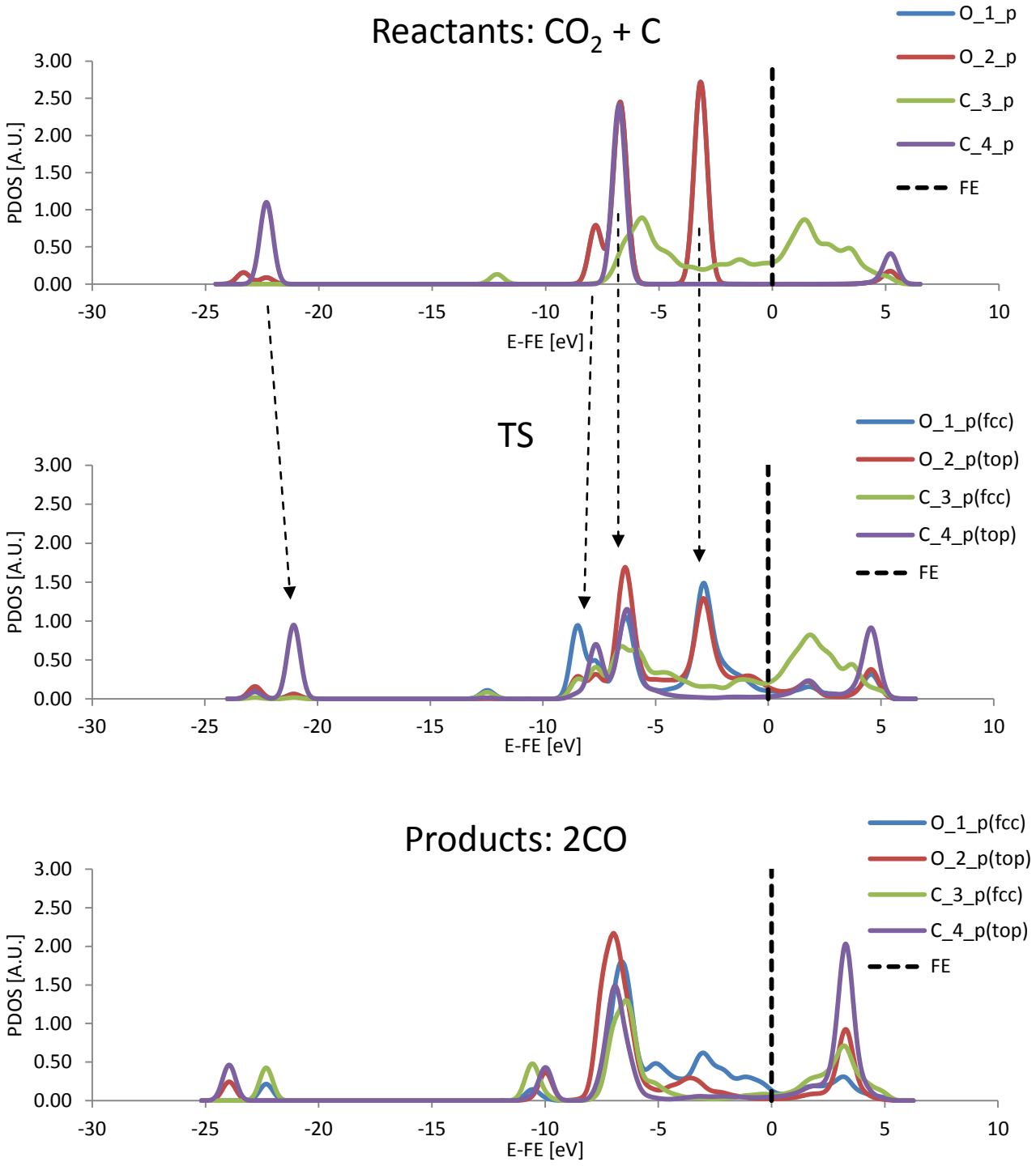

Figure 5.27: PDOS of the reactants, Transition State, and products for reaction (5.2) on Pt; FE = Fermi Energy (reference level); X_n_v means X = atomic type, n = label of the atom, v = valence orbital

On Rhodium:

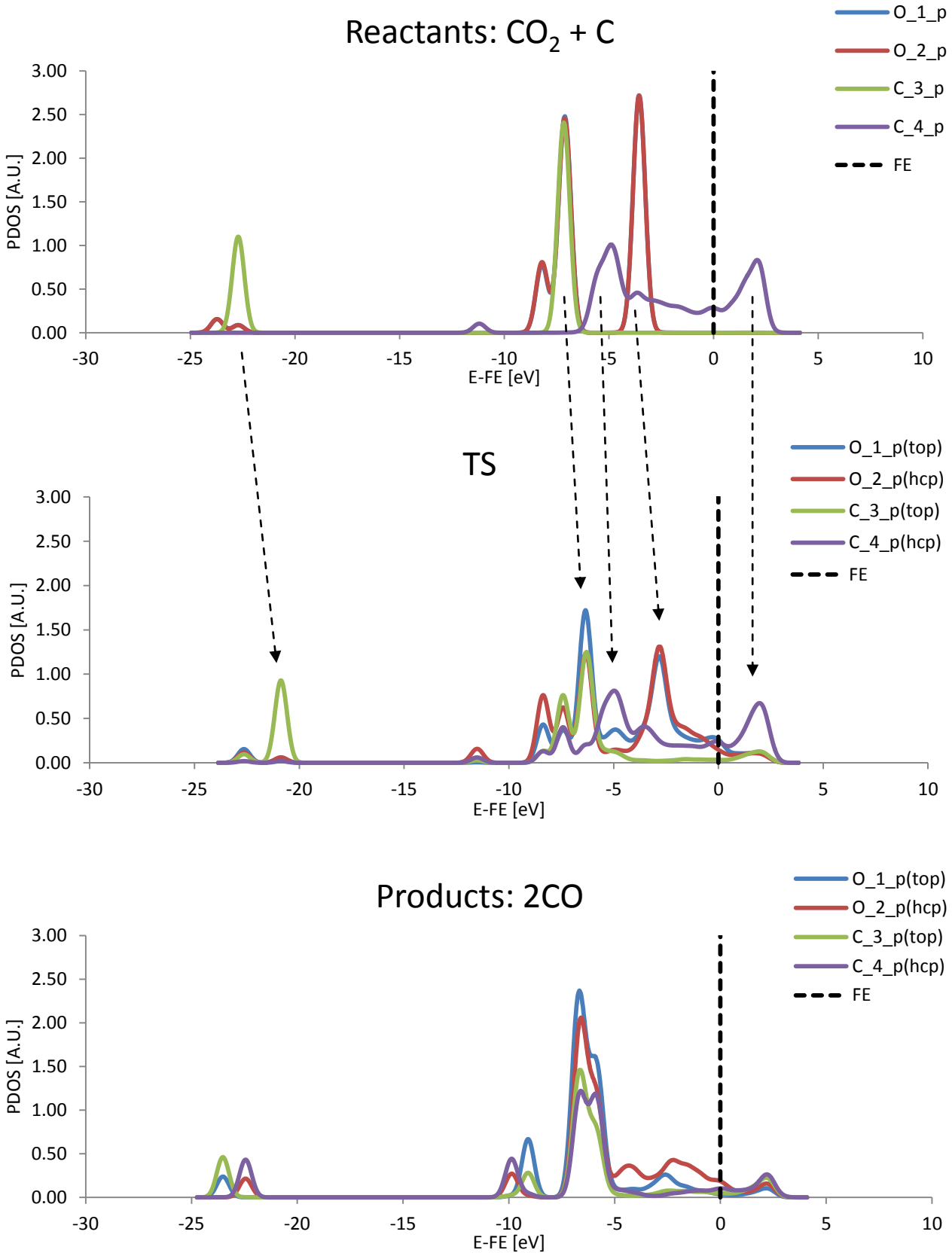

Figure 5.28: PDOS of the reactants, Transition State, and products for reaction (5.2) on Rh; FE = Fermi Energy (reference level); X_n_v means X = atomic type, n = label of the atom, v = valence orbital

On Nickel:

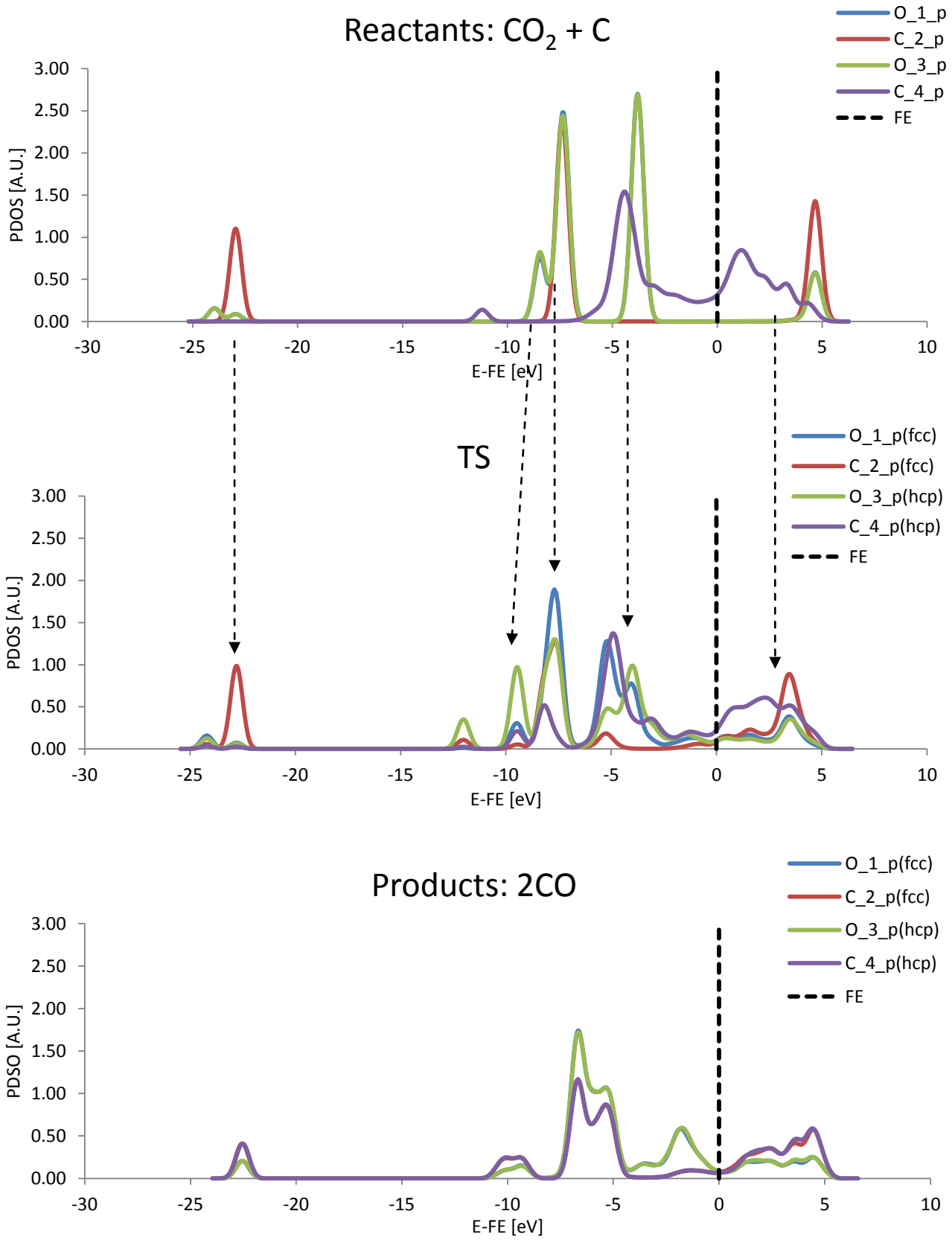

Figure 5.29: PDOS of the reactants, Transition State, and products for reaction (5.2) on Ni; FE = Fermi Energy (reference level); X_n_v means X = atomic type, n = label of the atom, v = valence orbital

Now the PDOS of the Transition State shows an electronic structure that resembles the one of the first image used to describe the MEP with the NEB method. Thus the Transition State may be considered "early" because it shares the electronic configuration of the reactants. This deeper analysis contributes to giving a description of the Transition State not only by considering geometrical properties and energies, but also the electronic configuration is studied, since it is fundamental in determine which bonds are allowed to be produced and which not.

According to geometrical and electronic structures, the Transition State always appears to be "early" [Table 5.17].

$CO_2+C \rightarrow 2CO$		
	Geometry	Electronic structure
Pt	Early	Early
Rh	Early	Early
Ni	Early	Early

Table 5.17: evaluation of the Transition State for reaction (5.2)

Conclusions:

- The atom of carbon at the metal surface has not notable influence on the forward activation energy,
- The Transition State is early but forward activation energy is slightly affected by reactants and backward activation energy directly depends on the binding energy of products,
- The early Transition State produces forward activation energies that do not appreciably vary from metal to metal, in fact the binding energy of the atomic carbon is almost identical for Pt, Rh and Ni; the TS configuration resembles the reactants and shows the same trend,
- Backward activation energy is influenced by the binding energy of the carbon monoxide.

5.5 Elementary Step: $CO_2 + nC \rightarrow 2CO + (n-1)C$

This elementary step is studied in order to understand how metals as Platinum, Rhodium and Nickel behave if atomic carbon is adsorbed on the slab. This condition represents a basic schematization for a coked (111) surface, as consequence surface chemistry will change because the carbon dioxide, now, not only experiences the metal potential, but also feels the potential due to a pseudo-layer of adsorbed carbons, that cause steric hindrance, in fact several adsorption sites are filled by C, and this prevents CO_2 to reach other active sites on the catalytic surface.

Platinum (111)

According to the previous calculations the same positions for reactants and products on Platinum, selected in Table 5.8 and Table 5.9, are used in the following dissertation.

The fcc site is identified as the strongest adsorption site for C on Platinum, as consequence all the allowable fcc sites of the 2x2 supercell used to represent the slab are filled with adsorbed carbons. The final state of the elementary step has just one molecule of carbon monoxide effectively adsorbed at the metal surface, at fcc. On the other hand the second molecule of carbon monoxide moves away from the adsorption site, which is the top site, and remains in gas phase at the end of the relaxation.

The Transition State research can start once the first and last images are selected. The required computational effort is notable since 4 atoms of Platinum belonging to the fourth layer of the slab are allowed to displace along the direction defined by the axis perpendicular to the four layers. Besides Platinum, even 5 atoms of carbon and 2 of oxygen are fully relaxed along all their spatial coordinates.

An upper and lateral view of the system at the initial, transition and final state is provided, forward and backward activation energies are indicated [Figure 5.30].

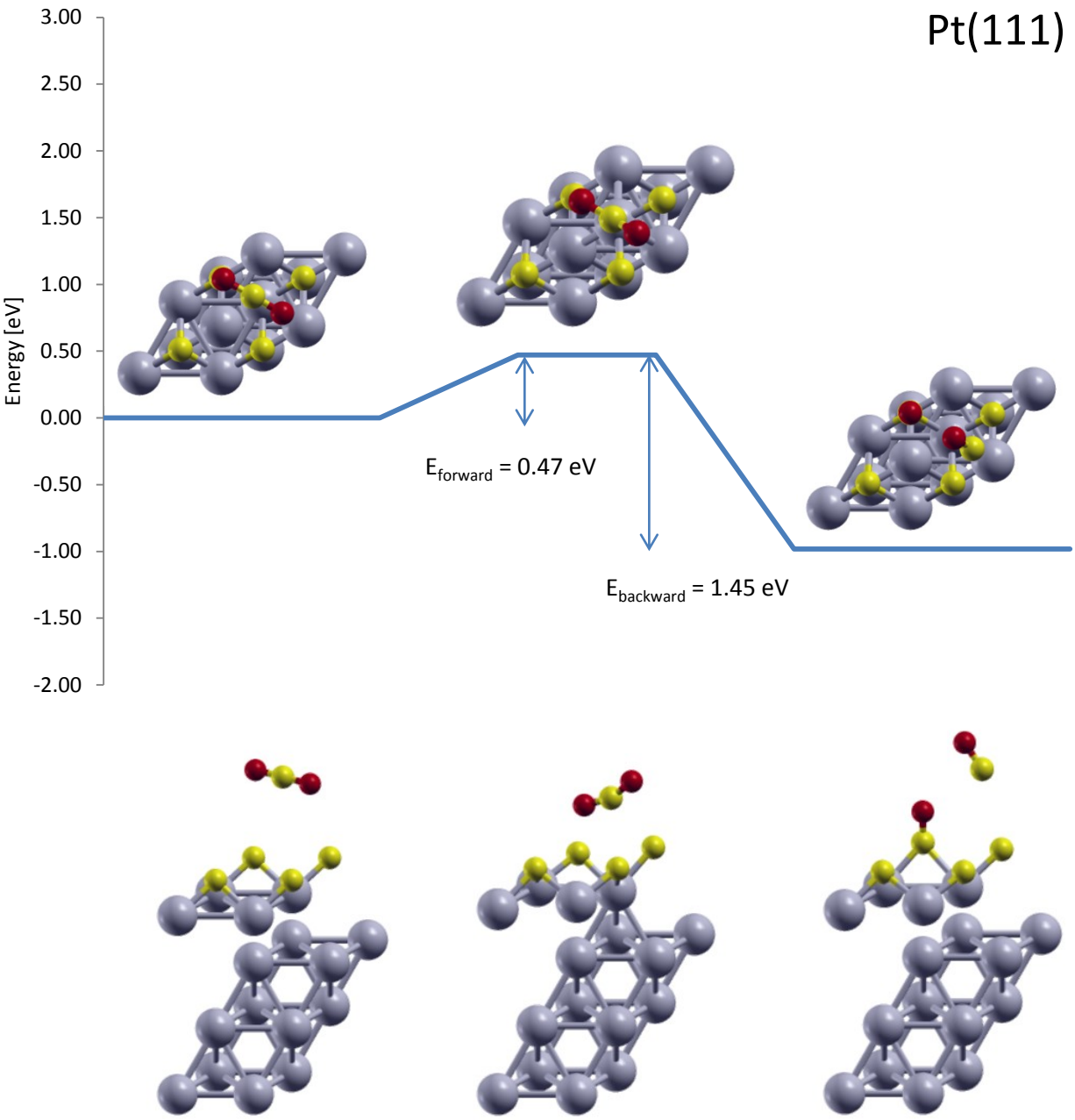

Figure 5.30: forward and backward activation energy of Boudouard reaction with higher coverage of carbon on Pt

CO_2 is always found to be in gas phase, 4.52 Å far from the metal surface, with a C-O distance of 1.17 Å and an O-C-O angle of 179.88° that demonstrate no interaction exists with the Platinum, in fact this is the typical structure of the gaseous CO_2. The carbon of CO_2 is over a top site, instead one of its oxygens is positioned over an adsorbed atom of carbon at the fcc site. The four adsorbed carbons experience a different interaction with the gaseous CO_2, in fact the carbons positioned under this molecule are slightly more pressed on the Platinum surface, but the average distance of the adsorbed atoms from the catalytic layer is 1.1 Å, with a Pt-C bond length of 1.97 Å and a C-C distance of 2.829 Å.

CO_2 gets closer to the surface, but at the Transition State CO_2 is no longer flat, but one oxygen is 3.03 Å above the metal, and the other instead is at 4.29 Å, instead C is positioned at 3.50 Å if the length is computed as the vertical distance of the oxygen from the nearest atom of Platinum. CO_2 can't land with its atom of carbon on the top site, since this site is surrounded by fcc sites, occupied by other atoms of carbon, that produce a carbon-carbon repulsion. However CO_2 experiences a potential that induce a distortion of the O-C-O angle, that is now 160.5°, this deformation is less important than the same experienced by CO_2 at lower coverage of carbon, in fact in the previous case CO_2 actually sits on top and feels a stronger potential due to the catalyst, that produces a more sharp angle (138.60°). One of the C-O bonds is compressed (1.169 Å) instead the other is stretched (1.206 Å) because the oxygen is interacting with the adsorbed carbon at fcc, a distance of 1.911 Å is computed between the former and the latter.

CO_2 completely breaks its C-O bond, and at the final state two carbon monoxides appear, one of them is on a fcc site, where previously the atom of carbon was adsorbed, the other instead is in gas phase. The C-O bond experienced by the adsorbed monoxide is 1.18 Å long, instead the gaseous C-O has a shorter bond distance (1.14 Å), this is due to the repulsion that the oxygen encounters when the carbon on the other side is electronically attracted by the surface. The CO in gas phase is not flat because it still experiences the surface potential in fact CO offers its carbon to the metal, the surface-C distance is 4.65 Å, while the surface-O distance is 5.54 Å. Gaseous CO tilted position is instead caused by the C-O repulsion that involves the oxygen of the adsorbed monoxide.

As a whole, it is possible to state that higher coverage of carbon causes both forward and backward activation energies to decrease [Figure 5.31].

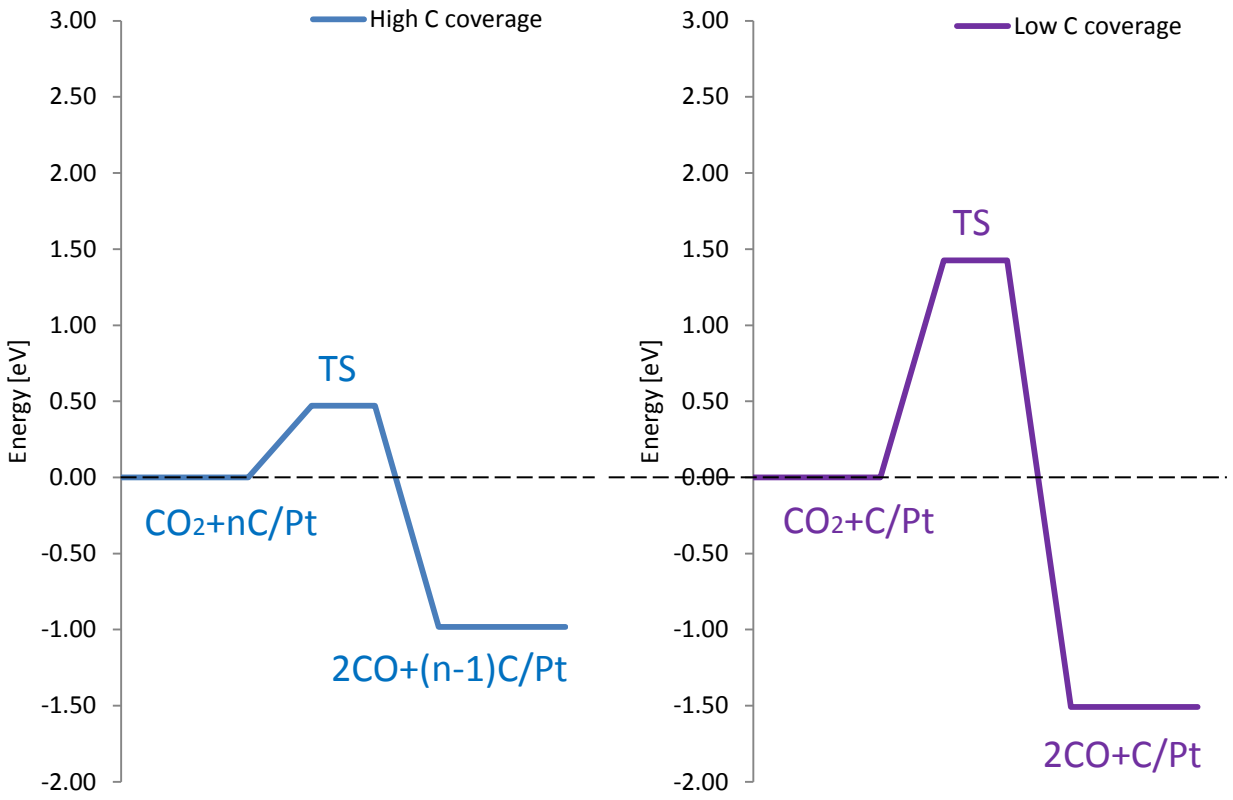

Figure 5.31: comparison between activation energies of the Boudouard reaction with high and low coverage of carbon on Pt

Rhodium (111)

The same elementary step is studied on the second metal of interest, the Rhodium, in order to understand how the different metals behave when a higher coverage of carbon is observed over the catalytic surface. The same approach as for Platinum is followed, according to the results shown in Table 5.11 and Table 5.12 CO_2 is set on a top site, while the atomic carbon is adsorbed on its favorite site, all the hcp sites of the 2x2 supercell (4 positions) are filled with one atom of carbon.

NEB calculations are performed and the Transition State is found with the CI method, electronic structures and energetic levels are illustrated in Figure 5.32.

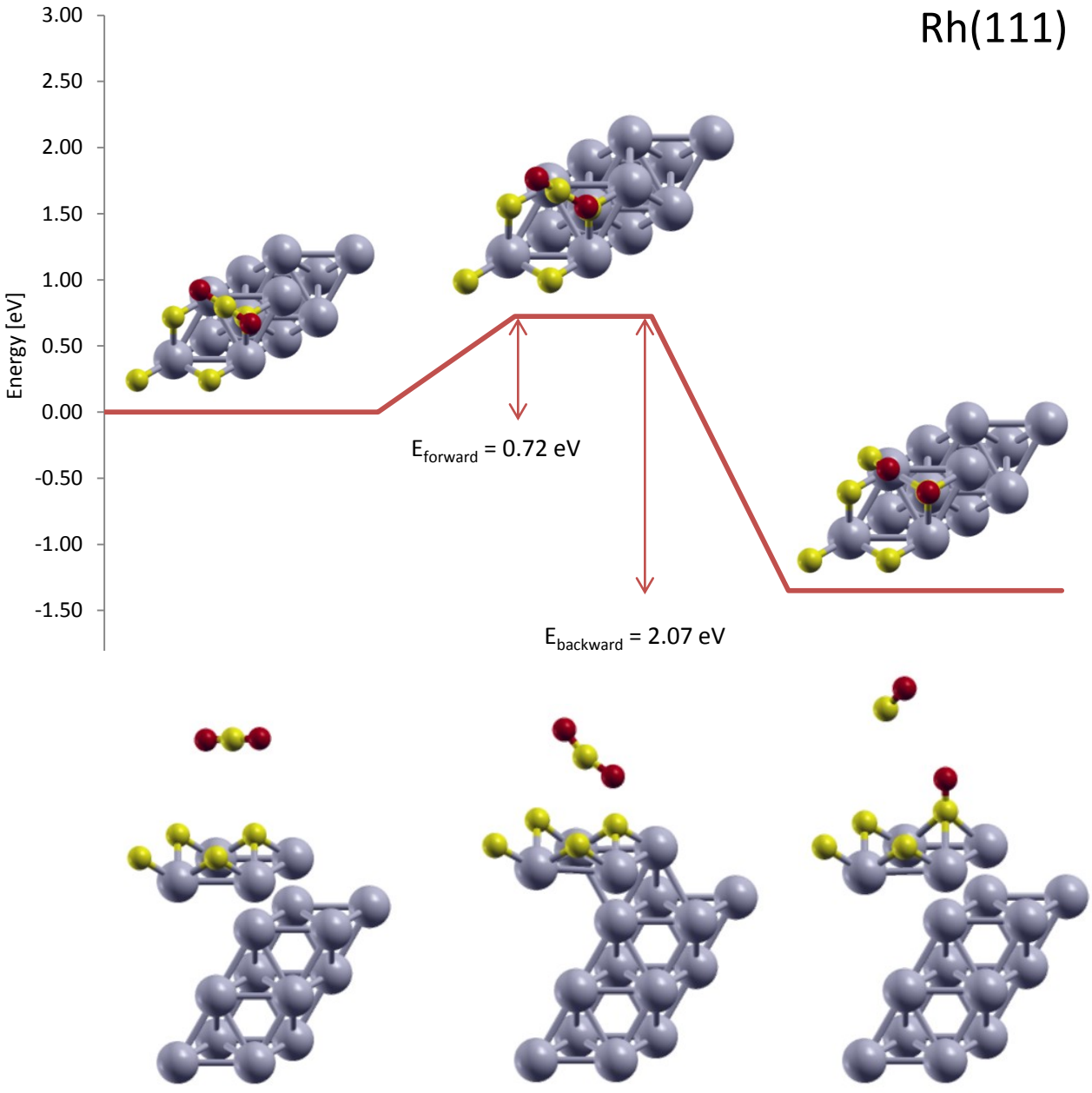

Figure 5.32: forward and backward activation energy of Boudouard reaction with higher coverage of carbon on Rh

At the initial state CO_2 is in gas phase, with one of its oxygens over a top site, and the other oxygen positioned over the atom of carbon adsorbed on the nearest hcp site. C-O bond is 1.17 Å long, and the O-C-O angle is 179.62°. CO_2 is 4.65 Å far from the Rhodium surface (distance surface-C) and is slightly tilted. All the hcp sites are filled with atoms of carbon that experience an average distance of 1.17 Å from the last metallic layer. This spacing is greater than the one calculated on Platinum, the reason of this is probably due to the Rhodium lattice constant, that is shorter than the Platinum lattice constant, and thus the threefold hollow is less broad.

The CO_2 turns in order to approach one of its oxygens to the atomic carbon on the surface. At the Transition State the geometrical structure of CO_2 resembles the gas phase structure but it is not exactly linear since the O-C-O angle is 158.77°, in fact C is just 3.45 Å far from the surface and begins to feel the potential due to the last layer of the slab, although, because of the potential due to the pseudo layer of adsorbed carbons and because of steric hindrance this molecule can't attach its carbon to the near top site, in fact 3.45 Å is a too large distance to give birth to a chemical bond. One C-O bond has a length of 1.167 Å, instead the other, that is going to be broken, shows a C-O distance of 1.213 Å. A new C-O bond is going to be formed, the C-O distance between the carbon at hcp and the oxygen of CO_2 is 1.774 Å. If the Transition State structure on Platinum and Rhodium are compared, it is possible to state that CO_2 bond length and its distance from the metal surface are very alike, in fact the substate-CO_2 interaction is the same for the three metals as previously seen. The only notable difference lies in the C-O distance of the new creating bond.

At the final state a C-O bond is destroyed and a new one appears. The monoxide that is adsorbed at the hcp site has a C-O bond 1.17 Å long, comparable with the length computed on Platinum, with a metal-C distance of 1.53 Å. The other CO, born by the gaseous CO_2, cannot settle on the metal and remains in gas phase, the C-O bond length is 1.14 Å, exactly as computed on Platinum. This result is conceptually correct since the gaseous molecule is far enough the surface and a moderate interaction with the surface potential can't affect the length of a strong bond as C-O. Although CO possesses a notable heat of adsorption on Rhodium, thus it would like to adsorbe but it cannot because of the high coverage of carbon, as consequence CO doesn't lay parallel to the surface but quite vertical, as it would like to land with its carbon upon an adsorption site. The carbon is found at 4.79 Å from Rhodium, and is tilted because of the repulsion induced by the atom of oxygen that belongs to the adsorbed monoxide.

As a whole, the higher coverage of carbon causes both forward and backward activation energies to decrease [Figure 5.33].

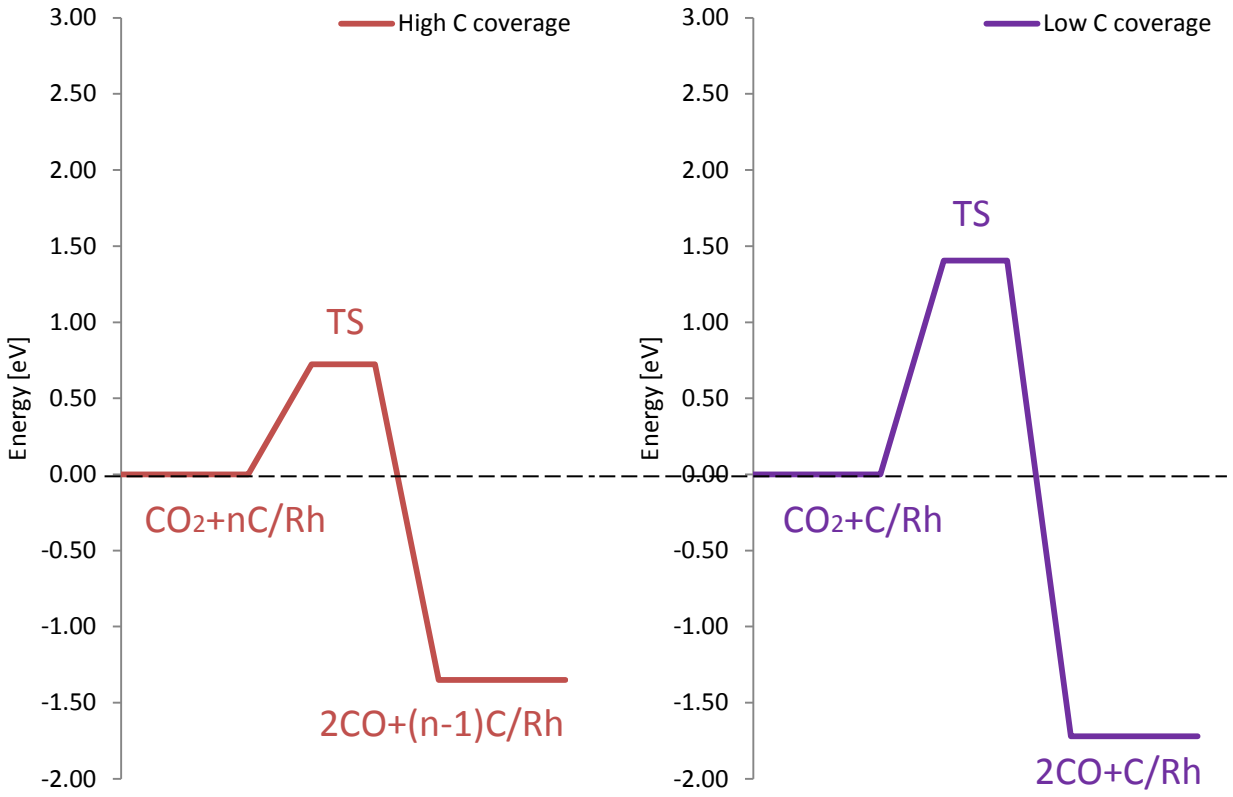

Figure 5.33: comparison between activation energies of the Boudouard reaction with high and low coverage of carbon on Rh

Nickel (111)

The last metal is Nickel, and the initial state of the elementary step involves CO_2 on top and atoms of carbon adsorbed at hcp, as illustrated in Table 5.14 and Table 5.15. The final state instead has a carbon monoxide adsorbed at hcp, and a CO in gas phase. NEB calculations allow to find the Transition State structure and to compute forward and backward activation energies [Figure 5.34].

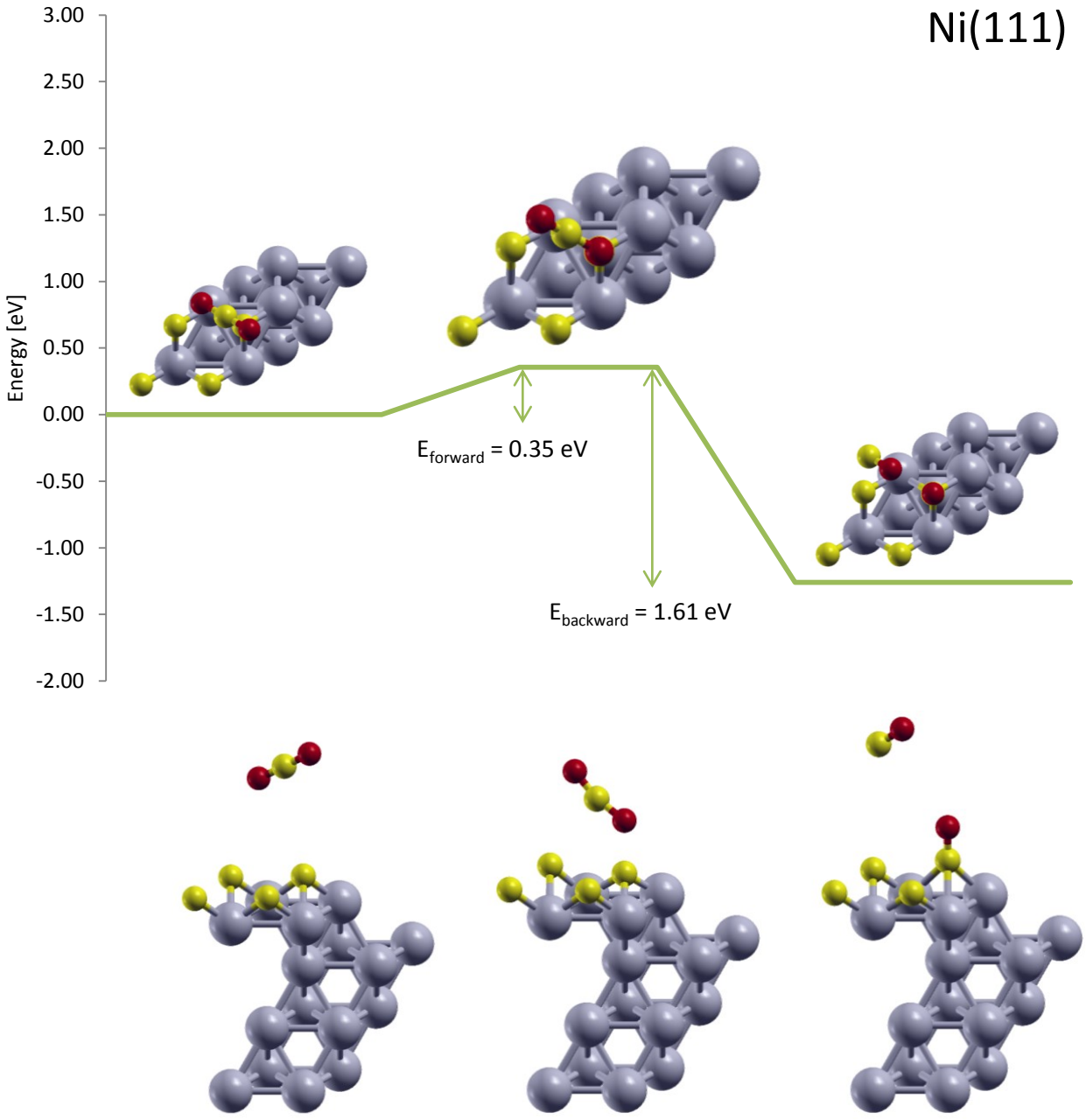

Figure 5.34: forward and backward activation energy of Boudouard reaction with higher coverage of carbon on Ni, upper view

At the initial state CO_2 is far from the surface, tilted, forming an angle of 32.06° with the plane of the surface. One of its oxygens is 4.48 Å above a top site and the other at 5.72 Å over a fcc site. The carbon is in the middle, at 5.09 Å, C-O bond length is 1.17 Å, and the O-C-O angle is 179.42°. The atoms of carbon adsorbed at the hcp sites are positioned at 1.22 Å from the catalytic surface, even if the binding energy of C on Nickel is the highest among the considered metals the distance is the greater because the threefold hollow is the most narrow, in fact the lattice constant for Nickel is shorter than the lattice constant for Platinum and Rhodium.

At the Transition State CO_2 is still far from the surface but looks down with its oxygen at the adsorbed carbon at hcp. The distance from the metal surface, computed by considering the atom of carbon of CO_2, is 3.49 Å, CO_2 structure is slightly distorted, with an O-C-O angle of 163.96°. The C-O bond opposite the surface is compressed (1.166 Å), instead the other is stretched (1.20 Å) because the oxygen is getting closer to the carbon at hcp.

At the final state the adsorbed CO is vertically positioned on an hcp site, with its carbon 1.50 Å far from the surface and a C-O bond length of 1.168 Å. Nickel seems to keep the atom of carbon closer to itself, but produces a longer C-O bond if compared with Platinum and Rhodium. The other monoxide is in gas phase, with the usual tilted configuration and the atom of carbon headed towards the surface. The C-O distance is 1.14 Å and the atom of carbon remains at 5.12 Å above the substrate.

According to Platinum and Rhodium substrates, if high coverage of carbon appears on the Nickel metal surface, both forward and backward activation energies decrease [Figure 5.35].

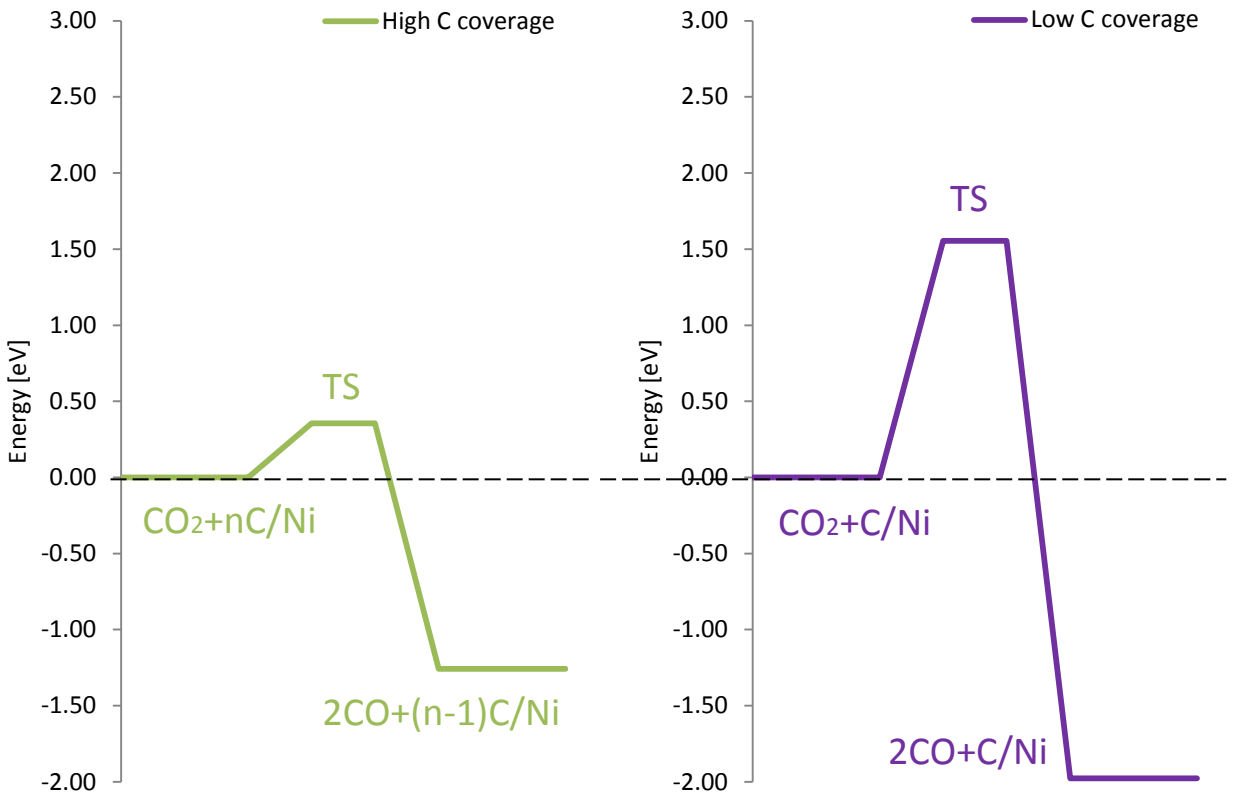

Figure 5.35: comparison between activation energies of the Boudouard reaction with high and low coverage of carbon on Ni

5.5.1 Reactivity Analysis of Metals:

$$CO_2 + nC \rightarrow 2CO + (n\text{-}1)C$$

The aim of this section is to rationalize the collected results and to elucidate differences and similarities among the surface chemistry of Platinum, Rhodium and Nickel. The effects of higher coverage of carbon on activation energies will be investigated, and relations among binding energies, activation energies and kind of metal are evaluated.

Figure 5.36 shows the energetic levels allowed by the different metals, and relative stability of reactants and products can be noticed to vary according to the selected metal.

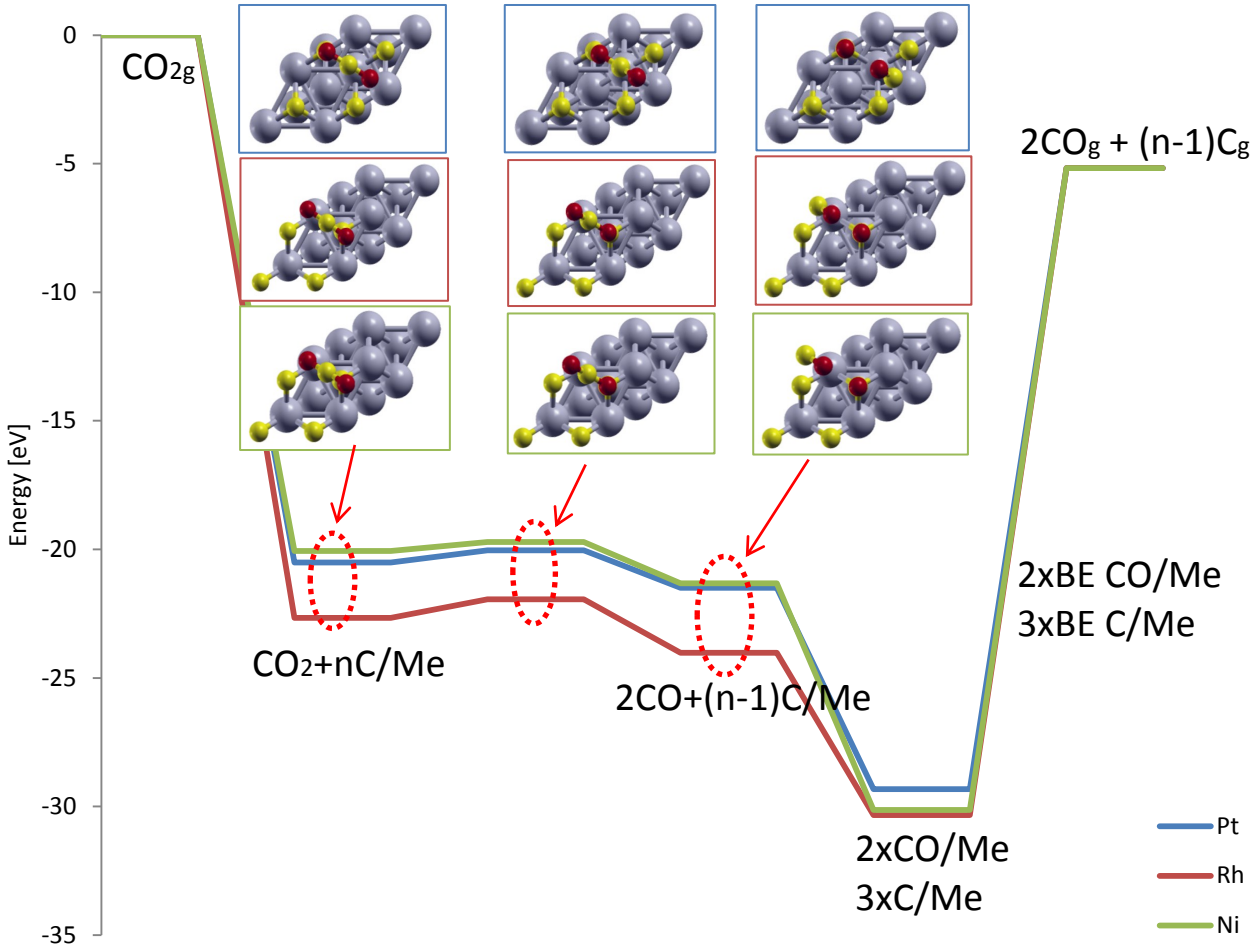

Figure 5.36: thermodynamic cycle of Boudouard reaction with higher coverage of carbon on Pt, Rh and Ni

These energetic levels appear to be quite different from the levels reached during the simple Boudouard reaction, in fact the energy associated to the initial state of the surface reaction (4.57) is strongly dependent on the kind of metal while the energy of the initial state of the surface reaction (4.58), with lower coverage of carbon, is almost the same, for all metals. Moreover the total energy of the final state of the elementary step (4.59) is strongly dependent on CO binding energy, instead for reaction (4.60) no clear relationship is found.

The dependence of activation energies and heats of reaction on the studied metals is displayed in Figure 5.37, a maximum for forward and backward activation energy is seen on Rhodium.

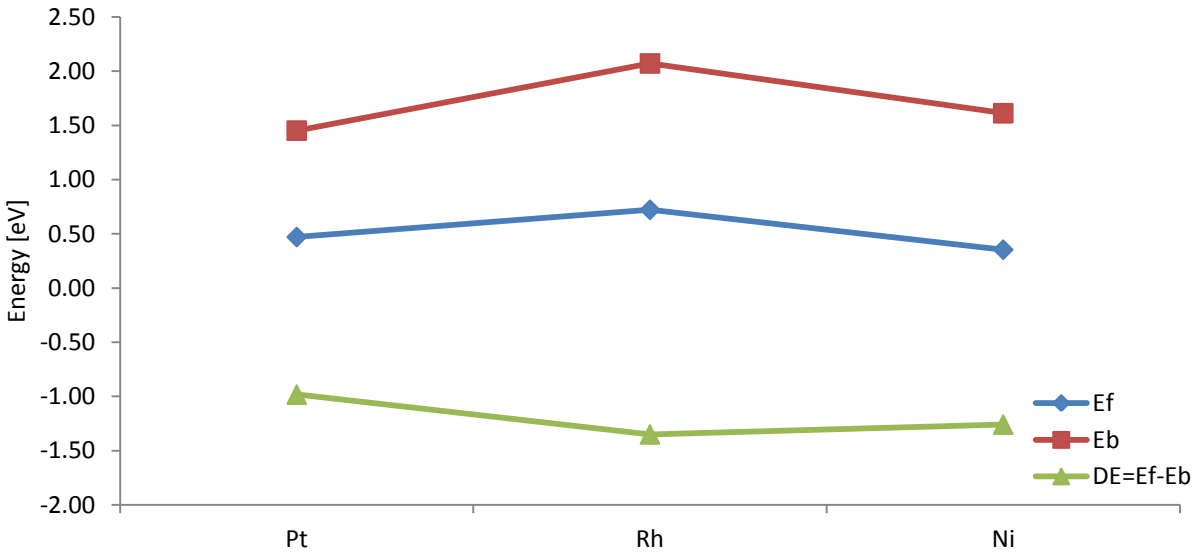

Figure 5.37: forward, backward activation energy, and heats of reaction (5.3) on the three metals

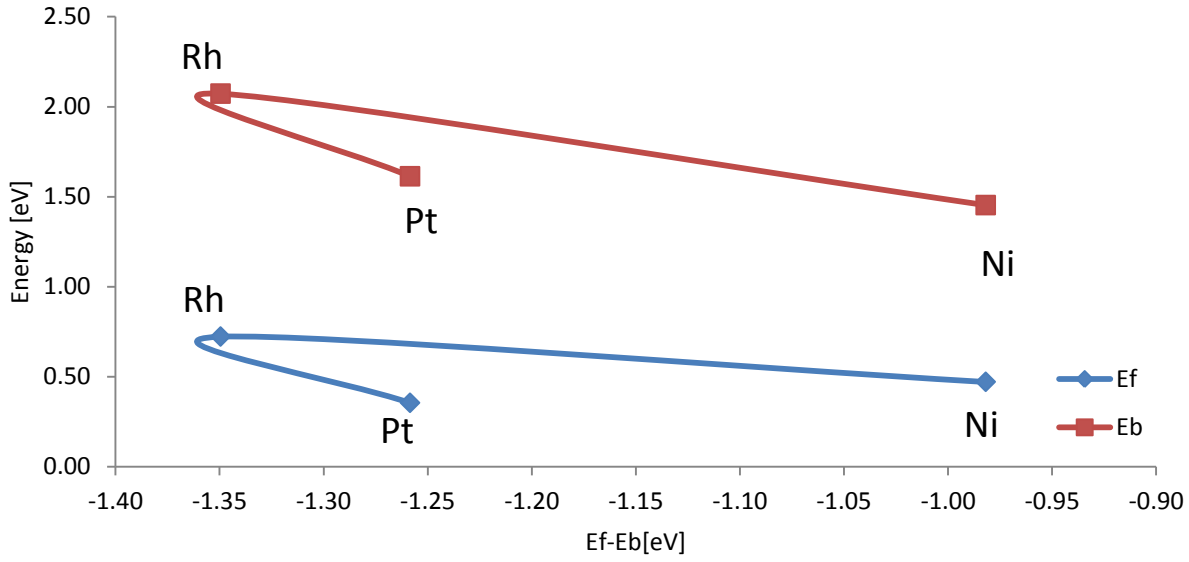

Figure 5.38: forward and backward activation energy dependence on heats of reaction (5.3)

Instead of being aligned with Platinum's and Rhodium's points, Nickel produces the less exothermic surface reaction, with low forward and backward activation energy, like Platinum [Figure 5.38], while Nickel provides the largest forward and backward activation energies if reaction (4.61) is considered.

An explanation to this particular behave is sought by considering the thermodynamic cycle in Figure 5.36.

Now Nickel appears to be the catalyst that experiences the lowest total binding energy for the system, in fact the energy of its initial state of the elementary step at the metal surface is the highest. The same trend can't be seen for the final state of the elementary step.

Nickel produces a binding energy for the atomic carbon that is just a bit smaller than the same binding energy computed on Rhodium, instead the "3d" metal causes the largest CO binding energy, thus the system should be found at the lowest energetic level (fourth step of Figure 5.36), instead the Nickel metal appears to be unable to strongly adsorbe the products as Rhodium does.

The motivation is clarified by the fifth step of Figure 5.36 and Figure 5.39.

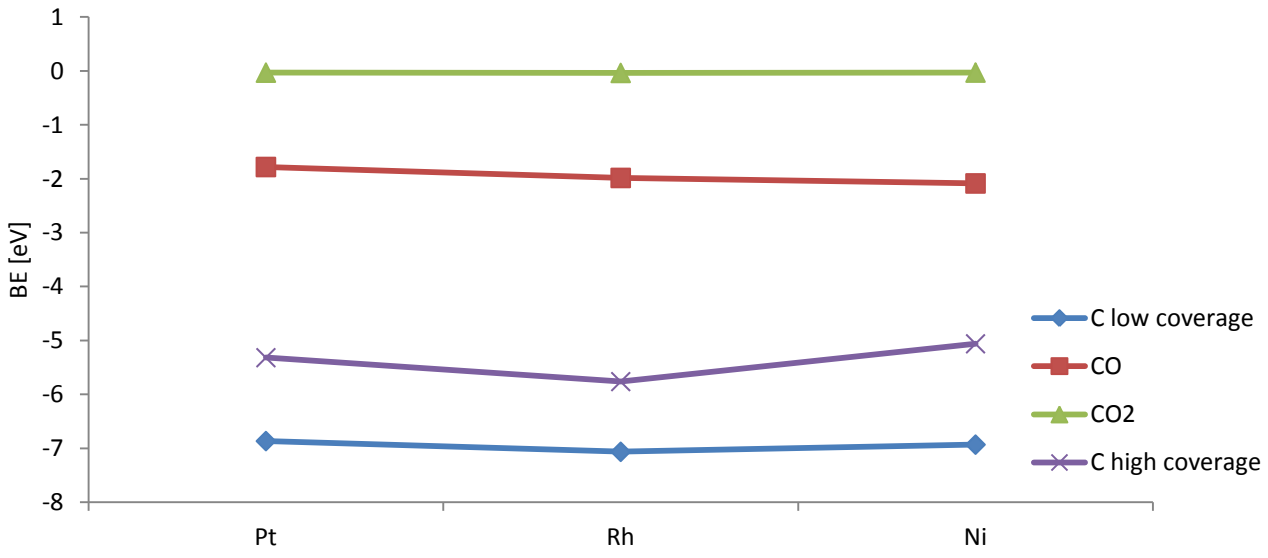

Figure 5.39: binding energies of reactants and products of reaction (5.3) on the three metals

The fifth step of the thermodynamic cycle [Figure 5.36] exhibits the difference between the binding energy of the final state of the elementary step and the binding energies of the products computed with se same 2x2 unit cell, but without other chemical species, that is to say that each unit cell only possesses one molecule of CO to determine the binding energy of the monoxide, and one atom of C

to compute the binding energy of the carbon, instead of having simultaneously 3 carbons and two monoxides on the same 2x2 slab:

$$\Delta_{4\to5} = 2 \cdot BE(CO) + 3 \cdot BE(C) - BE(2CO + 3C) \tag{4.62}$$

$$\begin{aligned}\Delta_{4\to5} = &+2 \cdot \left(E_{CO/slab} - E_{slab} - E_{CO}\right) \\ &+3 \cdot \left(E_{C/slab} - E_{slab} - E_{C}\right) \\ &-\left(E_{(2CO+3C)/slab} - E_{slab} - 2 \cdot E_{CO} - 3 \cdot E_{C}\right)\end{aligned} \tag{4.63}$$

Nickel experiences the greater gap between step 4-5 because the unit cell has the smallest volume of vacuum where reactants can be positioned, this leads to a strong interaction among the different species that are included in the unit cell. Thus the binding energy of the total system including products is very different from the sum of two times the binding energy of CO and three times the binding energy of C.

If 4 atoms of carbon are co-adsorbed on the surface, one fourth of the high coverage binding energy is smaller than the binding energy computed when just 1 atom of carbon is included in the supercell. The largest gap between these two quantities in experienced on Nickel.

As consequence the heats of reaction evaluated on the three metals [Figure 5.37] follow the trend of the binding energy of C when high coverage is considered [Figure 5.39], the level of the energy associated to the products on the different metals decreases from Platinum to Nickel to Rhodium [Figure 5.36], instead the surface-C interaction becomes stronger moving from Rhodium to Platinum to Nickel. Although if the binding energy of CO is considered (Ni-CO interaction is stronger than Pt-CO) becomes clear why the products' level of energy on Platinum is above the products' level of energy on Nickel.

As a whole the initial state's energy of the elementary step is affected by the binding energy of carbon with high coverage, instead the energy of the products no longer only depends on CO binding energy (as for reaction (4.64)) but it is dominantly determined by the binding energy of atomic carbon.

Electronic structure is examined by use of the PDOS, the distribution of the states is studied in order to deeply comprehend the effects of carbon coverage and how binding energies vary because of carbon-carbon interaction.

The projected density of states on "p" orbiltals belonging to the atoms of carbon is displayed, a comparison is made between the PDOS computed on a 2x2 supercell with just one atom of carbon (low coverage) and the PDOS computed on the same supercell with 4 atoms of carbon included (high coverage).

If more than one atom of carbon is adsorbed in the same unit cell, the shape of the PDOS does not show just two peaks as at low coverage, but it is more uneven, three or four bands can be identified, this is due to the fact that C does not only split its states in bonding and antibonding to interact with the substrate, but another splitting of the states happens because of carbon-carbon interaction [Figure 5.40 (B), Figure 5.41 (B), Figure 5.42 (B)].

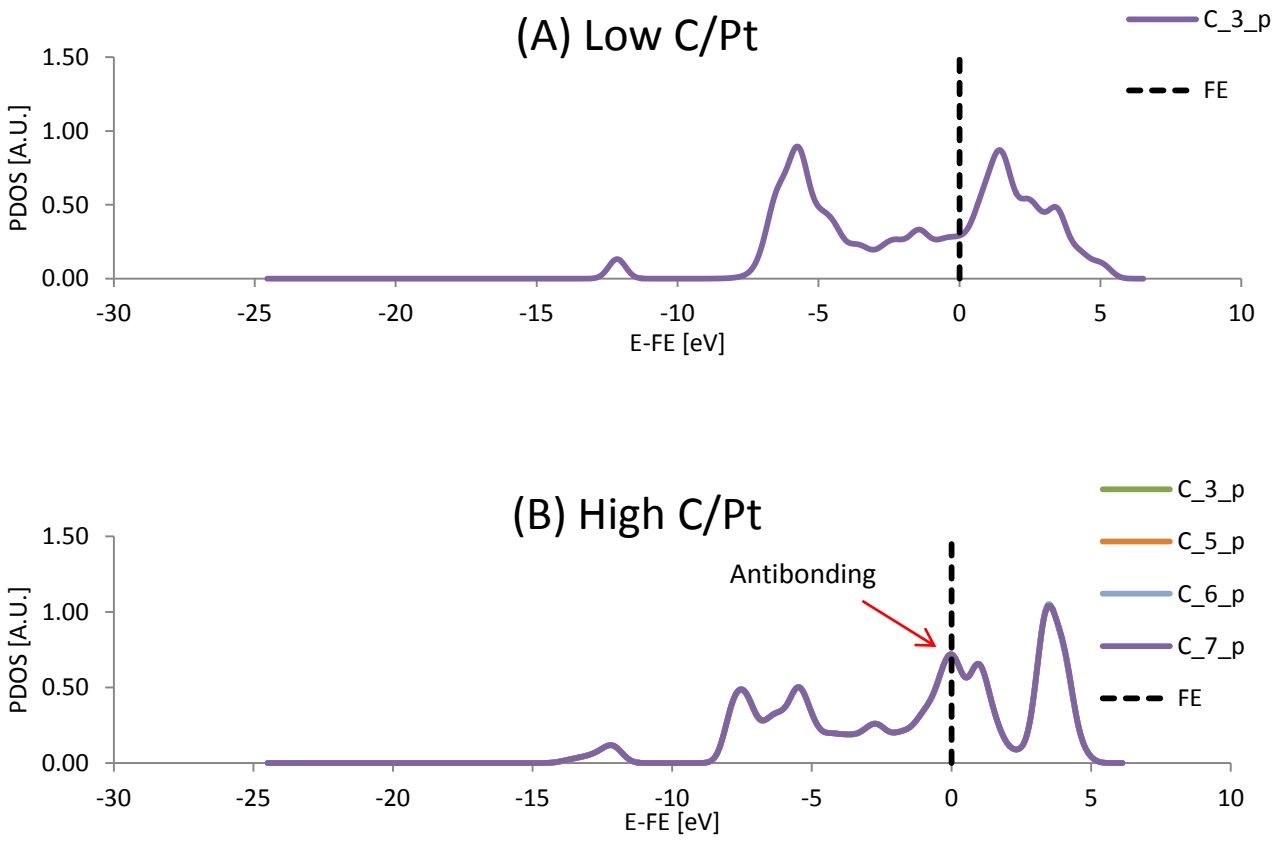

Figure 5.40: comparison between the PDOS of Pt with low (A) and high (B) coverage of carbon; FE = Fermi Energy (reference level); X_n_v means X = atomic type, n = label of the atom, v = valence orbital

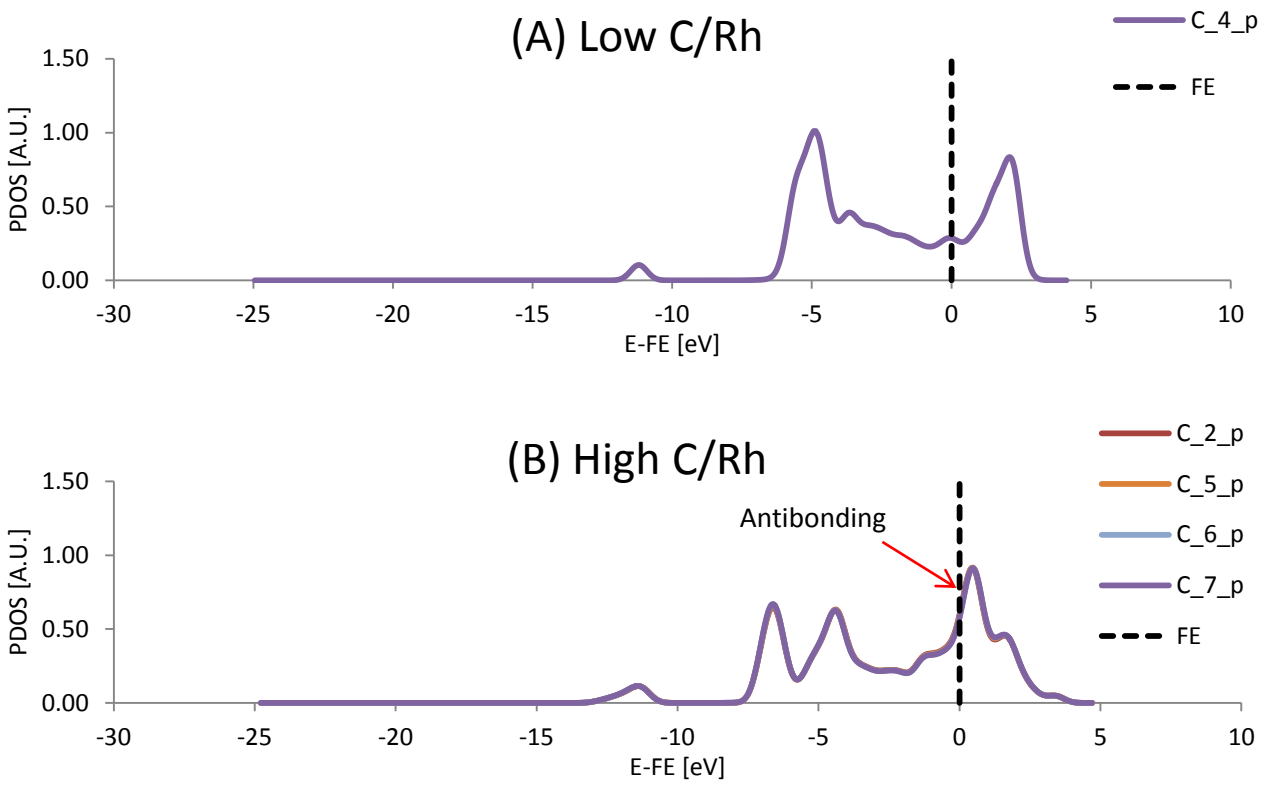

Figure 5.41: comparison between the PDOS of Rh with low (A) and high (B) coverage of carbon; FE = Fermi Energy (reference level); X_n_v means X = atomic type, n = label of the atom, v= valence orbital

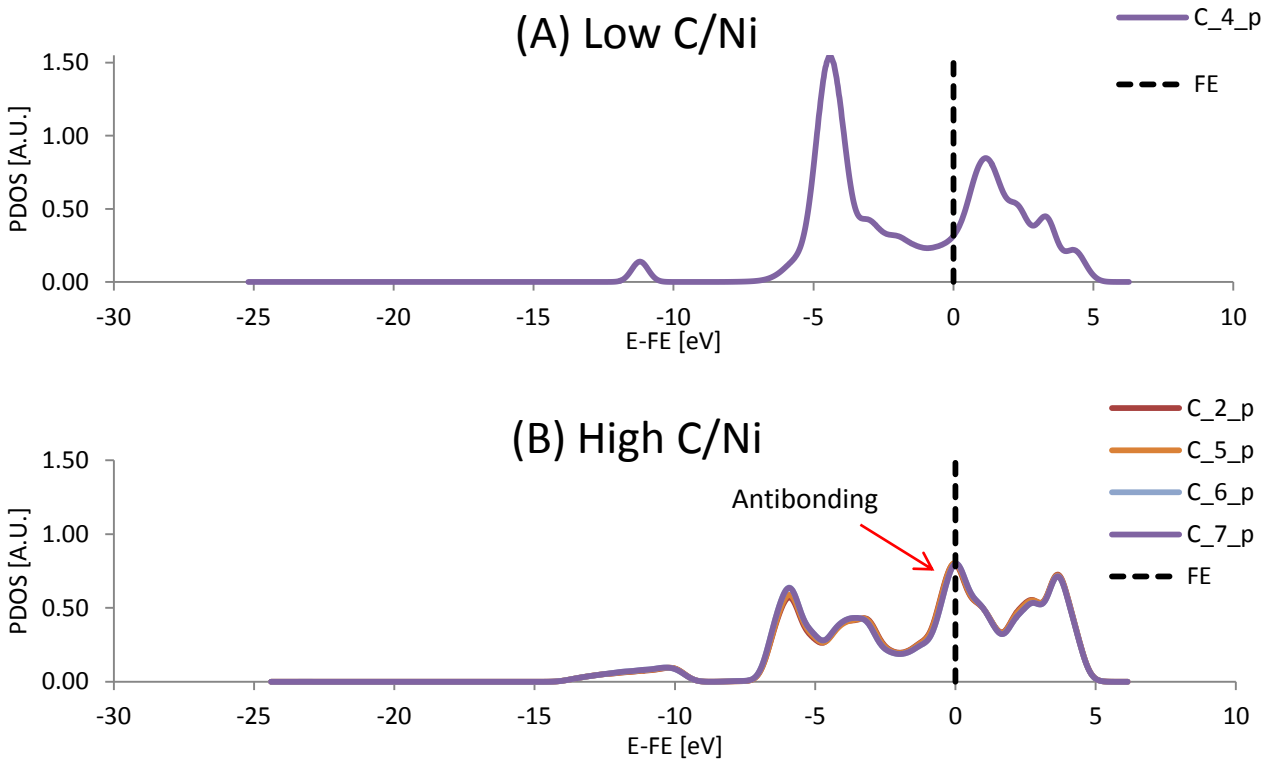

Figure 5.42: comparison between the PDOS of Ni with low (A) and high (B) coverage of carbon; FE = Fermi Energy (reference level); X_n_v means X = atomic type, n = label of the atom, v = valence orbital

The bonding states defined by two peaks around -5 eV are full, while the antibonding states are filling the third band, near 0 eV [Figure 5.40 (B), Figure 5.41 (B), Figure 5.42 (B)]. The greater is the portion of this band under the Fermi level the weaker is the strength of the bond, since half of the third peak is occupied by states for Platinum and Nickel, these metals produce a smaller binding energy rather than the binding energy for CO on Rhodium. In fact just a little fraction of the third band is filled on the Rhodium catalyst.

The binding energy of carbon, when high coverage is considered, is an important variable that can be connected with several properties of the system, in fact the larger is the binding energy of C (high coverage) and more stable are reactants at the surface, as consequence forward activation energy appears to increase according to the carbon binding energy [Figure 5.43]. Instead the energy of products at the metal surface depends on both CO and C binding energies, although a change in trend appears. Nickel does not possess the lowest backward activation energy, this trend is probably due to the reduction of carbon coverage and the consequential increment in carbon binding energy. One carbon leaves the surface and creates a gaseous carbon monoxide [Figure 5.43].

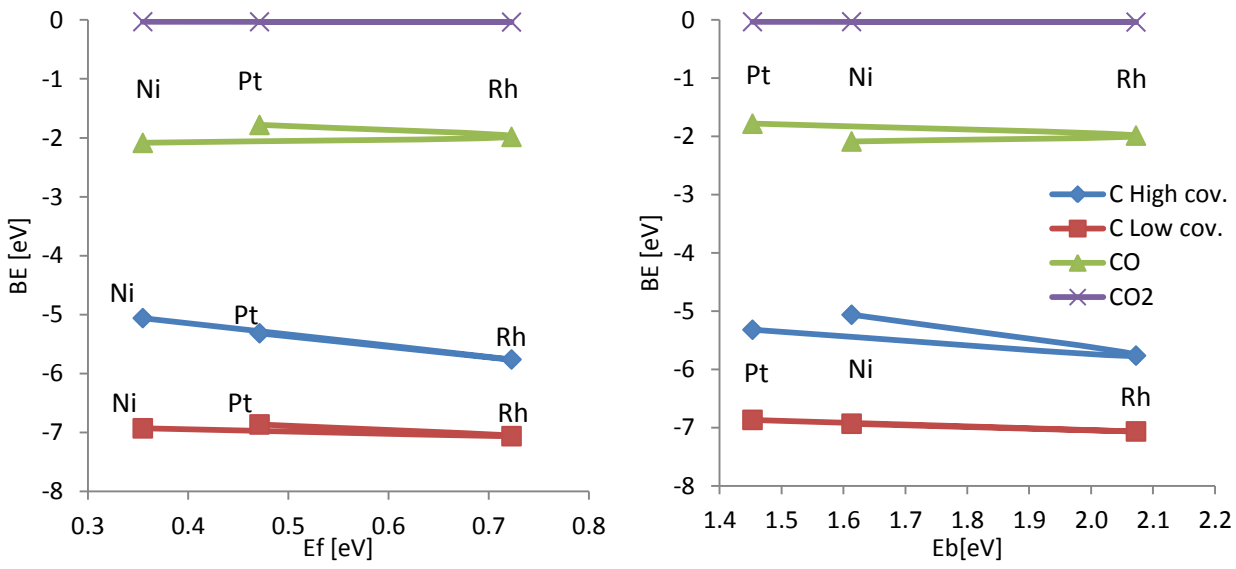

Figure 5.43: binding energies of reactants and products depending on forward and backward activation energy, for reaction (5.3)

To decide if the Transition State shares the same chemical reactivity of the reactants or of the products, its electronic structure has to be plotted and compared with the one of reactants and products. Thus the PDOS of the first (reactants at the surface), transition and last (products at the surface) states is depicted in the following figures.

On Platinum:

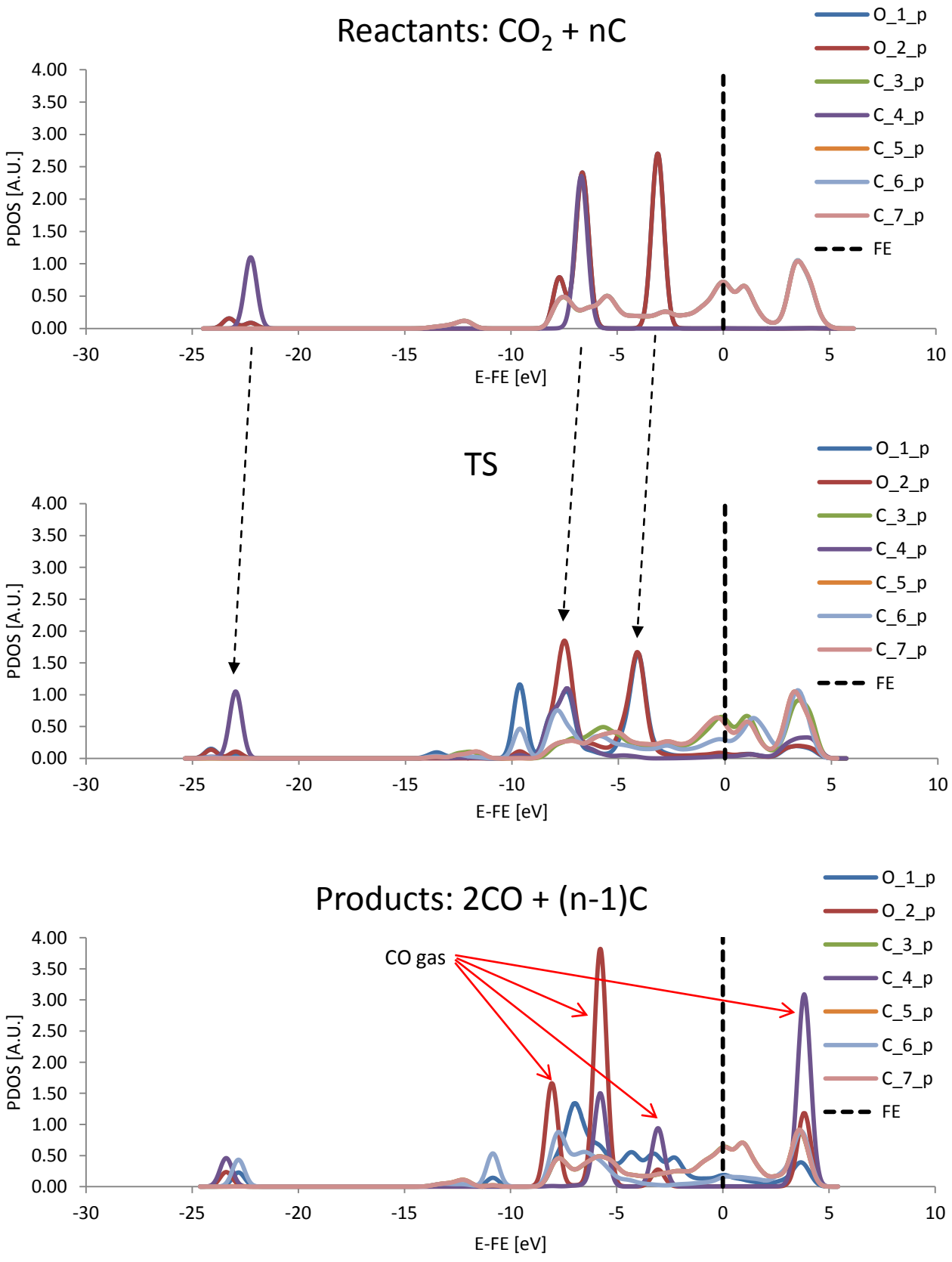

Figure 5.44: PDOS of the reactants, Transition State, and products for reaction (5.3) on Pt; FE = Fermi Energy (reference level); X_n_v means X = atomic type, n = label of the atom, v = valence orbital

On Rhodium:

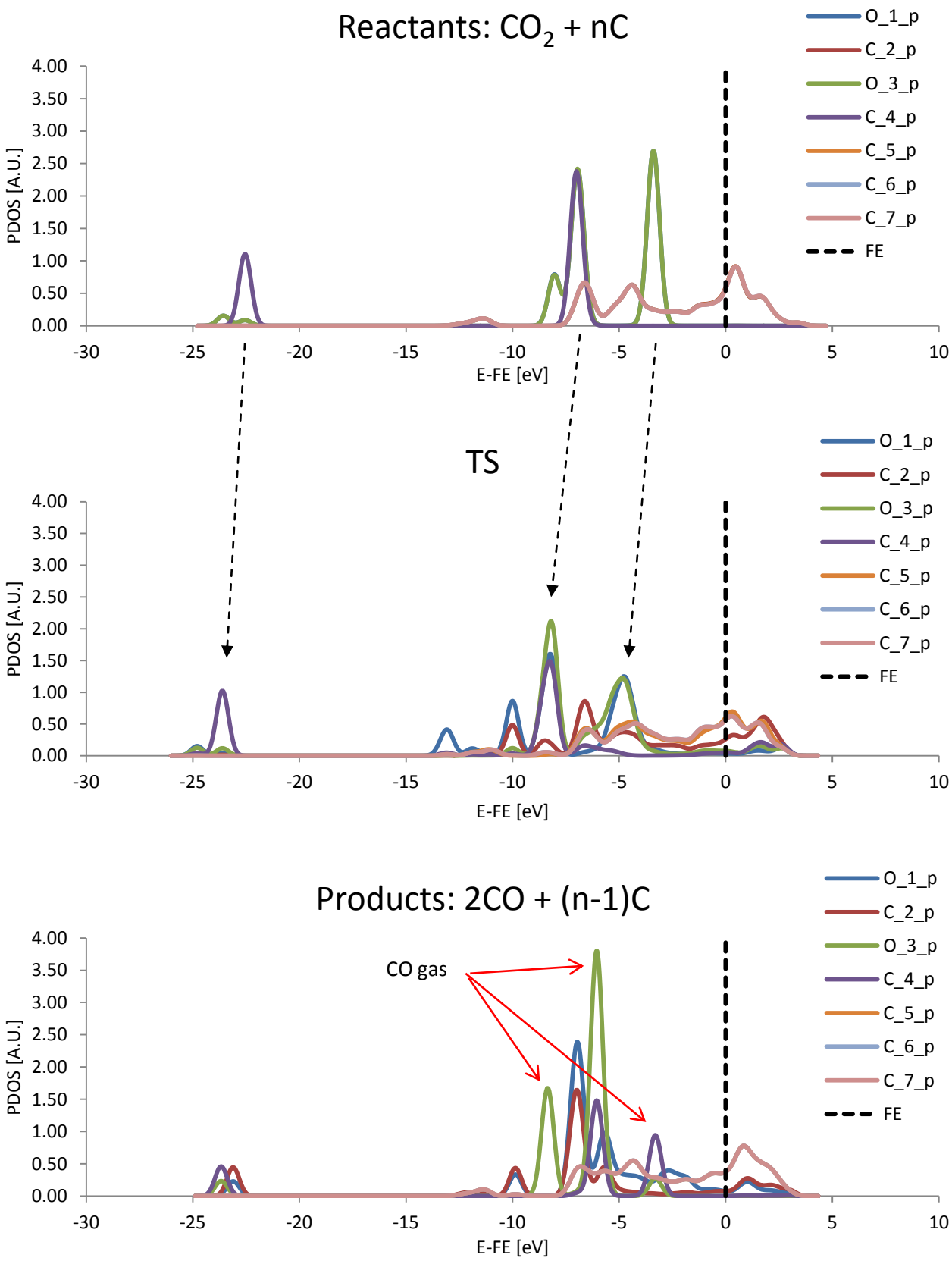

Figure 5.45: PDOS of the reactants, Transition State, and products for reaction (5.3) on Rh; FE = Fermi Energy (reference level); X_n_v means X = atomic type, n = label of the atom, v = valence orbital

On Nickel:

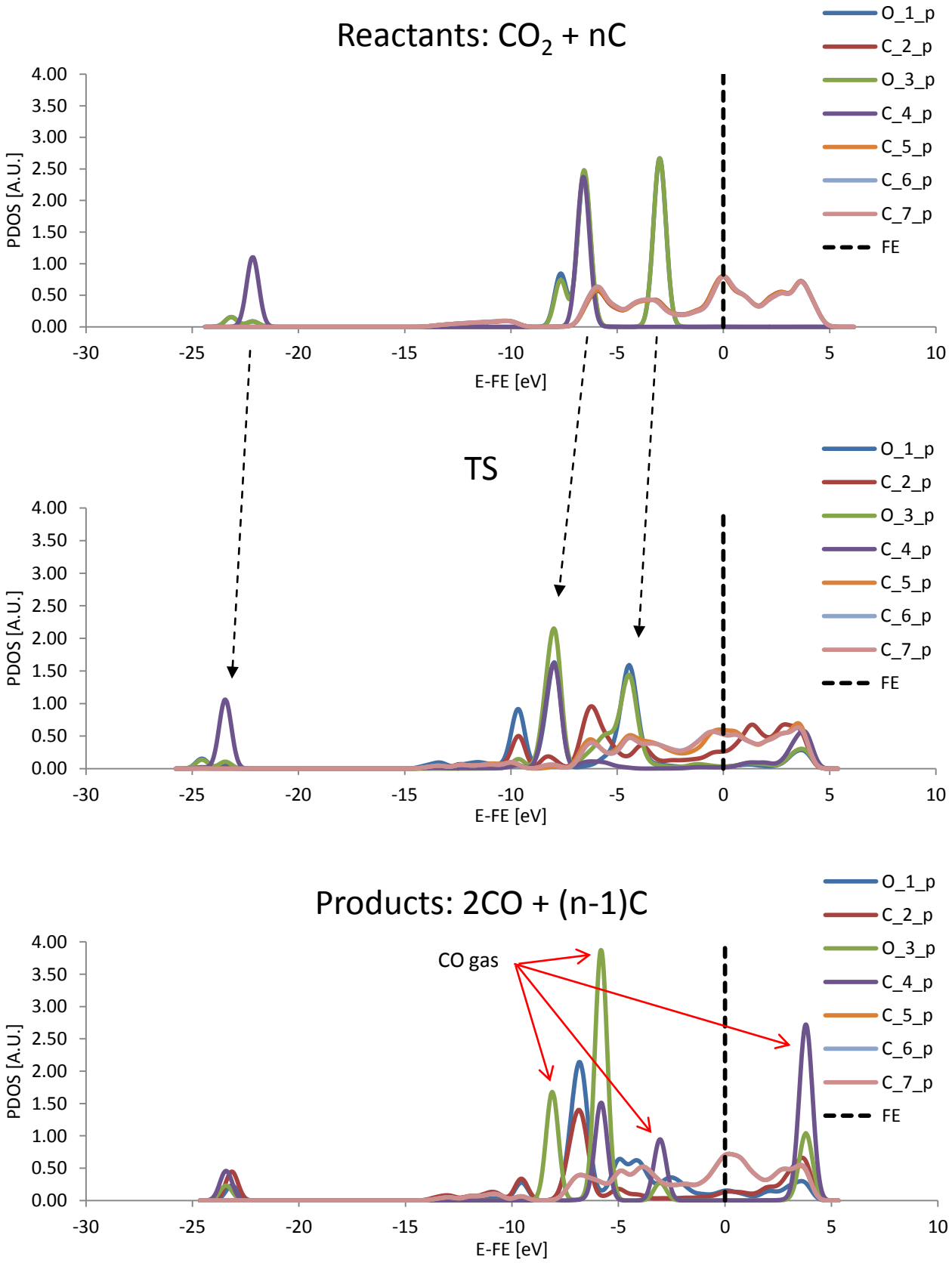

Figure 5.46: PDOS of the reactants, Transition State, and products for reaction (5.3) on Ni; FE = Fermi Energy (reference level); X_n_v means X = atomic type, n = label of the atom, v = valence orbital

In the PDOS of the first image of the NEB calculations the peaks of gaseous CO_2 are easily identified as well as the peaks of gaseous CO in the last image.

If the PDOS of the Transition State is accurately observed, the same peaks of the first image appear at the TS, in fact CO_2, even if slightly distorted, still exists on the saddle point of the MEP, and it is far from the surface. The bands of CO_2 are shifted towards lower energies, but they are very sharp, in fact electrons fill the bands associated with CO_2 bonding and antibonding molecular orbitals, and this means the C-O bonds are still well defined. Since the electronic structure at the Transition State resembles the electronic structure of reactants, the Transition State can be defined "early". An early Transition State shares the same electronic and often geometrical properties of reactants. The analysis on the nature of the Transition State has been done on two different levels, according to geometrical and electronic consideration [Table 5.18].

$CO_2+nC \rightarrow 2CO+(n-1)C$		
	Geometry	Electronic structure
Pt	Early	Early
Rh	Early	Early
Ni	Early	Early

Table 5.18: evaluation of the Transition State for reaction (5.3)

Conclusions:

- The binding energy of the atomic carbon is computed at high coverage to account for coverage effects,
- The binding energy of the atomic carbon with high coverage affects both forward and backward activation energy,
- Since one of the "n" carbons is a reactant and influences not only forward but even backward activation energy the Transition State is early,
- The Transition State is early, carbon binding energy with high coverage is reduced and even forward activation energy decreases if compared with the Boudouard reaction at low coverage.

5.6 Elementary Step: $CO_2 + H \rightarrow COOH$

Carbon dioxide can be activated by an atom of hydrogen adsorbed at the metal surface, thus the elementary step involving carbon dioxide hydrogenation on a (111) surface of Platinum, Rhodium and Nickel is studied to evaluate the activation energy of the process.

Platinum (111)

The research of the most stable adsorption sites for reactants and products is performed. The Platinum surface is studied in terms of potential energy surface, adsorbates are relaxed to the nearest local minimum and the binding energies are computed. The sites with the highest binding energy are selected to build the initial and final states of the elementary step.

CO_2	H	BE [eV]
Hcp	**Top**	-2.688
Top	**Fcc1**	-2.745
Top	**Fcc2**	-2.748
Top	**Hcp**	-2.710
Top	**Top**	-2.679
Fcc	**Hcp**	-2.709
Hcp	**Hcp**	-2.714
Fcc	**Top**	-2.681

Table 5.19: binding energy of carbon dioxide and atomic hydrogen at different combinations of adsorption sites on Pt

COOH	BE [eV]
Bridge	-2.301
Fcc	-2.304
Hcp	-2.303

Table 5.20: binding energy of the carboxyl group at different adsorption sites on Pt

Reactants are located at the fcc site for the hydrogen atom, instead CO_2 remains far from the surface with its carbon oriented towards a top site. The research of the initial configuration that defines the positions of reactants is very difficult since CO_2 experiences a flat potential, but even hydrogen

moves on a very smooth potential surface, in fact its binding energy slightly varies from an adsorption site to another [Table 5.19]. If initial COOH structure is far different from the relaxed one, the initial structure can be destroyed and split into co-adsorbed CO and OH, on the other hand if a good initial structure is built COOH always moves from the initial position on the surface to bring its carbon on a top site, with hydrogen in trans configuration, pointing at a Pt atom [22]. This statement explains why COOH binding energy does not change for site to site [Table 5.20].

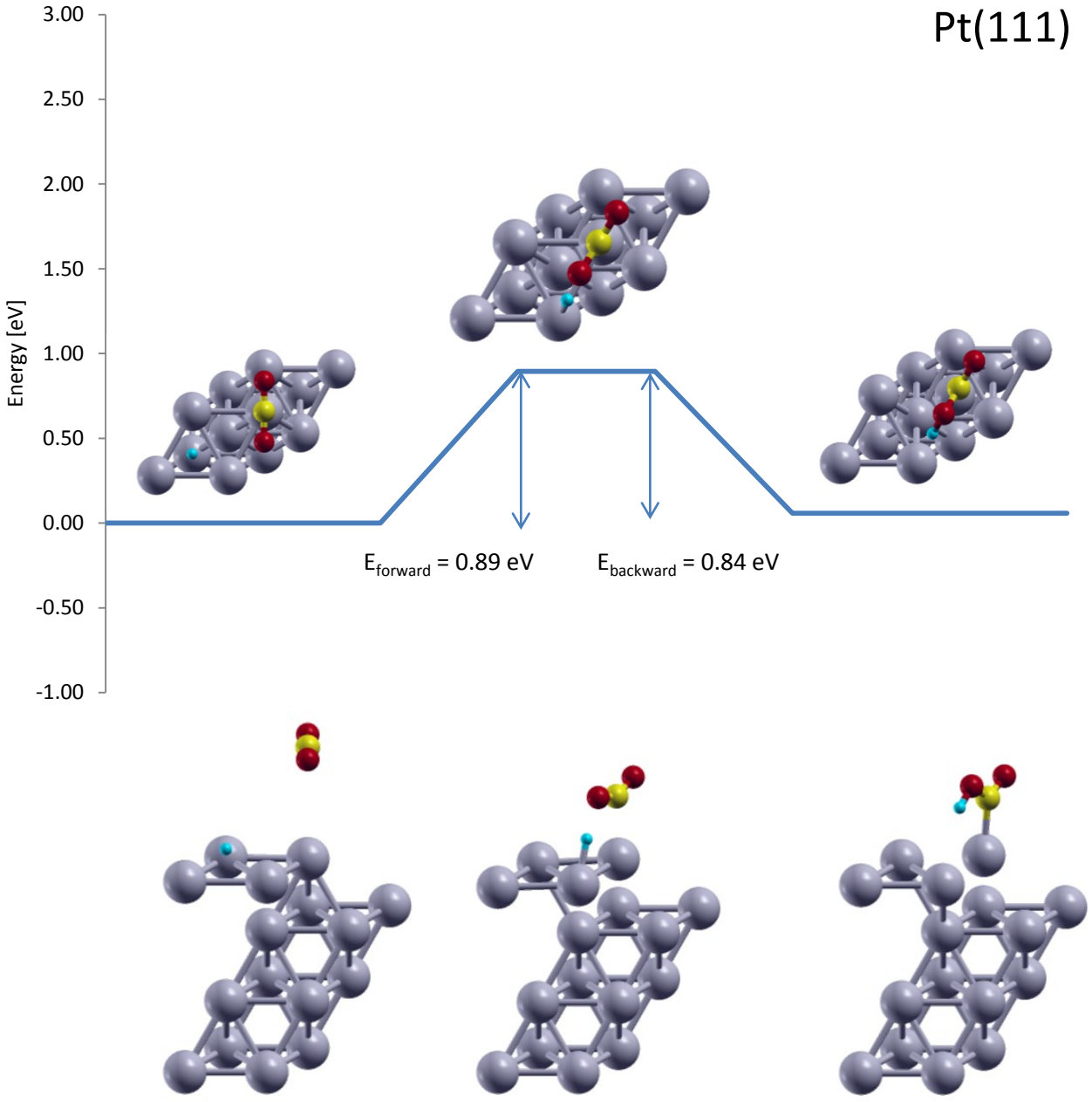

Figure 5.47: forward and backward activation energy of carbon dioxide hydrogenation on Pt

NEB calculations are performed to map the MEP, and CI method is used to exactly locate the Transition State [Figure 5.47]. Initial and final states of the elementary step that happens at the metal surface are chosen according to the previous research of the most stable adsorption sites.

As shown in Figure 5.47 it is possible to state that the energy of the reactants at the surface is quite the same as for the products at the surface. The energetic levels just differ by 0.058 eV, thus the surface reaction (4.65) is slightly endothermic.

At the initial state CO_2 is far from the surface, 4.098 Å of vacuum separate the carbon of CO_2 from the plane of the surface, thus no considerable interaction is expected; in fact the CO_2 structure is the typical one of an isolated gaseous CO_2. The C-O distance is 1.17 Å with an O-C-O angle of 179.94°. Hydrogen is instead positioned at the fcc site, the vertical distance is very short, 0.898 Å, this result is quite reasonable since hydrogen is a very small atom.

Then, at the Transition State, CO_2 lands on the surface, but the near metal induces a distortion of its linear structure, in fact the initial O-C-O angle is reduced from 179.94° to 147.16°. Pt-C distance is now 2.344 Å, instead the C-O bond is stretched, one of the two bond length is 1.196 Å, instead the other oxygen that is going towards the adsorbed hydrogen, produces a C-O distance of 1.223 Å. The adsorbed hydrogen shifts from the fcc to the top site, in order to get closer to the atom of oxygen that belongs to CO_2. The new Pt-H distance on the top site is 1.625 Å, and the O-H computed spacing is 1.569 Å.

The interaction between the valence electrons of oxygen and hydrogen becomes intense, CO_2 binds on a top site and gives rise to the new O-H bond. The final state of the elementary step involves a COOH species, with a Pt-C distance of 2.028 Å, a C-O bond of 1.215 Å, and a C-O-H group that displays a C-O distance of 1.335 Å, and a O-H spacing of 0.988 Å. Trans-COOH exhibits a O-C-O angle of 121.86°, that is less than the same angle measured on CO_2 at the Transition State. Hydrogen is directed towards a top site, 2.447 Å far from the last layer of the slab, it is also linked to an oxygen that is set at almost 3 Å from the surface, instead the other oxygen stays at 2.67 Å.

Rhodium (111)

Now, the second metal, Rhodium, is studied. Because of Rhodium "4d" valence states, heats of adsorption are different from the heats computed for Platinum, but not so diverse since they are both transition metals with d-bands partially filled. The initial and final configuration of the elementary step has to be found, to initialize the NEB method.

CO_2	H	BE [eV]
Hcp	**Top**	-2.502
Top	**Fcc1**	-2.825
Top	**Fcc2**	-2.821
Top	**Hcp**	-2.796
Top	**Top**	-2.484
Fcc	**Hcp**	-2.787
Fcc	**Fcc**	-2.834
Hcp	**Hcp**	-2.803
Fcc	**Top**	-2.797

Table 5.21: binding energy of carbon dioxide and atomic hydrogen at different combinations of adsorption sites on Rh

COOH	BE [eV]
Bridge	-2.510
Fcc	-2.510
Top	-2.510

Table 5.22: binding energy of the carboxyl group at different adsorption sites on Rh

CO_2 does not give an important contribution to the total binding energy, which is dominantly due to the adsorption of the atomic hydrogen. CO_2 is over a fcc site, instead the atom of hydrogen is attached to another threefold fcc site. The heats computed on Rhodium are a little stronger than the heats originated by the Platinum surface but similar. COOH instead has just one local minimum on the surface, that is on a top site, in fact if it is positioned at a fcc or at a bridge site it moves towards the nearest top.

Once the positions of reactants and products on the metal surface are known, NEB calculations can be performed to find the Transition State.

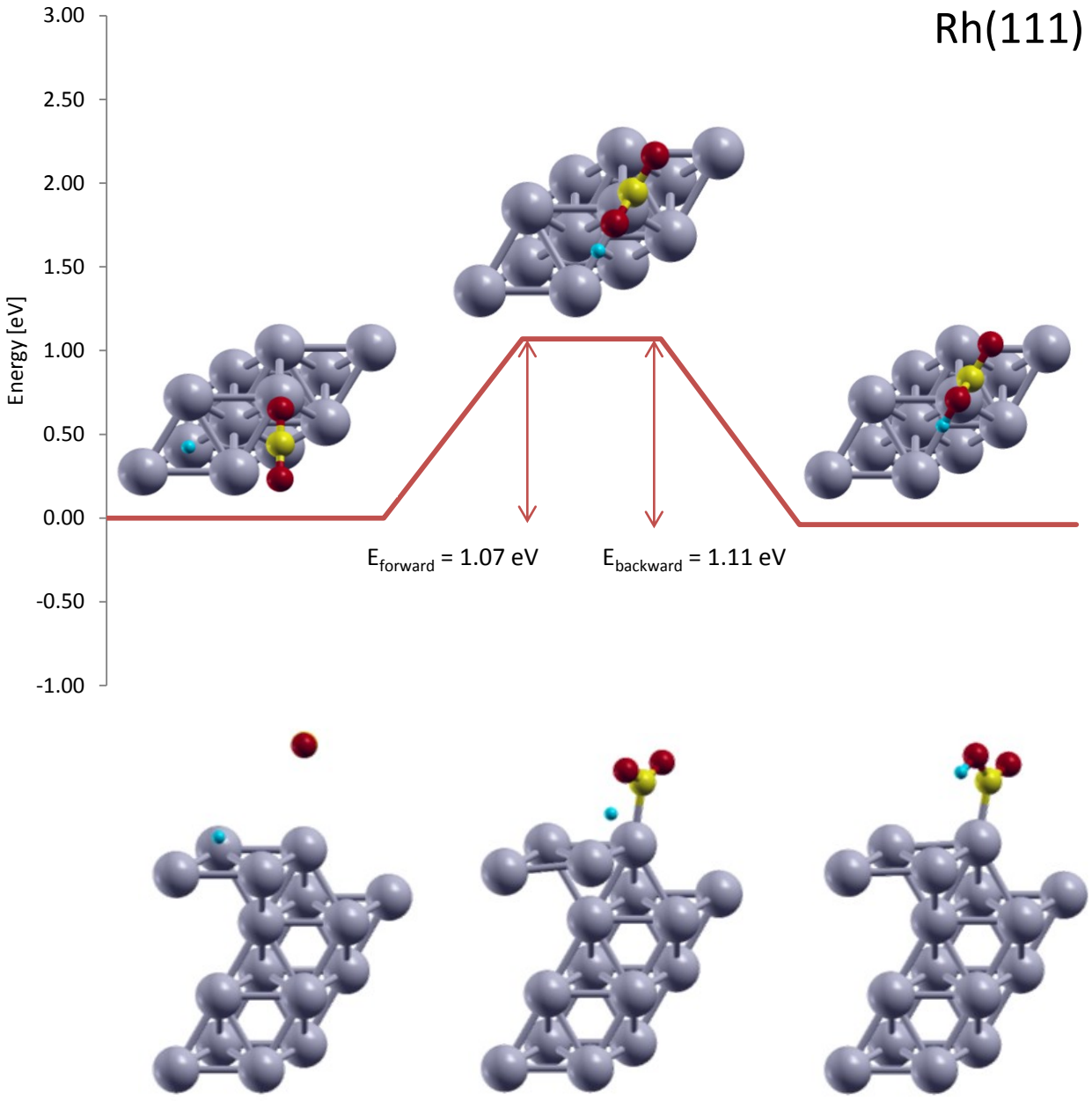

Figure 5.48: forward and backward activation energy of carbon dioxide hydrogenation on Rh

The surface reaction (4.66) on Rhodium is exothermic for -0.038 eV, that is to say it is almost athermic.

At the initial state, the reactants are CO_2 and H. CO_2 is in gas phase, its carbon is over a fcc site, with a distance of 4.13 Å from the surface, its linear structure is not flat, in fact an oxygen is pointing at a top site, the Rh-O distance is 3.76 Å, instead the other oxygen is 4.51 Å above the surface level. C-O bond length measures 1.17 Å, instead O-C-O angle is 179.93°. Hydrogen is at the fcc site, adsorbed on the catalyst, 0.99 Å far from the last layer of the slab, this distance appears to be larger than the same distance computed on Platinum, probably because the threefold hollow on Platinum is larger than on Rhodium, Rhodium lattice constant is shorter than Platinum one. In fact if the distance is not computed as vertical spacing from the surface plane, but as metal-hydrogen length, Rh-H bond is 1.859 Å long, on the other hand Pt-H bond is 1.865 Å long. This trend can be explained by considering hydrogen binding energy, since Rhodium exhibits a larger binding energy rather than Platinum, Rh-H distance is supposed to be shorter.

CO_2 approaches the metal and experiences the surface's potential, a Rh-C bond is created (2.013 Å), the carbon is not vertically set above the top site, but a Rh-Rh-C angle of 100.60° is computed. CO_2 structure still exists, but it is no longer linear, the O-C-O angle decreases till 131.31°. The C-O distance raises, the O opposite the adsorbed hydrogen is 1.262 Å far from the central carbon, instead the O near the hydrogen is 1.263 Å far from the carbon (the CO_2 structure is still symmetric) and 1.493 Å far from the atom of hydrogen. Meanwhile, the adsorbed hydrogen hops from fcc to a bridge site.

At the final state COOH is attached to a top site, the Rh-C bond length is 1.984 Å, with a Rh-Rh-C angle of 112.80°. COOH structure resembles the structure of CO_2 at the Transition State, with an O-C-O angle of 116.49°. On one end C-O distance is 1.265 Å (against 1.262 Å at TS), on the other end the C-O spacing increases from 1.263 Å to 1.337 Å because of O-H attraction. Obviously O-H distance is shorter than the one computed at the Transition State, in fact a hydroxyl bond of 0.985 Å is created, with its hydrogen 2.74 Å far from the surface and with a C-O-H angle of 108.83°.

Nickel (111)

The last metal, Nickel, is used to catalyze the reaction, the new substrate-adsorbate interaction has to be studied to determine the strongest adsorption sites for reactants and products, thus adsorbates are moved from site to site, and binding energies are calculated [Table 5.23, Table 5.24].

CO_2	H	BE [eV]
Hcp	**Top**	-2.936
Top	**Fcc1**	-2.962
Top	**Fcc2**	-2.960
Top	**Hcp**	-2.962
Top	**Top**	-2.387
Fcc	**Hcp**	-2.884
Fcc	**Fcc**	-2.965
Hcp	**Hcp**	-2.964
Fcc	**Top**	-2.954

Table 5.23: binding energy of carbon dioxide and atomic hydrogen at different combinations of adsorption sites on Ni

COOH	BE [eV]
Bridge	-2.476
Fcc	-2.328
Hcp	-2.474

Table 5.24: binding energy of the carboxyl group at different adsorption sites on Ni

Lots of binding energies for CO_2 and H co-adsorbed on the surface are near to -2.9 eV, but the highest is found when both CO_2 and H are at a fcc site. Instead, if the COOH structure is relaxed, the carboxyl group shifts from the bridge position to the top, and the same behave is observed if COOH is initially set on an hcp adsorption site. The most stable among the allowable initial and final states of the elementary step are identified for the Nickel catalyst; these states are the origin and the end of the MEP on which the Transition State has to be found. NEB calculations are performed, and forward and backward activation energies are estimated.

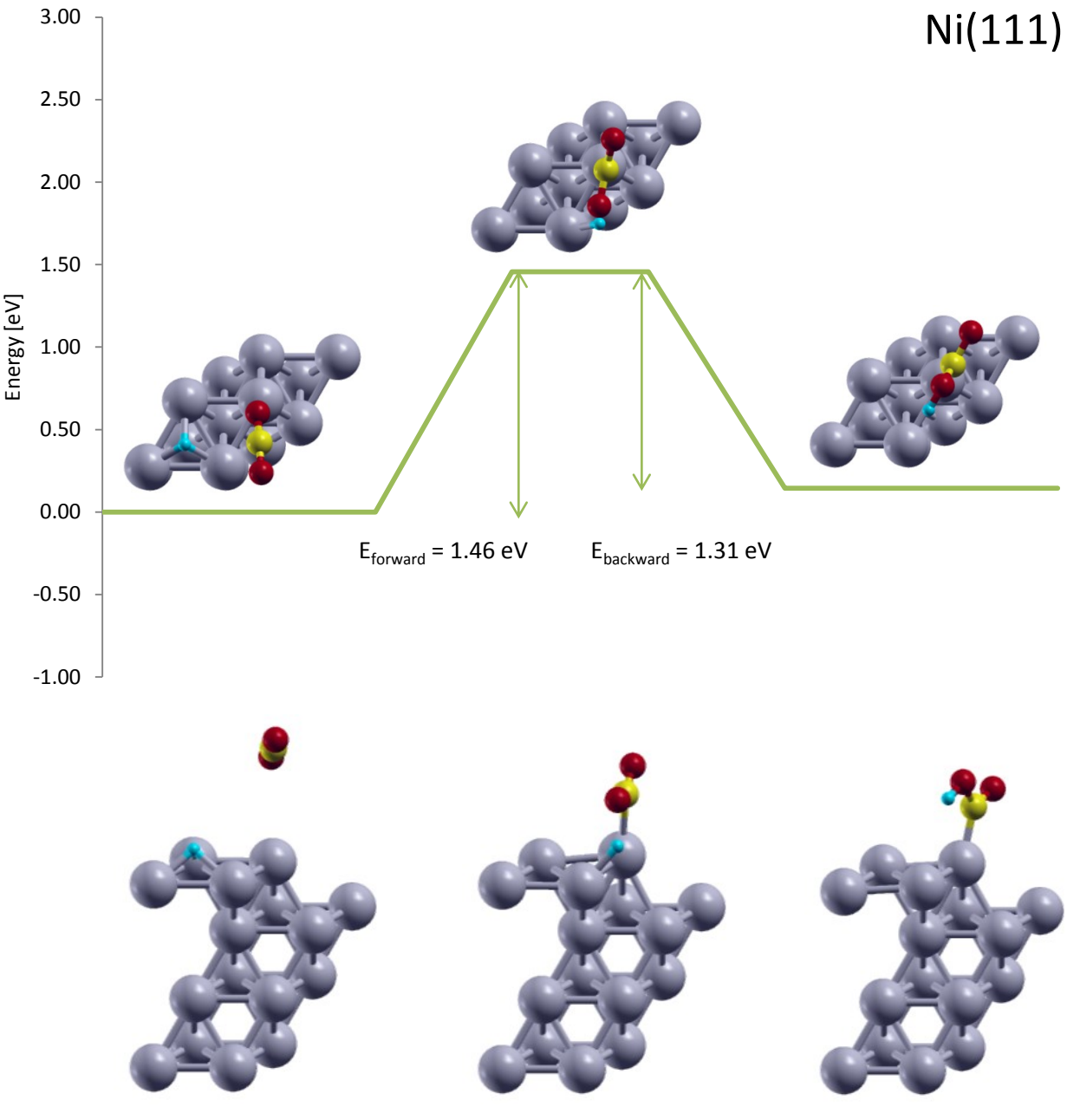

Figure 5.49: forward and backward activation energy of carbon dioxide hydrogenation on Ni

The surface reaction (4.67) on Nickel is endothermic as for Platinum. A difference of 0.145 eV between the energies of reactants and products at the surface is computed.

Gaseous CO_2 has a C-O bond length of 1.17 Å and an O-C-O angle of 179.99°. One of the carbon dioxide oxygens points at a top site, the vertical distance from the Nickel surface is 3.65 Å, the carbon atom is 4.29 Å over the surface, and the second oxygen 4.93 Å far from the outer layer of the slab. The atom of hydrogen is positioned inside a threefold fcc hollow site, the binding energy experienced by hydrogen on Nickel is larger than the binding energy computed on a Platinum or Rhodium surface, thus even if the available space inside the hollow is smaller, because of the shorter Nickel lattice constant, the perpendicular distance of H from the slab is little, 0.898 Å.

Then CO_2 shares electrons with the metal and adsorbes on a top site at the Transition State, the interaction with Nickel makes the Ni-C distance to be 2.08 Å, and causes an O-C-O angle of 140.01°. The CO_2 structure is no longer symmetric, since one C-O bond length is 1.201 Å, instead the other C-O bond is more extended, 1.265 Å, in fact the oxygen is moving towards the near adsorbed hydrogen. On the other end H goes from the fcc site to the near hcp, then it hops to the next fcc site and is found at bridge when the Transition State structure is defined, with an O-H distance of 1.449 Å.

Hydrogen gets closer to the atom of oxygen, until the distance of 0.988 Å is reached and the hydroxyl bond is created. At the final state the carboxyl is adsorbed on a top site, the “trans” configuration is preferred rather than the “cis” structure. The Ni-C bond length is 1.85 Å, one oxygen is adsorbed on the next top site, with a Ni-O distance of 2.02 Å. The other oxygen instead is positioned 2.81 Å above the plane of the metal while hydrogen is located 0.25 Å below the oxygen, 2.56 Å far from the catalytic layer. The C-O distance computed for the C-O-H chain is 1.33 Å, against the initial 1.265 Å, instead the other C-O distance is 1.269 Å against 1.201 Å computed at the Transition State. Carboxyl shape reminds the CO_2 structure at the Transition State, in fact the O-C-O angle is 116.55° and C-O-H group forms an angle of 110.19°.

5.6.1 Reactivity Analysis of Metals: $CO_2 + H \rightarrow COOH$

Here we want to establish if a correlation among Transition State properties and electronic structures of reactants or products exists. The following thermodynamic cycle [Figure 5.50] demonstrates that even if the initial and final states have the same energy, reactants and products in gas phase, what happens at the catalytic surface is strongly affected by the choice of the metal, that allows to reach particular energetic levels due to the different substrate-adsorbate feeling.

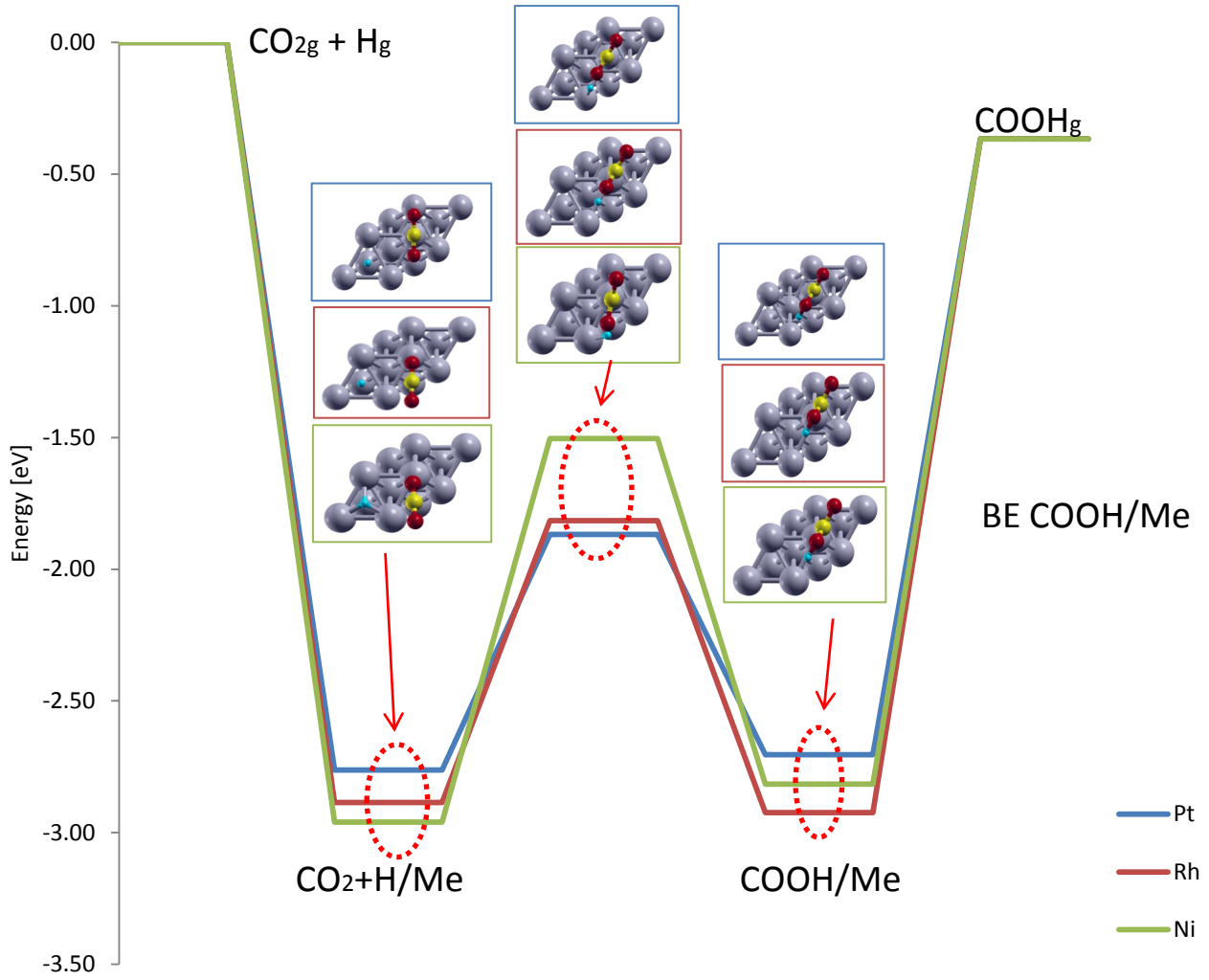

Figure 5.50: thermodynamic cycle of carbon dioxide hydrogenation on Pt, Rh and Ni

The thermodynamic cycle is built:

- The first step represents reactants in gas phase,
- Reactants are adsorbed at the metal surface,
- The third step is referred to the Transition State,
- Reactants are turned into products on the catalytic surface,
- The products desorbes from the surface and it remains in gas phase.

The dependence of forward and backward activation energies on the kind of metal is depicted in Figure 5.51, while heats of reaction are related to activation energies in Figure 5.52.

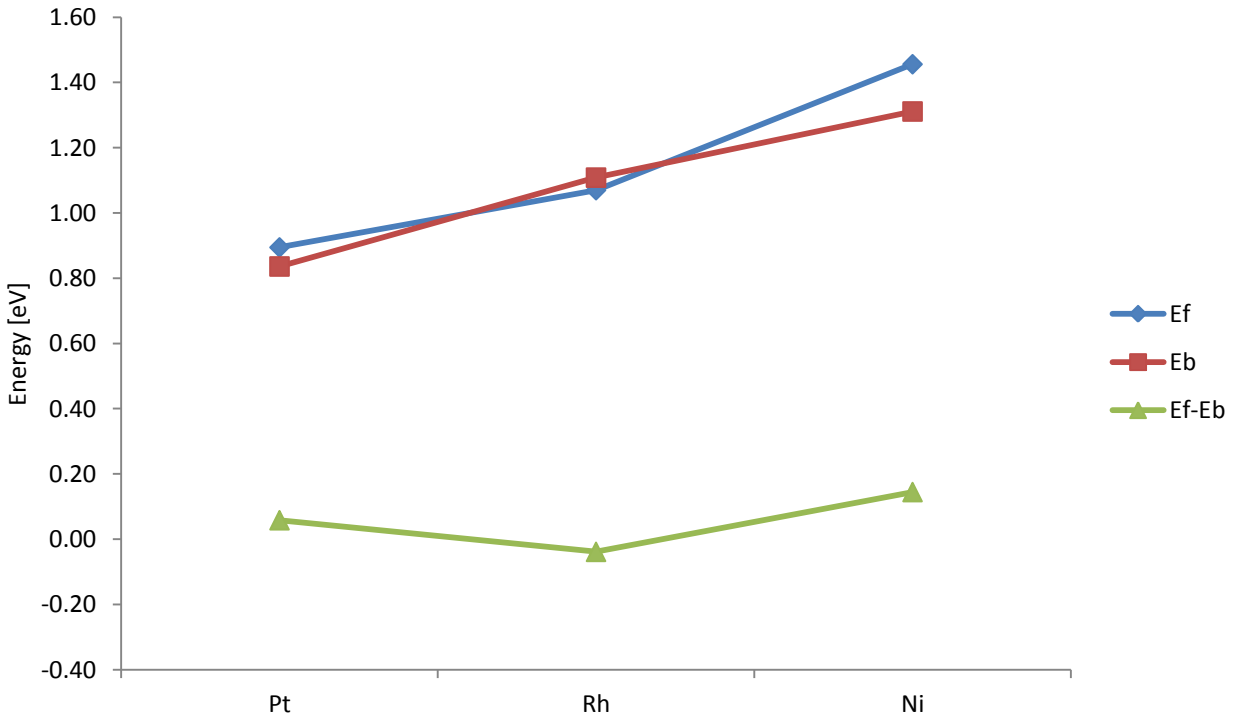

Figure 5.51: forward, backward activation energy, and heats of reaction (5.4) on the three metals

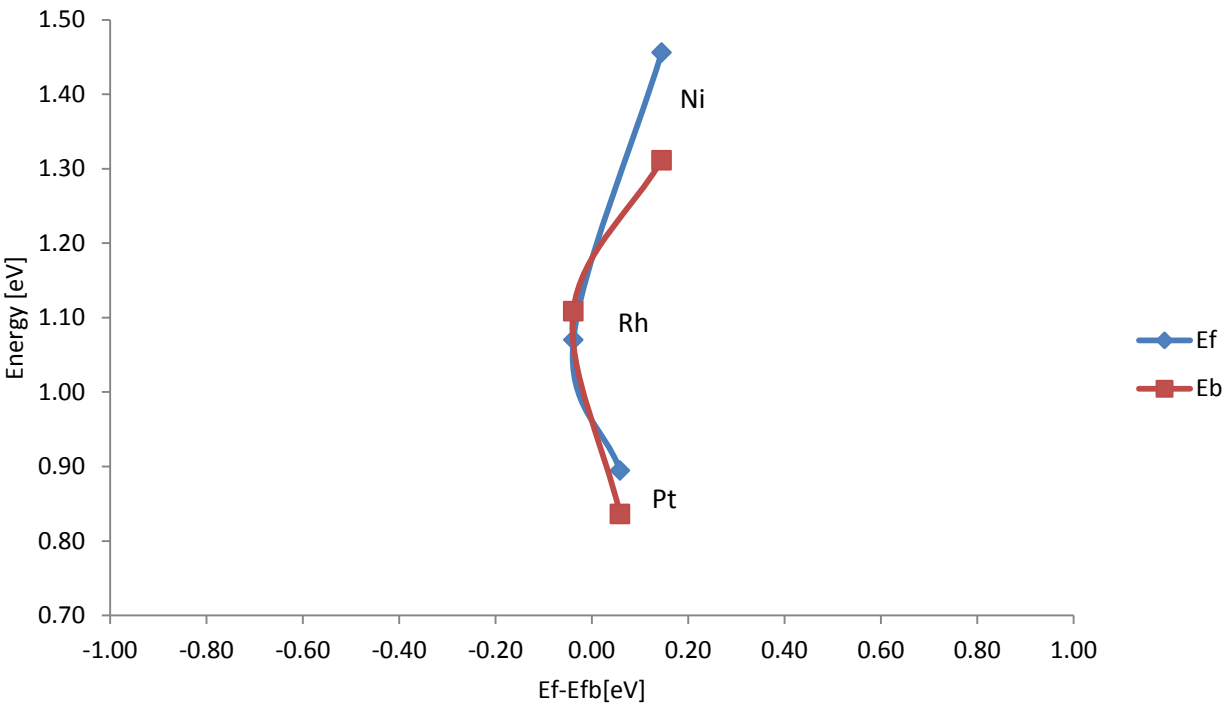

Figure 5.52: forward and backward activation energy dependence on heats of reaction (5.4)

Both forward and backward activation energies increase moving on the periodic table from Platinum to Rhodium and Nickel. A greater gap, that provokes a larger heat of reaction, is seen between forward and backward activation energy on Nickel.

The heats of reaction experienced on the three metals are all very close to 0 eV, thus no reasonable dependence can be found between activation energies and heats of reaction, in addition, it is possible to confirm that if forward activation energy grows even backward activation energy raises, as consequence Evans-Polanyi theory does not work for this class of reaction.

Binding energies of reactants and products are depicted in Figure 5.53 to explain and identify the chemical compound that acts on the energy of the initial, transition and final state of the elementary step at the different metal surfaces.

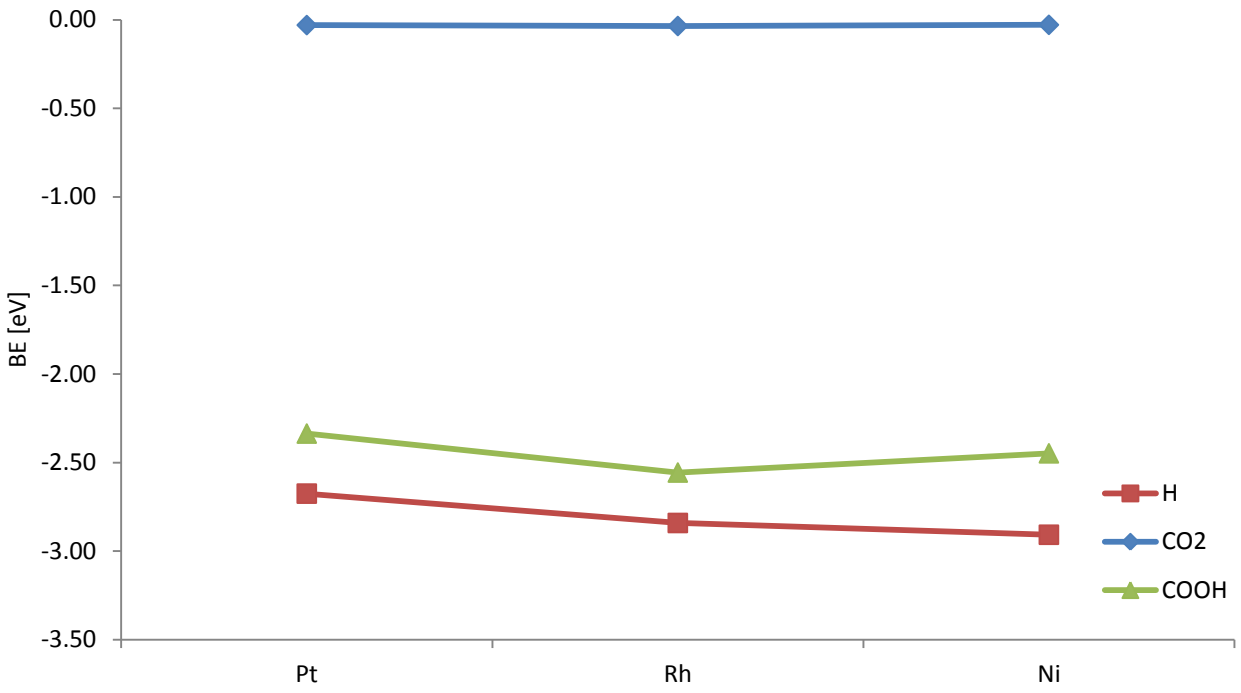

Figure 5.53: binding energies of reactants and products of reaction (5.4) on the three metals

CO_2, that is a closed shell molecule, with all bonding molecular orbitals doubly occupied, does not share electrons with the atoms of the surface, thus is always found in gas phase and doesn't interact with any of the three examined metals whereas the hydrogen-metal interaction can be analyzed by PDOS as shown in chapter 3 [Figure 3.46].

The greater is hydrogen binding energy and the greater are both forward and backward activation energy, thus hydrogen directly affects the relative energy of the Transition State.

On the other hand the carboxyl group experiences the same trend as for hydrogen only on Platinum and Rhodium, but it prefers to establish a chemical bond with Rhodium, rather than with Nickel, probably because of steric effects, in fact Nickel possesses the shortest lattice constant among the three metals, and thus the unit cell used to perform electronic structure calculations is smaller.

The stability of the initial state is determined by the atomic hydrogen adsorbed on the metal surface, since the binding energy of H decreases from Ni to Rh to Pt, reactants are more stable when they are adsorbed on Ni rather than on Pt or Rh. If H affects the total energy of the initial state thus affects the forward activation energy. The greater is hydrogen heat of adsorption and higher is the barrier energy. However, backward activation energy is also affected by hydrogen binding energy, the greater is the heat of adsorption and the higher becomes the backward activation energy. In fact

this means that the stability of the Transition State structure decreases as the stability of the adsorbed hydrogen grows.

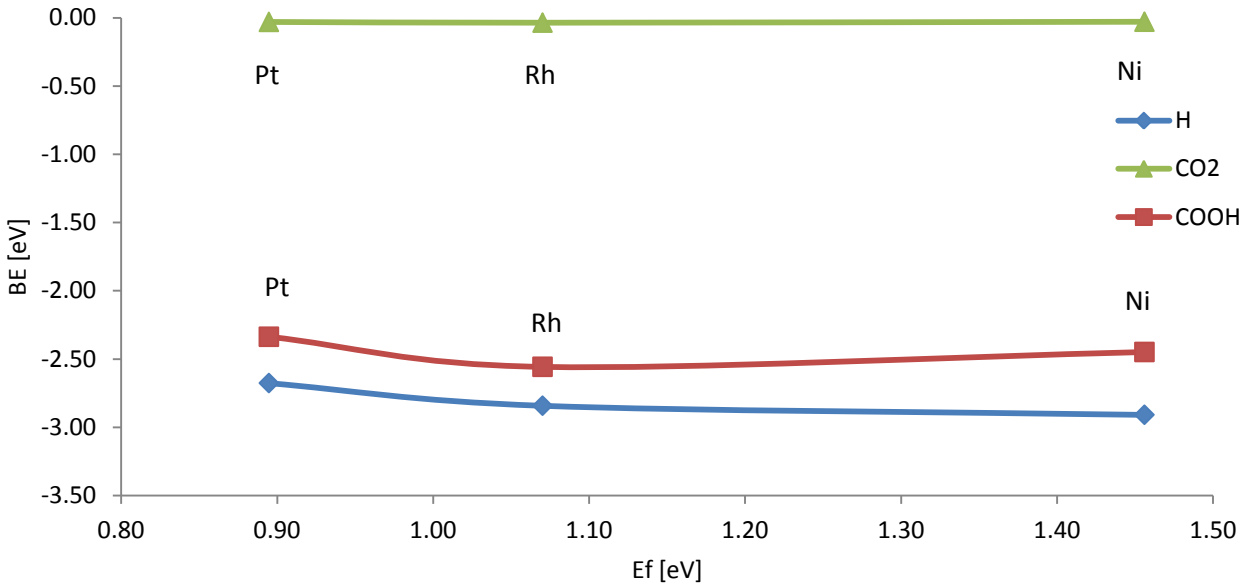

Figure 5.54: binding energies of reactants and products depending on forward activation energy, for reaction (5.4)

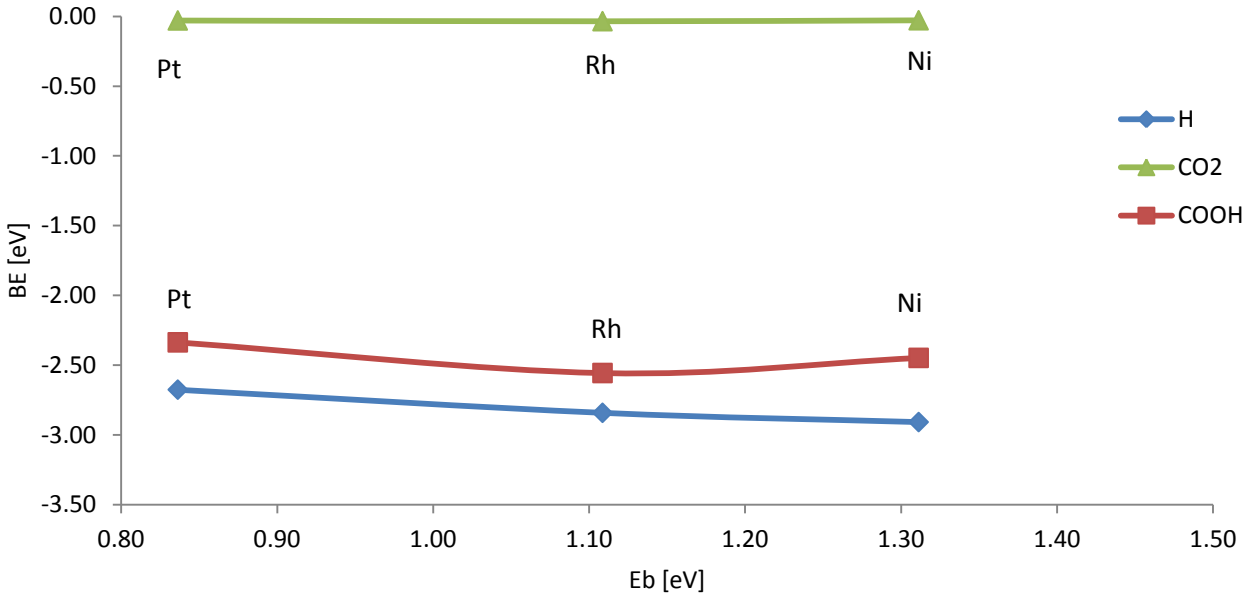

Figure 5.55: binding energies of reactants and products depending on backward activation energy, for reaction (5.4)

After defining the adsorbed hydrogen as the chemical compound that more strongly affects the energetic levels of the Transition State electronic structures computed on the Platinum, Rhodium and Nickel catalysts, now the projected density of states is applied on the initial, transition, and final states in order to define the shape of the Transition State structure and demonstrate the relationship that exists between reactants and molecular species at the Transition State, or between the products and the latter.

On Platinum:

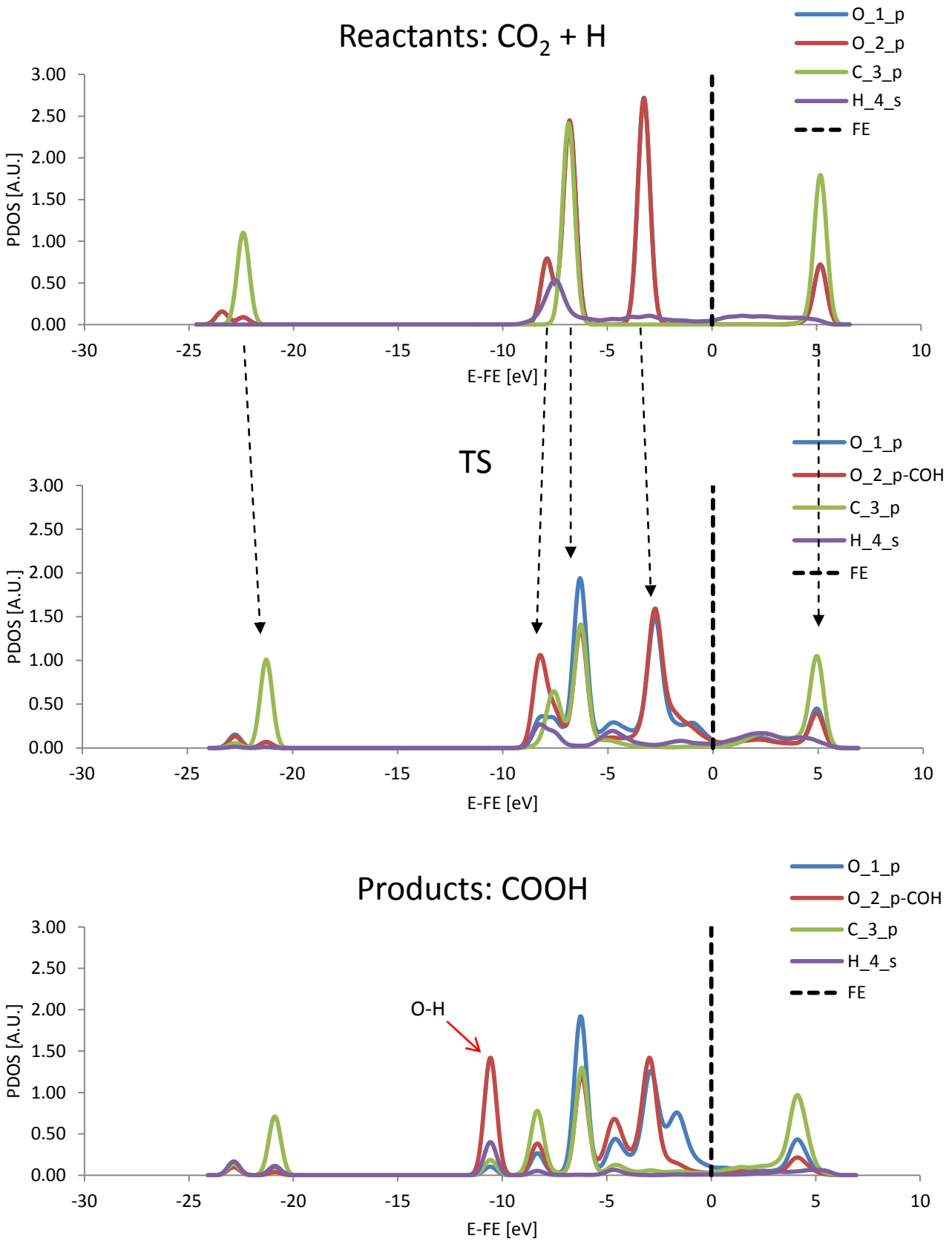

Figure 5.56: PDOS of the reactants, Transition State, and products for reaction (5.4) on Pt; FE = Fermi Energy (reference level); X_n_v means X = atomic type, n = label of the atom, v = valence orbital

On Rhodium:

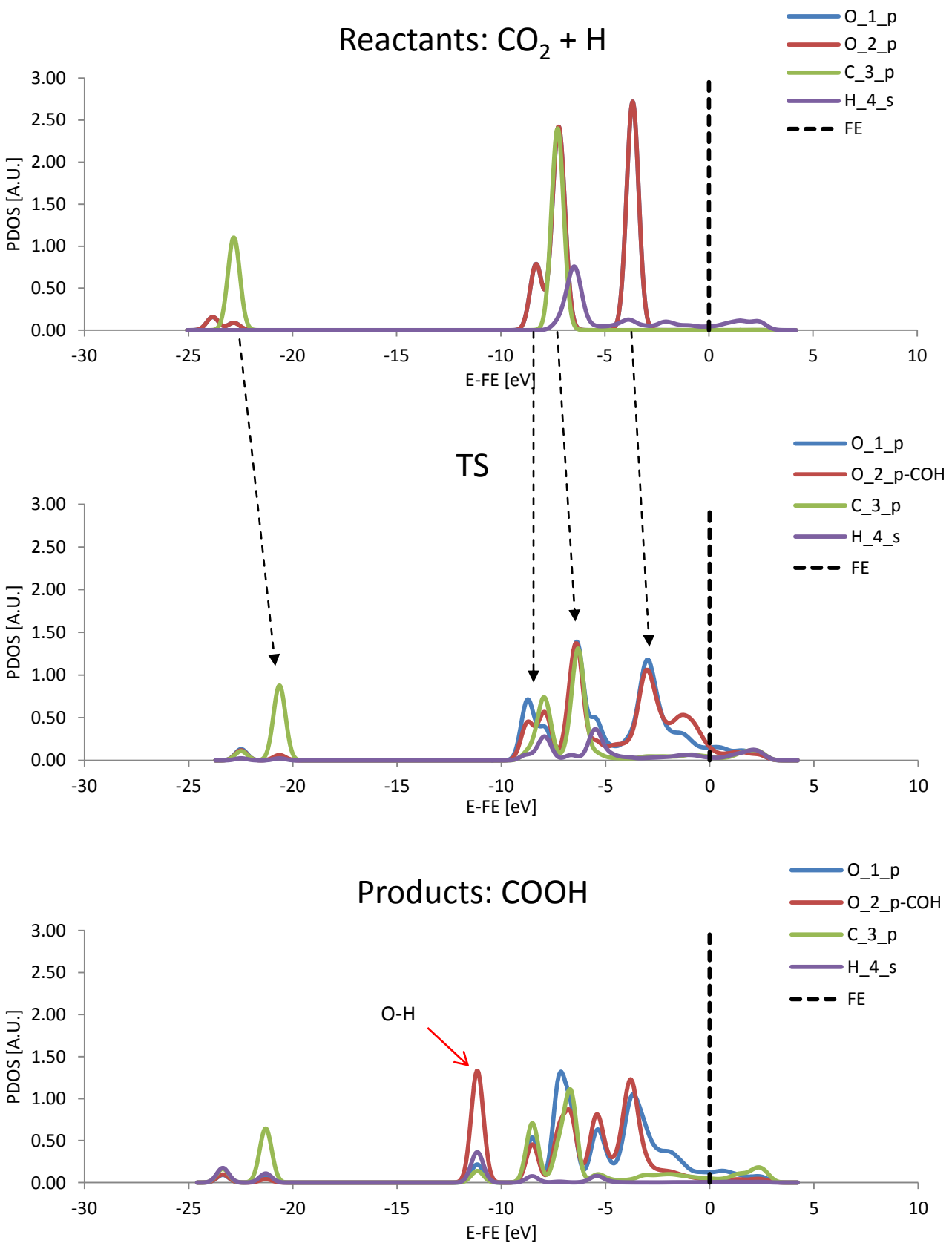

Figure 5.57: PDOS of the reactants, Transition State, and products for reaction (5.4) on Rh; FE = Fermi Energy (reference level); X_n_v means X = atomic type, n = label of the atom, v = valence orbital

On Nickel:

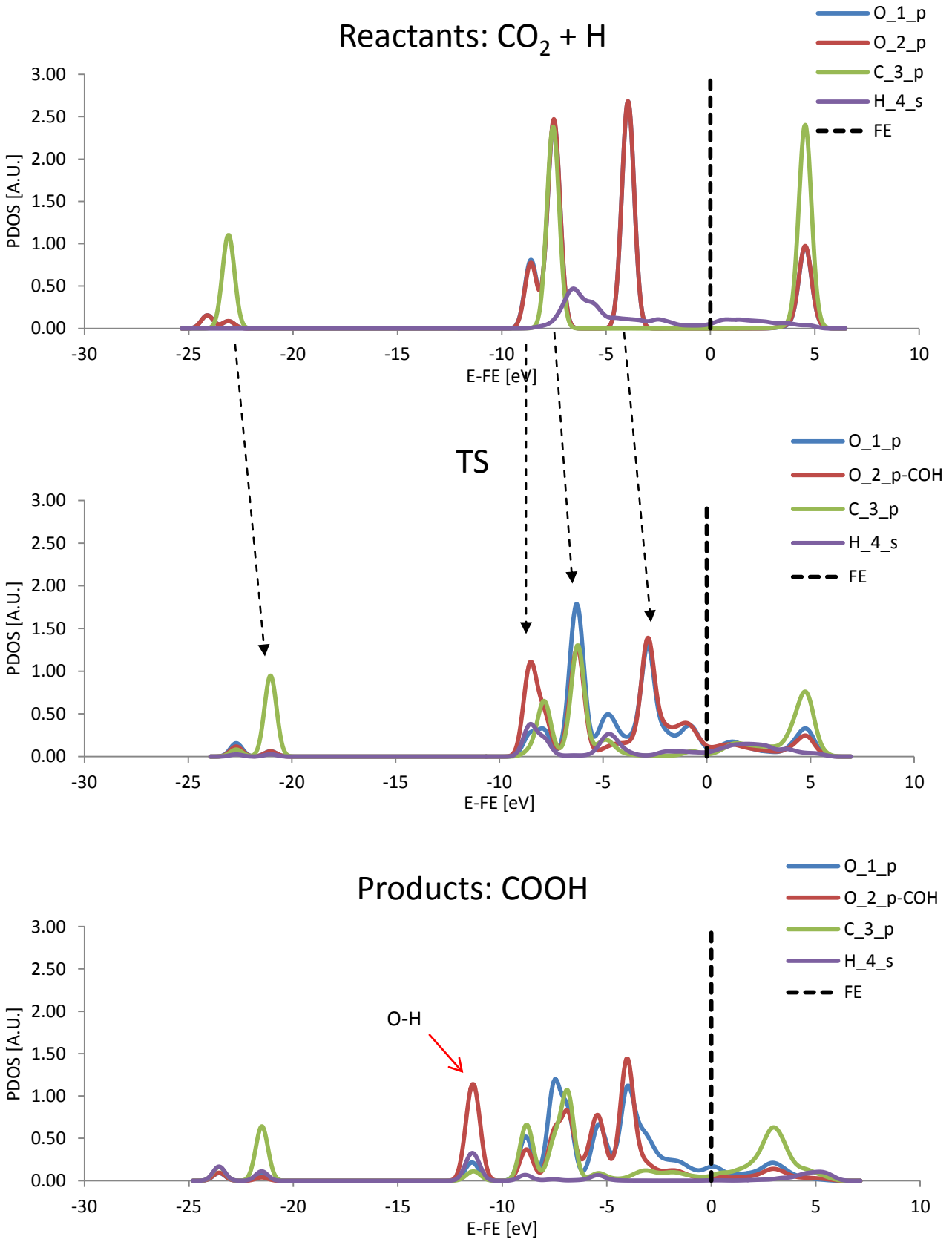

Figure 5.58: PDOS of the reactants, Transition State, and products for reaction (5.4) on Ni; FE = Fermi Energy (reference level); X_n_v means X = atomic type, n = label of the atom, v = valence orbital

The PDOS of the Transition State [Figure 5.56, Figure 5.57, Figure 5.58] possesses lower peaks if compared with the peaks of reactants, although the number of the peaks is the same, and the shape of the PDOS at the Transition State is the shape of the PDOS referred to CO_2 at the initial state of the elementary step. If instead the PDOS of the last state is observed, that is to say the PDOS referred to the products, a new peak is identified, with its center positioned at about -10 eV. This peak is due to the overlapping of the hydrogen state with the oxygen states, in order to create the O-H bond.

The Transition State analysis based on geometrical consideration seems to point out the lateness of the TS, since carbon dioxide is no longer linear, but at the same time it still since the atom of hydrogen is bound at the metal surface. Therefore the true nature of the Transition State is actually revealed by the PDOS that provides the electronic structure of the system, and this structure clearly appears to resemble the reactants electronic structure. As a whole the Transition State is "early" [Table 5.25].

CO_2+H → COOH		
	Geometry	Electronic structure
Pt	Late	Early
Rh	Late	Early
Ni	Late	Early

Table 5.25: evaluation of the Transition State for reaction (5.4)

Conclusions:

- Forward activation energy should depend on reactants binding energies while backward activation energy should change according to products binding energies, although both forward and backward activation energy are affected by hydrogen binding energy,
- The carboxyl group slightly affects backward activation energy,
- Since the binding energy of a reactant has consequence on backward activation energy the Transition State is early, in full agreement with PDOS.

Conclusions

We reported results of a systematic DFT study of CO_2 activation on Pt(111), Rh(111) and Ni(111) surfaces, consisting of 4 elementary-like steps and 6 surface species. Rh (111) has higher stability of C and COOH while Ni (111) exhibits the largest binding energy for O, H and CO.

The lowest energy barrier for CO_2 direct decomposition to CO and O appears on Ni(111), here carbon dioxide lays in gas phase and its binding energy does not exert any dependence on both forward and backward activation energies. However, atomic oxygen is recognized as the atomic compound that more strongly impacts over the energetic of the system, its binding energy can be related to both forward and backward activation energies in fact an Evans-Polanyi dependence has been detected. This relationship displays the late character of the Transition State, that is confirmed by the Transition State geometrical structure and PDOS.

The Boudouard reaction, is favored on Rh (111), though a very similar forward activation energy is produced by Pt(111). Carbon dioxide never considerably interacts with the catalyst and also the metal-carbon affinity is the same for Pt, Rh and Ni. CO instead determines the stability of the products at the catalytic surface, thus it is expected to increase backward activation energy as CO binding energy grows up. An Evans-Polanyi trend is identified, and the Transition State is supposed to be early, in fact as atomic carbon binding energy slightly varies from metal to metal, even forward activation energy is quite the same for Pt, Rh and Ni.

CO_2 can directly react with atomic hydrogen, strongly bound in a dissociated fashion at the metal surface. This elementary step is especially favored on Pt(111) where the lowest barrier energy is computed. Evans-Polanyi theory does not work with this class of reaction, thus the nature of the Transition State cannot be predicted this way and as consequence other trends are investigated. Hydrogen is marked as the chemical compound that affects both forward and backward activation energies. Since hydrogen influences backward activation energy, the Transition State can probably share the electronic properties of reactants. This statement is validated by the PDOS analysis that can be employed to definitely classify the Transition State as an early one.

The effects of a high carbon coverage have been discussed, carbon dioxide is no longer able to approach the active surface because of the carbon overlayer. Lots of adsorption sites are filled with atomic carbon, and as consequence the carbon of the monoxide does not experience such an intense interaction with the substrate and cannot reach the active top site. However the high coverage carbon binding energy decreases because of a carbon-carbon repulsion that occurs at the metal surface. The Boudouard reaction with low carbon coverage showed an early and fixed Transition State with forward activation energy identical for the three metals, although, carbon at high coverage appears to be less stable and the forward activation energy is expected to become smaller. The early character of the Transition State is recognized through PDOS and very low activation energies have been computed.

The analysis of energetic indicates that, for the CO_2 activation process, the carboxyl pathway is favored on Pt(111) while the direct route (carbon dioxide decomposition) dominates on Rh (111) and Ni (111). Although, if a high coverage of carbon appears at the metal surface, coking conditions change surface chemistry by producing lowest barrier energies, and as consequence CO_2 activation mechanism is no longer affected by the choice of the metallic substrate.

Index of Figures

Index of Tables

Bibliography

1. Wei, W. and G. Jinlong, *Methanation of carbon dioxide: an overview.* Frontiers of Chemical Science and Engineering, 2011. **5**(1): p. 2-10.
2. Cai, M., et al., *Methanation of carbon dioxide on Ni/ZrO2-Al2O3 catalysts: Effects of ZrO2 promoter and preparation method of novel ZrO2-Al2O3 carrier.* Journal of Natural Gas Chemistry, 2011. **20**(3): p. 318-324.
3. Centi, G. and S. Perathoner, *Opportunities and prospects in the chemical recycling of carbon dioxide to fuels.* Catalysis Today, 2009. **148**(3–4): p. 191-205.
4. Perkas, N., et al., *Methanation of Carbon Dioxide on Ni Catalysts on Mesoporous ZrO2 Doped with Rare Earth Oxides.* Catalysis Letters, 2009. **130**(3-4): p. 455-462.
5. Erhan Aksoylu, A. and Z. İlsenÖnsan, *Hydrogenation of carbon oxides using coprecipitated and impregnated Ni/Al2O3 catalysts.* Applied Catalysis A: General, 1997. **164**(1–2): p. 1-11.
6. Seo, J.G., et al., *Preparation of Ni/Al2O3–ZrO2 catalysts and their application to hydrogen production by steam reforming of LNG: Effect of ZrO2 content grafted on Al2O3.* Catalysis Today, 2008. **138**(3–4): p. 130-134.
7. Choudhary, V.R., S.A.R. Mulla, and V.H. Rane, *Surface basicity and acidity of alkaline earth-promoted La2O3 catalysts and their performance in oxidative coupling of methane.* Journal of Chemical Technology & Biotechnology, 1998. **72**(2): p. 125-130.
8. Ocampo, F., et al., *Effect of Ce/Zr composition and noble metal promotion on nickel based CexZr1−xO2 catalysts for carbon dioxide methanation.* Applied Catalysis A: General, 2011. **392**(1–2): p. 36-44.

9. Song, H., et al., *Methanation of Carbon Dioxide over a Highly Dispersed Ni/La2O3 Catalyst.* Chinese Journal of Catalysis, 2010. **31**(1): p. 21-23.
10. Inui, T., *Highly effective conversion of carbon dioxide to valuable compounds on composite catalysts.* Catalysis Today, 1996. **29**(1–4): p. 329-337.
11. Jacquemin, M., A. Beuls, and P. Ruiz, *Catalytic production of methane from CO2 and H2 at low temperature: Insight on the reaction mechanism.* Catalysis Today, 2010. **157**(1–4): p. 462-466.
12. Karelovic, A. and P. Ruiz, *CO2 hydrogenation at low temperature over Rh/γ-Al2O3 catalysts: Effect of the metal particle size on catalytic performances and reaction mechanism.* Applied Catalysis B: Environmental, 2012. **113–114**(0): p. 237-249.
13. Yu, K.-P., et al., *Pt/titania-nanotube: A potential catalyst for CO2 adsorption and hydrogenation.* Applied Catalysis B: Environmental, 2008. **84**(1–2): p. 112-118.
14. Kuśmierz, M., *Kinetic study on carbon dioxide hydrogenation over Ru/γ-Al2O3 catalysts.* Catalysis Today, 2008. **137**(2–4): p. 429-432.
15. Park, J.-N. and E.W. McFarland, *A highly dispersed Pd–Mg/SiO2 catalyst active for methanation of CO2.* Journal of Catalysis, 2009. **266**(1): p. 92-97.
16. Alavi, A., et al., *CO Oxidation on Pt(111): An Ab Initio Density Functional Theory Study.* Physical Review Letters, 1998. **80**(16): p. 3650-3653.
17. Eichler, A., *CO oxidation on transition metal surfaces: reaction rates from first principles.* Surface Science, 2002. **498**(3): p. 314-320.
18. Wang, G.-C., et al., *Cluster and periodic DFT calculations of adsorption and activation of CO2 on the Cu(hkl) surfaces.* Surface Science, 2004. **570**(3): p. 205-217.
19. Minot, C., *Modeling of high-pressure CO dissociation on Pt(1;0;0) and Pt(1;1;1).* Catalysis Today, 2004. **89**(3): p. 357-362.
20. Abild-Pedersen, F. and M.P. Andersson, *CO adsorption energies on metals with correction for high coordination adsorption sites – A density functional study.* Surface Science, 2007. **601**(7): p. 1747-1753.
21. Gokhale, A.A., J.A. Dumesic, and M. Mavrikakis, *On the Mechanism of Low-Temperature Water Gas Shift Reaction on Copper.* Journal of the American Chemical Society, 2008. **130**(4): p. 1402-1414.
22. Grabow, L.C., et al., *Mechanism of the Water Gas Shift Reaction on Pt: First Principles, Experiments, and Microkinetic Modeling.* The Journal of Physical Chemistry C, 2008. **112**(12): p. 4608-4617.

23. Flaherty, D.W., et al., *Mechanism for the water–gas shift reaction on monofunctional platinum and cause of catalyst deactivation.* Journal of Catalysis, 2011. **282**(2): p. 278-288.
24. Liu, C., T.R. Cundari, and A.K. Wilson, *CO2 Reduction on Transition Metal (Fe, Co, Ni, and Cu) Surfaces: In Comparison with Homogeneous Catalysis.* The Journal of Physical Chemistry C, 2012. **116**(9): p. 5681-5688.
25. Catapan, R.C., et al., *DFT Study of the Water–Gas Shift Reaction and Coke Formation on Ni(111) and Ni(211) Surfaces.* The Journal of Physical Chemistry C, 2012. **116**(38): p. 20281-20291.
26. Einstein, A., *Zur Elektrodynamik bewegter Körper.* Annalen der Physik 1905. **17**: p. 891.
27. Jensen, F., *Introduction to Computational Chemistry*. 2006: Wiley.
28. Schrödinger, E., *Quantisierung als Eigenwertproblem.* Annalen der Physik, 1926. **79**: p. 361,489.
29. Born-Oppenheimer, *Zur Quantentheorie der Molekeln.* Annalen der Physik, 1927. **389**(20): p. 457.
30. David S. Sholl, J.A.S., *DENSITY FUNCTIONAL THEORY: A Practical Introduction*. 2009: John Wiley & Sons, Inc.,Publication.
31. A. Szabo, N.S.O., *Modern Quantum Chemistry: Introduction to Advanced Electronic Structure Theory*. 1996: McGraw-Hill.
32. Prof. Dr. Wolfram Koch, D.M.C.H., *A Chemist's Guide to Density Functional Theory, Second Edition*. 2001.
33. Thomas, L.H., *The calculation of atomic fields.* Proc. Camb. Phil. Soc., 1927. **23** p. 542-548.
34. Hohenberg, P.K., W. , *Inhomogeneous Electron Gas.* Physical Review, 1964. **136**(3B).
35. Kohn, W. and L.J. Sham, *Self-Consistent Equations Including Exchange and Correlation Effects.* Physical Review, 1965. **140**(4A): p. A1133-A1138.
36. Payne, M.C., et al., *Iterative minimization techniques for ab initio total-energy calculations: molecular dynamics and conjugate gradients.* Reviews of Modern Physics, 1992. **64**(4): p. 1045-1097.
37. Ashcroft, N.W.a.M., N. D., *Solid State Physics*. 1976: Saunders.
38. Monkhorst, H.J. and J.D. Pack, *Special points for Brillouin-zone integrations.* Physical Review B, 1976. **13**(12): p. 5188-5192.
39. Clusius, *Einführung in die Quantenchemie. Von H. Hellmann. 350 S.,43 Abb., 35 Tab. Franz Deuticke, Leipzig u. Wien 1937. Pr. geh. RM. 20,-. geb. RM. 22.* Angewandte Chemie, 1941. **54**(11-12): p. 156-156.

40. Heine, M.W.F.a.V., *Theory of lattice contraction at aluminium surfaces.* J. Phys. Chem., 1973. **B 105**(L37).
41. Masel, R., *Chemical Kinetics and Catalysis*. 2001, New York: John Wiley and Sons.
42. Hammer, B. and J.K. Nørskov, *Theoretical surface science and catalysis—calculations and concepts*, in *Advances in Catalysis*, H.K. Bruce C. Gates, Editor. 2000, Academic Press. p. 71-129.
43. Marek, G., E. Andreas, and H. Jürgen, *CO adsorption on close-packed transition and noble metal surfaces: trends from ab initio calculations.* Journal of Physics: Condensed Matter, 2004. **16**(8): p. 1141.
44. Maestri, M. and K. Reuter, *Semiempirical Rate Constants for Complex Chemical Kinetics: First-Principles Assessment and Rational Refinement.* Angewandte Chemie International Edition, 2011. **50**(5): p. 1194-1197.
45. Honkala, K., et al., *Ammonia Synthesis from First-Principles Calculations.* Science, 2005. **307**(5709): p. 555-558.
46. Eyring, H., *The Activated Complex in Chemical Reactions.* The Journal of Chemical Physics, 1935. **3**(2): p. 107-115.
47. Sheppard, D., R. Terrell, and G. Henkelman, *Optimization methods for finding minimum energy paths.* The Journal of Chemical Physics, 2008. **128**(13): p. 134106-10.
48. Henkelman, G., B.P. Uberuaga, and H. Jonsson, *A climbing image nudged elastic band method for finding saddle points and minimum energy paths.* The Journal of Chemical Physics, 2000. **113**(22): p. 9901-9904.
49. Maestri, M. and K. Reuter, *Molecular-level understanding of WGS and reverse WGS reactions on Rh through hierarchical multiscale approach.* Chemical Engineering Science, 2012. **74**(0): p. 296-299.
50. Maestri, M., et al., *Dominant Reaction Pathways in the Catalytic Partial Oxidation of CH4 on Rh.* Topics in Catalysis, 2009. **52**(13-20): p. 1983-1988.
51. Maestri, M., et al., *Steam and dry reforming of methane on Rh: Microkinetic analysis and hierarchy of kinetic models.* Journal of Catalysis, 2008. **259**(2): p. 211-222.
52. Marzari, N., et al., *Thermal Contraction and Disordering of the Al(110) Surface.* Physical Review Letters, 1999. **82**(16): p. 3296-3299.
53. Bligaard, T., et al., *The Brønsted–Evans–Polanyi relation and the volcano curve in heterogeneous catalysis.* Journal of Catalysis, 2004. **224**(1): p. 206-217.